HHS Public Access

Author manuscript

Chem Rev. Author manuscript; available in PMC 2017 August 10.

Published in final edited form as:

Chem Rev. 2016 August 10; 116(15): 8693–8749. doi:10.1021/acs.chemrev.6b00180.

Hydrogenase Enzymes and Their Synthetic Models: The Role of Metal Hydrides

David Schilter[*,†,‡], **James M. Camara**[§], **Mioy T. Huynh**[‖], **Sharon Hammes-Schiffer**[‖], and **Thomas B. Rauchfuss**[‖]

[†]Center for Multidimensional Carbon Materials, Institute for Basic Science (IBS), Ulsan 44919, Republic of Korea

[‡]Department of Chemistry, Ulsan National Institute of Science and Technology (UNIST), Ulsan 44919, Republic of Korea

[§]Department of Chemistry, Yeshiva University, 500 West 185th Street, New York, New York 10033, United States

[‖]Department of Chemistry, University of Illinois at Urbana–Champaign, 600 South Mathews Avenue, Urbana, Illinois 61801, United States

Abstract

Hydrogenase enzymes efficiently process H_2 and protons at organometallic FeFe, NiFe, or Fe active sites. Synthetic modeling of the many H_2ases states has provided insight into H_2ase structure and mechanism, as well as afforded catalysts for the H_2 energy vector. Particularly important are hydride-bearing states, with synthetic hydride analogues now known for each hydrogenase class. These hydrides are typically prepared by protonation of low-valent cores. Examples of FeFe and NiFe hydrides derived from H_2 have also been prepared. Such chemistry is more developed than mimicry of the redox-inactive monoFe enzyme, although functional models of the latter are now emerging. Advances in physical and theoretical characterization of H_2ase enzymes and synthetic models have proven key to the study of hydrides in particular, and will guide modeling efforts toward more robust and active species optimized for practical applications.

Graphical abstract

[*]**Corresponding Author:** d.schilter@gmail.com.

Notes

The authors declare no competing financial interest.

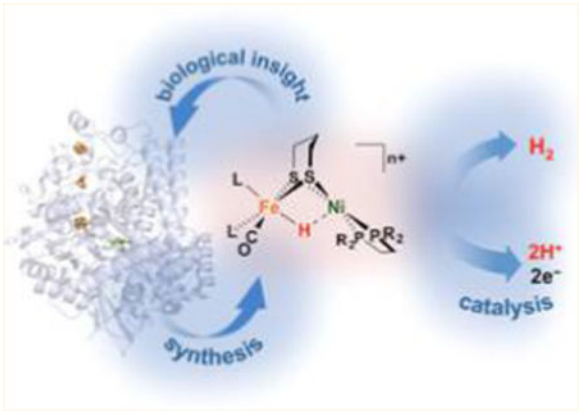

1. INTRODUCTION

Certain prokaryotes live off energy liberated from the metabolism of simple oxidants and dihydrogen. While this was known even in 1892,[1] it would be another 40 years before bacterial dehydrogenase enzymes were implicated in such processes. In what must have been a startling observation, *Bacterium aliphaticum liquefaciens*, grown under H_2, O_2, and CO_2, was found to reduce methylene blue (E = 11 mV vs NHE, the normal hydrogen electrode) under a stream of H_2.[2] This early work was followed by a landmark paper by Stephenson and Stickland, who described bacterial cultures from river mud that reduced NO_3^-, O_2, and fumarate.[3,4] They wrote that "hydrogen is in some way activated, and this activation can be conveniently expressed $H_2 \rightleftharpoons 2H$ without implying anything about the nature of the reaction", the catalyst for which was termed "hydrogenase". These H_2-processing metalloenzymes are the basis for many anaerobic bacteria, protozoa, fungi, and algae[5] collectively producing and consuming an estimated 0.3 Gt of H_2 each year.[6]

Three major classes of hydrogenase (H_2ase) have been identified, members of each featuring either an FeFe, a NiFe, or an Fe core.[7] The [FeFe]- and [NiFe]-H_2ases have been shown to mediate the interconversion of dihydrogen (H_2) with protons (H^+) and electrons (e^-) at high rates[8] and at potentials very close to those bounded by thermodynamics (eq 1).

$$H_2 \rightleftharpoons 2H^+ + 2e^- \quad (1)$$

In contrast to these two redox enzymes, the [Fe]-H_2ases (also known as H_2-forming methylenetetrahydromethanopterin dehydrogenases, Hmd) cleave H_2 to then deliver H^- to the organic substrate methenyltetrahydromethanopterin, with H^+ passing to the bulk solvent (eq 2).[9]

$$H_2 + \text{methenyl} - H_4\text{MPT}^+ \rightleftharpoons H^+ + \text{methylene} - H_4\text{MPT} \quad (2)$$

For each reaction, as was hypothesized in 1931, the catalysts are often bidirectional[3] and deactivated by CO. Unbeknownst to Stephenson and Stickland, the H_2ases each catalyze the isotope exchange between H_2O and D_2 (eq 3).[10, 11]

$$H_2+D_2O \rightleftharpoons HD+HDO \rightleftharpoons D_2+H_2O \quad (3)$$

A further hallmark of H_2ase behavior is their interconversion of ortho- and para-H_2 (eq 4),[12] the two nuclear spin isomers whose differing thermal properties have implications for H_2 storage.[13]

$$\text{ortho} - H_2 \rightleftharpoons \text{para} - H_2 \quad (4)$$

Interest in renewable, carbon-neutral energy technologies has motivated considerable biological research into the expression (including biosynthesis),[14] structure, and function of H_2ases. Each of the three enzyme cores and catalytic cycles is described in individual sections below (sections 3, 4, and 5). Before considering details, we must emphasize that the H_2ase families share several mechanistic themes—principal among them H_2 heterolysis—that are in no small part borne of the structural similarities revealed by even a cursory glance at their active sites (Figure 1).

Central to the H_2ases is Fe(II),[15] whose ligation to thiolate and CO sees it adopt low-spin configurations most suited to the binding of H^- and H_2. Despite the three enzyme classes being phylogenically unrelated,[16] "convergent evolution" causes expression of these common features that are apparently expedient for H_2 processing.[14] Inorganic chemists are motivated to prepare structural, spectroscopic, and/or functional mimics to elucidate the mechanisms of the very enzymes that inspired their synthesis.[17] Given that H_2 processing is championed by the Pt group metals, more cost-effective alternatives would involve the use of purely organic catalysts[18] or those based on earth-abundant metals, like the H_2ases.[19–27] Better yet, their synthetic models may be more robust and mass-producible, with smaller spatial footprints that allow densely decorated, highly active electrodes to be prepared and incorporated into devices such as fuel cells.[28–30]

Having identified the importance of Fe–CO–thiolato ensembles in H_2-processing enzymes, one can also reasonably expect complexes of H^- and H_2 to be somehow involved in Nature's plans. These substrate-bearing intermediates, and the synthetic models proposed to mimic them most closely, are the focus of this review. Particular emphasis is placed on work in the past decade, which has seen great progress not only in biochemical and chemical synthesis, but also in the development of experimental and computational methods for the characterization of metal dihydrogen and hydride complexes. Before turning to these themes, some background into the chemistry relevant to these natural and synthetic catalysts is presented.

2. FORMATION AND CHARACTERIZATION OF METAL HYDRIDES

2.1. Formation of Metal Hydrides from H^+ or H_2

Nature's handling of H^+ and H_2 with Fe and Ni follows patterns familiar in synthetic chemistry and catalysis.[31] For example, electron-rich, low-valent metal sites are susceptible to protonation (oxidative addition of H^+, Figure 2). In the case of a single metal center, the resulting hydride may vary greatly in its polarity and acid–base properties. When two metals are involved, consideration must also be paid to regiochemistry: will the product feature a terminal hydrido (t-H^-) or a bridging hydrido (μ-H^-) ligand?

When low- or mid-valent metal centers are exposed to H_2 instead of H^+, σ-complexes of the type M(η^2-H_2) may form, in which intact H_2 binds side-on to M (Figure 3).[32] This bonding motif has been described by analogy with the Dewar–Chatt–Duncanson model for metal complexes of olefins.[33] Since η^2-H_2 acts as a σ-base and π-acid, the bond between H atoms (bond dissociation energy (BDE) = 436 kJ mol^{-1} for free H_2)[34] is weakened upon coordination, and in the case of electron-rich metals, can be entirely broken to afford $M(H)_2$ dihydrides through a formal oxidative addition (homolysis).[35]

The homolytic route for hydride formation, while common for group 10 metals and previously proposed based on computations of the [NiFe]-H_2ases,[36] is no longer thought to be relevant to the H_2ases. Indeed, the kinetic barriers associated with homolytic H_2ase pathways are prohibitive, and the enzymes instead operate through heterolysis (Figure 4). Heterolysis typically involves higher-valent metals, suitably unsaturated examples of which can ligate H_2. The resulting M(η^2-H_2) complexes, when in the presence of a Brønsted base, may experience H_2 fission, but not in the homolytic sense. Rather, the base deprotonates acidic η^2-H_2 to afford a metal hydride and a conjugate acid. Such a tug-of-war over the H_2 substrate, which does not result in any change in metal oxidation state,[37] is typical of that played out between frustrated Lewis acid and base pairs (FLPs).[38,39] Cleavage is enabled by the remarkable influence electrophilic metal centers have on H_2, whose acidity when bound is highly variable, as is evident from the contrasting behaviors of *trans*-[Fe(dppe)$_2$(η^2-H_2)H]$^+$ (pK_a(THF) = 12; THF = tetrahydrofuran; dppe =1,2-bis(diphenylphosphino)ethane)[40,41] and *trans*-[Fe(dppe)$_2$(η^2-H_2)CO]$^{2+}$ (pK_a(THF) ≈ pK_a(CH_2Cl_2) = −5).[42,43] Such pK_a values depart greatly from that of the free gas (pK_a(THF) ≈ 50,[44] pK_a(MeCN) ≈ 50),[40] underscoring Nature's need for metals to activate this otherwise very strong bond.

Pentacoordinate, low-spin 16e$^-$ centers represent archetypal metal fragments for H_2 binding, and the H_2 adducts of three such motifs are presented in Figure 5. The Fe(II) electrophiles [Fe(dppe)$_2$CN]$^+$ ([**1**]$^+$ and [Fe(dppe)$_2$CO]$^{2+}$ ([**2**]$^{2+}$) both form stable η^2-H_2 complexes, despite the contrasting donor/acceptor properties of CN^- and CO. This is further astonishing in that it is the ligand *trans* to the H_2 binding site that has the most influence on whether or not a η^2-H_2 complex can persist. It turns out that η^2-H_2 complexes are stabilized by CN^- *and* CO ligands, although for different reasons in each case. According to Pauling's principle of electroneutrality, the strong σ-basicity of CN^- reduces the electron density Fe requires from the H–H σ-bond, such that the latter remains largely intact.[45] It may be somewhat counterintuitive that a strong donor such as CN^- does not, in this case, promote H_2 oxidative

addition. But since σ-bonding between Fe and H_2 is weak, the Fe(dπ)–H_2(σ*) π-backdonation is insufficient to induce splitting. When instead a strongly π-acidic CO ligand[35] is ligated to Fe, the system once more attracts the H–H σ-bond. Yet since CO competes for backdonation, the η^2-H_2 moiety persists as Fe(dπ)–H_2(σ*) interactions are weak.[33]

A continuum exists between labile M(η^2-H_2) and bona fide $M(H)_2$ complexes, between which are metal complexes where H_2 is activated to the point that heterolysis, but not homolysis, can occur. Residing in the middle of the first row of transition metals, Fe seems to be in such a "sweet spot". With the judiciously chosen coligands CO and CN^-, Fe(η^2-H_2) species not only form readily, but, as demonstrated by the three H_2ase families, often do so in preference to binding ubiquitous substrates such as H_2O or N_2. Once formed, η^2-H_2 complexes may undergo heterolysis to afford hydrido species, general aspects of which are discussed in section 2.2.

2.2. Properties of Hydride Complexes

The strong donor properties of H^- are very familiar to inorganic chemists. In general, the donicity of a given ligand L can be quantified by several parameters, including the so-called P_L value.[46] Defined in terms of ligand effects on the $Cr^{+/0}$ couple ($P_L = E_{1/2}[Cr(I/0)(CO)_5L] - E_{1/2}[Cr(I/0)(CO)_6]$), $P_L \equiv 0$ V for CO, with NO^+ (1.4 V) and OH^- (−1.55 V) having the expected opposite effects on redox. The value for H^- (−1.22 V) is less negative than the latter extreme, but more negative than the value for CN^- (−1.00 V), consistent with the strong donicity and anionic nature of H^-. Closely related to the P_L value is the Lever parameter (E_L), which describes redox effects of ligands on Ru(III/II) couples.[47] The E_L parameter estimated for H^- is −0.5 V, in the −0.63 to 0 V range characteristic of strongly donating ligands and π-bases including OH^- and RS^-. While the two scales are certainly influenced by ligand charge, they do provide useful measures of donicity, although they do not account for any steric interactions and synergistic effects between ligands.

Other ligands can be quantitatively compared to H^-, but how can different complexes of H^- be compared? Nominally an anionic ligand, hydride can exist in anything from "hydridic" M–$H^{\delta-}$ moieties to "protic" M–$H^{\delta+}$ groups. A key parameter in describing hydrides is pK_a, which, for an arbitrary species MH^+ (eq 5), is found by treating it with a comparable amount of a suitable base (denoted B, eq 6) with a known pK_a (BH^+) in the solvent being used. If the Brønsted acidities of MH^+ and BH^+ differ greatly, then only an upper or lower bound for pK_a(MH^+) is measurable in practice. If the acidities are comparable, then K_{eq} (eq 7) and pK_a(MH^+) may be easily determined.

$$MH^+ \rightleftharpoons M + H^+;\ K_a(MH^+) = [M][H^+]/[MH^+] \quad (5)$$

$$BH^+ \rightleftharpoons B + H^+;\ K_a(BH^+) = [B][H^+]/[BH^+] \quad (6)$$

$$MH^+ + B \rightleftharpoons M + BH^+;\ K_{eq} = [M][BH^+]/[MH^+][B] \quad (7)$$

Matters are more complicated when a base forms an H-bonded adduct with its conjugate acid (eq 8), a process referred to as homoconjugation or self-association.[48]

$$B + BH^+ \rightleftharpoons B_2H^+;\ K_f = [B_2H^+]/[B][BH^+] \quad (8)$$

For certain weak acid/base pairs in organic solvents (e.g., RCO_2^-/RCO_2H in MeCN), such effects must be taken into account when the concentration of added base exceeds $1/K_f$.[49] Homoconjugation constants K_f for several acids are known,[50] and $pK_a(MH^+)$ can still be computed in a straightforward manner (see the Appendix).[48] Homoconjugation can be largely avoided by employing aniliniums/anilines, which are expected to exhibit low values of K_f.[51] Values for $pK_a(MH^+)$ span a wide range,[44] and rough predictions based on metal and ligand parametrization are possible.[41] The values are typically lower for electron-poor metal complexes and higher for their electron-rich counterparts, with a $M–H^{\delta-}$ description perhaps being more relevant in the latter case (eq 9).

$$MH^+ \rightleftharpoons M^{2+} + H^- \quad (9)$$

The reaction in eq 9 is clearly related to that in eq 5, with the metal hydride now releasing H^- rather than H^+. The Gibbs free energy change associated with eq 9, known as the hydricity ($\Delta G^\circ(H^-)$),[52] is readily computed if MH^+ can transfer H^- to acceptors of known hydricity, such a competitive binding method being analogous to determining pK_a by adding a base. Alternatively, if $pK_a(MH^+)$ and the half-wave potentials ($E_{1/2}$) of the $1e^-$ couples $[M]^{+/0}$ and $[M]^{2+/+}$ (or the $2e^-$ couple $[M]^{2+/0}$) are known, hydricity (expressed in J mol^{-1}) can also be calculated according to eq 10 or 11, derivations of which are in the Appendix.[52,53]

$$\Delta G^\circ(H^-) = (RT/\log_{10}e)pK_a + FE_{1/2}([M]^{+/0}) + FE_{1/2}([M]^{2+/+}) - 2FE_{1/2}([H]^{+/-}) \quad (10)$$

$$\Delta G^\circ(H^-) = (RT/\log_{10}e)pK_a + 2FE_{1/2}([M]^{2+/0}) - 2FE_{1/2}([H]^{+/-}) \quad (11)$$

where $F = 96\,485$ C mol^{-1}, $R = 8.314$ J K^{-1} mol^{-1} and T is reported in kelvin. It is noted that very few H_2ase models have two consecutive reversible $1e^-$ couples (or, alternatively, a reversible $2e^-$ couple) necessary for this calculation.

The hydricity of a compound is a measure of its propensity to donate H^-, with the lowest values corresponding to the most hydridic species. As with the pK_a's of metal complexes, hydricities are also strongly influenced by solvation,[54] with a narrower range of values expected for more polar solvents. For example, H_2, {Ni[(1,2-bis(dihydroxylmethylphosphino)ethane]$_2$H}$^+$, and HCO_2^- have vastly different hydricities in MeCN (76.6, 57.4, and 44.0 kcal mol^{-1}, respectively), the solvent most commonly used for such determinations. The values measured in the stronger dielectric H_2O are much closer (34.2, 30.0, and 24.1 kcal mol^{-1}).[54] Hydricity is intuitively also related to the electron density at the metal in question, with $\Delta G^\circ(H^-)$ for the relatively electron-rich and -poor complexes [Ni(dmpe)$_2$H]$^+$ (dmpe =1,2-bis(dimethylphosphino)ethane) and [Ni(dppe)$_2$H]$^+$ determined as 48.9 and 62.7 kcal mol^{-1}, respectively.[53] Lastly, hydricity is also sensitive to coordination geometry, an aspect that has been explored with [M(diphosphine)$_2$H]$^+$ complexes, and one that is not surprising given that bite angles of chelating ligands can favor certain coordination numbers.[55,56] In particular, ligands that span large angles will stabilize a hydride-free complex, leading to lower hydricity values. Overall, the many factors contributing to hydricity mean that it is certainly possible for a species to have a high pK_a and modest hydricity, as the influence of redox may swing the result either way.

The interrelation between hydride redox, pK_a, and hydricity is summarized in Figure 6. Simple thermodynamic cycles enable determination of free energies, such as hydricity ΔG° (H^-, II), from experimentally determined pK_a(II), E°(II/I), and E°(I/0) (or E°(II/0)) values as in eq 10. In this context, pK_a(n), $\Delta G^\circ(H^\bullet,n)$, and $\Delta G^\circ(H^-,n)$ are respectively associated with equilibria for H^+, $H^\bullet$, and H^- donation from $[M^nH]^{(n-1)+}$.

Until now, metal hydrides have been viewed here as potential sources of H^+ or H^-. Yet another important scenario is homolysis of an M–H bond,[58,59] which in practice does not involve free $H^\bullet$ but rather its delivery to a substrate.[60] The facility of the homolysis reaction can be calculated analogously to hydricity: if pK_a(II) and E°(I/0) (written in eq 13 as pK_a and $E_{1/2}([M]^{+/0})$, respectively) are known, one can compute the $H^\bullet$ donor strength ($\Delta G^\circ(H^\bullet)$, eq 12, 13). Once more, details of the cycles used to derive eqs 12 and 13 are presented in the Appendix.

$$MH^+ \rightleftharpoons M^+ + H^\bullet \quad (12)$$

$$\Delta G^\circ(H^\bullet) = (RT/\log_{10}e)pK_a + FE_{1/2}([M]^{+/0}) - FE_{1/2}([H]^{+/0}) \quad (13)$$

Our discussion now returns to considering pK_a's of metal hydrides and the significant and intuitive perturbations redox has on these.[61,62] Indeed, the oxidation of metal hydrides causes large increases in acidity, as the reductive elimination of H^+ is certainly more favorable when the metal site is more electron poor. One family of species for which the thermodynamics are well studied are the bis(diphosphine) complexes of Ni.[57] Consider tetrahedral [Ni(dppe)$_2$], which readily protonates to give the respective 5-coordinate divalent

hydride $[Ni(dppe)_2H]^+$ (eq 14, $pK_a(II) = 16.7$). The same cannot be said for oxidized $[Ni(dppe)_2]^+$, whose protonation product $[Ni(dppe)_2H]^{2+}$ is a strong acid in MeCN (eq 15, $pK_a(III) = -8.6$).[57]

$$[Ni(dppe)_2H]^+ \rightleftharpoons [Ni(dppe)_2] + H^+; \quad K_a(II) = [Ni(dppe)_2][H^+]/[Ni(dppe)_2H^+] \quad (14)$$

$$[Ni(dppe)_2H]^{2+} \rightleftharpoons [Ni(dppe)_2]^+ + H^+; \quad K_a(III) = [Ni(dppe)_2^+][H^+]/[Ni(dppe)_2H^{2+}] \quad (15)$$

The marked drop in pK_a upon oxidation of $[Ni(dppe)_2H]^+$ is a typical consequence of redox on a mononuclear metal hydride, with this acidity increase often leading to hydride-related redox events being irreversible. One reason the [FeFe]- and [NiFe]-H_2ases employ bimetallic active sites may be to disperse the strong effects of redox over two metal sites.[63] This dampens the impact felt by the H^- ligand, enhances the reversibility of redox couples, and perhaps lowers activation barriers to catalysis. The [Fe]-H_2ase active site, which is a Lewis acid *not* required to perform redox, features only a single Fe center, with Nature apparently dispensing with the need for a second metal. A detailed understanding of redox and acid–base properties of H_2ases and functional models requires a number of experimental techniques. Some key methods are discussed in section 2.3, particularly in the context of characterizing hydride-containing species.

2.3. Physical Characterization of Hydrogenase Enzymes and Models

2.3.1. Electrochemistry—In addition to the two hydrogenic substrates H^+ and H_2, the [FeFe]- and [NiFe]-H_2ases also handle electrons to drive eq 1 in a forward or reverse sense. According to the Nernst equation, at pH 7, $p(H_2) = 1$ bar, and $T = 298$ K, the $2H^+/H_2$ couple is at −414 mV vs NHE. Yet hydrogenases only have access to H_2 partial pressures of 1–10 Pa (10^{-5}–10^{-4} bar), such that they must operate between −266 and −296 mV, the narrow range mandated by thermodynamics.[6] In vivo, electrons travel via Fe–S clusters positioned close enough together (<14 Å is optimal)[64] to allow tunneling to and from an electron transport protein as the source/sink. In place of the transport protein, in vitro studies of H_2ases instead often employ suitable small molecule electron donors (e.g., methylviologen radical, $E_{1/2} = -446$ mV vs NHE) and acceptors (e.g., benzylviologen, $E_{1/2} = -358$ mV), whose potentials lie on either side of the $2H^+/H_2$ couple at $p(H_2) = 1$ bar.[65] Such redox reagents are also used when studying model compounds, which, with notable exceptions,[66,67] almost always lack redox-active Fe–S clusters or other electron shuttling moieties. Organic solvents may be necessary, as many models feature lipophilic ligands (e.g., phosphines) to stabilize their low-valent states. These studies have benefited from a growing body of work on electrochemistry in polar aprotic solvents,[68] and although pK_a scales are still not uniform, certain reference couples have become standard.[69] While redox potentials of the enzymes in aqueous solutions are typically reported relative to NHE, potentials of model complexes are most often reported against $Fc^{+/0}$ (Fc = $FeCp_2$; Cp^- =

cyclopentadienide), a couple which lies at 0.4, 0.63, and 0.69 V relative to NHE in H_2O,[68] MeCN,[69] and CH_2Cl_2, respectively.[68] In terms of electrolyte salts, model studies make extensive use of noncoordinating anions,[70] with the borates BF_4^-, $B(C_6F_5)_4^-$, and $BAr^F{}_4^-$(3,5-$(CF_3)_2C_6H_3)_4B^-$),[71] as well as PF_6^-, being typical counteranions for both voltammetry[72] and synthesis. Such anions possess diffuse charge and allow for coordinatively unsaturated cations to be studied "in isolation" and to be given every possible chance to interact with weak ligands like H_2.

An important alternative to sacrificial electron donors and acceptors is the use of an electrode as the electron source/sink, with voltammetric methods[73] (as well as associated spectroelectrochemical techniques)[74] proving extremely useful for characterizing analytes when immobilized or in solution,[75] and for determining catalytic rates[76,77] and overpotentials (vide infra).[49,78,79] Cyclic voltammetry (CV) has become popular in the study of synthetic hydrides, and many hydride-bearing mimics of [FeFe]- and [NiFe]-H_2ase exhibit electrochemistry that has informed their HER mechanisms, including uncovering the existence of paramagnetic ($S = 1/2$) hydrides. In contrast to conventional metal hydride chemistry, focused for example on hydrogenation reactions, H_2ases characteristically operate by one-electron ($1e^-$) pathways. As described for [Ni-$(dppe)_2H]^{2+/+}$, redox imparts large changes in the acidity of hydride species, leading to the reductions and oxidations often being rather irreversible. This reflects the high reactivity of certain hydrides and may hint at desirable catalytic properties.

Redox waves of hydrides are often perturbed when H_2 or H^+ substrate is present. Consider the latter case, for which CV is a typical assay for the hydrogen evolution reaction (HER, the reverse of eq 1) catalytic activity. Assume, for instance, a metal hydride gives rise to a $1e^-$ reduction mechanistically relevant to the HER. The potential of this couple in the absence of H^+, denoted here E_{redox}, will certainly depend on the relative electron density at the metal(s) and thus the donor set. When an acid substrate HA is titrated into the hydride/electrolyte mixture, the growth of a wave implicates a situation in which the hydride complex is continually regenerated, and thus participates in a catalytic reaction involving protons. The resultant "catalytic wave" is often described by its potentials at full height (E_{cat}) or half-height ($E_{cat/2}$),[80] values that may differ from E_{redox}. The current associated with the catalytic wave, i_c, can be several times i_p, the current at E_{redox} in the absence of HA. The value i_c will be clear for an ideal (sigmoidal) wave, such that the potentials E_{cat} and $E_{cat/2}$ are precisely determined.[79] More complicated examples can introduce variance in i_c and, correspondingly, the potentials E_{cat} and $E_{cat/2}$. The latter value is least affected by nonidealities, and is thus the more reliable. If the quotient i_c/i_p is proportional to [HA], then the process is second order in $[H^+]$, consistent with the HER. At a certain point, one reaches the so-called "acid-independent regime", in which the addition of HA no longer leads to an increase in i_c, and pseudo-first-order conditions with respect to the catalyst are reached. The maximum obtainable i_c/i_p is proportional to the square root of the turnover frequency (TOF) for H_2 evolution. The latter is an important metric, yet some have questioned its general applicability and instead advocate use of other values including catalytic efficiency (CE = i_c[catalyst]/i_p[HA]).[81]

Catalytic currents and/or TOF values are key descriptors of reactivity, yet these kinetic parameters should not be quoted without their associated potentials, on which they are dependent. The potentials E_{cat} and $E_{cat/2}$ ideally will be more positive than the HA reduction in the absence of hydride catalyst, a wave associated with direct reaction at the electrode (e.g., glassy carbon).[82] Such a process may compete with catalyst-mediated HER at strongly reducing potentials, and one must be aware that currents arising from direct reductions have often been erroneously ascribed to catalysis from model complexes. In any case, $E_{cat/2}$ will be more negative than $E(H_2/HA)$, the thermodynamic potential for the H_2/HA couple, although $E_{cat/2}$ for an ideal catalyst will be very close to this upper bound. When comparing catalysts, the values $E_{cat/2}$, E_{cat}, and E_{redox} are to be used in preference to the oft-quoted but rather subjective term "onset potential" (E_{onset}), the voltage near the base of the catalytic wave at the "onset" of catalysis.[49,73]

An important electrochemical figure of merit is overpotential ($\eta = E(H_2/HA) - E$), defined as the additional voltage, beyond that required thermodynamically, used to drive a reaction at a specific rate.[83] The reaction is driven at a potential E, which may be taken as $E_{cat/2}$, E_{cat}, or another potential. Whatever potential (and thus overpotential) one selects, it is essential that this thermodynamic value is reported if and only if a kinetic value derived from the current is reported.[80,84] Given that η is proportional to the excess electrical energy required, its minimization, while maintaining an acceptable rate of reaction, is highly desirable. Although electron-rich metal catalysts give rise to more negative $E_{cat/2}$ values than their electron-poor counterparts, the former can still have reasonably small overpotentials if they can catalyze H_2 evolution from weaker acids, which have more negative thermodynamic potentials $E(H_2/HA)$. In general, one aims to find the weakest acid that will quantitatively protonate the reduced form of the catalyst, whence η and TOF will be optimized. In addition to these catalytic data, stoichiometric conversions can allow one to develop a picture of the HER mechanism(s) at play. Two photons and two electrons must be transferred during the catalytic cycle; these reactions are often denoted as C (chemical) and E (electrochemical) steps. As will become clear, the sequence of these steps (e.g., ECEC vs CEEC) varies from catalyst to catalyst.

Cyclic voltammograms associated with catalytic reactions may be complicated by certain processes including acid homoconjugation, whence H_2 evolves not only following reduction of HA, but also from other sources such as the homoconjugated species $H^+[AHA]^-$.[49] Digital simulation of voltammograms and supplementary data from chronoamperometry are often beneficial in elucidating mechanisms.[85] Overall, information from CV contributes in no small part to a detailed picture of processes involved in catalytic H_2 evolution or oxidation. Some case studies involving CV in catalysis are presented in the [FeFe]- and [NiFe]-H_2ase sections 3 and 4. Readers unfamiliar with electrocatalysis and its figures of merit are referred to some useful introductions.[73,80,86,87]

2.3.2. Crystallography—Possessing only a single electron, H atoms are often challenging to locate by X-ray crystallography, as any bond they form automatically means a significant amount of electron density is in this bond rather than about the H nucleus. Furthermore, metal hydrides can be difficult to characterize in that Fourier truncation ripples surrounding heavy atoms can overwhelm smaller electron density peaks. These two effects result in H

atoms being difficult to locate and their M–H bond lengths typically being underestimated.[88] Despite these problems, laboratory X-ray analysis of high-quality small molecule metal hydride crystals routinely allows identification and refinement of H^- ligand positions. In contrast, synchrotron X-ray diffraction of protein crystals can only afford H atom positions under very favorable circumstances. The sample must diffract to <1 Å (high resolution by protein standards), and only then can careful modeling and refinement reveal hydrides and other H nuclei.[89,90] The resulting crystallographic models are best compared to those from neutron diffraction,[91,92] a technique that exploits the larger scattering cross section of D vs H, and is suitable to the study of macromolecules.[93] For example, one might characterize a H_2ase or its hydride-bearing model by X-ray diffraction and compare the metrics to neutron data of the relevant small molecule deuteride (crystals of suitable size for neutron diffraction are realistically more accessible for small molecules than for H_2ases). Such deuterides are typically simple to prepare owing to the H/D exchange properties of many metal hydrides.

2.3.3. Magnetic Resonance Spectroscopy—When considering metal hydrides in particular, certain spectroscopic methods are more informative than others. Among the most useful is nuclear magnetic resonance (NMR) spectroscopy, with spin–orbit coupling causing even diamagnetic Fe–^{1}H moieties to resonate over a wide range, although typically in the region upfield of $Si(CH_3)_4$ in which other ligand signals are rarely observed. The chemical shift, as will become clear, is not only dependent on spin–orbit interactions[94] and the electron-rich or -poor character of the metal(s) to which H^- is bound, but also on the terminal or bridging nature of its coordination. NMR has not been successfully applied to the [FeFe]- and [NiFe]-H_2ase enzymes themselves, even in cases where H^- is ligated at an $S = 0$ core. In cases where H^- is bound to open-shell metal centers ($S > 0$), electron paramagnetic resonance (EPR) spectroscopy, as well as its pulsed variants electron nuclear double resonance (ENDOR) and electron spin echo envelope modulation (ESEEM),[95] have proven extremely powerful. Indeed, the first direct evidence for a metal hydride in Nature was obtained by ENDOR spectroscopic measurement of a [NiFe]-H_2ase (vide infra).[96] Overall, the latter two techniques are particularly useful for resolution of anisotropic coupling between unpaired spins and ^{1}H nuclei diagnostic of H^- ligation.

2.3.4. Vibrational Spectroscopy—Vibrational spectroscopy provided early breakthroughs in H_2ase structure elucidation, particularly the identification of the CO and CN^- cofactors present at the active sites. These cofactors represent key spectroscopic handles because ν_{CO} and ν_{CN} bands appear in spectral regions devoid of protein bands. The number and intensities of ν_{CO} and ν_{CN} bands not only report on the number of such moieties but also the C–M–C angles between them. In turn, the vibrational frequencies report on metal electron density and the extent to which π-backbonding occurs. But what of M–H and M–H–M chromophores—how easily detected and assigned are their vibrations? Although their intensities are often rather low, ν_{MH} modes can be identified using infrared (IR) and Raman spectroscopies,[97] in the latter case taking due consideration of the photolability of many CO- and H^--containing complexes. Terminal hydride ν_{MH} bands often appear in IR spectral regions populated by ν_{CO} stretches (particularly those of bridging CO ligands).[98] Bridging hydrides give rise to weaker, lower energy vibrations best observed with resonance Raman, although vibrational mixing with other bands can

convolute matters. The challenges discussed here can partly be overcome by studying M–D and M–^{13}CO isotopologues, in which case the bands are shifted to lower energy ($\nu_{MH} \approx 2^{1/2}\nu_{MD}$ and $\nu_{12CO} \approx (91/87)^{1/2}\nu_{13CO}$, assuming uncoupled harmonic vibrations and $m_M \gg m_D$).[97] Nevertheless, unambiguous assignment of hydride bands is not always possible, and such data are unknown for many hydrides.

The difficulties in identifying metal hydride bands are well met by using a technique known as either nuclear resonance vibrational spectroscopy (NRVS) or nuclear inelastic scattering (NIS),[99–101] which now represents a valuable complement to the two more established vibrational methods. While Raman provides vibrational information following electronic excitation, NRVS does the same with nuclear excitation, requiring inelastic scattering of highly monochromatic (meV-resolved) synchrotron γ- or X-rays[102] by Mössbauer-active nuclides (e.g., ^{57}Fe, ^{61}Ni). The resulting spectra feature bands corresponding to only (and all) vibrations in which the metal nuclide moves. The unparalleled selectivity for probing the inner coordination sphere (even when surrounded by many kilodaltons of proteic mass) has already proven invaluable, as examples in this review will highlight. The intensities of NRVS bands are related to the displacement of the Mössbauer-active nuclide along the beam path. Many NRVS studies focus on low energy vibrations, such as bending and wagging modes, as they often involve large amplitude motion of metals and thus have relatively large NRVS intensities. The disadvantage in using these modes is that their coupled nature necessitates detailed density functional theory (DFT, vide infra) analyses for confident assignments. On the other hand, high energy vibrations, such as M–H/D stretches, see the metal move only very slightly, as the mass of M is large relative to that of H or D. Pure ν_{MH} modes are thus difficult—although not impossible—to observe.[103]

The inherently high frequency and low intensity of M–H/D modes leads to such NRVS measurements being far from routine, but this will inevitably change given the ever-increasing flux and resolution of synchrotron light sources. At the time of this review, NRVS-equipped facilities include beamlines at the Advanced Photon Source (Chicago, IL, USA), European Synchrotron Radiation Facility (Grenoble, France), and SPring-8 (Hyogo, Japan). Alternatively, seeded free-electron lasers can also provide the necessary monochromatic radiation, although such facilities are currently of limited accessibility and their applications to NRVS are yet to be well developed.[104]

When a complex exists for only a short time, its characterization calls for stopped-flow techniques and transient (time-resolved) spectroscopies. For example, the pulsed nature of free-electron lasers, while resulting in lower average fluxes, would enable NRVS measurements on the femtosecond scale. The most widespread transient methods use more traditional laser sources to obtain vibrational[105] and optical spectra.[106] These have been applied to H^+ transfer dynamics in H_2ases[107] as well as the detection of synthetic mixed-valent hydride species,[108] and are well complemented by computational investigations into such fleeting species. Described in section 2.4 are some of the theoretical approaches used to understand H_2ases and their models, as well as the information that is afforded by such work.

2.4. Theoretical Characterization of Hydrogenase Enzymes and Models

2.4.1. Approaches—The physical characterization of synthetic H_2ase models is typically much simpler than analogous studies on the proteins themselves. The same can be said for computational investigations, and thus while many synthetic species are amenable to in silico characterization, the enzyme structures are typically truncated to contain only the active site and perhaps the second coordination sphere for fully quantum mechanical calculations. Alternatively, mixed quantum mechanical/molecular mechanical (QM/MM) methods, in which only the active site is treated quantum mechanically while the remainder of the enzyme and solvent are treated with a MM force field,[109–113] have been used to study the larger H_2ase enzyme systems.[114–116] The computationally expensive nature of metallic cores, as well as the intractability associated with high levels of theory such as coupled cluster methods, have led to DFT[117,118] being widely used in the study of H_2ases and synthetic models.[119–121] As used with other molecular transition metal electrocatalysts,[122–124] popular functionals include B3LYP,[125,126] BP86,[127,128] B3P86,[126,127] PBE0,[129–131] TPSSh,[132] M06-L,[133] and ωB97XD.[134] These functionals are typically used with double- or triple-ζ basis sets, as well as polarization for specific atoms including moving H^+ or H^- groups,[135] and diffuse basis functions for anionic systems.[136] Additionally, effective core potentials and their corresponding basis sets, such as those of Hay and Wadt (LANL)[137] or Stuttgart–Dresden (SDD),[138] may be used for the transition metals to decrease computational cost.[139] The application of DFT to such complexes has been reviewed in detail.[140]

2.4.2. Predicting Observables—Molecular geometries of H_2ase models optimized using the above functionals have been shown to agree quite well with X-ray crystal structures. Geometries can be optimized either in the gas phase, subsequently including solvation free energies using a Born–Haber thermodynamic cycle, or in the solution phase directly.[141] Solvation effects are typically incorporated with a polarizable continuum model, in which the solvent is represented as a homogeneous dielectric. These models, such as PCM,[142–144] C-PCM,[145] SMD,[146] and COSMO,[147] are advantageous for treating solute–solvent interactions without requiring conformational sampling, although they do so by inherently neglecting specific solute–solvent interactions such as hydrogen bonding.

With optimized structures in hand, DFT calculations are invaluable for the prediction of further observables such as redox potentials and pK_a values. Accurate predictions of these parameters are necessary given their importance in the H^+ reduction reaction. The accuracy of calculated reduction potentials and pK_a values has been assessed for many molecular electrocatalysts and provides validation for the computational methods employed.[57,141] Several methods can be implemented to account for the reference electrode in the calculations to allow comparison with experimental measurements. One option is to subtract an experimental or theoretical value for the absolute reduction potential of the reference electrode.[148–152] An alternative is to subtract the value of the reduction potential of the reference electrode calculated using the same level of theory and basis set.[153–156] Yet another option is to calculate the reduction potential of a related half-cell reaction, which has been experimentally measured under similar experimental conditions and with respect to the same reference electrode.[52,57,141,157,158] Application of a thermodynamic cycle, also called

an isodesmic reaction, results in the reference electrode potentials canceling, as has been demonstrated for the calculation of quantitatively accurate redox potentials for synthetic H_2ase models.[159–161] This approach may also be applied to calculate pK_a values, although experimental pK_a measurements are not performed as often. One particular advantage of this approach is the cancellation of systematic errors associated with the level of theory and specified functional and basis set. Furthermore, application of a thermodynamic cycle also avoids the calculation of the free energies of H^+ and e^-, as well as the potential of the reference electrode. The application of this thermodynamic cycle is equivalent to the calculation of reduction potentials and pK_a's relative to related systems with experimentally measured values. Such an approach appears to be the most reliable at the current time.

Along with redox and acid–base behavior, spectroscopic observables are also available through DFT calculations. In particular, the diagnostic IR signatures of the CN^- and CO ligands are readily observed and can also be predicted by DFT calculations. However, since the harmonic approximation is often invoked to compute vibrational frequencies, calculated absolute frequencies are generally shifted systematically. For this reason, empirical scaling factors, dependent on the functional and basis set used, are often employed.[162,163] While the absolute vibrational frequencies calculated with DFT are often not quantitatively accurate, shifts in frequencies due to protonations and/or reductions are generally reliable. Nevertheless, absolute vibrational frequencies calculated using the BP86 functional tend to agree remarkably well with the experimental data without the use of scaling factors, which has been attributed to a fortuitous cancellation of errors.[164]

Although EPR spectroscopy is widely used to characterize paramagnetic states of the enzyme and models,[95] the accurate calculation of magnetic spectroscopic parameters is typically a challenging computational task. When calculated within the framework of DFT, the accuracy of parameters such as *g*-values, hyperfine couplings, zero-field splittings, and quadrupole couplings are very sensitive to the particular system being studied, especially the metal center(s). For example, while DFT calculated values are in good agreement with measurements for organic radicals and biradicals,[165–167] the calculated values for transition metal complexes typically deviate from those observed. In particular, *g*-shifts are notably underestimated by many functionals for transition metal complexes.[168,169] Hyperfine couplings for transition metal complexes present an additional challenge due to the significant contributions from spin–orbit coupling and spin polarization,[170] with the latter commonly underestimated by DFT.[171,172] However, predicted magnetic spectroscopic parameters are not always unreliable,[173] with calculated Mössbauer isomer shifts for ^{57}Fe being especially promising.[174–176] It has also been suggested that hybrid functionals, which contain a portion of Hartree–Fock exchange, tend to provide better agreement with experiment,[169,177] although at the risk of spin contamination.[178] Nonetheless, the application of these approaches to H_2ase models has seen successes over the years.[179–185]

The value of theoretical calculations is not limited to rationalizing experimental observations. The rapid nature of many H^+ and e^- transfers ensures that many species may evade conclusive identification even by transient spectroscopies. Indeed, calculations come to the fore when practical experimental solutions are not to be found. Computational studies are not only useful for the characterization of known H_2ase models, but also have guided the

design of new synthetic targets.[186–189] Experimental and theoretical studies in the field are thus driven by one another to a deeper understanding of H_2ases and their models. Our general discussion on characterization ends here, and we now present the state-of-the-art in the characterization and synthetic modeling of the [FeFe]-H_2ases (section 3), [NiFe]-H_2ases (section 4), and [Fe]-H_2ases (section 5).

3. [FeFe]-H_2ASES

3.1. Enzyme Structure and Function

Expressed in bacteria and lower eukaryotes,[190] the [FeFe]-H_2ases are arguably the fastest and most evolved of the H_2ases. While the [FeFe]-H_2ases vary in size (45–130 kDa), each features an active site ensemble known as the H-cluster. With six Fe centers in total, the H-cluster comprises a [4Fe–4S] metallocubane linked to an apical Cys-S$^-$ ligand in a [2Fe] moiety of formula $\{(Cys\text{-}S)(NC)(OC)Fe[(SCH_2)_2NH]Fe\text{-}(CO)_2(CN)\}^{2-/3-}$ (Figure 7).

Perhaps the more striking feature of the H-cluster structure is the [4Fe–4S] cluster, a common redox cofactor positioned in an uncommon location—covalently bound at the active site—that emphasizes the importance of e$^-$ transfer in catalysis. The Fe centers in the [2Fe] unit are labeled Fe^p ("proximal" to 4Fe–4S) and Fe^d ("distal" to 4Fe–4S), with the latter featuring a vacant site for substrate binding. The low-spin Fe^p and Fe^d centers are linked through S atoms of the azadithiolate (adt^{2-} = $^-SCH_2N\text{-}(H)CH_2S^-$) cofactor. While the 4Fe–4S unit and three or four "auxiliary" Fe–S clusters define an e$^-$ transport chain,[192] azadithiolate plays a key role in shuttling H$^+$ to or from the active site. Poised over the apical site of Fe^d, the secondary amine influences interconversion of Fe, Fe–H, and Fe(η^2-H_2) species by virtue of its acid–base properties. Beyond this, the amine further participates in N···H–S-Cys hydrogen-bonding interactions, beginning a pathway for H$^+$ transfer between the active site and the protein surface. The arrangement of the amine and Fe^d is constrained such that no bond can form between the two, with this Lewis base and acid constituting a FLP.[39] However, this system is unlike most synthetic FLPs in that the [2Fe] site is also redox-active, and is thus well-suited to perform electrocatalysis.

Completing the H-cluster are five "organometallic ligands" (3 × CO, 2 × CN$^-$), whose presence at the active site initially came as a surprise, although foreshadowed by the crystallographic analysis of [NiFe]-H_2ases. These chromophores absorb strongly in an uncluttered IR region,[191,193] serving as crucial reporters on the purity of protein samples, which is greatly decreased by any exposure of [FeFe]-H_2ases to O_2. The diatomic ligands are key spectroscopic handles, and while ν_{CN} modes are less sensitive to H-cluster redox (CN$^-$ is a weak π-acceptor), the ν_{CO} energies can vary over a 200 cm^{-1} range.[7] Consequently, IR analyses of [FeFe]-H_2ases are particularly informative, although interpretation can be complicated by the highly coupled nature of these modes.

After accounting for all the ligands, one can now consider the geometry of the [2Fe] unit. If the μ-CO ligand were *trans* to its current location, at a terminal Fe^d site, one might consider the [2Fe] unit as a pseudosymmetric union of two pyramidal Fe units, much like the vast majority of synthetic $[L_3Fe(SR)_2FeL_3]$ complexes (see section 3.2.1). But the presence of the CO bridge stabilizes an unsymmetrical "rotated" structure, wherein a coordination site

on the Fe^d *trans* to this π-acid is free for substrate binding. The "rotated" structure is further rigidified by a strong $Fe^dCN\cdots{}^+H_3N$-Lys358 interaction involving a conserved residue.[194] In addition to the structural role played by the CN^- ligands, cyanides also enhance the basicity and lower the redox potentials of the [2Fe] site and, along with the CO ligands, enforce low-spin configurations ideal for H_2 binding.[35]

On the other hand, *have* all the ligands been accounted for? Structural analyses suffer from a major complication: protein X-ray crystallography is typically unable to resolve the presence —much less the location—of hydrogenic substrates. Consequently, the protonation state of the amine is not clarified by crystallography. The presence of substrate at the Fe^d binding site is also an open question, and even if an Fe^d–H terminal hydride were a long-lived intermediate, the ligand would typically not be crystallographically locatable. Furthermore, Fe–H and Fe(η^2-H_2) moieties are very weak IR and Raman chromophores (see section 2.3.4), and are usually EPR-inactive, such that their identification based on hyperfine interactions is unlikely. Despite the lack of direct evidence for hydride ligation,[195] Fe^d–H intermediates are assumed to exist at least transiently in the catalytic cycle.[24,196] It is altogether conceivable that hydrides might not exist as stabile entities on a nearly flat potential energy landscape associated with an efficient catalytic cycle. While often slow,[197] the protonation and deprotonation of metal centers might be accelerated by proton-coupled electron transfer (PCET), which would exploit the juxtaposition of [4Fe–4S] and adt^{2-} cofactors to keep Fe^d hydride-free. Information on Fe–H species, albeit indirect, has been obtained by studying a mutated [FeFe]-H_2ase from *Chlamydomonas reinhardtii*. Such work builds on the hypothesis that Fe–H intermediates are destabilized by the PCET machinery. Indeed, introduction of Ser in place of Cys in the H^+ transfer pathway results in a significant drop in activity, and IR and EPR analyses of the reduced mutant indicated a new form with a H-cluster best described as $[4Fe–4S]^+$/Fe(II)Fe(II). Such an assignment is consistent with an Fe–H species, and the presence of the hydride is further indicated by the shift in the bridging CO band upon changing the solvent from H_2O to D_2O.[198]

Taking in the active site as a whole, the H-cluster is conformationally rigid, and its overall structure persists throughout the catalytic cycle. Despite this, there is some flexibility within certain components. First, substrate turnover necessitates interaction at the apical site on Fe^d, a metal that must switch between octahedral and square-pyramidal geometries. Second, to function as a H^+ relay, the secondary amine in the adt^{2-} cofactor is required to undergo rapid inversion (this aspect is illustrated in Appendix A.1, Figure 58). Lastly, the CO bridging Fe^p and Fe^d serves as a "shock absorber", with its linearity dependent on redox and the chemistry occurring at Fe^d. This reactive site is the location for H^-/H_2 binding, and its coordination to exogenous CO leads to deactivation of the enzyme. In contrast, H_2O does not poison the active site, consistent with a low-spin π-donor description for Fe^d.

Particularly important structure–function relationships have been elucidated by reconstitution of the semi-apoenzyme derived from algal H_2ases. The semi-apoenzyme, which contains the Fe_4S_4 cofactor but not the [2Fe] subunit, is readily reconstituted to a fully active enzyme upon treatment with the synthetic diiron complex $[NC(OC)_2Fe(adt)Fe(CO)_2CN]^{2-}$ ($[\mathbf{3}]^{2-}$, Figure 8). The reconstitution is accompanied by loss

of CO, attachment of the [4Fe–4S] cluster, repositioning of CN^- ligands to transoid, basal positions, and adoption of a "rotated" structure.[199,200]

The artificial maturations have also been performed using isostructurual, although subtly different, diiron dithiolates including $\{Fe_2[(SCH_2)_2–X](CN)_x(CO)_{6–x}\}^{–/2–}$, where X = CH_2, O, S, NMe and x = 1, 2.[201,202] While these abiological analogues are readily accepted by the protein, catalytic activity assays indicated that the $adt^{2–}$ cofactor is crucial for H^+ transfer, and the only semisynthetic [FeFe]-H_2ase that exhibits significant activity is that obtained by reconstitution with $[(OC)_3Fe(adt)\text{-}Fe(CO)_2CN]^-$. With the functional importance of each H-cluster component now clear, our discussion moves to the various enzyme states and their roles in the catalytic cycle.

The understanding of enzyme mechanisms rests on the identification of characterized states,[203] which number three in the case of [FeFe]-H_2ase. Several crystallographic and spectroscopic studies confirm that the structure of the H-cluster is virtually invariant in all redox forms. In considering the proposed catalytic cycle (Figure 9), focus is consequently placed on the oxidation and protonation states of the Fe centers and $adt^{2–}$ cofactor. Spectroscopic parameters for the three known [FeFe]-H_2ase states are presented in Table 1, and the properties of each are now individually discussed.

The most common state for biophysical studies is H_{ox}, so denoted as it is "oxidized", although not oxygenated (an important distinction for such O_2-sensitive organometallic enzymes). Early Mössbauer studies on H_{ox} indicated strong coupling between the proximal $[4Fe–4S]^{2+}$ cofactor and the [2Fe] center, with the latter initially described as a low-spin (S = 1/2) Fe(II)Fe(III) tandem.[204] Yet, the inadequacy of Mössbauer spectroscopy in distinguishing oxidation states of low-spin Fe led some astray, particularly when low oxidation states such as Fe(I) ("subferrous") were not considered to be biologically relevant.

A suite of advanced EPR techniques has greatly informed the current picture of H_{ox}. While its EPR signals at g = 2.10, 2.04, and 2.00 shift slightly depending on the organism, these invariably are consistent with an Fe(II)Fe(I) description for the [2Fe] core. Although biophysical reports indicate Fe^p to be monovalent, analyses of synthetic models consistently point to the reverse assignment, supported on general grounds by considering the favorability of a +I oxidation state for pentacoordinate sites such as Fe^d in H_{ox}. In any case, the electronic coupling of the $[4Fe–4S]^{2+}$ cofactor and [2Fe] core allows mixing of excited states and enhanced hyperfine coupling (isotropic $A(^{57}Fe)$ ≈11–12 MHz for each moiety). The value of paramagnetic centers as spectroscopic handles also comes to the fore in the identification of ^{14}N hyperfine, which represented the first evidence for the identity of the $adt^{2–}$ cofactor.[205]

Poised to bind H_2, the H_{ox} state also strongly binds CO at the apical Fe^d site adjacent to the secondary amine.[206] The binding of ^{13}CO is stereospecific,[207] which adds weight to our picture of the relatively rigid active site. When exogenous CO is taken up by H_{ox}, its spin becomes more delocalized across the H-cluster, although EPR analysis indicates that the cubane remains in a $[4Fe–4S]^{2+}$ state. An Fe(1.5)Fe(1.5) description for [2Fe] is thus logical, given that both Fe^p and Fe^d are now octahedrally coordinated with similar ligand

sets. The deactivated, CO-bound state features strong coupling between the [4Fe–4S] and [2Fe] units, which is significant mechanistically in that binding of H_2 (and especially of H^-) might also enhance interaction between these two subsites and thus be involved in PCET.[208]

When [FeFe]-H_2ase exists at potentials more negative than −395 mV, it is not H_{ox}, but rather its product H_{red}, that predominates. The latter state is EPR-silent and is thought to feature a $[4Fe–4S]^{2+}$ cluster (also EPR-silent) and an $S = 0$ [2Fe] site. It was formerly assumed that H_{red} features a H^- ligand as part of an Fe(II)Fe(II), H^- core. However, X-ray spectroscopy does not support the presence of an Fe–H moiety in H_{red}, which is instead considered to be an isoelectronic Fe(I)Fe(I) form. This description is consistent with IR data indicating that the H_{red} core is more electron-rich than that of H_{ox}, with the terminal ν_{CO} bands undergoing, on average, a bathochromic shift of 25 cm^{-1} on forming H_{red}. The two states also differ in the geometry of the semibridging CO ligand. In H_{ox}, the CO bridges to Fe^p, with the Fe^d–C–O unit being highly bent,[209] perhaps in order to enable some spin delocalization. In the diamagnetic H_{red} state, the Fe^d–C–O is almost linear.

A third active state has been uncovered through studies on an [FeFe]-H_2ase that, unlike most such proteins, lacks Fe–S clusters outside of the H-cluster. This recently identified H_{sred} (“super reduced”) form in *Chlamydomonas reinhardtii* is observed at or below −540 mV, about 150 mV more negative than the $H_{ox/red}$ couple. Both the $[4Fe–4S]^+$ cubane and the Fe(I)Fe(I) [2Fe] site adopt their lowest oxidation states, a situation that would not be long-lived were auxiliary Fe–S clusters present to accept electrons. Nevertheless, H_{sred} is assumed to be a transient intermediate in all [FeFe]-H_2ases. Its IR spectrum features ν_{CO} bands more similar to H_{ox} than H_{red}, but one ν_{CN} band shifts by 45 cm^{-1} to lower energy, perhaps indicating a structural change as such stretches are insensitive to metal electron density.[210] Described now are current proposals regarding the enzyme catalytic cycle and mechanism, subjects that are still topics of debate.

In considering the stoichiometry of the catalytic cycle, one notes that the two redox equivalents demanded by the $H_2/2H^+$ couple cannot be provided by the $H_{ox/red}$ couple alone, a problem conveniently addressed by invoking H_{sred}, which is $2e^-$ more reduced than H_{ox} (Figure 9). Consistent with present biophysical information, it is suggested that oxidation of H_2 involves its binding at the Fe^d site in H_{ox} to give H_{ox} (H_2).[203] The Fe(η^2-H_2) fragment in the latter species is deprotonated by the amine of the adt^{2-} cofactor, resulting in the ammonium hydride heterolysis product $H_{ox}(H^+, H^-)$. A PCET step is now proposed, in which deprotonation is associated with e^- transfer from [2Fe] to the $[4Fe–4S]^{2+}$ cluster. The resulting $[4Fe–4S]^+$,Fe(II)Fe(II),H^- species may tautomerize to H_{sred}, whose rapid oxidation (e^- transfer) affords H_{red} and then H_{ox}, thereby completing the cycle. The reverse processes apply to H^+ reduction, which involves H^+ transfer from adt^{2-} to a reduced Fe^d center in concert with e^- transfer from $[4Fe–4S]^+$ to give the same intermediate invoked for H_2 oxidation.

The catalytic mechanism can be further appreciated from the perspective of e^- counting. Summing 3d electrons and electron pairs for each Fe–ligand bond in the [2Fe] subsite, one notes that H_{ox} is a $33e^-$ dimer, and H_{red} is a $34e^-$ dimer (Figure 9), with $34e^-$ being consistent with a bimetallic complex featuring a metal–metal bond. In order to maintain this

electron count, binding of exogenous CO to Fe^d in H_{red} is accompanied by dissociation of the Cys-S–Fe^p bond.[211] If the [2Fe] site carried a H^- ligand, as seems likely in at least a transient form, the 18e$^-$ rule is still obeyed, since the H^- complex would remain 34e$^-$ regardless of its description as Fe(II)Fe(II),H^- or Fe(I)Fe(I),H^+. To reiterate, as the H_{ox}/H_{red} couple differs by only one electron, it is clear that [4Fe–4S] must supply the extra electron or hole required for the $H_2 \rightleftharpoons 2H^+ + 2e^-$ reaction.

While characterization data for each catalytic intermediate are not available, what we do know is that the [FeFe]-H_2ases are some of the fastest enzymes.[14] Rates vary by 2 orders of magnitude for H_2 evolution but only by a factor of 2 or 3 for H_2 oxidation. Compared to the rates for H_2 evolution, H_2 oxidation is always faster, sometimes by as much as 3 orders of magnitude.[212] Perhaps the best characterized in terms of structure and rates is the H_2ase I (note: organisms often have two or more different H_2ases) from *Clostridium pasteurianum*. In this case, the turnover frequencies (TOFs) at 30 °C for H_2 oxidation and evolution are 25 000 and 5700 s^{-1}, respectively.[212]

The remarkably high catalytic rates of [FeFe]-H_2ases are competitive with those exhibited by Pt metal.[213] Yet, as stated in the Introduction, one motivation for the study of [FeFe]-H_2ases is the preparation of base metal catalysts with the hope that reproducing the native structure will afford the native function. While long-lived hydrides are unlikely to be involved in the [FeFe]-H_2ase mechanism, it is assumed that complexes of the form Fe(II/I)Fe(II),H^- do have a transient presence (Figure 9). Presented in section 3.2 are synthetic hydrides relevant to the FeFe active site. The high fidelity hydride models are typically terminal, but, for historical purposes, some bridging species will be described in discussion of early work. Moreover, catalytically important bridging hydrides will also be considered.

3.2. [FeFe]-H_2ase Synthetic Modeling

3.2.1. Early Diiron Dithiolates and Their Hydrido Complexes—

The crystallographic analysis of [FeFe]-H_2ase attracted particular interest from organometallic chemists, for whom the active site immediately brought to mind “classic” diiron dithiolates that predated the determination of the enzyme structure by 70 years.[214] Renewed attention was paid to Fe(I)Fe(I) carbonyls such as $[(OC)_3Fe(SEt)_2Fe(CO)_3]^{23}$ and, later, $[(OC)_3Fe(pdt)Fe(CO)_3]$ ([**4**], pdt^{2-} = 1,3-propanedithiolate; Figure 10),[215] owing to the presence of Fe, RS^-, and CO in these complexes as well as the diiron (and, in fact, all) H_2ase active sites.

There exists an uncanny and promising resemblance between [FeFe]-H_2ase active sites and the archetypal synthetic low-valent hexacarbonyls, with their 34e$^-$, stable Fe–Fe bonded motif.[216] Yet, in reality the latter are *too* stable, to the point that their oxidations are strongly anodic (e.g., $E_{1/2}([\mathbf{4}]^{+/0}) = 0.65$ V vs $Fc^{+/0}$)[217] and their Brønsted basicities are low. As discussed above, a requirement of the [FeFe]- and [NiFe]-H_2ases is their participation in both acid–base and redox at mild pH and potentials. Although [**4**] is inert to $HBF_4{\cdot}Et_2O$, it is protonated by HOTf (trifluoromethanesulfonic acid) such that lower and upper bounds for the acidity of $[\mathbf{4}(\mu\text{-H})]^+$ in C_6D_5F are known: $-9 < pK_a([4(\mu\text{-H})]^+) < 0$.[44] However, protonation with HOTf does not proceed smoothly, and isolation of an Fe(II)(μ-H)Fe(II) derivative of [**4**] was found to necessitate action of the superacid generated from

$[SiEt_3]B(C_6F_5)_4$ and HCl.[218] In the preparation of $[\mathbf{4}(\mu\text{-H})]^+$ from [**4**], while the 2e⁻ Fe–Fe bond in the latter formally reduces H^+ to afford a H^- ligand, the internuclear separation in the resulting hydride is still typically comparable to twice the covalent radius[219] of low-spin Fe (2 × 1.32 Å = 2.64 Å). Thus, although the $3d^6$ Fe(II) sites are not expected to interact strongly with each other, a dashed bond between metals is nevertheless an oft-adopted notation. While not used in this review, a more rigorous notation exists for the representation of Fe(μ-H)Fe systems and three-center two-electron bonds in general.[220] This convention avoids depicting direct Fe–Fe bonds (Figure 10, bottom), and employs the typical arrows for L-type (charge-neutral, 2e⁻) donors, and a half-arrow for the bridging hydride. Such a method is useful when counting electrons, with the half-arrow making clear that Fe(μ-H)Fe units involve three-center two-electron rather than three-center four-electron bonds, as the simple line drawing might imply.

The acid–base and redox reactivity of the diiron(I) dithiolato hexacarbonyls is greatly enhanced upon replacement of π-acidic CO ligands with stronger donors—a strategy that has proven very generalizable. For example, the installation of one or two CN^- ligands occurs under mild conditions to afford, in the latter case, a complex bearing all the diatomic ligands present in the [FeFe]-H_2ase active site.[221] While acids only protonate the N atom in $[(OC)_3Fe(pdt)Fe(CO)_2CN]^-$ (the Fe–Fe bond being insufficiently basic), the dicyanide $[\mathbf{3}]^{2-}$ protonates to give hydrides.[222–224] In situ analysis revealed an N-protonated intermediate prior to the formation of $[NC(OC)_2Fe(pdt)(\mu\text{-H})Fe(CO)_2CN]^-$ ($[\mathbf{3}(\mu\text{-H})]^-$).

The asymmetric derivative $[Me_3P(OC)_2Fe(pdt)Fe\text{-}(CO)_2CN]^-$($[\mathbf{5}]^-$) could be converted to its stable conjugate acid $[Me_3P(OC)_2Fe(pdt)(\mu\text{-H})Fe(CO)_2CN]$ ([**5**(μ-H)], Figure 11),[23] which exhibits a ^{1}H NMR resonance at −17 ppm typical of a μ-H^- ligand. The charge-neutral hydride [**5**(μ-H)] undergoes electrochemical reduction at −1.57 V vs $Fc^{+/0}$, the pseudoreversibility of which indicates that a mixed-valent complex is accessible (vide infra). Further protonation of [**5**(μ-H)] affords $[Me_3P(CO)_2Fe(pdt)(\mu\text{-H})Fe(CO)_2(CNH)]^+$ ($[\mathbf{5}(\mu\text{-H})H]^+$), whose irreversible reduction at E_{pc} = −1.47 V is accompanied by H_2 evolution. In what is a common indirect indicator of catalytic activity, the reductive current increases upon titration with strong acids, including HCl, H_2SO_4, and toluenesulfonic acid (HOTs), with a TOF of 0.0067 s^{-1} at −1.2 V vs Ag/AgCl in the latter case.[225] While modest, the activity of species such as [**5**(μ-H)] contrasts the inactivity of the related bis(phosphine) hydride $[Me_3P(CO)_2Fe(SMe)_2(\mu\text{-H})Fe\text{-}(CO)_2PMe_3]^+$ ($\delta(^1H)$ −15.6 ppm),[226] which lacks an effective H^+ relay. This role is apparently well-served by CN^-, despite its arrangement perhaps not being ideal for H^+ transfer to the metal sites. Overall, these findings highlight an important design feature for functional [FeFe]-H_2ase (and [NiFe]-H_2ase) models: the basic/oxidizable metal(s) must be proximal to a basic moiety.

The ambidentate nature of CN^- was recognized as a complicating factor that saw it largely replaced in models by simpler ligands of (ideally) comparable σ-donicity. While donors such as carbenes,[227–231] isonitriles,[232–235] and even nitrosyls[236,237] have been used, tertiary phosphines have proven the most useful.[23]

3.2.2. Mixed-Valent Hydrides—The 34e⁻ Fe(II)(μ-H)Fe-(II) species discussed above represent models for a putative [FeFe]-H_2ase form tautomeric to the H_{sred} state, an

unobserved species which likely bears a terminal hydride (Figure 9, bottom right). The catalytic cycle for H_2 evolution necessitates the reduction of diferrous hydrides to mixed-valent derivatives, both for synthetic catalysts and in the native catalytic cycle (the state H_{ox} (H^+, H^-)). While there is reason to believe that synthetic versions of these hydrides may be unstable (e.g., toward bimolecular decomposition and H_2 evolution), the pseudoreversibility of Fe(II)(μ-H)Fe(II/I) couples in certain complexes suggested that a mixed-valent species might be persistent. Such odd-electron dinuclear species are often classified according to the system of Robin and Day.[238,239] A Robin–Day class I complex features structural asymmetry associated with localization of the singly occupied orbital on one site. A class III complex features structurally indistinguishable metal sites, each with a "genuinely nonintegral valence".[240] Between these two extremes lie the class II complexes, whose metal sites are distinguishable, but not very different.

At this point it is important to acknowledge a large, but quite distinct body of work concerning hydrogen evolution reaction (HER) electrocatalysis mediated by hexacarbonyls [$(OC)_3$Fe-(dithiolate)Fe$(CO)_3$] and pentacarbonyls [$(OC)_3$Fe-(dithiolate)Fe$(CO)_2$L]. Such ligand sets, in contrast to that of the CN^--containing active site and models, result in higher oxidation potentials but make accessible very reduced (but abiological) states such as Fe(0)Fe(I),[241] particularly when electron-poor ligands, such as 3,6-dichloro-1,2-benzenedithiolate,[242] are used. The protonation of these (often monoanionic) Fe(0)Fe(I) complexes would afford mixed-valent Fe(II)Fe(I)/Fe(1.5)Fe(1.5) hydrides, species that have been invoked during the HER as mediated by the [FeFe]-H_2ases. However, the necessary formation of Fe(0)Fe(I) species leads to hexa- and pentacarbonyls displaying high overpotentials,[67] and these parent compounds can be considered to have less fidelity to [FeFe]-H_2ases than their more substituted analogues, with which this subsection is now concerned.

An early study on mixed-valent diiron hydrides reported the reduction of [$Me_3P(OC)_2$Fe(pdt)(μ-H)Fe$(CO)_2PMe_3]^+$ ([**6**(μ-H)]$^+$) with acenaphthylene anion radical to generate the neutral complex [$Me_3P(OC)_2$Fe(pdt)(μ-H)Fe$(CO)_2PMe_3$] ([**6**(μ-H)], Figure 12).[108] The product features an EPR resonance at $g = 2.0066$ (near that of the free electron $g_e = 2.0023$) split by ^{1}H ($A_{iso} = -41.7$ MHz) and two equivalent ^{31}P nuclei ($A_{iso} = -75.8$ MHz). A Robin–Day class III delocalized Fe(1.5)(μ-H)Fe(1.5) description for the complex was supported by DFT studies, which suggested that 70% of the unpaired spin density resides on the two Fe centers, with approximately 35% on each site.[108]

The radical hydride [**6**(μ-H)] is rather labile, as evidenced by its poorly reversible oxidation and an estimated $t_{1/2}$ ~ 1 s at 25°C. Relatives of the present system include Fe(edt)(μ-H)Fe (edt^{2-} = 1,2-ethanedithiolate),[108] Fe(bdt)(μ-H)Fe (bdt^{2-} = 1,2-benzenedithiolato),[243] and Fe$(SH)_2$(μ-H)Fe derivaties,[244] all of which are similarly fragile. However, protonation of [dppv-(OC)Fe(pdt)Fe(CO)dppv] ([**7**], dppv =1,2-bis-(diphenylphosphino)ethene) affords a more sterically encumbered diferrous hydride [dppv(OC)Fe(pdt)(μ-H)Fe(CO)-dppv]$^+$ ([**7**(μ-H)]$^+$, Figure 13), which sustains reduction to afford the isolable neutral hydride [dppv(OC)Fe(pdt)(μ-H)Fe(CO)dppv] ([**7**(μ-H)]).[245] X-ray crystallography revealed the product to feature an asymmetric Fe(II)(μ-H)Fe(I) core. The structural and EPR data are consistent with DFT calculations indicating that the Fe(I), which bears two-thirds of the spin

density, is more distant from the hydride than is Fe(II) (1.82 vs 1.61 Å), on which most of the remaining spin resides. In solution, a small fraction of this asymmetric Robin–Day class II species converts to a C_2-symmetric complex with the expected Fe(1.5)(μ-H)Fe(1.5) class III description. The latter product features dppv ligands with so-called "apical–basal" stereochemistry, in which they each bind an apical site that is *trans* to μ-H, as well as a basal site *trans* to pdt^{2-}.

Treatment of mixed-valent bis(dppv) hydride [**7**(μ-H)] with D^+ yields the diferrous hydride and 1/2D_2 rather than [dppv(OC)Fe(pdt)Fe(CO)dppv]$^+$ ([**7**]$^+$) and HD. This surprising observation implicates a spectator role for μ-H^- in this complex during HER, probably reflecting the influence of the two bulky diphosphines and the robustness of Fe(II)(μ-H)Fe(II) motifs in general.

The relatively high-valent paramagnetic hydride [(Cp*)Fe-(bdt)(μ-H)Fe(Cp*)] (Cp^{*-} = pentamethylcyclopentadienide) is generated by reduction of the unusual diferric species [(Cp*)Fe(bdt)(μ-H)Fe(Cp*)]$^+$ ($E_{1/2}$ = −0.91 V vs $Fc^{+/0}$). Protonation of the Fe(II)(μ-H)Fe(III) complex returns the Fe(III)(μ-H)Fe(III) complex and induces evolution of H_2 (0.5 equiv).[246] These bridging hydride ligands, even on reduced diiron cores, can often be so inert they resist protonation even with strong acids. Indeed, the HER reactions described here can be considered to proceed by an outer-sphere mechanism, throughout which the coordination sphere of the catalyst is unchanged. If instead HER occurs with protons contacting the metal site(s), then it corresponds to an inner sphere mechanism, involving the intermediacy of a mixed-valent dihydride complex. Diiron dihydrides are described in section 3.2.3.

3.2.3. Dihydrides—The privileged bis(dppv) motif is well-suited to stabilizing many Fe oxidation and protonation states, among which are FeFe complexes in which two hydride ligands are present. Displacement of CO from [**7**(μ-H)]$^+$ in MeCN affords the activated species [dppv(OC)Fe(pdt)(μ-H)Fe-(MeCN)dppv]$^+$ ([**8**(μ-H)(MeCN)]$^+$), and subsequent treatment with BH_4^- cleanly gives [dppv(OC)Fe(pdt)(μ-H)Fe(*t*-H)dppv] ([**8**(μ-H)(*t*-H)], Figure 14).[247] The displacement of a labile MeCN ligand by a hydride source was inspired by the related synthesis of [$(Me_3P)_2$(CO)Fe(edt)Fe(CO)$(PMe_3)_2$(*t*-H)]$^+$ discussed below. The product features not only a bridging hydride but also a terminal hydride (denoted *t*-H^-); these cis ligands give rise to ^{1}H NMR resonances at δ −18.9 and −12.2 ppm, respectively (intramolecular exchange rate ≈1 s^{-1} at −25°C).

While sequential addition of H^+ and H^- to an Fe(I)Fe(I) precursor represents one route to dihydrides, perhaps a more obvious (and generally applied) method is oxidative addition of H_2. In the case of [dppv(OC)Fe(edt)Fe$(CO)_3$] ([**9**], Figure 15), photolytic decarbonylation affords a transient 32e$^-$ species that binds and cleaves H_2 to afford [dppv(OC)Fe(edt)(μ-H)Fe(*t*-H)$(CO)_2$] ([**10**(μ-H)(*t*-H)], δ −12.8 (*t*-H), −14.9 ppm (μ-H)).[248] DFT calculations indicate a product of C_s symmetry, with the trans nature of the hydride ligands contrasting the *cis* arrangement in [**8**(μ-H)(*t*-H)].[248]

A closely related process of CO dissociation and H_2 activation occurs for diruthenium analogues. For example, irradiation of [$Cy_3P(OC)_2$Ru(pdt)Ru$(CO)_2PCy_3$] under an H_2

atmosphere affords the *trans* dihydride $[Cy_3P(OC)_2Ru(pdt)(\mu\text{-}H)Ru(t\text{-}H)(CO)PCy_3]$,[249] which yields $[Cy_3P(CO)_2Ru(pdt)(\mu\text{-}H)Ru\text{-}(\eta^2\text{-}H_2)(CO)PCy_3]^+$ on treatment with $[H(OEt_2)_2]BAr^F{}_4$ in CH_2Cl_2. When $[D(OEt_2)_2]BAr^F{}_4$ is instead used, D incorporation is only observed as η^2-HD and not as a D^- ligand, a result that highlights the inherent stability of μ-H^- over t-H^- ligands.

The discussion on synthetic models has, until now, focused on bridging hydride complexes. Yet, both [**8**(μ-H)(t-H)] and [**10**(μ-H)(t-H)] feature t-H^- ligands that are a key motif in the [FeFe]-H_2ase mechanism. The preparation of terminal hydride complexes has been the subject of intense research activity, much of which is summarized in section 3.2.4.

3.2.4. Terminal Hydrides—In considering the structure of dihydride [**8**(μ-H)(t-H)], one might say that the presence of the strongly donating μ-H^- ligand directs the second H^- to adopt the important terminal position. But what of the situation when only a single H^- ligand is present? Can a terminal *mono*hydride, similar to that proposed in the enzyme mechanism, be observed in a model complex?

The large number of bridging hydrides reported is in part due to such species typically being thermodynamic products of $[L_3Fe(dithiolate)FeL_3]$ protonation. Yet it just so happens that terminal hydrides, of varying kinetic stability, feature commonly (but not always)[250] as intermediates in this reaction. Their presence was initially inferred from electrochemical studies on the HER activity of the related diphosphide $[(OC)_3Fe(\mu\text{-}PPh_2)_2Fe(CO)_3]$.[251] The first direct observation of terminal hydrides arising from protonation was found by studying the action of $HBF_4{\cdot}Et_2O$ on $[OC(dppe)Fe(pdt)Fe(CO)_3]$.[252] At 298 K in CH_2Cl_2 solution, the sole product was bridging hydride $[(dppe)(CO)Fe(pdt)(\mu\text{-}H)Fe(CO)_3]^+$, in which a dibasal phosphine (i.e., C_s symmetry) was indicated by a characteristic high-field ^1H NMR triplet at −14.1 ppm ($^2J_{PH}$ = 21 Hz). When protonation was instead monitored at 203 K, a singlet at −4.33 ppm could be observed, such a shift being significantly downfield of resonances expected for bridging hydrides. The lack of coupling to any ^{31}P nuclei indicated that initial protonation, perhaps counterintuitively, occurred at the relatively electron-poor $Fe(CO)_3$ fragment to afford $[(dppe)(OC)Fe(pdt)Fe\text{-}(CO)_3(t\text{-}H)]^+$. This terminal hydride, upon warming to 243 K, converts to a mixture of apical–basal and dibasal forms of the bridging hydride, with the latter being the only FeFe species at 298 K. As many further examples will demonstrate, low-temperature protonation studies of this type are a powerful tool in studying the formation of terminal hydrides for a variety of FeFe systems.

Despite efforts in monitoring protonations of Fe(I)Fe(I) species, the first diiron terminal hydride complex to be fully characterized arose from a rather different route involving hydride transfer to an Fe(II)Fe(II) precursor. Treatment of $[(Me_3P)_2(CO)Fe(edt)Fe(CO)(PMe_3)_2MeCN]^{2+}$ ($[\mathbf{11}(MeCN)]^{2+}$) with either AlH_4^- or BH_4^- at −25°C induced the formation of $[(Me_3P)_2(CO)Fe(edt)Fe(CO)(PMe_3)_2(t\text{-}H)]^+$ ($[\mathbf{11}(t\text{-}H)]^+$) by displacement of MeCN (Figure 16). Isolated as a strikingly green species,[253] $[\mathbf{11}(t\text{-}H)]^+$ exhibits a ^1H NMR resonance at −4.6 ppm coupled to just two ^{31}P nuclei. The product features an IR-active ν_{FeH} band at 1844 cm^{-1}, consistent with the terminal nature of the hydride ligand. While M–H vibrations are often not easily assigned,[254] the frequency is comparable to that

calculated using DFT (1908 cm^{-1}), with two lower frequency bands (1352 and 1151 cm^{-1}) predicted for the analogous bridging isomer.[253]

Although terminal hydride [**11**(*t*-H)]$^+$ could be crystallized (r_{FeFe} = 2.565 Å, r_{FeFe}= = 1.498 Å), it is of limited thermal stability; in solution at room temperature it isomerizes to the red, C_2-symmetric bridging hydride ([**11**(μ-H)]$^+$ (−20.6 ppm, r_{FeFe} = 2.610 Å, rFeFe= = 1.656, 1.602 Å) by a first-order process (k = 2 × 10^{-4} s^{-1} at 294 K). Both *t*-H and μ-H isomers are unreactive toward H_2O, but the terminal form does liberate H_2 upon treatment with the strong acids HOTf or [$H(OEt_2)_2$]$BAr^F{}_4$ in the presence of MeCN to give back [**11**(MeCN)]$^{2+}$.[255] This finding highlights the considerably more hydridic nature of *t*-H^- ligands.[249] Such work further emphasizes the need to suppress the isomerization of terminal to bridging species. This process is typically irreversible, although theoretical work has suggested that excitation of Fe(pdt)(μ-H)Fe species to a low-lying triplet state can afford the terminal isomer.[256]

The *t*-H → μ-H isomerization has been examined using DFT calculations on [(dppv)(CO)Fe(edt)Fe$(CO)_3$(*t*-H)]$^+$ ([**12**(*t*-H)]$^+$), [(dppv)(CO)Fe(edt)Fe$(PMe_3)(CO)_2$(*t*-H)]$^+$, and [$(Me_3P)_2$(CO)Fe(edt)Fe$(PMe_3)_2$CO(*t*-H)]$^+$ ([**11**(*t*-H)]$^+$). These isomerizations may conceivably occur through Bailar (trigonal) or Ray–Dutt (rhombic) twists, with the pathway dependent on the ligand set.[257] For these complexes, the free energy barriers to Ray–Dutt twisting are lower by 4.4–7.7 kcal/mol. When bulky ligands are present, certain isomerizations are unlikely to occur by Ray–Dutt twists since these would involve high-energy intermediates such as bridging phosphine complexes (Figure 17). Such motifs need not be invoked if isomerization proceeds through Bailar twists. For example, [**12**(*t*-H)]$^+$ was predicted to convert to its bridging tautomer through a multistep pathway involving only Ray–Dutt twists, while [**11**(*t*-H)]$^+$ was calculated to isomerize by both Ray–Dutt and Bailar twists.

Since the first preparation of a diiron terminal hydride, several more such complexes of varying stability have been prepared. Their syntheses typically follow a biomimetic route involving (low-temperature) protonation of Fe(I)Fe(I) species. In the case of the bis(dppv) complex [dppv(OC)Fe(pdt)Fe(CO)dppv] ([7]) protonation with strong acids such as HBF_4·Et_2O (weak acids will not suffice) at −25 °C affords the terminal hydride [dppv(OC)Fe(pdt)Fe(CO)(*t*-H)dppv]$^+$ ([7(*t*-H)]$^+$, $\delta(^1H)$ −3.5 ppm) as an isolable kinetic product. Solutions of this species are stable for minutes at 0 °C,[258] an effect of the bulky, strongly electron-donating ligands that hinder isomerization.[259] At room temperature, the hydride converts to asymmetric and symmetric isomers of the bridging species [dppv(OC)Fe(pdt)-(μ-H)Fe(CO)dppv]$^+$ ([7(μ-H)]$^+$, $\delta(^1H)$ −14.5 and −15.6 ppm, respectively) described above. While stereodynamics and HER mechanisms are discussed in section 3.2.6, both the *t*- and μ-H propanedithiolates catalyze the HER, although with modest TOFs of 5 and 3 s^{-1}, respectively.

Protonation at a terminal site in preference to the Fe–Fe bond is puzzling[260] because most synthetic Fe(I)Fe(I) species do not have an empty apical coordination site. Due consideration must also be paid to the thiolate S atoms, whose nonbonding electron pairs allow for thiol intermediates in the protonation reaction. The S atoms in synthetic [FeFe]-

H_2ase models have indeed been shown to be competent Brønsted bases. For example, protonation of $[(OC)_2(Me_3P)Fe(edt)(\mu\text{-}H)Fe(CO)_2(PMe_3)]$ affords, according to IR spectroscopy, the expected hydride $[(OC)_2(Me_3P)Fe(edt)(\mu\text{-}H)Fe(CO)_2(PMe_3)]^+$, as well as the thiol $[(OC)_2(Me_3P)Fe(Hedt)Fe(CO)_2(PMe_3)]^+$.[261] Similarly, treatment of $[(OC)_3Fe(3,4\text{-dichlorobenzene-1,2-dithiolate})Fe\text{-(dppp)CO}]$ with $HBF_4{\cdot}OEt_2$ (1 equiv) results in the protonation of one S atom.[262] The involvement of heteroatom-protonated species can greatly influence the regiochemistry of hydride formation because heteroatom proton relays are known to play key roles in reducing barriers in what would otherwise be intermolecular protonations of metal sites. Indeed, heteroatom bases of comparable thermodynamic basicity to low-valent metal centers have much greater kinetic basicities.[263] These effects are borne out in the contrasting protonations of dithiolate $[dppv(OC)Fe(pdt)Fe(CO)_3]$[264] ([**13**], Figure 18) and a related diphosphide $[dppv(OC)Fe(pdpp)Fe(CO)_3]$ ([**14**], $pdpp^{2-}$ = 1,3-propanedi(phenylphosphide)).[265] Treatment of [**13**] with $[H(OEt_2)_2]BAr^F{}_4$ at −90 °C rapidly affords $[dppv(OC)Fe\text{-(pdt)}Fe(t\text{-}H)(CO)_3]^+$ ([**13**(t-H)]$^+$), which undergoes slow isomerization to the bridging hydride [**13**(μ-H)]$^+$. Under identical conditions, the diphosphide transforms slowly and exclusively to the bridging species $[dppv(OC)Fe(pdpp)(\mu\text{-}H)Fe(CO)_3]^+$ ([**14**(μ-H)]$^+$) with no intermediates observed. With lone electron pairs available on ligated pdt^{2-} but not $pdpp^{2-}$, it is apparent that heteroatom participation not only accelerates metal protonation, but also directs it to terminal sites.

Assuming the dppv(CO)Fe^I fragment is more basic than $Fe^I(CO)_3$, it may seem strange that the t-H^- ligands in complexes such as [**12**(t-H)]$^+$ are located at the tricarbonyl sites. This stereochemistry is rationalized in terms of the steric bulk of the diphosphine, as well as by considering a "rotated" form of the neutral complex in which a bridging CO ligand is *trans* to a vacant terminal Fe site (Figure 19). In the extreme case, one CO ligand moves to a bridging position to afford $[dppv(CO)Fe(edt)(\mu\text{-}CO)Fe(CO)_2]$. This isomer may be considered a $2e^-$ mixed-valent species in which the pseudooctahedral site is Fe(II), with the square-pyramidal basic site being Fe(0). According to DFT calculations, the two isomers of this "rotated" species are both transition states, of which an asymmetric form, in which dppv occupies an apical and basal site (apical–basal), is only slightly more stable.[265]

The role of S atoms in hydride formation was also implicated in the protonation and isomerization of the electron-rich tetraphosphine $[(Me_3P)_2(OC)Fe(pdt)Fe(CO)(PMe_3)_2]$ ([**15**], Figure 20).[250] Its treatment with $[H(OEt_2)_2]BAr^F{}_4$ at −90 °C gave a 2:1 mixture of symmetrical bridging hydride and a terminal hydride ($\delta(^1H)$ −18.8 and −2.2 ppm, respectively). Also formed was a nonhydride (putatively thiol) species that converts to both bridging and terminal hydrides at −60 °C, with the t-H → μ-H conversion being, encouragingly, rather slow ($t_{1/2}$ = 2.5 h at 20 °C) in the absence of acid catalyst.

While models discussed in this section share much in common with the [FeFe]-H_2ase active site, the synthetic terminal hydrides lack the conformational rigidity of the enzyme H-cluster. In the latter case, the distal Fe adopts a reactive "rotated" state in which a terminal site is available for binding H^- or H_2 substrate.[266] This rotated structure is perhaps stabilized by hydrogen bonding to the protein, but electronic factors may also be important. In model systems, this geometry can only be reproduced in unsymmetrically substituted complexes,

including the Fe(I)Fe-(I) compounds [dppv(OC)Fe(2,2-diethyl-1,3-propanedithiolate)(μ-CO)Fe(CO)$_2$][266] and [dmpe(OC)Fe-(adt^{Bn})Fe(CO)$_3$].[267]

3.2.5. Comparison of Bridging and Terminal Hydrides—While the thermal stability of bridging hydrides was discussed above, these isomers are also typically more resistant to electrochemical reduction than their terminal counterparts. In view of the strong σ-donicity of the H$^-$ ligand,[47] 1e$^-$ reduction of Fe(II)Fe(II)(t-H) occurs at the ferrous center not bound to the hydride (analogous to Fe^p in [FeFe]-H$_2$ase). This situation is not possible in the case of Fe(II)(μ-H)Fe(II), as H$^-$ exerts its cathodic effect on the couples of both metals.[259] A corollary is that H$^-$ binds Fe(II) considerably more tightly than Fe(I), as is illustrated by the disparate Fe–H distances in the mixed-valent complex [dppv(OC)Fe(pdt)(μ-H)Fe(CO)dppv] ([**7**(μ-H)]). Theoretical calculations also indicate that reductions of terminal hydrides occur at more positive potentials than those of bridging hydrides,[186] although some special cases have been identified in which this trend is reversed. These situations arise when bulky ligands are present, with reduction of the μ-H complex alleviating strain by allowing the metals to distance themselves from one another.[186]

Discussion of μ-H isomers can be illustrative and guide the synthesis of more stable terminal hydrides, but one must keep in mind that μ-H species do not come into consideration in the [FeFe]-H$_2$ase mechanism. For the enzyme catalytic cycle (Figure 9), DFT studies indicate that t-H to μ-H isomerization comes with a prohibitively large electronic energy barrier (29 kcal mol^{-1}),[268] in no small part due to the H-bonding of CN$^-$ ligands to nearby residues preventing turnstile rotation. Moreover, direct protonation of the Fe–Fe bond—bypassing any t-H species—is even more unlikely, and the endothermic H$^+$ transfers from Lys358 to H$_{ox}$ and H$_{red}$ are accompanied by kinetic barriers of 52 and 39 kcal mol^{-1}, respectively. These large barriers arise because direct H$^+$ transfer would require movement of Lys358 and cleavage of its H-bond to Glu361. In contrast to such processes, terminal hydride formation is exothermic and requires an electronic activation energy of only 6.9 kcal mol^{-1}, with the barrier to H$_2$ formation being 4.1 kcal mol^{-1}.[268] The redox properties of diiron dithiolates allows one to estimate rates of protonation of the Fe–Fe bond (the highest occupied molecular orbital (HOMO)).[217] In the case of an [FeFe]-H$_2$ase protein operating at –414 mV vs NHE at pH 7, the estimated rate is an order of magnitude lower than the observed rates for the enzyme. This once more underscores that the enzyme operates through terminal hydrides, and it does so because of distinct kinetic advantages. Of course, the key component facilitating terminal protonation is the azadithiolate cofactor. Synthetic models featuring adt^{2-} (or its derivatives) are discussed in section 3.2.6, along with their mechanisms for H$_2$ evolution.

3.2.6. Azadithiolato Hydrides—The synthesis of the archetypal [(OC)$_3$Fe(pdt)Fe(CO)$_3$] simply involves treatment of an Fe(0) carbonyl with the dithiol H$_2$pdt. In contrast, the instability of free H$_2$adt or H$_2$adt^R ((adt^R)$^{2-}$ = $^-$SCH$_2$N(R)-CH$_2$S$^-$); R = alkyl, etc.) species or simple salts thereof[269] necessitates indirect synthetic routes for [(OC)$_3$Fe(adt)Fe-(CO)$_3$] derivatives. Among the methods used, the Mannich-type condensation of CH$_2$O, amines, and [(OC)$_3$Fe(SH)$_2$Fe(CO)$_3$] has proven useful in affording [(OC)$_3$Fe(adt)Fe(CO)$_3$],[270] N-substituted species [(OC)$_3$Fe(adt^R)Fe(CO)$_3$], as well as oxadithiolate

$[(OC)_3Fe(odt)Fe(CO)_3]$ (odt^{2-} = $(^-SCH_2)_2O$).[271] Conveniently, the ligand substitution chemistry of these heteroatom-bridged hexacarbonyls mirrors that of the pdt^{2-} parent, and several tertiary phosphine- and CN^--substituted derivatives are known. These models thus feature an ideal arrangement with an Fe(I)Fe(I) core of high thermodynamic basicity proximal to an amine proton relay with high kinetic basicity.

A major contributor to the kinetic favorability of terminal hydrides is the azadithiolate cofactor, which plays a key role in the catalytic activity of models and the enzyme. The azadithiolate in the enzyme was confirmed by an elegant series of experiments in which apo-HydA (the [FeFe]-H_2ase from *Chlamydomonas reinhardtii* lacking the [2Fe] subsite) was reconstituted ("maturated") with the synthetic diiron dicyanides $[NC-(CO)_2Fe(adt)Fe(CO)_2CN]^{2-}$ ([**3**]$^{2-}$), $[NC(CO)_2Fe(odt)Fe-(CO)_2CN]^{2-}$, and $[NC(CO)_2Fe(pdt)Fe(CO)_2CN]^{2-}$.[199,200,272] Each maturation product exhibited ν_{CO} and ν_{CN} bands matching those of native HydA, indicating that the diiron complexes had been accepted by the apoprotein. Yet only the apo-HydA + $[NC(CO)_2Fe(adt)Fe(CO)_2CN]^{2-}$ product (believed to be the holoenzyme) could reproduce the activity of authentic HydA. Because the activity of the enzyme is so high, the protein maturated with the flawed cofactor pdt^{2-} is still catalytically competent, albeit with <1% activity of HydA.[201] Such work confirms not only that the dithiolate cofactor contains an amine, but further that this H^+ relay is essential to the efficiency of [FeFe]-H_2ases.

The divergent reactivity of propanedithiolates and azadithiolates, apparent also in purely synthetic species, is of great importance. While $[(Me_3P)_2(OC)Fe(pdt)Fe(CO)(PMe_3)_2]$ ([**15**]) converts primarily to the bridging hydride upon treatment with $[H(OEt_2)_2]BAr^F{}_4$ (vide supra), azadithiolate $[(Me_3P)_2(OC)Fe(adt)Fe(CO)(PMe_3)_2]$ ([**16**]) converts rapidly and exclusively to the terminal hydride $[(Me_3P)_2(OC)Fe-(adt)Fe(t\text{-}H)(CO)(PMe_3)_2]^+$ ([**16**(*t*-H)]$^+$, $\delta(^1H)$ −2.29 ppm).[250] Considering the similar electronic properties of the low-valent species (ν_{CO} = 1860, 1839 and 1857, 1836 cm^{-1} for pdt^{2-} and adt^{2-} complexes, respectively), this regiochemical selectivity is ascribed to the influence of the secondary amine, which provides a kinetic protonation pathway via an ammonium intermediate. The effect is so marked that even weak acids (e.g., NH_4PF_6) can induce rapid *t*-H formation in the azadithiolate complex, with no reactivity observed for the propanedithiolate complex. While S-protonation was invoked when describing the reactivity of [**15**], such thiol intermediates are no longer relevant when a basic amine is present, especially when it is poised above the terminal site. Such an arrangement has been crystallographically confirmed in the diiron azadithiolato terminal hydrides $[(Me_3P)_2(OC)Fe(adt)Fe(t\text{-}H)(CO)-(PMe_3)_2]^+$([**16**(*t*-H)]$^+$) and $[dppv(CO)Fe(adtH)Fe(t\text{-}H)-(dppv)(CO)]^{2+}$ ([**17**(*t*-H)H]$^{2+}$, Figure 21).[250,258]

The structure of [**16**(*t*-H)]$^+$ features not only the synergistic trans arrangement of the *t*-H^- donor and μ-CO acceptor, but also a positioning of the amine such that N–H···H–Fe dihydrogen bonding (2.042 Å) is possible, as also indicated by one-dimensional nuclear Overhauser effect NMR experiments. It does not take much imagination to see that the Fe–H (1.487 Å) moiety could arise from tautomerization of an ammonium intermediate, followed by inversion at N such that this interaction (as well as the anomeric-type interactions featuring the lone pair) can be established. The related tetraphosphine [**17**(*t*-H)H]$^{2+}$, perhaps

owing to the lower donicity of dppv versus bis(PMe_3) ligation, has a slightly shorter Fe–H bond (1.438 Å). Given that the dppv complex was crystallized with the dithiolate in the ammonium state, the difference could also be ascribed to the stronger dihydrogen bonding (1.879 Å) of this now more acidic moiety to the H^- ligand. DFT studies have shown that the N–H···H–Fe interaction is strongly affected by the presence of H-bond acceptors such as BF_4^-, and that in the absence of the counteranions the H···H distance contracts to 1.40 Å.[161] The participation of an ammonium hydride state for the enzyme has been proposed, with such a species (Figure 9, middle right) arising from the protonation of H_{sred}.

The thermodynamic influence of dihydrogen bonding has been the subject of many experimental and theoretical studies. In particular, vibrational frequency shifts induced by such bonding, as well as the final H···H distances, have been used in combination with DFT calculations to correlate observables with the strengths of these interactions.[273] In the present case of $[\mathbf{16}(t\text{-H})]^+$ and $[\mathbf{17}(t\text{-H})\text{H}]^{2+}$, the stabilization afforded by dihydrogen bonding amounts to approximately 2 and 4 kcal mol^{-1}, respectively, based on the H···H distances. In all, such interactions play a small but not insignificant role in reactivity, and they have also been implicated in the [Fe]-H_2ase catalytic cycle (section 5.1).[274]

Although the amine group plays a key role in second coordination sphere interactions and directing terminal protonation, it is perhaps unfortunate that the t-H → μ-H isomerization in synthetic models occurs regardless of which dithiolate is present.[264] Thus, both complexes in Figure 21 irreversibly convert to their respective bridging hydride thermodynamic products. In the dppv-containing system, the conformational dynamics have been extensively studied both in situ and in silico (Figure 22). DFT calculations indicate the kinetic protonation product of [**17**] to be the ammonium $[\mathbf{17}\text{H}]^+$.[161] The proton is rapidly relayed to a terminal coordination site at the nearest Fe center, which is 1.3 pK_a units (on an MeCN scale) more basic than the amine. Experimentally, low-temperature protonation of [**17**] readily affords terminal hydride $[\mathbf{17}(t\text{-H})]^+$ ($\delta(^1\text{H})$ −4.2 ppm), which eventually isomerizes to bridging hydrides of pseudo C_2 and then C_1 symmetry. The final hydride complex $[\mathbf{17}(\mu\text{-H})]^+$ (−14.3 ppm; Figure 22, center left) is much less acidic (pK_a > 18.6) than $[\mathbf{17}(t\text{-H})]^+$ (pK_a = 16), reflecting the higher thermodynamic basicity of the Fe–Fe bond relative to the terminal sites in Fe(I)Fe(I) species. Consistent with NMR data, the pK_a values suggest the conversion should be almost quantitative, as $[[\mathbf{17}(\mu\text{-H})]^+]/[[\mathbf{17}(t\text{-H})]^+] > 10^{2.6}$.[258] A similar t-H → μ-H isomerization process is at play for the doubly protonated derivatives. The ammonium terminal hydride $[\mathbf{17}(t\text{-H})\text{H}]^{2+}$ is 9.5 pK_a units more acidic than $[\mathbf{17}(t\text{-H})]^+$, in line with the former only being relevant when strong acids are employed. It turns out that $[\mathbf{17}(t\text{-H})\text{H}]^{2+}$ plays an important role in catalysis. Having addressed the stoichiometric protonations of diiron species, the discussion now moves to their catalytic reactions. As will become clear, such complexes—most notable of which is the dication $[\mathbf{17}(t\text{-H})\text{H}]^{2+}$—can exhibit a broad range of HER activity that can be readily appreciated by considering their structures.

3.2.7. Proton Reduction Catalysis—Understanding the protonation of [FeFe]-H_2ase models is a prerequisite for the study of HER electrocatalysis, in which acid–base chemistry plays a central role. Hydrides of the form FeFe(t-H) or Fe(μ-H) Fe are important intermediates, but few HER investigations on diiron models include conclusive

characterization of hydride-bearing states. Several surveys on the HER mediated by FeFe species are available,[81,275–277] and presented here is rather a description of the salient components of diiron dithiolate catalysts, such that one can identify the often subtle structural and electronic differences between systems and rationalize their influence on catalytic H^+ reduction. For instance, the donicity of ligands bound to the FeFe cores will govern which oxidation states are accessible during the catalytic cycle. The electron density at the metal further influences which protonation states predominate, an aspect that is also affected by protic groups in the second coordination sphere and the nature of the acid employed. With these aspects in mind, the design challenges associated with [FeFe]-H_2ase modeling, as well as some potential solutions, will become more apparent. In terms of evaluating electrocatalysis, it is once more emphasized that a description should include both thermodynamic information (e.g., potential) and a corresponding kinetic parameter (e.g., TOF).[73] In all, catalysts acting at low overpotentials and high turnover frequencies are the most desirable.

Before turning to specific examples, possible pathways for inner-sphere HER mediated by an arbitrary reduced metal complex L_nM are presented in Figure 23. With respect to FeFe complexes, catalysis typically involves conversion of an Fe(I)-Fe(I) species (an H_{red} model denoted L_nM) to the doubly protonated and doubly reduced state L_nMH_2. Poised to release H_2, this latter state may take the form of a dihydrogen complex $L_nM(\eta\text{-}H_2)$, a dihydride $L_nM(H)_2$, or another tautomer. The exact nature of the relevant hydride-bearing intermediates for a given catalyst depends on the mechanism at play, which is influenced by metal coordination environment, Brønsted acid strength, and catalytic conditions. As described in section 3.2.2, a scarce few diiron hydrides have been characterized aside from the $34e^-$ diferrous systems.[196] Furthermore, it is rare for even the latter well-studied compounds to be directly observed in catalysis.

Discussed now are examples of $[(OC)_3Fe(dithiolate)(CO)_3]$ catalysts, the "first-generation" [FeFe]-H_2ase models on which the majority of HER studies have focused,[276] in part due to the straightforward preparation and robust nature of such hexacarbonyl compounds. With respect to the archetypal $[(OC)_3Fe(pdt)Fe(CO)_3]$ ([**4**]), the use of electrochemical and spectroelectrochemical measurements, digital simulations,[278,279] and DFT calculations has revealed much about its HER mechanism (Figure 24).[280] The electron-poor Fe(I)Fe(I) core in [**4**] is not readily protonated (section 3.2.1), and catalytic reduction of HOTs instead begins with reduction of [**4**] ($E_{1/2} = -1.55$ V vs $Fc^{+/0}$). The monoanion is now sufficiently basic to undergo protonation by HOTs, and the resulting μ-H species is more easily reduced ($E > -1.55$ V) than $[\mathbf{4}]^-$ such that an additional reduction occurs. The formally Fe(I)Fe(I) anion $[(OC)_3Fe(pdt)(\mu\text{-H})Fe(CO)_3]^-$ ($[\mathbf{4}(\mu\text{-H})]^-$) can now undergo protonation at either of its Fe or S atoms. Protonation at a metal site affords an Fe(II)Fe(II) dihydride poised to release H_2 and regenerate [**4**] (albeit slowly) in an overall ECEC mechanistic cycle. Another possible form of the doubly-protonated species is a Fe(I)Fe(I) hydride in which one thiol binds only one Fe site. The latter species readily undergoes reduction (−1.75 V) and quickly releases H_2 as part of a CECE cycle. A common reduced hydride intermediate can thus perform catalysis by two separate mechanisms occurring at distinct potentials and rates.

Electrocatalytic proton reduction by the 1,2-benzenedithiolate congener $[(OC)_3Fe(bdt)Fe(CO)_3]$ ([**18**]) proceeds by a mechanism different from those described above. While the exact pathway is dependent on the acid pK_a, experimental and DFT studies indicate that this very electron-poor complex must receive $2e^-$ (−1.31, −1.33 V vs $Fc^{+/0}$ in MeCN) to give the formally Fe(0)Fe(0) dianion $[\mathbf{18}]^{2-}$, protonation of which yields the Fe(I)(μ-H)Fe(I) species $[\mathbf{18}(\mu\text{-H})]^-$ (Figure 25).[85] This hydride product is susceptible to further reaction with acids of pK_a < 23 (e.g., HOTs), resulting in slow release of H_2 that regenerates [**18**] and completes the EECC catalytic cycle. Additional reduction of $[\mathbf{18}(\mu\text{-H})]^-$ is necessary when weaker acids (pK_a > 23, e.g. HOAc) are used. This is followed by protonation and rapid H_2 release to complete an overall ECEC mechanism.

The reader may recall that it is an Fe(I)Fe(I) form of [FeFe]-H_2ase, namely H_{sred}, that is proposed to undergo tautomerization/protonation to afford a terminal hydride (section 3.1). Contrasting the HER mechanism of the enzyme with those of its hexacarbonyl models allows one to tease out the influences of ligand sets and acid–base cofactors: the first and second coordination spheres. With respect to ligand effects, electron-poor models (i.e., those with six CO ligands) require reduction below an Fe(I)Fe(I) state before their protonation can occur. Even then, it is a μ-H rather than t-H species that invariably forms. In terms of the second coordination sphere, the presence of Brønsted basic sites within a model complex can have a strong influence on the electrocatalytic mechanism and potential at which catalysis occurs.[281] Basic residues are protonated in acidic media, resulting in the catalyst bearing less negative charge and giving rise to milder reductions relative to those of more anionic species. For example, the mechanism proposed for HOTs reduction[282] catalyzed by $[(OC)_3Fe(adt^R)Fe(CO)_3]$ ([**19**], R = ^{i}Pr, $CH_2CH_2OCH_3$) begins with protonation of the amino group to form $[\mathbf{19}H]^+$ (Figure 26). The resulting Fe(I)Fe(I) cation can be reduced at −1.2 V vs $Fc^{+/0}$, nearly 450 mV more positive than the wave for the neutral complex $[(OC)_3Fe(adt^R)Fe(CO)_3]$. The reduced ammonium [**19**H] is then protonated to generate a mixed-valence ammonium hydride $[\mathbf{19}(\mu\text{-H})H]^+$, which immediately reduces at potentials below −1.2 V and slowly releases H_2. While the structure of the $[\mathbf{19}(H)_2]$ product is not obvious, what is clear is that an acid–base cofactor enables a mechanism involving mixed-valence hydrides in place of abiological, highly reduced Fe(I)(μ-H)Fe(I) intermediates. In the presence of the strong acid $HBF_4{\cdot}Et_2O$, $[\mathbf{19}(H)_2]$ can not only undergo slow H_2 loss, but instead may also be protonated to afford $[\mathbf{19}(H)_3]^+$, whose reduction (−1.4 V) causes fast release of H_2. Of the two CECE mechanisms, as was illustrated in the previous two examples, the reduction occurring at the more negative potential results in faster H_2 production.

The low basicity of hexacarbonyl derivatives means that their conversion to hydride-bearing species necessitates either the use of superacids or electrochemical reduction prior to protonation. The second process requires highly negative potentials and, thus, can incur significant overpotentials, even when an azadithiolate $(adt^R)^{2-}$ is present. At no point does ammonium $[\mathbf{19}H]^+$ convert to an amine hydride form, reflecting a poorly basic metal core. The observation that another Fe(I)Fe(I) species, namely H_{red}, readily protonates to form a hydride indicates deficiencies in the inner coordination sphere of these “first-generation” models. As described earlier in this section, these are addressed by substitution of CO

ligands for strong σ-donors such as CN^-, phosphines, and *N*-heterocyclic carbenes. But how many substitutions must be made? Replacing two carbonyls is apparently insufficient, as exemplified in the reduction of HOTs catalyzed by [(dppe)(OC)Fe(pdt)$Fe(CO)_3$]. In this case, HER requires reduction of either a bridging hydride [(dppe)(OC)Fe(pdt)(μ-H)$Fe(CO)_3]^+$ (−1.3V vs $Fc^{+/0}$) or the parent complex (−1.5 V).[283] Of course, Nature eschews bridging hydrides and does not operate via Fe(I)Fe(0) intermediates, allowing for much milder HER potentials. The first model to exhibit H^+ reduction electrocatalysis through a terminal hydride was [(OC)(dppv)Fe(pdt)Fe(dppv)(CO)] ([**7**]), whose treatment with $HBF_4{\cdot}Et_2O$ affords the Fe(II)Fe(II)(*t*-H) complex [7(*t*-H)]$^+$, a species that persists for minutes at 20 °C. The hydride reduces at −1.64 V vs $Fc^{+/0}$, and catalytic reduction of $HBF_4{\cdot}Et_2O$ at this potential proceeds with a TOF of 5 s^{-1}. In contrast, the Fe(II)(μ-H)Fe(II) isomer [**7**(μ-H)]$^+$ reduces at −1.84 V with an associated TOF of 3 s^{-1} (Table 2).

The above example illustrates that, as described in section 3.2.5, terminal hydrides are privileged in that their reductions are both mild (due to the availability of a hydride-free Fe(II) site as an oxidant) and can give rise to higher TOFs (due to *t*-H^- ligands being more reactive than μ-H^- ligands). The 1e^- reduction of [7(*t*-H)]$^+$ is likely followed by direct protonation of its *t*-H^- ligand to evolve H_2, a process in which no doubly protonated and singly reduced derivative of [**7**] (analogous to H_{ox} (H^+, H^-)) is formed. A much faster HER would result if a heteroatom base, proximal to H^-, could serve as a "landing site" for H^+. The important combination of an electron-rich bimetallic core and a pendant base is present in [dppv(OC)Fe(adt)Fe(dppv)(CO)] ([**17**], Figure 27), whose terminal hydride derivative [dppv-(OC)Fe(adt)Fe(*t*-H)(dppv)(CO)]$^+$ ([**17**(*t*-H)]$^+$) is relatively long-lived and catalyzes the mild and rapid HER (−1.49 V vs $Fc^{+/0}$, TOF = 5000 s^{-1}) from $ClCH_2CO_2H$ in CH_2Cl_2. The bridging hydride tautomer [**17**(μ-H)]$^+$ is an inferior catalyst: E_{cat} = −1.72 V, TOF = 20 s^{-1}. Furthermore, a remarkable effect is observed if [**17**(*t*-H)]$^+$ acts on the stronger acid CF_3CO_2H, whence catalysis occurs at −1.11 V with a TOF of 58 000 s^{-1}. The improvement in both catalytic potential and TOF was attributed to the high activity of the oxidizing, doubly protonated dication [dppv(OC)Fe(adtH)Fe(*t*-H)(dppv)(CO)]$^{2+}$ ([**17**(*t*-H)H]$^{2+}$).

The attractive catalytic properties of [**17**] have motivated computational investigations into its activity.[160] Unlike other synthetic models described in this review so far, the two protonations of [**17**] precede any reduction events, a situation that parallels [FeFe]-H_2ase. Reduction of [17(*t*-H)H]$^{2+}$ induces a contraction of the N–H···H–Fe interaction, such that a spin-delocalized intermediate Fe(1.5)Fe(1.5)(η^2-H_2) forms.[95,208] Release of H_2 from this labile species affords a substrate-free Fe(II)Fe(I) species, whose rapid reduction affords the starting Fe(I)Fe(I) complex. This study underscores once more the synergistic roles that terminal hydrides and proximal protic moieties play in efficient HER catalysis.

The FeFe HER catalysts discussed here make use of an electrode to mimic the native [4Fe–4S] electron relay cluster. An electron relay can be incorporated into synthetic models in the form of a redox-active moiety that may serve as an electron source/sink. Pentacarbonyl [**20**] features such a ligand—a phosphole—and the mechanism of its HER has been studied in CH_2Cl_2 solution.[284] Precatalyst [**20**] enters the HER cycle upon double protonation and 2e^- reduction (−1.44 V vs $Fc^{+/0}$, Figure 28). An ECCE mechanism affords the active species [**20**(μ-H)H], which takes the form of a mixed-valence bridging hydride featuring a singly

reduced, protonated ligand. Catalytic reduction of $[Et_3NH]BF_4$ occurs at −2.0 V, at which [**20**(μ-H)H] undergoes a second 2e$^-$ reduction and protonation in an ECE process, resulting in an Fe(I)(μ-H)Fe(I) species of formula [**20**(μ-H)$(H)_2]^-$. This species is indicated by spectroelectrochemical and DFT studies to adopt a structure in which an Fe–S bond is cleaved and a doubly protonated, doubly reduced ligand is present. Intermediate [**20**(μ-H)$(H)_2]^-$ is the catalyst resting state; its protonation and release of H_2 is rate-determining (k_{cat} = 10^5 M^{-1} s^{-1}). Overall, the phosphole ligand serves as a reservoir of reducing equivalents, enhancing PCET in a system that is both O_2-tolerant and very fast. This system also catalyzes reduction of H_2SO_4 at −0.66 V at TOF = 70 000 s^{-1} (k_{cat} = 3.5 × 10^4 M^{-1} s^{-1} in acid-independent regime). The value of the redox-active ligand is emphasized in that catalysis by [**20**(μ-H)$(H)_2]^-$ is so fast even though its mechanism is "handicapped" by operation via bridging hydrides.

3.2.8. Hydrides from H_2—Mimicking the catalytic activity of [FeFe]-H_2ases requires a synthetic FeFe complex to mediate not only the evolution of H_2, but also its oxidation. Such a conversion is of interest for many reasons, a principle one being the need for cost-effective alternatives to Pt electrodes in fuel cells. As noted in section 2.1, the heterolysis of H_2 is challenging in that free H_2 is only weakly acidic (pK_a(THF)[44] ≈ pK_a(MeCN) ≈ 50),[40] a hurdle that can be overcome by its binding to a cationic metal site such as Fe(II). While successes in catalytic H_2 oxidation are less numerous than those in the HER, several synthetic Fe catalysts can cleave H_2. Some of these bear little structural resemblance to the [2Fe] subsite; these "bioinspired" models have been reviewed elsewhere.[24,26,281] The focus here is on "biomimetic" systems—diiron thiolates in particular—that either catalytically oxidize H_2 or convert to a hydride form under H_2. The ideal biomimetic system would mimic H_{ox}, the Fe(I)Fe(II) enzyme state that binds and cleaves H_2, using it as a source of H^-.

Early work on H_2 activation by [FeFe]-H_2ase models did not result in oxidation of H_2 or its conversion to hydrides. Rather, it was shown that $[(Me_3P)(CO)_2$ Fe(pdt)(μ-H)Fe-$(CO)_2(PMe_3)]^+$ ([**6**(μ-H)$]^+$), a Fe(II)(μ-H)Fe(II) complex, mediates H/D scrambling under D_2 and ambient light (Figure 29).[285] The process is rather slow, with exchange of the hydride in CH_2Cl_2 solution under 7–8 bar of D_2 requiring 4 weeks. In a related experiment, a H_2/D_2 mixture, exposed to direct sunlight and [**6**(μ-H)$]^+$ in CH_2Cl_2, afforded HD. H/D exchange was markedly slower in the absence of light, and did not occur at all when the coordinating solvent CH_3CN was used. It was thus proposed that light opens a coordination site by inducing either reversible decarbonylation or isomerization of the bridging hydride to a terminal hydride (the latter possibility was addressed in section 3.2.4).[256] Further studies of H/D exchange with [**6**(μ-H)$]^+$ or $[(Me_3P)(CO)_2Fe(pdt)(\mu\text{-}SMe)_2Fe(CO)_2(PMe_3)]^+$ indicated that both complexes catalyzed D_2/H_2O exchange, a characteristic reaction of H_2ases. The basic requirements for H/D exchange catalysis could thus be formulated: one needs a pentacoordinate Fe(II) Lewis acid to bind $(H/D)_2$ and an accessible Brønsted base to deprotonate coordinated $(H/D)_2$. These roles are possibly fulfilled by the μ-H complex and water, respectively.

While the [2Fe] subsite extracts a H^- ligand from the H_2 substrate, early models could not replicate this activity. Photolytic decarbonylation of [(dppv)(CO)Fe(edt)$Fe(CO)_3$] ([**9**])

affords an all-important free Fe site, yet the unsaturated intermediate, instead of heterolyzing H_2, oxidatively adds it through a very slow process.[248] As mentioned above, oxidative addition of H_2 is not observed for H_2ases, which operate exclusively by heterolysis. It is also conceivable that metals extract H^+ (rather than H^-) from H_2, as in the complete conversion of [**6**] to its hydride [**6**(μ-H)]$^+$ under H_2 (1 atm) in the presence of the H^- acceptor $B(C_6F_5)_3$. This FLP can be viewed as the reverse of the enzymatic system, in which the amine accepts H^+ and Fe^d receives H^-.

Initial attempts at activating and oxidizing H_2 with synthetic [FeFe]-H_2ase models utilized compounds in their Fe(I)Fe(I) or Fe(II)Fe(II) forms, neither of which is relevant to the biological mechanism, which proceeds through an Fe(I)Fe(II) state. As discussed in section 3.1, the mixed-valent core of H_{ox} exhibits a rotated Fe^d coordination geometry exposing a site on an electrophilic Fe center to bind H_2 (or the inhibitor CO). More recent synthetic studies have thus involved the preparation and reactivity studies of H_{ox} models. While the first such complexes, obtained by oxidation of Fe(I)Fe(I) H_{red} models, were only observed transiently in spectroelectrochemical and stopped-flow studies,[286] a series of stable H_{ox} models appeared following reports of $[(CO)_2(PMe_3)Fe(pdt)Fe(CO)_2(IMes)]^+$(IMes =1,3-bis(2-mesityl)imidazolylidine) and $[Me_3P(CO)_2Fe(edt)\text{-}Fe(CO)(dppv)]^+$.[230,287] The products, readily prepared by oxidation of Fe(I)Fe(I) parent complexes with Fc^+, reproduced many features of H_{ox}. For example, the $[(CO)_2(Me_3P)Fe]$ fragment in $[(CO)_2(Me_3P)Fe(pdt)Fe(CO)_2(IMes)]^+$ adopts a rotated structure with a semibridging CO ligand. Meanwhile, $[Me_3P(CO)_2Fe(edt)Fe(CO)(dppv)]^+$ mimics H_{ox} behavior in that it binds CO.

A more complete H_{ox} model also contains an azadithiolate ligand, $[Me_3P(CO)_2Fe(adt^{Bn})Fe(CO)(dppv)]^+$ ([**21**]$^+$). In considering the structure of [**21**]$^+$, one notices that it features not only the mixed-valent core but also a H^+ relay poised for H_2 heterolysis.[200,288,289] This prototype was the first H_{ox} model to activate H_2 and afford a hydride product, albeit in a bridging form and at very high H_2 pressure (Figure 30).[290] The reaction mechanism is not obvious a priori, but could be proposed based on the redox potentials of the relevant species. A likely scenario involves [**21**]$^+$ binding and heterolyzing H_2 to afford the mixed-valence ammonium hydride [**21**(t-H)H]$^+$. An additional [**21**]$^+$ complex may then oxidize and deprotonate (or abstract $H^\bullet$ from) [**21**(t-H)H]$^+$. The slow nature of the H_2 activation is likely due to a combination of weak H_2 binding, as well as the necessity for two complexes to act on a single H_2 molecule, one as an H_2 binder and the other as an oxidant.

The above result prompted investigation of a potentially catalytic and biomimetic route, in which external base and oxidant were employed.[291] In fact, [**21**]$^+$ effects H_2 heterolysis in the presence of the mild oxidant $[FeCp^*_2]^+$ (Fc^{*+}) as well as the (optional) weak base P(o-tolyl)$_3$. The reaction proceeds over the course of hours under only 2 atm H_2 at 0 °C to quantitatively afford [**21**(μ-H)]$^+$ and $[HP(o\text{-tolyl})_3]^+$ ($k_{obs} = 2.2 \times 10^{-5}$ s^{-1} at 0°C). Given that the rate-determining step is likely H_2 binding, it was thought that the stronger electrophile $[(OC)_3Fe(adt^{Bn})Fe\text{-}(CO)(dppn)]^+$ ([**22**]$^+$, dppn = 1,8-bis(diphenylphosphino)-naphthalene) might more effectively cleave H_2. Under identical conditions (although using the slightly stronger oxidant Fc^+) [**22**]$^+$ heterolyzes H_2 20 times faster ($k_{obs} = 4.8 \times 10^{-4}$ s^{-1}

at 0 °C) than [**21**]$^+$ and ~10^4 times faster than [**21**]$^+$ in the absence of oxidant at room temperature. The kinetic isotope effect measured for H_2/D_2 heterolysis by [**22**]$^+$ and Fc^+ was inverse (KIE = 0.8).

The above results bring to light the three requirements for H_2 activation. Not only does the system require a Lewis acidic Fe site and a Brønsted basic amine, but it also requires an electron sink. In Nature, these roles are served by Fe^d, adt^{2-}, and the proximal [4Fe–4S] cluster, respectively. The first synthetic model addressing these three design principles was an analogue of [**21**]$^+$ in which the PMe_3 ligand was replaced by the redox-active phosphine $Cp^*Fe(C_5Me_4CH_2PEt_2)$ (abbreviated FcP*).[66] In this way, the complex $[(FcP^*)(CO)_2Fe(adt^{Bn})Fe(CO)(dppv)]$ ([**23**], Figure 31) preserves the electronic properties of [**21**], as the redox auxiliary is insulated by a CH_2 spacer group. The triiron complex reversibly oxidizes at its Fe(I)Fe(I) core (−700 mV vs $Fc^{+/0}$) and at the FcP* metalloligand (−393 mV) to afford the unique H_{ox} model [**23**]$^{2+}$ featuring Fe(I), Fe(II), and Fe(III) centers. Encouragingly, [**23**]$^{2+}$ exhibited increased affinity toward CO, such that at low temperature the diamagnetic triferrous complex [**23**(CO)]$^{2+}$ forms quantitatively. While the inclusion of redox cofactor Fc*P resulted in only a 2-fold increase in H_2 activation rate relative to the [**21**]$^+$/Fc*$^+$ system, [**23**]$^{2+}$ *catalytically* oxidizes H_2 to protons and electrons. Exposure of [**23**]$^{2+}$ to H_2 in the presence of excess Fc^+ and P(*o*-tolyl)$_3$ resulted in complete conversion to Fc and [HP(*o*-tolyl)$_3$]$^+$, although at an extremely slow rate (TOF = 0.4 h^{-1}). However, the triiron system is bidirectional in that the H_{red} model [**23**] is a catalyst for the HER,[98] such that its combination with $[H(OEt_2)_2]BAr^F{}_4$ (10 equiv) and Fc* (5 equiv) resulted in three turnovers during a 3 h experiment. The functional [FeFe]-H_2ase model [**23**] represented a significant step forward, although its activity does not approach that of the native system. The markedly lower activity of [**23**]$^{2+}$ is thought to result from its low affinity for H_2. DFT calculations on [**23**]$^{2+}$ indicate that H_2 binding requires the relatively bulky benzyl group to shift to an energetically unfavorable conformation to allow H_2 access to an open Fe site.[188]

Catalytic H_2 oxidation and formation mediated by the triiron system are plagued by the formation of μ-H complexes, which are more inert than their active *t*-H tautomers. The bridging species [**23**(μ-H)]$^+$ is not a HER catalyst, although it maintains some H_2 oxidation activity. This deactivation is apparent as rates for catalytic reactions are much lower than those for stoichiometric reactions, implying sluggish deprotonation of the μ-hydride might restrict catalytic turnover.

The oxidation of H_2 by H_{ox} models does not require the acid–base cofactor to take the form of an azadithiolate, nor does it require the redox cofactor to be attached to the FeFe core. This is demonstrated with $[(OC)_3Fe(pdt)(\mu\text{-dppf})Fe(CO)]$ (dppf =1,1′-bis(diphenylphosphino)ferrocene), which catalyzes H_2 oxidation at the surface of an electrode in the presence of pyridine as the base.[293] A separate body of work on azadiphosphines[294] culminated in the preparation of $[(OC)_3Fe\text{-}(pdt)Fe(PNP)(CO)]$ ([**24**], Figure 32), whose H^+ relay $Ph_2PCH_2N(^nPr)CH_2PPh_2$ (PNP)[295] causes bridging hydride [**24**(μ-H)]$^+$ to undergo rapid H/D exchange with CH_3CO_2D. Importantly, these hydrides are almost instantaneously deprotonated by relatively weak bases such as aniline and water, suggesting μ-H complexes might undergo turnover during H_2 oxidation.

It was found that [**24**]$^+$ catalytically oxidizes H_2 in the presence of excess Fc^+ and P(*o*-tolyl)$_3$, illustrating that the redox auxiliary need not be directly appended to the FeFe core to achieve catalytic turnover.[296] However, the proximity of the H^+ relay is absolutely necessary, as replacement of PNP's ^{n}PrN group with a nonbasic CH_2 fragment affords a catalytically inactive species. Oxidation of H_2 by the [**24**]$^+$/Fc^+ system (TOF = 0.6 h^{-1} at 25 °C) is only marginally greater than the triiron system (0.4 h^{-1}), suggesting that the extremely low rates of catalytic H_2 oxidation by model complexes are primarily a result of their inherently poor affinity for H_2.

3.3. Concluding Remarks and Future Challenges

Considerable efforts have gone into synthetic modeling of the [FeFe]-H_2ases, no doubt targeted at reproducing the activity of these remarkably efficient enzymes. The ease with which "first generation" models (i.e., hexacarbonyls) can be prepared has led the majority of synthetic and catalytic studies to focus on these systems. Yet their structural and functional resemblance to the active site is inferior to that of more substituted, electron-rich systems. The latter can operate biomimetically through terminal hydride intermediates and at oxidation states matching those proposed for [FeFe]-H_2ase. Synthetic studies concerned with fine-tuning the first and second coordination spheres by CO substitution and acid–base incorporation, respectively, have been rewarded with HER activities comparable to the enzymatic catalysts, albeit at overpotentials greater than 0.5 V. The quest for fully functional bidirectional models has led to the development of sophisticated models featuring not only a pendant base proximal to an electron-rich FeFe core, but also a redox cofactor.[297] These complete models for the H-cluster mediate H_2 oxidation, yet they do so at rates several orders of magnitude less than the native system.

Given the successes and shortcomings of functional models, what avenues seem promising from the vantage? Certainly the [FeFe]-H_2ase active site is subject to an array of weak interactions that are difficult to replicate in small molecule models. Further, the highly evolved mechanisms allowing for H_2 and H^+ transport to and from the Fe^d site cannot be found in purely synthetic systems. Whereas chemists are jubilant in replicating the role of the first and even the second coordination spheres, mutation studies make it clear that the third coordination sphere is also crucial to high catalytic rates.[298]

Despite the challenges inherent to synthetically approximating the protein environment around the active site, there are some specific shortcomings in current models that restrict their activities. In the case of H_{ox} models, these are poised to activate H_2 yet bind it rather weakly. This relative unreactivity of H_{ox} models is also reflected in their weak binding of CO, a strong inhibitor of [FeFe]-H_2ase. Until synthetic models show higher affinity for CO, they are unlikely to exhibit high rates for H_2 oxidation.[297] Remarkably little emphasis has been placed on a rather important design aspect—matching redox potentials of synthetic models to those of [FeFe]-H_2ases, which must operate between −266 and −296 mV vs NHE. Most desirable are diiron dithiolates with reversible electrochemistry around −900 mV vs $Fc^{+/0}$ mimicking the Fe(I)Fe(II/I) H_{ox}/H_{red} couple. This criterion is satisfied by only a handful of models, including bis(dppv) complexes. While H_2ases operate at low H_2 pressures, the most sought after synthetic catalysts are those that can handle higher pressures

by exhibiting more cathodic redox waves. Such reducing models are yet to be reported, and the cationic nature of most systems contrasts the tetra- and trianionic H_{red} and H_{ox} states, respectively (assuming adt^{2-} is not doubly N-protonated). Finally, one obvious problem with models is that reduced states almost invariably adopt nonbiomimetic structures, not unlike the age-old $[(OC)_3Fe(SR)_2Fe(CO)_3]$ species. In the enzyme, the [2Fe] subsite adopts a preorganized rotated structure necessary for catalysis. Reproducing this is naturally a difficult task as CO and CN^- are free to move and are not functionalizable. But by employing bulky dithiolates and unsymmetrical substitution, the rotated structure can be stabilized in select cases.[266,267,299] It will be necessary to target more conformationally rigid models to enforce this geometry and prevent bridging hydride formation.

It is anticipated that efforts in further tuning biomimetic FeFe models will bring us closer to the enzyme activity. This goal may also be approached from an entirely different angle, and much success has been reported in research concerning bioinspired systems, whose structures are considerably different from that of the native catalyst. Among these is a remarkably active monoiron PNP (azadiphosphine) complex,[300] which merges the pendant base motif of [**24**] into an otherwise rather different structure that nevertheless serves as an efficient bidirectional catalyst. The discussion concerning [FeFe]-H_2ases and their models ends here, and we now consider the [NiFe]-H_2ases in section 4. As will become apparent, despite being biologically unrelated, these two classes of H_2ase share similar mechanistic themes that make their study even more instructive.

4. [NiFe]-H_2ASES

4.1. Enzyme Structure and Function

The [NiFe]-H_2ases are older[301] and more abundant and O_2-tolerant[302] than the [FeFe]-H_2ases. The former, more robust family of catalysts is expressed in bacteria, but unlike [FeFe]-H_2ases is also found in archaea and cyanobacteria (though not in lower eukaryotes).[190] The [NiFe]-H_2ases are heterodimeric (63 + 29 kDa),[303–305] with the larger subunit housing an active site featuring a redox-active $Ni(S\text{-}Cys)_4$ center, of which two $^-$S-Cys ligands bridge to an organometallic, redox-inactive $Fe\text{-}(CN)_2(CO)$ fragment (Figure 33).

A striking aspect of the active site is the unusual arrangement of S donor atoms around the Ni center. While (Cys546-S)Ni(S-Cys84) defines an almost straight line (176.3°), the (Cys549-S)Ni(S-Cys81) angle is considerably smaller (107.9°) such that Ni adopts a seesaw geometry approaching that of SF_4. As for the $(Cys\text{-}S)_2Fe(CN)_2(CO)$ center, it is best described as a distorted square pyramid in which CO occupies the apical site. The structural parameter τ, which ranges from 0 to 1 for the square-pyramidal and trigonal bipyramidal extremes, is in this case equal to (173.7° − 162.7°)/60° = 0.18.[306] The metals are separated by a distance (2.57 Å) comparable to the sum of the Ni and Fe covalent radii (1.24 Å + 1.32 Å = 2.56 Å).[219] The $(Cys\text{-}S)_2Ni(\mu\text{-}S\text{-}Cys)_2Fe(CN)_2(CO)$ core is common to all enzyme states, and while the metrics described here are for the Ni-R form (vide infra), they are very similar to those determined experimentally or computationally for other states. One aspect that does change between redox states is the nature of a third coordination site between the metals. When occupied, this site completes the distorted square-pyramidal and octahedral ligand arrangements about Ni and Fe, respectively. The reduced, active forms of [NiFe]-

H_2ase have the site either vacant or home to a bridging hydrido ligand. These catalytically relevant states are presented in Figure 34.

The name "Ni-R" is given to the most reduced enzyme state. In a biophysical context, the "most reduced" species has the greatest number of electrons and prevails at low redox potentials ("reduced" does not necessarily refer to low metal oxidation states, as might be understood by synthetic chemists). Although (t-H)Ni(II)(μ-H)Fe(II) dihydrides[181,308] and Ni(II)Fe(II)(η-H_2) dihydrogen-bound formulations have been proposed based on computations,[309] the current picture for Ni-R is that of a 34e$^-$ Ni(II)(μ-H)Fe(II) core. This is further believed to be low-spin,[103] despite some earlier computational predictions to the contrary.[310,311] While the identities of the active site heavy atoms have been agreed upon for some time, only recently has X-ray crystallographic data been of sufficient resolution to allow unambiguous location of the μ-H$^-$ ligand.[89] The hydrido binds Ni (1.58 Å) somewhat tighter than Fe (1.78 Å), and its presence has since been verified by ^{57}Fe NRVS, with the observation of a characteristic δ_{NiHFe} bending vibration at 675 cm^{-1}.[103,312]

IR spectroscopy indicates the existence of three isoelectronic Ni-R subspecies, whose pH-dependent speciation indicates that they differ in their protonation states. More basic than bridging thiolates, the terminal thiolates are the most obvious H$^+$ acceptors. The highest-resolution X-ray diffraction data for Ni-R have been modeled with an active site featuring protonated Cys546 (Figure 33).[89] However, as the difference map has electron density on either side of the Cys546 S atom, an argument can be made for S to be unprotonated and undergo anisotropic motion perpendicular to the Ni–S bond. Indeed, aside from the terminal thiolates, an Arg509 residue proximal to Ni represents another viable H$^+$ relay (vide infra).[313] In any case, the situation is much clearer when it comes to electron transport, with a chain of 4Fe–4S, 3Fe–4S, and 4Fe–4S clusters clearly defining a tunneling path to and from the active site.

The stepwise oxidation and deprotonation[107] (−436 mV vs NHE, pH 7.4)[314] of EPR-silent Ni-R affords the 33e$^-$ Ni-C state (Ni(III)(μ-H)Fe(II), "catalytic intermediate"), perhaps the most well-characterized of the active forms. This EPR-active (g = 2.21, 2.15, 2.01) low-spin (S = 1/2) species has been the subject of several X-ray structural determinations, although none with sufficient resolution to unambiguously locate the μ-H$^-$ ligand. Rather, this moiety has been confirmed by the pulsed EPR methods HYSCORE and ENDOR, with signals for the paramagnetic Ni(III) site featuring anisotropic spin coupling to a ^{1}H nucleus.[96,315] The five anionic ligands surrounding the Ni center undoubtedly play a role in taming the otherwise oxidizing +III state, whose polarizing nature results in terminal cysteinato ligands almost certainly being deprotonated,[316] in contrast to the situation with Ni-R.

Oxidation and deprotonation (−375 mV vs NHE, pH 7.4)[314] of Ni-C gives Ni-SI$_a$ ("silent active"), a low-spin hydride-free 32e$^-$ Ni(II)Fe(II) state. This electron count does not take into account a weakly Ni-bound H_2O ligand,[316] upon release of which an electrophilic core is exposed to heterolyze H_2. Yet before this transformation is described, the potentially important 33e$^-$ Ni-L (Ni(I)Fe(II), "light") form, intermediary between Ni-C and Ni-SI$_a$, should also be acknowledged. Originally observed by low-temperature irradiation of Ni-C, the isoelectronic Ni-L is a tautomer in which reductive elimination of the proton allows

formation of a Ni–Fe bond,[179] although with little change in the internuclear separation.[85] ENDOR and HYSCORE point to the proton residing on a terminal Cys546,[317] with prolonged irradiation leading to H^+ departure from the active site.[318] Should interconversion between Ni-C and Ni-SI_a involve concerted PCET, then Ni-L need not be invoked in mechanisms. Computational studies had proposed involvement of Ni-L in catalysis,[36] but this was contraindicated by the apparent need for light irradiation that would not necessarily be available in vivo. However, Ni-L formation has been demonstrated to occur in the dark[319] as well as during catalysis, although its presence is fleeting.[107,307,320] The divergent observations regarding the stability of Ni-L have been attributed to the redox state of the proximal $[4Fe–4S]^{2+/+}$ cluster.[321] When this cluster is oxidized, Ni-C converts to Ni-SI_a, either directly through PCET, or by tautomerization to Ni-L and donation of an e^- to the cluster. If instead the cluster is in its reduced state, the intermediate Ni-L may persist. Analogous to these redox effects, pH also has an influence on the Ni-C to Ni-SI_a conversion. At low pH, this reaction is slowed, presumably due to the protonation of the residue that must accept a proton from the Ni(III)HFe(II) core of Ni-C.[322] While the participation of Ni-L in turnover is still a point of contention, selected data for this state, as well as the three confirmed catalytic states Ni-R, Ni-C, and Ni-SI_a, are given in Table 3.

With the active states described, one can now complete a catalytic cycle by activation of H_2 with Ni-SI_a. Upon dissociation of any aquo ligand present, Ni-SI_a features seesaw Ni(II) and square-pyramidal Fe(II), both of which are electrophilic $16e^-$ metal centers that may conceivably bind and cleave H_2. On general grounds, one might consider this to be more likely to occur at Fe(II), a middle transition metal with just enough nuclear charge to impart electrophilicity while still retaining π-basicity for synergistic H_2 binding. Yet the consensus is that while both metals may participate, Ni does the bulk of the work, not only because it is optimally positioned near the end of a hydrophobic H_2 transport channel,[324] but also because its unusual geometry is particularly reactive, as indicated by DFT calculations.[310,325] Recent work has suggested that the orientation of Cys ligands has a strong influence on spin densities at Ni and S.[326,327] Furthermore, several computational studies on truncated active sites indicate that rotation of terminal Cys modulates the relative stability of low- and high-spin Ni,[310,328,329] although the protein environment may also have nontrivial effects on Ni electronic structure.[325,330] In the case of a Ni(II)Fe(II) core such as that in Ni-SI_a, one would expect square-planar and tetrahedral Ni to give rise to $S = 0$ and 1 states, respectively. The seesaw Ni(S-Cys)$_4$ coordination present in all states is rigidly poised between these two typical geometries, and while Ni-SI_a has no EPR signal, its singlet–triplet gap is not large.[329]

The conversion of Ni-SI_a to Ni-R involves the reactive Ni(II)Fe(II) core being “tamed” upon receiving the μ-H^- ligand, with the fate of the other heterolysis product, a proton, still unclear. A substantial body of computational work[331] as well as the high-resolution Ni-R X-ray structure[89] implicates Cys546, although questions have arisen as to whether the terminal thiolate is sufficiently basic[24] to deprotonate the as-yet-unobserved Ni(II)(η^2-H_2)Fe(II) intermediate. In an alternative mechanism, a more basic Arg509 serves as the H^+ acceptor, much as the azadithiolate cofactor does for [FeFe]-H_2ase (Figure 35). Notably, Arg509 is highly conserved, and its basic guanidine group ($pK_a \approx 13.8$)[332] is only 4.5 Å away from Ni.[313]

While there is debate as to exactly how [NiFe]-H_2ases process H_2, there is little doubt that they do it incredibly quickly. A graphite-supported film of [NiFe]-H_2ase isolated from *Allochromatium vinosum* exhibited diffusion-limited TOF values for H_2 oxidation (>6000 s^{-1}, pH 7, 45 °C, 0.2 V vs SHE). The corresponding current density was similar to that of a Pt electrode, although for the latter case this could be achieved at lower potentials of −0.4 V.[333] Given the large footprint of [NiFe]-H_2ases, their activity must be superior to that of the individual Pt sites, although the accessibility of the active site to the substrate is cited as a source of overpotential.[334] Alternatively, the H_2 oxidation can be driven using benzylviologen as a sacrificial electron acceptor, as demonstrated with [NiFe]-H_2ase from *Desulfovibrio gigas* (2200 s^{-1}, 30 °C, −358 mV).[335] Many examples of [NiFe]-H_2ase are bidirectional, and the same *Desulfovibrio gigas* enzyme also catalyzes H^+ reduction (640 s^{-1}, 30 °C, methylviologen at −446 mV).[335]

The activities of [NiFe]-H_2ases can vary greatly. These differences may arise from several factors, an important one being the strength with which the protein binds H_2. Stronger H_2 binding is exhibited by enzymes expressed for H_2 uptake, such as the *Ralstonia* [NiFe]-H_2ases. Their H_2 production rates are modest (70 s^{-1}, pH 5.5, 40 °C, −0.45 V vs SHE), yet they can operate in the presence of O_2. Indeed, the strong binding of H_2 makes it an even more potent inhibitor than O_2 and CO.[336] Notably, O_2 and CO irreversibly deactivate [FeFe]-H_2ase and Pt catalysts, respectively.

Inhibition of the HER by H_2 can be quantified by considering the Michaelis constant K_M,[337,338] which is related to how much the activity is attenuated by a given H_2 concentration.[339] In the case of [NiFe]-H_2ases, K_M values are typically ~10^{-7}–10^{-4} M, whereas those for [FeFe]-H_2ase are greater and fall in the range ~10^{-4}–10^{-3} M.[339] Thus, while trace H_2 can inhibit the HER in many [NiFe]-H_2ases, the [FeFe]-H_2ases bind H_2 more weakly and are less prone to product inhibition. Such measurements are consistent with the typical biasing of [FeFe]-H_2ases toward H_2 formation, with [NiFe]-H_2ases usually being expressed to oxidize H_2. Interestingly, under high pressures of H_2, certain [FeFe]-H_2ases can still mediate H_2 oxidation faster than [NiFe]-H_2ases.

As has been described above, hydrides are central to the catalytic activity of [NiFe]-H_2ases, the only H_2ases for which hydride-bearing species have been confirmed. Further comparison of the H_2ases points to the contrasting bridging hydride cores of Ni-R and Ni-C with respect to the terminal hydride proposed for [FeFe]-H_2ase. Lacking azadithiolate, the [NiFe]-H_2ases shuttle protons around entirely with amino acid residues (and a H-bonded H_2O network) and feature a dinuclear core more strongly anchored to the protein scaffold. Relative to the diiron enzymes, one might say that the [NiFe]-H_2ases make up for in robustness what they lose in activity. The heteronuclear active sites represent attractive targets for synthetic modeling studies, which, through reproducing [NiFe]-H_2ase structure and spectroscopy (Table 3), aim to reproduce enzyme function. Several reports have described NiFe complexes strongly resembling the [NiFe]-H_2ase active site. These efforts are summarized in section 4.2, with particular emphasis placed on complexes bearing hydride ligands.

4.2. [NiFe]-H_2ase Synthetic Modeling

4.2.1. Hydrides from H^+—Synthetic modeling of the [NiFe]-H_2ases, relative to that of the [FeFe]-H_2ases, is a much younger area of study.[340,341] The low-spin $Fe(CN)_2(CO)$ fragment in the former is reminiscent of the distal $Fe(CN)(CO)_2$ site in the latter, and has similarly caught the eye of synthetic chemists. Certain difficulties associated with preparing heterobimetallics led early [NiFe]-H_2ase modeling to be directed toward mononuclear Ni or Fe models of their respective subsites. With respect to metal hydrides, particular attention was paid to Fe–CN–CO systems, including $[Fe(CN)_2(CO)_3]^{2-}$. This dianion undergoes protonation, not at the N atoms, but rather at Fe(0) to give three isomers of the octahedral Fe(II) product $[HFe(CN)_2(CO)_3]^-$, one of which is shown in Figure 36.[342] With four of the six ligands in the Ni-R state of the enzyme, this hydride remains an attractive synthetic module, and its potential aqueous solubility may lend itself to reconstitution studies akin to those of [FeFe]-H_2ases.

Two CO ligands in $[HFe(CN)_2(CO)_3]^-$ are liberated during its conversion to $[Fe(dppv)(CO)(CN)_2H]^-$ ($[\mathbf{25}]^-$), a product that replicates the enzyme structure well, with the diphosphine dppv representing a prosthesis for the bridging Cys thiolates. IR spectroscopy (ν_{CO} = 1936 cm^{-1}; ν_{CN} = 2087, 2080 cm^{-1}) indicates the monocarbonyl product to be electronically similar to the enzyme subsite, although the ν_{CN} values are lower than those for Ni-R, whose CN^- ligands participate in H-bonding.

Hydrides containing both Fe and Ni are rare, and at one point examples of these were limited to clusters such as the μ^3-H^--containing $[NiFe_3H(CO)_{12}]^-$ metallotetrahedron[343] or the μ-H^--bridged $[NiFe_5HN(CO)_{14}]^{2-}$ and $[Ni_2Fe_4HN(CO)_{14}]^{2-}$ octahedra bearing interstitial N^{3-}.[344] Of much greater relevance to the [NiFe]-H_2ase active site was the report of the first NiFe *thiolato* hydride, $[(dppe)Ni(pdt)(\mu\text{-}H)Fe(CO)_3]^+$ ($[\mathbf{26}(\mu\text{-}H)]^+$, Figure 37).[345]

Yet before discussing hydride $[\mathbf{26}(\mu\text{-}H)]^+$ and its derivatives, one must consider the low-valent conjugate bases from which they are prepared. The Ni(I)Fe(I) species $[(dppe)Ni(pdt)Fe\text{-}(CO)_3]$ ([**26**]),[346] diamagnetic on account of its metal–metal bond (2.467 Å),[347] is a 34e^- complex similar to the homobimetallic $[dppe(OC)Fe(pdt)Fe(CO)_3]$. Comproportionation of the Ni(II) complex [(dppe)Ni(pdt)] with an Fe(0) source such as [Fe(benzylideneacetone)$(CO)_3$] or $[Fe_2(CO)_9]$ affords [**26**], which was initially purported to be unstable,[346] but is in fact rather robust. A more generalizable synthesis for [**26**] was later developed in which [(diphosphine)Ni(dithiolate)] and *cis*-$[FeI_2(CO)_4]$ are combined, with 2e^- reduction of the resulting iodide $[(diphosphine)Ni(dithiolate)(\mu\text{-}I)Fe(CO)_3]^+$ affording the neutral species $[(diphosphine)Ni(dithiolate)Fe\text{-}(CO)_3]$.[348] Such complexes reproduce the $Ni(SR)_2Fe$ "butterfly" and apical CO ligand at the [NiFe]-H_2ase active site, although differences in the coordination spheres of the synthetic and native systems are not insignificant. Much like the modeling of [FeFe]-H_2ases, in which phosphines are extensively used as prostheses for CN^- groups and the Cys-S–[4Fe–4S] metalloligand, the diphosphine in $[(diphosphine)Ni(dithiolate)Fe\text{-}(CO)_3]$ is a substitute for terminal Cys-S^- ligands. Another significant difference can be found in the set of diatomic ligands, with the three CO ligands in these models contrasting Nature's choice of one CO and two CN^- groups. The

stereoelectronic consequences of these changes will be discussed in the context of the first generation of synthetic NiFe hydrides.

The finding that the archetypal Ni(I)Fe(I) complex [**26**] sustains protonation to afford a well-defined hydride product represented a significant advance in the field of [NiFe]-H_2ase modeling. This protonation reaction was found to proceed via a $2e^-$ mixed-valent conformer, with dppe rotation resulting in a square-planar environment around Ni (see section 4.2.3).[160] Oxidized (divalent) Ni is now strongly stabilized, with concomitant cleavage of the NiFe bond resulting in Fe being in a reduced state. Overall, this redox isomerization closely parallels the "rotation" of Fe(I)Fe(I) to afford a reactive Fe(II)Fe(0) species. In the present case, DFT calculations indicate that the latent Ni(II)Fe(0) isomer is ~10^8 times more basic than the Ni(I)Fe(I) form and is geometrically preorganized to form hydride [**26**(μ-H)]$^+$.[160] With its Ni(II)(μ-H)Fe(II) core, the robust, air-stable product [**26**(μ-H)]$^+$ represented the first model for the Ni-R enzyme state. However, Ni-R does not form by protonation of a low-valent species—indeed no [NiFe]-H_2ase states feature a Ni(I)Fe(I) or Ni(II)Fe(0) core. The **26** to [**26**(μ-H)]$^+$ reaction is rather a low-valent analogue of the Ni-L to Ni-C conversion, in which oxidative addition of a H^+ transforms Ni(I)Fe(II) to Ni(III)(μ-H)Fe(II). Yet [**26**(μ-H)]$^+$ is nevertheless an important model with instructive characterization. Curiously, the H^- ligand gives rise to a high-field ^{1}H NMR resonance (−3.53 ppm) that appears in a chemical shift region typical of FeFe(t-H) terminal hydrides rather than Fe(μ-H)Fe species. The ligand was found by X-ray crystallography (Figure 38) to be somewhat closer to Fe (1.460 Å) than to Ni (1.637 Å).[345] Relative to [**26**], the metals in [**26**(μ-H)]$^+$ are further apart (2.613 Å) such that they are out of bonding distance, although a Ni···Fe interaction is sometimes drawn. The H^- ligand has a rigidifying influence on the structure, resulting in a single sharp ^{31}P NMR resonance for the dppe ligand and two ^{13}C resonances for the CO ligands.

The structure of [**26**(μ-H)]$^+$ is supported by vibrational spectroscopy in the form of Raman[349] and ^{57}Fe NRVS measurements.[103] The latter method, applied to ^{57}Fe-labeled isotopologue [(dppe)Ni(pdt)(μ-H)^{57}Fe(CO)$_3$]$^+$ ([**26′**(μ-H)]$^+$), indicated that H^- does indeed bond more strongly to Fe (ν_{HFe} = 1479 cm^{-1}) than to Ni (ν_{NiH} = 1022 cm^{-1}). The vibrational frequencies of the corresponding deuteride agree with the $\nu_{MH} \approx 2^{1/2}\nu_{MD}$ approximation for M–H/D harmonic oscillators in which M is much heavier than H/D. Relative to stretches, bending modes associated with μ-H^- ligands are much lower in energy, with the frequency of the δ_{NiHFe} bending vibration for [(dppe)Ni(pdt)(μ-H)^{57}Fe(CO)$_3$]$^+$ (758 cm^{-1}) approaching that for the enzyme (675 cm^{-1}). The asymmetric hydride binding in [**26**(μ-H)]$^+$ has also been probed by valence-to-core X-ray emission spectroscopy.[350] In this case, the Fe spectra exhibit strong Fe–H signatures, while the Ni spectrum shows no evidence for its interaction with a light bridging atom. The method further allows estimation of M–H bond lengths, and although these come with moderately high uncertainties (~0.15 Å), such information is a useful complement to other analyses.

The tightness with which hydride binds Fe is rationalized in terms of the high electrophilicity of the Fe(CO)$_3$ center in [**26**(μ-H)]$^+$, whose weighted average ν_{CO} frequency (2043 cm^{-1}) is considerably higher than that of the Fe(CO)(CN)$_2$ fragment in Ni-R (1944 cm^{-1}). The electronic influences described here result in [**26**(μ-H)]$^+$ being somewhat acidic (pK_a = 10.7, Table 4), with the μ-H group being rather protic (e.g., it readily exchanges with

D_2O) and insensitive to excess acid. The latter fact simplifies the synthesis of this and related NiFe hydrides, and is in contrast to the preparation of FeFe hydrides, which often involve strictly stoichiometric quantities of acid to avoid H_2 formation.

Several derivatives of [**26**(μ-H)]$^+$ have been prepared in order to bring the structure and spectroscopy of models more in line with Ni-R. One component in such compounds that is not often varied is the dithiolate, with pdt^{2-} and edt^{2-} giving rise to the most stable species owing to their high basicity and favorable chelate ring sizes. Indeed, while FeFe complexes of many mono-and di-, alkyl-, and arylthiolates are known, the NiFe systems are less modular. Although the variety of diphosphines at Ni is not large (dppe, dcpe, and dppv have been reported), the $Fe(CO)_3$ center allows more substitutional scope. The hydrides [(diphosphine)Ni(pdt)(μ-H)$Fe(CO)_3$]$^+$ undergo reaction with mono-[63] and diphosphines[351] to afford [(diphosphine)Ni-(pdt)(μ-H)$Fe(PR_3)(CO)_2$]$^+$ and [(diphosphine)Ni(pdt)(μ-H)Fe(diphosphine)(CO)]$^+$ complexes, respectively (Figure 39). One limitation of this method is its potential incompatibility with highly basic phosphines such as PCy_3, which deprotonate [**26**(μ-H)]$^+$ rather than participate in ligand substitution at Fe.

Complexes of the type [(diphosphine)Ni(pdt)(μ-H)$Fe(PR_3)$-$(CO)_2$]$^+$ feature basal PR_3 ligands and are thus of lower symmetry than their C_s-symmetric tricarbonyl parents. When edt^{2-} is present, appreciable quantities of C_s-symmetric apical PR_3 isomers coexist with the C_1-symmetric species. In either case, substitution of one CO ligand for PPh_3 causes negligible change in $\Delta G°(H^-)$, although the weighted average ν_{CO} decreases by ~50 cm^{-1} and the pK_a increases by 3–4 units.[63] Even greater effects are observed when diphosphines are employed, and the first such complex [(dppe)Ni(pdt)(μ-H)Fe(dppe)(CO)]$^+$ ([**34**(μ-H)]$^+$) was initially prepared by decarbonylation of [(dppe)Ni(pdt)Fe(dppe)$(CO)_2$]$^{2+}$ with BH_4^-. A cleaner and more general route involves photolysis of a solution containing tricarbonyl hydride [(diphosphine)Ni(pdt)(μ-H)$Fe(CO)_3$]$^+$ and diphosphine. The complexes [(diphosphine)Ni(pdt)(μ-H)Fe(diphosphine)(CO)]$^+$ typically exist as two isomers: one with the Fe-ligated diphosphine being apical–basal and another in which it is dibasal. The structure of the latter isomer corresponds well to that of Ni-R, whose two basal CN^- ligands are mimicked by the diphosphine in the present species. Such bis(diphosphine) species also approach Ni-R in terms of their electron density at Fe, with the two isomers of [**26**(μ-H)]$^+$ exhibiting low ν_{CO} frequencies (1954 and 1938 cm^{-1}). The effect of substitution on the weighted average ν_{CO} is approximately additive, with these values being ~100 cm^{-1} lower than that for the tricarbonyl. As expected, changes in Fe ligation have large effects on ν_{CO} and pK_a, and the latter is consistent with the μ-H^- being closely associated with the Fe site. Changes at Ni (e.g., substitution of dppe with dcpe) are less influential on these parameters but do affect redox (section 4.2.3).

The present complexes feature Ni(μ-H)Fe cores whose geometries certainly vary with the identity of the coligand(s). While the bond length difference $r_{Ni–H} - r_{Fe–H}$ is 0.177 Å in the case of [**26**(μ-H)]$^+$, this doubles to 0.370 Å for the Ni(dcpe) analogue [**27**(μ-H)]$^+$.[348] This latter complex features the most electron-rich Ni site and the most electron-poor Fe site, and one might argue that an increase in donicity of the Ni ligand set means that it need not bind H^- so tightly. However, a conclusive trend in H^- binding is difficult to tease out as ligand substitution often has steric consequences. Indeed, interactions between the phosphine

substituents in the PPh_3 complex [(dppe)Ni(pdt)(μ-H)Fe(PPh_3)$(CO)_2$]$^+$ ([**29**(μ-H)]$^+$)[63] lead to a bond length difference of 0.403 Å that is *greater* than that in [**26**(μ-H)]$^+$, a counterintuitive result if just considering electronic effects. Such steric interactions are also at play in the bis(diphosphine) complexes, and while there is structural variation, it is significant that the $r_{Ni–H} - r_{Fe–H}$ value for [(dppe)Ni(pdt)(μ-H)Fe-(dppbz)(CO)]$^+$ ([**35** (μ-H)]$^+$, dppbz = 1,2-bis-(diphenylphosphino)benzene)[351] of −0.010 Å indicates that increasing electron density at Fe can shift H^- toward Ni such that the structures approach that of [NiFe]-H_2ase.

4.2.2. Related Dithiolato Hydrides—As might be expected, the properties of heterobimetallic dithiolato hydride complexes are sensitive to not only variations in the ligand sets, but also changes in the metals used. The ease of preparation and high stability of the Ni(pdt)(μ-H)Fe models above have inspired the synthesis of congeners in which Ni or Fe is replaced by other metals, typically heavier elements from their respective groups. While such work departs somewhat from replicating the [NiFe]-H_2ase active site, it may provide information about the factors governing reactivity of NiFe systems. It is also possible that these "less biomimetic" systems perform even better catalytically. The ligand set chosen for Fe (or its replacement) often varies, with that of the group 10 metal typically bearing two neutral donors in addition to two thiolates. For example, square-planar building blocks of the form $[ML_2(SR)_2]$ feature prominently, and although the following examples have phosphines as the neutral ligand (e.g., L_2 = dppe), the formation of bimetallics can in principle occur with a range of building blocks.

The most closely related complexes to [**26**(μ-H)]$^+$ are its analogues [(dppe)Pd(pdt)(μ-H)Fe$(CO)_3$]$^+$ ([**37**(μ-H)]$^+$) and [(dppe)Pt(pdt)(μ-H)Fe$(CO)_3$]$^+$ ([**38**(μ-H)]$^+$). These are spectroscopically almost identical to their NiFe relative [**26**(μ-H)]$^+$ and are also isostructurual, including the asymmetry of the μ-H^- bridge toward Fe. Additionally, each is prepared in high yield by treatment of a [(dppe)M(pdt)Fe$(CO)_3$] precursor with HBF_4·Et_2O. A distinguishing feature of the PtFe example is that the low-valent species [(dppe)Pt(pdt)Fe$(CO)_3$] ([**38**]) is a bona fide M(II)Fe(0) complex. No Pt–Fe bond exists in this species, which is "frozen" in a reactive conformation rather than in a tetrahedral arrangement observed for the NiFe system.

More often than is the case with the Ni site, the Fe site can also be altered to feature other elements. The most common substitute is Ru, which has rich organometallic chemistry and forms strong, stable bonds to H^-, H_2, and C-donor ligands, as evidenced by the formation of [$Cy_3P(CO)_2$Ru(pdt)(μ-H)Ru(*t*-H)(CO)PCy_3] from H_2 (section 3.2.3).[249] Indeed, the synthesis of NiRu complexes [(dxpe)Ni(pdt)Ru(cymene)] ([**39**], dxpe = dppe; [**40**], dxpe = dcpe; Figure 40)[352] suggests that 14e$^-$ FeL_3 and Ru(cymene) fragments are to some extent interchangeable. The tetrahedral Ni coordination might suggest a Ni(I)Ru(I) description for these complexes, but the geometry is also consistent with a Ni(0)Ru(II) assignment, to which DFT calculations point. Combination of either [**39**] or [**40**] with $[H(OEt_2)_2]BAr^F{}_4$ affords the corresponding hydrides [**39**(μ-H)]$^+$ and [**40**(μ-H)]$^+$. The zerovalent Ni center is thought to be the initial site of protonation, although the X-ray structure of [**39**(μ-H)]$^+$ reveals a familiar motif in which the H^- ends up closer to Ru (1.54 Å) than to Ni (1.65 Å).

There is no particular reason why the metal to replace Fe must be chosen from group 8. However, it is thought that 14e$^-$ fragments are most suitable, and indeed $Mo(CO)_4$ and $W(CO)_4$ fragments readily bind the Ni chelates $[Ni(R_2PCH_2CH_2S)_2]$ and $[(R_2PCH_2CH_2PR_2)Ni(pdt)]$ to form Ni(II)M(0) bimetallics.[354] While the products do not feature metal–metal bonds and M is octahedrally bound, the propensity of group 6 metals to form 7-coordinate complexes can be exploited to prepare the Ni(II)(μ-H)W(II) species ([**41**(t-H)]$^+$).[353] The high acidity of this hydride (which is deprotonated by excess Et_2O) and low catalytic activity result from the electron-poor nature of the W(II) center (average ν_{CO} = 2006 cm^{-1}), and perhaps also from its coordination geometry not allowing H$^-$ to interact with Ni.

An ever-increasing number of hydrides have been prepared that reproduce many aspects of the [NiFe]-H_2ase active site. In terms of structure and spectroscopy, some are certainly closer than others to Nature's blueprint, while some do not even include Ni and/or Fe. The key question is, how do the differences between the enzyme and its models affect catalysis? This question is addressed in section 4.2.3 with respect to some complexes already described here, as well as some further examples.

4.2.3. Electrochemistry and HER Catalysis—With active sites that exhibit both acid–base and redox behavior, the [NiFe]-H_2ases are suitably equipped to mediate proton reduction (HER). The acid–base and redox criteria are met by several synthetic [NiFe]-H_2ase models, and their electrochemistry, studied using methods described in section 3.2.7, is now described. Considered first are the family of complexes [(diphosphine)Ni(dithiolate)(μ-H)Fe$(CO)_{3-n}L_n$]$^+$, not only because they were the first HER-active models to be reported, but also because variation in the ligand sets allows development of structure–function relationships. All but the most electron-rich of these Ni(μ-H)Fe species are not oxidizable. Surprisingly, the oxidation of the bis(dppe) complex [**34**(μ-H)]$^+$ occurs at a mild potential (0.15 V vs $Fc^{+/0}$), although with low reversibility. When treated with a chemical oxidant (acetylferrocenium) at −25 °C, the ν_{CO} bands are shifted by large amounts (68 cm^{-1}), indicative of a Ni(II)(μ-H)Fe(III) product whose oxidation states are reversed relative to the Ni(III)(μ-H)Fe(II) description for Ni-C. In contrast to the oxidations, the reductions of Ni(μ-H)Fe are more well-defined and more relevant to the HER mechanisms of these synthetic catalysts. Some key electrochemical measurements are presented in Table 5.

Potentials for the [(diphosphine)Ni(dithiolate)(μ-H)-FeL_3]$^{+/0}$ couple are strongly related to the nature and number of phosphine donors at both the Ni and Fe sites, being most negative when strongly donating ligand sets are involved. As is the case with the reduction of Fe(II)(μ-H)Fe(II) species, the initial 1e$^-$ reduction product of Ni(II)(μ-H)Fe(II) may take multiple forms, viz., Ni(I)(μ-H)Fe(II), Ni(II)(μ-H)Fe(I), and Ni(1.5)(μ-H)Fe(1.5). The reversibility of this couple varies greatly and correlates with the stability of the radical hydride complex, the formation of which is a key step in catalysis (vide infra). The reduction is irreversible in the case of tri- and dicarbonyls with the exception of [**31**(μ-H)]$^{+/0}$, where the [**31**(μ-H)]^0 radical is thought to be stabilized by spin delocalization onto the $P(OPh)_3$ ligand in a manner similar to that observed for [**31**]$^+$.[180] When two diphosphines are incorporated into Ni(II)(μ-H)Fe(II) species, the reversibility of the 1e$^-$ reductions approaches unity (e.g., for [**36**(μ-H)]$^+$, Figure 41, $|i_{pa}/i_{pc}| = 0.94$ at 0.1 V s^{-1}, room temperature). Electron transfer can also be

induced chemically, and treatment of [(dppv)Ni(pdt)(μ-H)Fe(dppv)CO]$^+$ with $CoCp^*_2$ allows isolation of the stable charge-neutral hydride. Reduction causes only a modest red shift, with $\Delta\nu_{CO} = -37$ cm^{-1}, consistent with Ni-centered redox and thus a Ni(I)(μ-H)Fe(II) description. This is further corroborated by EPR and DFT studies, the latter indicating that significant spin density resides on Ni.[351]

The electron-rich di- and monocarbonyl catalysts operate at high rates, although their $E_{cat/2}$ values are, unsurprisingly, rather negative. Such electron-rich catalysts give rise to more negative $E_{cat/2}$ values, yet can still have reasonably small overpotentials if they can mediate H_2 evolution from weaker acids. As stated in section 2.3.1, one should find the weakest acid that will protonate the reduced form of the catalyst, which is the Ni(I)Fe(I) species in the present case. As is clear from the data in Table 5, the more cathodic $E_{cat/2}$ values have yet to be offset by employing weaker acids for the NiFe systems. Overpotentials for the current catalysts remain >0.5 V, and reducing this key metric while maintaining high TOFs is a fundamental challenge in HER catalysis.

The mechanism by which [(diphosphine)Ni(dithiolate)(μ-H)FeL$_3$]$^+$ catalysts operate involves sequential e$^-$ and H$^+$ transfers. Hydrides of the form Ni(II)(μ-H)Fe(II) (Figure 42, top right) are typically unaffected by acid, and the catalytic cycle thus involves their 1e$^-$ reduction to a mixed-valent complex. Examples of these reduced species have been observed to react instantaneously with acid,[351] perhaps with S atoms serving to relay protons to the metal sites. Following protonation, loss of H_2 affords mixed-valent species Ni(II)Fe(I) complexes (for tri- and dicarbonyls) or Ni(I)Fe(II) complexes (for monocarbonyls), the latter case matching the assignment for the Ni-L state of [NiFe]-H_2ase. Reduction of the $S = 1/2$ intermediates gives the neutral, hydride-free species. The reduced hydride-free species can exist in a reactive Ni(II)Fe(0) form in which Ni is planar, as well as a Ni(I)Fe(I) resting state with tetrahedral Ni.[160] The tetrahedral isomer can readily convert to the reactive form (with a DFT-calculated free energy barrier of $\Delta G^{\ddagger} \approx 6.7$ kcal mol^{-1} and an experimentally estimated barrier of 9.5 kcal mol^{-1} for [**26**][160]), whose high basicity allows for protonation and completion of the catalytic cycle.

Given that HER catalysts featuring a mono- or diphosphine at Fe operate at the highest rates, it is likely that the basicity conferred by these ligands is important for catalysis. Indeed, one or both of the H$^+$ transfers may be rate-determining, and the lack of an effective H$^+$ relay apart from the bridging pdt^{2-} may represent a shortcoming of these models, despite the negligible effect replacing PPh_3 with P(2-pyridyl)Ph_2 has on the TOF. This relay aspect has been investigated with the unusual Ni(I)Fe(I) complex Ni(xbsms)Fe(CO)$_3$ ([**43**], Figure 43), in which only one of the thiolates is bridging.[355] The xbsms^{2-} ligand and its relatives are popular ligands in [NiFe]-H_2ase synthetic modeling, with flexible polydentate donors of this type often being referred to as podands. Treatment with $HBF_4{\cdot}Et_2O$ affords conjugate acid [**43**H]$^+$, whose average ν_{CO} is only modestly (43 cm^{-1}) shifted relative to [**43**] (cf. 66 cm^{-1} for [**26**] → [**26**(μ-H)]$^+$). Crystallographic analysis confirms the product as a Ni(I)Fe(I) thiol, although DFT calculations suggest that the Ni(II)(μ-H)Fe(II) hydride tautomer is only slightly higher in free energy (~5 kcal mol^{-1}). Cyclic voltammetry studies indicate [**43**] mediates electrocatalytic reduction of CF_3CO_2H ($E_{cat/2} = -1.43$ V vs Fc$^{+/0}$, $\eta = 540$ mV), although bulk electrolysis suggests that the TOF is low in this case (0.0014 s^{-1} at −1.6 V).

The poor basicity of [**43**], which is not completely protonated by CF_3CO_2H, may well be responsible for this sluggishness. The use of stronger acids and/or substitution of CO ligands for more basic donors is likely to increase the activity of the present system.

Given the scope of this review, the focus here has largely been on bimetallic HER catalysts that are isolable in one or more hydride-bearing forms. However, these represent a subset of catalytically active [NiFe]-H_2ase models, and many others have not been characterized as their hydride derivatives, although hydrides are assumed as HER intermediates.[356,357] Consider the Ni(I)Fe(II) radical [CpNi(pdt)Fe(dppe)CO] ([**44**], ν_{CO} = 1901 cm^{-1}),[159] a very electron-rich model for the Ni-L state. The conjugate acid [CpNi(pdt)(μ-H)Fe(dppe)CO]$^+$ ([**44**(μ-H)]$^+$, Figure 44), also a radical, is predicted by DFT studies to have spin density localized mainly on the Ni coordination sphere, with almost twice as much density at Ni than Fe. Such a finding is significant, as the Ni(III)(μ-H)Fe(II) core implicated would match that of Ni-C. The hydride [**44**(μ-H)]$^+$ has so far eluded characterization, as while it is generated by addition of acid (1 equiv) to [**44**], the hydride is instantly reduced to [**44**(μ-H)] by surrounding [**44**]. After reaction of [**44**(μ-H)] with remaining acid, the overall stoichiometry is [**44**] + $H^+ \rightarrow$ [**44**]$^+$ + 1/2H_2, a reaction that also proceeds electrocatalytically using CF_3CO_2H as the H^+ source ($E_{cat/2}$ = −1.16 V, TOF = 4 s^{-1}). The DFT calculations suggest that the H^+ reduction mechanism can proceed through one of two pathways, depending on whether the dppe ligand is dibasal or apical–basal. Overall, this example demonstrates well that the challenges in [NiFe]-H_2ase modeling cannot solely be met by preparing more electron-rich NiFe dithiolates. The DFT structure calculated for [**44**(μ-H)]$^+$ features asymmetrically bound μ-H^-, with the Ni–H bond (1.80 Å) being longer than the Fe–H bond (1.60 Å).[159] Despite the presence of the Cp^- ligand, the Ni(III) site remains a strong oxidant, as it does not bind H^- as tightly as Fe. The oxidizing power and reducing power of [**44**(μ-H)]$^+$ and [**44**], respectively, illustrate the large effects protonation can have on redox (and vice versa). Such NiFe models rely on the geometric persistence of the NiCp subunit, and the square planar $\rightleftharpoons$ tetrahedral isomerization accompanying the reduction of 4-coordinate Ni^{II} does not come into play here.

This review has so far highlighted examples from the growing list of thiolate- and hydride-containing heterobimetallic complexes, many of which exhibit electrocatalytic behavior.[356,358] Even rather electron-poor bimetallic species can often be converted to hydrides because the proton chemical potential is readily increased by changing acid concentration and/or employing a superacid. The preparation of Ni(μ-H)Fe species from H_2 is an arguably more challenging matter and is addressed in section 4.2.4.

4.2.4. Hydrides from H_2—As is the case for the modeling of [FeFe]-H_2ases, very few [NiFe]-H_2ase models exist in which a H^- ligand is derived from H_2 heterolysis.[26] Before these examples are described, two less-biomimetic situations are addressed, in which model complexes instead accept either a H^+ or a $H^\bullet$ from H_2.

The first case is exemplified by the conversion of the Ni(I)Fe(I) species [(dppe)Ni(pdt)Fe(CO)$_3$] ([**26**]) to the Ni(II)Fe(II) hydride [(dppe)Ni(pdt)(μ-H)Fe(CO)$_3$]$^+$ ([**26**(μ-H)]$^+$) not by using the typical acid $HBF_4{\cdot}Et_2O$, but rather by using a combination of H_2 (1 atm) and $B(C_6F_5)_3$.[63] This presumably heterolytic pathway makes use

of the [**26**]/$B(C_6F_5)_3$ FLP, although the roles are reversed relative to the enzyme. Indeed, the Ni-SI_a + H_2 ⇌ Ni-R conversion involves a Lewis acidic metal site and a basic Cys (or Arg) residue. The present situation is perhaps more relevant to the [Fe]-H_2ase mechanism (vide infra), in which the Lewis acidic substrate methenyl-H_4MPT^+, whose role here is played by $B(C_6F_5)_3$, accepts H^- in a metal-mediated process.

Metal complexes can also use H_2 as a source of $H^•$, although this does not necessarily implicate a homolytic activation pathway. Consider the low-valent Ni(0)Ru(II) species [**39**], which is readily oxidized by Fc^+ to afford the Ni(I)Ru(II) cation [**39**]$^+$ (Figure 40). Under H_2, the latter complex converts to the diamagnetic Ni(II)(μ-H)Ru(II) product ([**39**(μ-H)]$^+$), whose alternative synthesis is from [**39**] and $[H(OEt_2)_2]BAr^F{}_4$. The reaction with H_2 is slow (~12 h) and poorly understood,[359] and it is as yet unclear whether the process is first or second order in [**39**]$^+$. The latter case would be less relevant to the H_2ases, whose active sites are deeply nested in their protein shells and cannot work in concert with a second H_2ase.

Biomimetic [NiFe]-H_2ase models that utilize H_2 as a H^- source are best designed by mimicking the structure of Ni-SI_a, whose electrophilic Ni(II)Fe(II) core is amenable to the binding and cleavage of H_2. A popular class of building blocks exists in Ni complexes of N_2S_2- (2 × amine + 2 × thiolate) or S_4-donor (2 × thioether + 2 × thiolate) podands.[360] As with (diphosphine)-Ni(dithiolate) species, low-spin Ni(II) podands have been incorporated into many bimetallic systems, one example of which is [Ni($podand^{Me}$)Ru(OH_2)(C_6Me_6)]$^{2+}$ ([**45**(OH_2)]$^{2+}$, Figure 45, top left).[361]

As proposed for Ni-SI_a, the Ni(II)Ru(II) complex [**45**(OH_2)]$^{2+}$ incorporates a weakly bound OH_2 ligand into its structure, with a 14e$^-$ Ru(C_6Me_6) fragment serving as a Fe(CN)$(CO)_2$ surrogate. Under H_2 (1 atm) at room temperature, diamagnetic [**45**(OH_2)]$^{2+}$ converts to the paramagnetic hydride [**45**(μ-H)(OH_2)]$^+$ with concomitant release of H^+ to the (buffered) solution. Octahedral on account of an apical aquo ligand, the Ni(II) site in the product (S = 1) contrasts that in Ni-R (S = 0), wherein no H_2O is bound. Precise atomic coordinates of the synthetic model were obtained by X-ray and neutron diffraction, the latter utilizing deuteride [**45**(μ-D)(OH_2)]$^+$ (prepared from [**45**(OH_2)]$^{2+}$ and D_2) and affording accurate Ni–D (1.859 Å) and Ru–D (1.676 Å) distances. The two proposed mechanisms for H_2 activation are (i) arene slippage to η^4-hapticity, with subsequent H_2 ligation and cleavage at Ru, and (ii) H_2 ligation and cleavage at Ni. In both cases it was suggested that the Ru-bound aquo deprotonates η^2-H_2, but an alternative route that appears at least as likely involves a free H_2O molecule serving as the base.

Hydride [**45**(μ-H)(OH_2)]$^+$ is a catalyst for H_2 oxidation, mediating 2e$^-$ reduction of excess Cu^{2+} under H_2, with the concomitant release of $2H^+$. The proposed mechanism is unusual in that each cycle requires activation of *two* molecules of H_2 and involves a putative dihydride intermediate.[362] The latter species is invoked based on H/D-exchange experiments, as well the observation that [**45**(μ-H)(OH_2)]$^+$, despite its protic nature, requires H_2 to convert to the low-valent Ni(I)Ru(I) complex. The hydride [(H_2O)Ni($podand^{Me}$)(μ-H)Ru(C_6Me_6)]$^+$ was further demonstrated to mediate hydrogenation of aldehydes to their corresponding alcohols,[363] as well as to serve as an anodic catalyst in a fuel cell[28,29] in which the cathodic reaction was mediated by [Ni($podand^{Me}$)(η^2-O_2)Ru(Cp*)]$^+$.[364] The processing of H_2 is

accompanied here also by O_2 activation, with the more electron-rich Cp^{*-} derivative allowing access to Ni(II)-Ru(IV) peroxos. More recently, the Ni(II)Fe(IV) peroxo $[Ni(podand^{Me})(\eta^2\text{-}O_2)Fe(Cp^*)]^+$ could also be prepared from O_2,[365] a reaction mimicking the oxidase behavior exhibited by certain O_2-tolerant [NiFe]-H_2ases.[366]

The structure of hydride $[\mathbf{45}(\mu\text{-}H)(OH_2)]^+$ certainly differs from that of Ni-R, not least in the use of Ru(II) for Fe(II). The promising reactivity and aqueous solubility of the synthetic model[362] inspired further research into related podand complexes, including those with NiFe cores. A close relative of $[\mathbf{45}(\mu\text{-}H)(OH_2)]^+$ is the 34e$^-$ complex $\{Ni(podand^{Et})Fe\text{-}(MeCN)[P(OEt)_3]_3\}^{2+}$ ($[\mathbf{46}(MeCN)]^{2+}$, Figure 46), which preserves many important features while also having the targeted NiFe composition. The organometallic $Fe(CN)_2(CO)$ site at [NiFe]-H_2ase is mimicked here by a $Fe[P(OEt)_3]_3$ fragment, with the phosphite ligands chosen for their σ-donating and π-accepting properties.[367]

Demonstrating reactivity akin to its NiRu analogue, $[\mathbf{46}(MeCN)]^{2+}$ transforms under H_2 to the hydride $[\mathbf{46}(\mu\text{-}H)]^+$, although not without the use of a strong base to accept the H^+ byproduct. The product here is diamagnetic, allowing for assignment of the H^- resonance ($\delta(^1H)$ −3.57 ppm), whose shift is on par with values for [(diphosphine)Ni(dithiolate)(μ-H)$Fe(CO)_{3-n}L_n]^+$. The use of D_2 in place of H_2 confirms both the resultant hydride structure and the origin of the new bridging ligand identified according to IR (ν_{NiHFe} = 1687 cm^{-1}, ν_{NiDFe} = 1218 cm^{-1}) and ESI-MS data. X-ray crystallography of the hydride afforded bond lengths for Ni–H (2.16 Å) and Fe–H (1.57 Å) slightly smaller than those obtained by neutron diffraction using the deuteride (Ni–D 2.18 Å, Fe–H 1.577 Å). The latter measurements provide a better picture of the true nuclear positions, although in both cases the Fe-biased binding of H^- is clear. Nevertheless, the complex $[\mathbf{46}(\mu\text{-}H)]^+$ is interesting in that it exhibits hydridic properties, liberating H_2 upon treatment with $HBF_4{\cdot}Et_2O$. Similar to Ni-R, it also undergoes oxidation, although only irreversibly and at a rather high potential (0.45 V). A reversible wave at −0.42 V may arise from a $[\mathbf{46}(\mu\text{-}H)]^{+/0}$ couple, which indicates that the mixed-valent hydride $[\mathbf{46}(\mu\text{-}H)]$ is potentially isolable.

The report that hydride $[\mathbf{46}(\mu\text{-}H)]^+$ could be prepared from H_2 was followed almost immediately by one describing synthetic hydrides of even higher fidelity to Ni-R, both in structure and in function. One model in question was prepared from [(dppe)-Ni(pdt)$Fe(CN)_2(CO)_2$], one of many complexes that mimic the Ni-SCO state (Ni-SI_a + CO ⇌ Ni-SCO), an inactive enzyme form in which Fe(II) is coordinatively saturated due to its 2CO + 2CN$^-$ ligands. The bis(triarylborane) adduct ($[\mathbf{47}(CO)]$) undergoes decarbonylation with Me_3NO to presumably afford a coordinatively unsaturated electrophile that, despite its lack of a positive charge, extracts H^- from H_2 in the presence of the Me_3N decarbonylation coproduct (Figure 47).[368]

The product $[\mathbf{47}(\mu\text{-}H)]^-$ and its relatives are the first [NiFe]-H_2ase models containing both CN^- *and* H^- groups. Aside from its CO occupying a basal site, the Fe coordination sphere in $[\mathbf{47}(\mu\text{-}H)]^-$ completely reproduces that in Ni-R, with the BR_3 groups simulating the H-bonding exhibited by the CN^- ligands in Ni-R. Nevertheless, the H^- ligand ($\delta(^1H)$ −7.05 ppm) is still closer to Fe (1.516 Å) than to Ni (1.710 Å), although the asymmetry is less pronounced than in $[\mathbf{46}(\mu\text{-}H)]^-$. A subtlety differentiating $[\mathbf{47}(\mu\text{-}H)]^-$ from the many Ni(II)

(pdt)(μ-H)Fe(II) species is the distortion in the Ni coordination, with the lesser of the P–Ni–S angles (147.7°) departing from linearity, although not to the extent of the respective S–Ni–S angle in Ni-R (107.9°). The distorted Ni geometry in these systems is unlikely to be reproduced by podand-containing complexes such as those described above, for which square-planar Ni sites are apparently favored.

The hydridic behavior of [**47**(μ-H)]$^-$ is evidenced in its dihydrogen bonding interactions with weak acids (e.g., Fe– H$^-$···$^+$HNMe$_3$) and its liberation of H_2 when treated with the stronger acid $PhNH_3^+$. These interactions are no doubt promoted by the anionic nature of [**47**(μ-H)]$^-$, an aspect that also affects redox. Hydride [**47**(μ-H)]$^-$ and its dcpe analogue [**48**(μ-H)]$^-$ oxidize at −0.08 and −0.10 V vs $Fc^{+/0}$, respectively, with the similarity of these values suggesting that oxidation is Fe-centered and generates a Ni(II)(μ-H)Fe(III) species (cf. Ni-C Ni(III)(μ-H)Fe(II)). Significantly, [**47**(μ-H)]$^-$ is an electrocatalyst for H_2 oxidation ($E_{cat}/2 \approx -0.08$ V, TOF = 0.98 s^{-1}) in the presence of 1,8-diazabicycloundec-7-ene (DBU, pK_a = 24.3 in MeCN) as a base. The observation that DBU does not deprotonate [**47**(μ-H)]$^-$ mandates that the anion first be oxidized in the catalytic cycle, with the implicated Ni(II)(μ-H)Fe(III) species serving as a rare example of a synthetic high-valent NiFe hydride. Work aimed at a more accurate synthetic model for Ni-C will certainly address the $^-$CNBR$_3$ ligands, whose high ν_{CN} frequencies (2162, 2137 cm^{-1}) and low donicity (2 × $^-$CNBR$_3$ is less donating than dppe) contrast the $^-$CN ligands in the enzyme. Concomitantly, the installation of stronger donors at Ni will be required to ensure that Ni(II) is more easily oxidized than Fe(II) in complexes of the present type.

4.2.5. Bioinspired Systems—The mechanism by which [NiFe]-H_2ase operates involves redox at Ni, with the Fe center serving as a Lewis acid permanently in the +II oxidation state. This observation has led many chemists to investigate mononuclear Ni catalysts with the requisite redox and acid–base properties. Such species are often termed “bioinspired” as they have less in common with H_2ases than the “biomimetic” examples described here thus far. Although several Ni complexes, particularly those featuring dithiolenes,[369] are known to mediate the HER, discussed here are the more privileged examples that exhibit H_2 activation. There are certainly fewer stable examples of Ni(η^2-H_2) complexes than of Fe(η^2-H_2) analogues, in part a reflection of η^2-H_2 complexes almost always being octahedral. This rarity had initially led to doubts about Ni performing H_2 cleavage in [NiFe]-H_2ase, although this is now thought to be the case. Early evidence for Ni interaction with H_2 could be found from [**49**H], which converts to its D isotopologue [**49**D] under D_2 (Figure 48).[370] The formation of a short-lived D_2 complex is thought to be followed by heterolysis of D_2, with Ni receiving D^- and thiolate accepting D^+.

One isolable dihydrogen complex is [**50**(η^2-H_2)]$^+$, whose ^{1}H NMR resonance at −3.21 ppm is characteristic of a η^2-H_2 ligand. Illustrating the H_2 heterolysis reaction, this cation reacts with NEt_3 to afford the corresponding hydride [**50**(H)].[371] A similar example exists in [**51**(η^2-H_2)]$^+$, although this H_2 adduct exhibits H_2 fission without the need for an external base.[372] Indeed, the amido group is well-placed to accept a H^+ while remaining bonded to Ni, resulting in the low thermal stability of [**51**(η^2-H_2)]$^+$. In general, it is important to note that observation of H_2 heterolysis does not rule out a homolytic pathway. Indeed, an

oxidative addition route involving a Ni(IV) dihydride is proposed in the case of [**51**(η^2-H_2)]$^+$. Lastly, the most stable Ni(II)(η^2-H_2) complex to date is {[(2-$Ph_2PC_6H_4$)$_3$Si]Ni(η^2-H_2)}$^+$, which features a tetradentate, anionic SiP_3-donor tripod.[373] In a sense, this complex mirrors the 5-coordinate Ni(II) center in the (Cys-S)$_2$Ni(η^2-H_2)(Cys-S)$_2$Fe(CN)$_2$(CO) species proposed as an enzyme intermediate. While the complexes [**50**(η^2-H_2)]$^+$ and [**51**(η^2-H_2)]$^+$ illustrate biorelevant facets of nickel hydrides, their redox chemistry has not been developed.

Molecular Ni complexes with favorable acid–base and redox properties allow mediation of both H_2 oxidation and evolution. Such bidirectional catalysts remain key synthetic targets. One prominent class of these blends the well-understood protonation behavior of bis(diphosphine)nickel complexes[55] with the H^+ relay motif in [FeFe]-H_2ases. These complexes feature heterocycles with phosphine donor groups and amine relays (denoted "P_2N_2", Figure 49).[86]

Variation of R and R′ substituents in [Ni(P_2N_2)$_2$] allows tuning of steric and electronic properties such that certain reactions are favored. For example, when R = Cy and R′ = ^{t}Bu, the Ni derivative is a fast H_2 oxidation electrocatalyst, at least by synthetic standards (TOF = 51 s^{-1} under H_2 (1 atm) at −0.77 V vs $Fc^{+/0}$).[27,374] When instead R = Ph and R′ = CH_2CH_2OMe, a bidirectional catalyst is afforded, albeit one that effects H_2 oxidation and production very slowly. Bidirectional catalysts typically operate at low overpotentials, in this case possibly facilitated by concerted PCET.[375,376] It was later found that the HER activity of the Ni complexes is greatly enhanced by using a "P_2N" ligand, a seven-membered analogue of "P_2N_2" ligands bearing only one NR′ substituent. When R = R′ = Ph, [Ni(P_2N)$_2$] mediates the HER from protonated N,N-dimethylformamide (pK_a = 6.1) extremely rapidly (TOF > 100 000 s^{-1} at −1.13 vs $Fc^{+/0}$), albeit at a high overpotential (η = 625 mV).[377] Whether performing H_2 oxidation or evolution, it is clear that H^+ relays play a large role in facilitating substrate transfer. The present class of compounds combines Ni with amines reminiscent of adt^{2-}, the latter being positioned far enough away such that Ni–N bonding is unfavorable, yet close enough to rapidly relay H^+ to and from the metal.[281]

4.3. Concluding Remarks and Future Challenges

The synthetic modeling of [NiFe]-H_2ases has afforded an ever-growing collection of heterobimetallic complexes, the structures and reactivities of which are incrementally approaching those of Nature's blueprint. The high efficiency of H_2ases requires that each catalytically active state be of similar free energy[375] and exist in an almost flat free energy landscape in which kinetic barriers to H_2 oxidation or evolution are minimized.[141] Reproducing these rates in synthetic systems will necessitate more rigid complexes, and no doubt motivate the synthesis of new polydentate ligands. Indeed, Ni(diphosphine)$_2$-based catalysts oscillate between tetrahedral Ni(0) and planar Ni(II) during catalysis in contrast to the rigid NiS_4 coordination sphere of the enzyme. This molecular reorganization may well be a contributing factor to the high overpotentials several conformationally flexible models exhibit. While rigidity appears important, not just any ligand will suffice, and ideal designs include those that constrain the complex, particularly the Ni center, in the unique geometry between square planar and tetrahedral. The seesaw coordination, indicated by DFT studies to

be important in H_2 scission,[325] has yet to be replicated. Synthetic chemists will need to look beyond classic ligands, such as podands, which strongly bias square-planar coordination. This biasing of one redox state over another may be a reason why no biomimetic catalyst has been characterized in all of the states proposed for its catalytic cycle. On the other hand, ligand flexibility has been shown to be important for PCET in the $[Ni(P_2N_2)_2]$ and related catalysts with proton relays. In such cases, thermal motions enable the pendant amine to move closer to the Ni center with a relatively low energy penalty in order to facilitate proton transfer.[376] Although the geometry of the Fe site in models is more easily managed, holding the CO ligand trans to the hydride binding site poses a challenge.[378]

A key shortcoming with models prepared thus far is that no system can exist in a Ni(III)(μ-H)Fe(II) form analogous to Ni-C. The continuing quest to prepare more electron-rich complexes can be readily tracked by considering redox potentials and ν_{CO} frequencies. This work will involve shifting the μ-H^- ligand toward Ni to stabilize a +III oxidation state.[379,380] Additionally, this state would be favored by the inclusion of stronger anionic ligands including thiolates or possibly even phosphides or amides. Such ligands may also serve as H^+ relays, although their propensity to bridge metals must be suppressed. The innovations necessary to tackle these and other challenges in the modeling of [NiFe]-H_2ases will not only bring chemists closer to useful synthetic analogues, but also deepen our understanding of the unusual chemistry in Nature's toolkit.

5. [Fe]-H_2ASES

5.1. Enzyme Structure and Function

Of all the H_2 produced in Nature, approximately half is used in the conversion of CO_2 to CH_4, a process that underpins the metabolism of methanogens. To this end, these archaea express four [NiFe]-H_2ases, as well as, when starved for Ni, one [Fe]-H_2ase[381] (the "third hydrogenase", 43 kDa).[382] Discovered after[383] the more O_2-sensitive FeFe and NiFe proteins,[384] [Fe]-H_2ase is not a redox enzyme and thus does not feature Fe–S clusters. In fact, it was initially purported to be completely free of Fe,[385] although it is now known as a metalloenzyme after all,[386] whose activity centers around a Cys-ligated Fe-guanylylpyridinol cofactor (Fe-GP). This structure was shown by IR (ν_{CO} = 2011, 1944 cm^{-1})[387] and NRVS[388] analyses to contain a $Fe(CO)_2$(S-Cys) fragment bound to a unique guanylylpyridinol/pyridonate (GP) through its acyl (ν_{CO} = 1697 cm^{-1}) and pyridyl donors. The GP ligand can be isolated, although in a form with the acyl group oxidized to the corresponding carboxylate.[389] Initial holoenzyme structural studies included this additional O atom, although subsequent mutagenesis and crystallography[390] confirmed that the acyl form is indeed at the active site (Figure 50).[391]

The $Fe(CO)_2$(S-Cys)(guanylylpyridinol/pyridonate) unit is square pyramidal (τ = (175.1° – 173.7°)/60° = 0.02),[306] with the two CO ligands being *cis*: one *trans* to the basic thiolate and the other *trans* to the pyridine/pyridonate. The acyl ligand exerts its *trans* effect on a sixth site, which when not passivated by a H_2O ligand, is available to bind H_2 (as well as inhibitors such as CO). When the enzyme adopts an "open" state, H_2O is displaced by methenyl-H_4MPT^+ (Figure 51). After folding to the closed state, there remains a 4 Å-wide hydrophobic channel accessible to solvent and H_2. Diffusion of the latter to the active site

and release of a proton from the pyridinol moiety to a neighboring His residue affords a Fe(η^2-H_2)$(CO)_2$(S-Cys)-(guanylylpyridonate) complex proximal to methenyl-H_4MPT$^+$. The H_2 substrate is now primed to undergo heterolysis, with the basic O atom of the pyridonate[392] and methenyl-H_4MPT$^+$ serving as the H^+ and H^- acceptors, respectively. Release of the product and ligation of H_2O completes the cycle.[393] Overall, the consumption of H_2 is close to isoergic ($\Delta G = -5.5$ kJmol^{-1}), as one would expect given the comparable potentials for the H^+/H_2 (−414 mV) and methenyl-H_4MPT$^+$/methylene-H_4MPT (−390 mV) couples at pH 7, as well as the rates of H_2 splitting (TOF = 215 s^{-1}, pH 7.5) and formation (TOF = 555 s^{-1}, pH 6.5) mediated by [Fe]-H_2ase.[383]

Inasmuch as pyridonate is similar to CN^- in terms of donor/acceptor properties,[394] the active site of [Fe]-H_2ase shares certain features with that of [FeFe]-H_2ase.[395] Each has a basic cofactor (secondary amine or pyridonate O atom) adjacent to the transiently vacant Fe coordination site. Yet [Fe]-H_2ase does not perform redox and is not highly O_2-sensitive,[394] and its Fe site is invariably found to exist in a low-spin *di*valent state, certainly a good fit for H_2 binding and heterolysis.

The catalytic cycle for [Fe]-H_2ase, like that for [FeFe]- or [NiFe]-H_2ase, is proposed to involve hydride species. One mechanism, based on DFT calculations of a truncated active site model, invokes an elongated dihydrogen bond of the form Fe(II)–H···H–$O_{pyridinol}$.[274] However, calculations in which all amino acids are considered indicate that Fe hydrides need not be considered if H_2 scission is concerted. In such a case, the Fe(η^2-H_2)(guanylylpyridonate) group, in which the Fe(η^2-H_2) moiety has an estimated pK_a of 9,[396] converts to Fe(guanylylpyridinol) without the intermediacy of a hydride, as H^+ abstraction by pyridonate and H^- migration to the substrate occur simultaneously.[397] The methylene-H_4MPT product then leaves the active site, but not before the protein undergoes large-scale movement to open its binding pocket. This study employs molecular dynamics (MD) simulations to probe the opening and closing of the binding pocket, and quantum mechanical/molecular mechanical (QM/MM) calculations to investigate H_2 splitting on select MD snapshots.[397] In contrast to [Fe]-H_2ase, no large displacements are required to shuttle small substrates to the cores of [FeFe]-H_2ase and [NiFe]-H_2ase.

While not an electrocatalyst (and thus not relevant to fuel cell applications), [Fe]-H_2ase does deliver H^- stereoselectively to its substrate. The enzyme could thus serve as a basis for catalysts in organic synthesis, although perhaps due to the many specific supramolecular interactions involved in binding substrate, no molecules other than methenyl-H_4MPT$^+$ induce H_2 cleavage.[398] Time will tell whether the methenyl-H_4MPT$^+$/H_2/Fe-GP ternary complex is absolutely necessary or whether the H^- delivery can be generalized. Motivated by this, as well as the prospect of learning more about the catalytic cycle, synthetic chemists have taken to reproducing the [Fe]-H_2ase active site.[399]

5.2. [Fe]-H_2ase Synthetic Modeling

5.2.1. Models of CO-Inhibited [Fe]-H_2ase—H_2ases are inhibited by CO, which often (but not always, see section 3.1) outcompetes H_2 for metal binding sites, thereby filling their coordination spheres. In the case of [Fe]-H_2ase, the inhibited enzyme features a low-spin facial Fe(II)$(CO)_3$ fragment giving rise to ν_{CO} bands at 2074, 2020, and 1981 cm^{-1} (Table

6). Synthetic modeling of [Fe]-H_2ase began with mimics of the inhibited enzyme, which are described here before highlighting efforts to mimic the coordinatively unsaturated Fe site in the active states.

The finding in 2009 that existing X-ray data for [Fe]-H_2ase indicated an Fe-bound acyl ligand inspired a flurry of synthetic activity to reproduce this common organometallic fragment. Despite the multitude of octahedral ferrous complexes, the enzyme has a unique ligand set, and work in the area has focused on reproducing the structure (inner coordination sphere) and spectroscopy (IR bands). For example, the first acyl thiolato monoiron complex $[Fe(CO)_3(SPh)$(2-diphenylphosphinobenzoyl)] ([**52**], Figure 52) features five of the six donors present at the [Fe]-H_2ase active site and gives rise to ν_{CO} bands closely matching those of the enzyme.[400,401] Moreover, the synthesis of [**52**] by oxidative addition of a thioester to Fe(0) is biomimetic in that the guanylylpyridinol/pyridonate (GP) cofactor is also derived from a thioester.[402] Much like the CO-inhibited enzyme, [**52**] readily loses CO, although the 5-coordinate product converts to a dinuclear species.

Complexes of Fe featuring 2-pyridonate moieties have also been reported, one example of which is $[Fe(CO)_2(PPh_3)$I(6-methyl-2-pyridonate)] ([**53**]).[403] A dicarbonyl, this complex further contrasts the active site in that the pyridonate group in [**53**] binds through both N *and* O atoms.[404] A key feature of [Fe]-H_2ase is the positioning of the basic O atom near but not bonded to the Fe site. Early efforts toward octahedral analogues of Nature's 5-ccordinate FLP are now described.

Synthetic investigations into 2-pyridylcarbamoyl[405,406] and pyridylacyl complexes have afforded models closely resembling the CO-inhibited [Fe]-H_2ase active site. Indeed, this motif has been incorporated into complexes of the form $[Fe(CO)_2$(2-pyridinethiolate)(2-pyridylacetyl)] ([**54**–**56**], Figure 53), which feature donors resembling the native ligands, with an additional N-donor.[407–409] While [**54**–**56**] feature protected acylpyridinols, Fe complexes of the unmasked ligand have also been prepared, the coordination sphere in tricarbonyl [**57**] being similar to that in the CO-inhibited enzyme with I^- in place of Cys-S^-. These pyridylacyl complexes are not assembled through a biomimetic thioester oxidative addition, but instead form by more traditional organometallic routes. In the case of [**54**]–[**56**], this involves nucleophilic attack of $[Fe(CO)_4]^{2-}$ onto a 2-picolyl tosylate, with subsequent insertion of CO into the Fe–alkyl bond.[408–410] In the synthesis of [**58**], Fe instead serves as an electrophile, with $[Fe(CO)_5]$ undergoing addition of 2-picolide anion such that a CO ligand is converted to an acyl.[407]

The tricarbonyls [**57**] and [**58**] were employed in an [Fe]-H_2ase reconstitution study analogous to that described for [FeFe]-H_2ase (vide supra). Incubation of [**57**] or [**58**] with apo-[Fe]-H_2ase, which lacks the Fe-GP cofactor,[411] afforded products whose IR spectra indicated ligation of $Fe(CO)_2$(acylpyridinol/acylmethylpyridinol) to Cys176. Although the methylated derivative was unreactive toward H_2/methenyl-H_4+MPT^+ or H^+/methylene-H_4MPT, the acylpyridinol-containing protein catalyzed these reactions. The semisynthetic system was 2 orders of magnitude slower than the native one, a result attributed to subtle electronic differences between GP and the acylpyridinol ligand. Nevertheless, this work

highlights the importance of pyridinol/pyridonate as a H^+ relay, and refutes some older DFT studies that, by analogy with [NiFe]-H_2ases, implicated Cys-S^- as a relay.[114,274]

Given that pentacoordinate Fe is crucial to the activity of H_2ases, section 5.2.2 highlights $16e^-$ Fe complexes that most closely mimic the [Fe]-H_2ase active site in both structure and reactivity. This will serve as a prelude to studies into H_2 activation with [Fe]-H_2ase models.

5.2.2. Models of Active [Fe]-H_2ase States—A significant breakthrough in modeling the [Fe]-H_2ases came with the finding that a combination of thiolate, pyridylacyl, and other π-bonding ligands can stabilize unsaturated Fe(II) sites. Addition of thiolate to [**58**] replaces not only I^- but also CO, such that square-pyramidal complex [**59**] forms (Figure 54).[412] However, this species does not bind H_2O or H_2 (or O_2), a result attributed to its electron richness. Although the similarity of its ν_{CO} frequencies to those of the enzyme suggests that other factors may also play a role, DFT calculations indicate that H_2 binding is thermodynamically unfavorable ($\Delta G = 10.2$ kcal mol^{-1}).[413]

Building on the chemistry of [**59**], the higher-fidelity structural model [**60**] features the hydroxyl group characteristic of [Fe]-H_2ase.[414] The species was identified according to NMR and IR spectroscopies, but was found to be rather labile (although less so than its 2,6-dimethylphenylthiolato and 1-propanethiolato congeners). Although spectroscopically and structurally similar to the active site, it is unreactive toward H_2. This may indicate that secondary interactions involving the [Fe]-H_2ase pocket, the inclusion of methenyl-H_4MPT^+, and the presence of a more substituted pyridyl ligand are important factors in the activation of H_2.[26]

Another example of a five-coordinate [Fe]-H_2ase model could be prepared from dehydrobromination of octahedral Fe(II) carbamoyl [**61**HBr] (Figure 55).[415] Similar in structure to [**60**], the proposed kinetic product could not be characterized, as it rapidly converted to the cyclometalated species [**62**]. The latter product can also be prepared from hydride [**61**(H)H] ($\delta(^1H)$ −5.1 ppm), which, in turn, is generated from [**61**HBr] and $HBEt_3^-$. While displacement of Br^- with H^- is not a biomimetic transformation, the donor atoms around [**61**(H)H] match those of the active site in a transient hydride-bearing intermediate. Such an enzyme state has yet to be experimentally confirmed, although some theoretical studies invoke it as a short-lived species, very similar to [**61**(H)H], which is unstable above −40 °C. While the generation of [**61**(H)H] indicates that the present type of carbamoyl species can support a hydride ligand, the second coordination sphere of [**61**(H)H] does not feature a basic moiety to engage in H_2 heterolysis.

The close resemblance that the Fe coordination spheres of acylpyridine [**61**] and related species have to that of [Fe]-H_2ase indicates that differences in reactivity may arise from secondary interactions. In search of H_2 heterolysis, such structural models have been modified to incorporate more basic fragments into their architecture, even though this may decrease their resemblance to the active site. For example, combination of tricarbonyl [**58**] with the bidentate ligand $Et_2PCH_2N(Me)\text{-}CH_2PEt_2$ affords monocarbonyl [**63**I], from which I^- dissociation can occur (Figure 56).[416] The putative 5-coordinate species is well set up to cleave H_2, although no direct evidence of the ammonium hydride has been reported, even

under high H_2 pressures. The activation of H_2 by [**63**]$^+$ was evidenced in the scrambling of H_2/D_2 mixtures, with the additional scrambling of H_2 and CH_3CO_2D suggesting a heterolytic mechanism is at play. Bearing some similarity to bioinspired Ni(PNP) and Fe(PNP) electrocatalysts, the present species represents the first functional model for [Fe]-H_2ase and underscores the importance of a proximal base for FLP activity. Even though no hydride complex could be detected, such work importantly demonstrates that an Fe-based [Fe]-H_2ase model can activate H_2 outside of the enzyme in the absence of the native methenyl-H_4MPT$^+$ substrate.

The inertness toward H_2 shown by many 5-coordinate Fe complexes described above comes as a disappointment, but is unsurprising given that ferrous dihydrogen complexes are characteristically cationic.[35] Furthermore, when observed, either directly with [**61**(H)H] or indirectly in the case of [**63**]$^+$, the hydrides are unstable. This has led efforts in functional mimicry to also consider structures departing from the Fe(pyridylacyl) paradigm. For example, triarylimidazolium salts of [RuCp-$(CO)_2$]$^-$ represent FLPs that parallel the biological combination of methenyl-H_4MPT$^+$ and the Fe-GP cofactor (Figure 57).[417] Indeed, the electrophilic C centers of the triarylimidazolium ($\delta(^{13}C)$ 169.6 ppm) and methenyl-H_4MPT$^+$ (165.34 ppm)[418] would appear to be comparably reactive. When treated with H_2, the synthetic Lewis pair heterolyzes H_2 with the cation receiving H^- and the Ru^0 center accepting a H^+ by oxidative addition.

The heterolysis reaction proceeds fastest when a polymeric Ru–CO–Cp species is used in place of [RuCp$(CO)_2$]$^-$. A slightly more biomimetic choice would of course be [FeCp-$(CO)_2$]$^-$, but it directly reduces the imidazolium cation. Overall, H_2 heterolysis is similar to the H_2 fission mediated by the [(dppe)Ni(pdt)Fe$(CO)_3$]/B$(C_6F_5)_3$ FLP (section 4.2.3).[63] Since the H^- and H^+ heterolysis products are delivered respectively to the organic substrate and metal center, the process is *not* biomimetic.

5.3. Concluding Remarks and Future Challenges

Synthetic modeling of [Fe]-H_2ases, particularly since the clarification of the active site structure in 2009, has afforded several high-fidelity structural mimics. This work began with the preparation of octahedral Fe(II) complexes featuring some or all of the thiolate, carbonyl, acyl, and pyridonate/pyridinol ligands present in the native protein. More relevant to the active enzyme are 5-coordinate species, in which a site is free for H_2 or H^- binding. Such 16e$^-$ species have been reported, but typically do not exhibit [Fe]-H_2ase reactivity despite closely mimicking the structure and spectroscopy. This points to the need for tuning the second coordination sphere, the importance of which is demonstrated by artificial reconstitution studies of [Fe]- and [FeFe]-H_2ase. Indeed, the high H–H bond strength means that H_2 heterolysis can only be facile when both Lewis acidic and basic components are present and well arranged. To this end, incorporation of an artificial amine H^+ relay in [**63**]$^+$ afforded a catalyst that activates and transfers H_2. No η^2 –H_2 or H^- complex intermediates have been identified in this case, yet the same is true for [Fe]-H_2ases, with the possible role of Fe–H moieties still a subject of debate. Future efforts in this area may address these questions and also aim to synthetically replicate the cooperative binding of methenyl-H_4MPT$^+$ and H_2 to the enzyme active site.

6. CONCLUSIONS

The study of H_2ases reminds us that organometallic chemistry is literally alive and well, providing the machinery that allows Nature to process the most abundant element in the universe. It is worth mentioning here that examples of metal hydrides in biology are not limited to H_2ases. For example, ENDOR studies on nitrogenase (N_2ase) suggest the presence of two hydrides attached to its Fe_7MoS_9C cofactor during H^+ reduction.[419] Each of the chemically equivalent hydrides is thought to bridge two Fe centers, a situation rather reminiscent of Fe(pdt)(μ-H)Fe model complexes. It is hardly surprising that hydrides play a role in N_2ases, as these exhibit H_2ase behavior in that they can process protons and electrons independently of N_2 reduction to NH_3.[420] An inner sphere mechanism for this HER would necessitate metal hydride participation. Such chemistry is also at play in the related enzyme nickel–iron carbon monoxide dehydrogenase ([NiFe]-CODHase), which utilizes protons and electrons in the interconversion of CO_2 with CO and H_2O.[421] In this case, the Fe_4NiS_4 cofactor can feature a Ni–H or Ni–H–Fe moiety, into which CO_2 inserts during the catalytic cycle.[422,423] The similarities between the enzymes discussed here indicate that acid–base and redox reactions are tasks carried out well by FeS-containing enzymes, especially when they are low-spin.

Returning to the H_2ases, each of their unique organoiron sites[15] facilitates rapid H_2 cleavage and/or formation, motivating chemists to unravel the mechanisms by which they operate. Characterizing the many H_2ase intermediates, including key hydride-bearing states, necessitates the use of several complementary experimental and theoretical techniques. These techniques are also applicable to synthetic hydrides inspired by the H_2ase active sites, with small molecules often being more tractable and easily studied. Many catalytically competent examples are known, and the prospect of their use in a future hydrogen economy is attractive.

One reality of H_2ase modeling is that there will always be differences between enzymes and their small molecule analogues. The [FeFe]- and [NiFe]-H_2ases tightly encapsulate their active sites, ruling out bimolecular pathways and permitting only minor solvation changes and ligand reorganization during catalysis.[424] This is not the case for model complexes, which are conformationally less restricted, as exemplified by the t-H $\rightarrow$ μ-H conversion at play in [dppv(OC)Fe(adt)Fe(H)(dppv)-(CO)]$^+$ ([**17**(H)]$^+$),[258] which does not occur for the [FeFe]-H_2ases, whose cores are held in place by intricate H-bonding networks. Similarly, Ni isomerization in [(dppe)Ni(pdt)Fe-$(CO)_3$] ([**26**]) is necessary to accommodate protonation or oxidation,[160] contrasting the [NiFe]-H_2ases, in which Ni is rigidly held in a seesaw coordination. Indeed, preorganized, rigid metal sites and second coordination spheres play key roles in minimizing both overpotential and the possibility of side reactions. On the other hand, some degree of conformational flexibility is required for the systems to find the optimal distances and angles for intramolecular proton or hydride transfer reactions.[376]

Incorporated into H_2ase protein scaffolds are hydrophobic channels for H_2 propagation to and from their active sites. This is advantageous in selectively introducing substrate to the catalytic metals, but in the case of [NiFe]-H_2ase, its channels may be prone to blockage when H_2 partial pressures are high.[337] The more exposed nature of model catalysts relative

to the enzyme active sites ensures that the former will not suffer from this blockage, and access to H_2, protons, and electrons (as well as inhibitors) is enhanced. With compact profiles, model complexes may also bind electrode surfaces closely and densely such that electron transfer might be rapid and catalytic current densities might be high.[425] Ideally, synthetic catalysts would operate at high rates and low overpotentials, as well as exhibit a robustness that enables operation over wide temperature and pH ranges that may be necessary for implementation in fuel cells.[426]

The amino acids surrounding the H_2ase active sites serve to shield mixed-valent or coordinatively unsaturated states from participating in any reactions other than those of the catalytic cycle. Many mimics of coordinatively saturated, inactive enzyme states have been prepared, but certainly the reactive forms have proven more elusive. For example, terminal Fe(II)Fe(II)(*t*-H) models for [FeFe]-H_2ase have been isolated, yet their $1e^-$ reduced mixed-valent forms have not. Absent from [NiFe]-H_2ase modeling are satisfactory $33e^-$ Ni(I)Fe(II) models for Ni-L, an isolable $32e^-$ Ni(II)Fe(II) model for Ni-SI_a (without its coordinated H_2O), as well as any Ni(III)(μ-H)Fe(II) complex that would resemble the key hydride-bearing Ni-C state. Efforts toward the latter two will involve incorporation of strongly basic ligands to stabilize coordinatively unsaturated and/or high-valent metal sites.

In general, it is debatable whether characterizing catalysts in their many states is necessary or even possible if the species in question is highly active. But it is undeniable that the native H_2ases are significantly faster and more energy-efficient than model complexes. While many models show reactivity toward protons, the discrepancy is most apparent when considering H_2 activation.[427] Despite considerable progress over the past decade, the few H_2ase models that heterolyze H_2 do so very slowly. Thus, bidirectional synthetic catalysts are scarce, and those that exist exhibit slow rates for electrocatalytic H_2 oxidation and/or evolution arising from significant overpotentials associated with their mechanisms. The bidirectionality of many [FeFe]- and [NiFe]-H_2ases has evolved not only from a biological need to both consume and dispense reducing equivalents, but also to operate in very narrow potential ranges and at low concentrations of H_2 and H^+.[6] Furthermore, for a H_2-processing catalyst to be bidirectional, it follows that interconversion of H_2 and hydrides must be rapid and close to isoergic.[428] Such a transformation has been identified as a major challenge in organometallic chemistry,[429] and the viability of H_2 as an energy vector is reliant on both its efficient production and consumption. Electrocatalysis is certainly not the only means of H_2 processing, but it is notable that the reaction of H_2 and O_2[430] in fuel cells is potentially more efficient than traditional combustion, in which energy losses from the Carnot cycle are unavoidable.

Regardless of the motivation for modeling the H_2ases—be it fundamentally learning more about enzymes or perhaps developing base-metal hydrogen-processing catalysts—this work is invariably instructive, and intricacies associated with apparently simple reactions are continually uncovered. At the heart of H_2ases and their functional models are metal hydrides,[431] which are more pervasive and of broader relevance than many would have guessed. A deeper understanding of these hydrides, obtained through a confluence of biological and organometallic chemistry research, will place us closer to a sustainable future.

Acknowledgments

D.S. is supported by the Institute for Basic Science (IBS-R019-D1). T.B.R. is supported by the National Institutes of Health (GM061153, GM-65440). S.H.-S. acknowledges support from the National Science Foundation (CHE-13-61293). M.T.H. acknowledges support from the National Science Foundation Graduate Research Fellowship Program under Grant DGE-1144245.

Biographies

David Schilter was educated at The University of Sydney, from which he received B.Sc. (Hons.) and Ph.D. degrees in 2005 and 2009, respectively. These studies were followed by postdoctoral research at the University of Illinois at Urbana–Champaign and at the IBS Center for Multidimensional Carbon Materials at UNIST, where he has served as a research scientist since 2014. His interests include coordination, organometallic, and materials chemistry.

James M. Camara earned his Ph.D. in chemistry from Columbia University in 2009, where he studied the polymerization and transmetalation chemistry of zirconium and aluminum complexes. Following the completion of his Ph.D., he was a postdoctoral fellow at the University of Illinois at Urbana–Champaign where he conducted synthetic and mechanistic studies on models of the [FeFe]-H_2ase active site. He is currently an assistant professor of chemistry at Yeshiva University in New York City. His research interests are centered around various aspects of mechanistic organometallic chemistry including the use of redox-active ligands in catalysis, development of new transmetalation reactions, and small molecule activation by metal centers.

Mioy T. Huynh received his B.S. in chemistry from the University of California, Los Angeles, in 2012. He is currently a graduate student at the University of Illinois at Urbana–Champaign in Sharon Hammes-Schiffer's research group. His research interests include the investigation of proton-coupled electron transfer reactions in catalytic systems.

Sharon Hammes-Schiffer received her B.A. in chemistry from Princeton University in 1988 and her Ph.D. in chemistry from Stanford University in 1993, followed by two years at AT&T Bell Laboratories as a postdoctoral research scientist. She was the Clare Boothe Luce Assistant Professor of Chemistry and Biochemistry at the University of Notre Dame from 1995 to 2000 and spent the next 12 years at The Pennsylvania State University, initially as the Shaffer Associate Professor of Chemistry and later as the Eberly Professor of Biotechnology. In 2012 she became the Swanlund Chair and professor of chemistry at the University of Illinois Urbana–Champaign. Dr. Hammes-Schiffer's research centers on the investigation of electron, proton, and proton-coupled electron transfer reactions in chemical, biological, and interfacial processes. Her work encompasses the development of analytical theories and computational methods, as well as applications to a wide range of experimentally relevant systems.

Thomas B. Rauchfuss was born in 1949 in Baltimore, MD. He received his undergraduate degree from the University of Puget Sound (1971) and his Ph.D. from Washington State University (1976). After a postdoc with David Buckingham at the Australian National

University, he started his independent career at the University of Illinois at Urbana–Champaign in 1978, where he has remained. He has also studied at the following institutions: the University of Auckland, University of Louis Pasteur, and the Technical University of Karlsruhe. His research focuses on synthetic inorganic and organometallic chemistry, with an emphasis on environmentally motivated themes. For the past decade, his group has conducted research on synthetic modeling of the active sites of the hydrogenase enzymes.

APPENDIX

A.1. Proposed Pyramidal Inversion of Azadithiolate During Catalysis

Figure 58 shows proton transport to and from the [2Fe] site in [FeFe]-H_2ase.

A.2. Determining the pK_a of a Metal Hydride

If titrating a metal hydride MH^+ with a base B[50,51]

$$\begin{gathered}
\mathrm{MH^+ + B \rightleftharpoons BH^+ + M} \\
K_{\mathrm{eq}} = \text{unknown equilibrium constant} \\
\mathrm{MH^+ \rightleftharpoons M + H^+} \\
K_{\mathrm{a}}(\mathrm{MH^+}) = \text{unknown acid dissociation constant} \\
\mathrm{BH^+ \rightleftharpoons B + H^+} \\
K_{\mathrm{a}}(\mathrm{BH^+}) = \text{known acid dissociation constant (ref 51)} \\
\mathrm{BH^+ + B \rightleftharpoons BHB^+} \\
K_{\mathrm{f}}(\mathrm{BH^+}) = \text{known acid homoconjugation constant (ref 50)}
\end{gathered}$$

1. A known amount of base B (=$[B]_{total}$) is added to a known amount of MH^+. The values $[MH^+]$ and [M] in solution are determined, typically using IR or NMR spectroscopy with an internal standard.

2. $[BH^+]$ is determined according to

$$\begin{gathered}
[\mathrm{BH^+}]^2 + \{[\mathrm{B}]_{\mathrm{total}} - 2[\mathrm{M}] + 1/K_{\mathrm{f}}(\mathrm{BH^+})\}[\mathrm{BH^+}] \\
- [\mathrm{M}]/K_{\mathrm{f}}(\mathrm{BH^+}) = 0 \\
\Rightarrow [\mathrm{BH^+}] = \{\{\{[\mathrm{B}]_{\mathrm{total}} - 2[\mathrm{M}] + 1/K_{\mathrm{f}}(\mathrm{BH^+})\}^2 \\
+ 4[\mathrm{M}]/K_{\mathrm{f}}(\mathrm{BH^+})\}^{1/2} - \{[\mathrm{B}]_{\mathrm{total}} \\
- 2[\mathrm{M}] + 1/K_{\mathrm{f}}(\mathrm{BH^+})\}\}/2
\end{gathered}$$

3. $[BHB^+]$ is determined using mass balance on M:

$$\begin{gathered}
[\mathrm{MH^+}]_{\mathrm{initial}} = [\mathrm{M}] + [\mathrm{MH^+}] \\
[\mathrm{MH^+}]_{\mathrm{initial}} = [\mathrm{BH^+}] + [\mathrm{MH^+}] + [\mathrm{BHB^+}] \\
[\mathrm{M}] = [\mathrm{BH^+}] + [\mathrm{BHB^+}] \\
\Rightarrow [\mathrm{BHB^+}] = [\mathrm{M}] - [\mathrm{BH^+}]
\end{gathered}$$

4. [B] is determined using mass balance on B:

$$[\mathrm{B}] = [\mathrm{B}]_{\mathrm{total}} - \left[\mathrm{BH}^{+}\right] - 2\left[\mathrm{BHB}^{+}\right]$$

5. All the values [B], [BH^+], [M], and [MH^+] are now known such that K_{eq} and thus $pK_a(MH^+) = pK_{eq} + pK_a(BH^+)$ can be computed.

If titrating a metal complex M with a weak acid HA:

$$\mathrm{M} + \mathrm{HA} \rightleftharpoons \mathrm{MH}^{+} + \mathrm{A}^{-}$$
$$K_{\mathrm{eq}} = \text{unknown equilibrium constant}$$
$$\mathrm{MH}^{+} \rightleftharpoons \mathrm{M} + \mathrm{H}^{+}$$
$$K_{\mathrm{a}}\left(\mathrm{MH}^{+}\right) = \text{unknown acid dissociation constant}$$
$$\mathrm{HA} \rightleftharpoons \mathrm{H}^{+} + \mathrm{A}^{-}$$
$$K_{\mathrm{a}}\left(\mathrm{HA}\right) = \text{known acid dissociation constant}$$
$$\mathrm{HA} + \mathrm{A}^{-} \rightleftharpoons \mathrm{AHA}^{-}$$
$$K_{\mathrm{f}}\left(\mathrm{HA}\right) = \text{known acid homoconjugation constant}$$

1. A known amount of acid HA (=$[A^-]_{total}$) is added to a known amount of M. The values [MH^+] and [M] in solution are determined, typically using IR or NMR spectroscopy with an internal standard present.

2. [A^-] is determined according to

$$\begin{gathered}\left[\mathrm{A}^{-}\right]^{2} + \left\{\left[\mathrm{A}^{-}\right]_{\mathrm{total}} - 2\left[\mathrm{MH}^{+}\right] + 1/K_{\mathrm{f}}(\mathrm{HA})\right\}\left[\mathrm{A}^{-}\right] \\ - \left[\mathrm{MH}^{+}\right]/K_{\mathrm{f}}\left(\mathrm{HA}\right) = 0 \\ \Rightarrow \left[\mathrm{A}^{-}\right] = \left\{\left\{\left\{\left[\mathrm{A}^{-}\right]_{\mathrm{total}} - 2\left[\mathrm{MH}^{+}\right] + 1/K_{\mathrm{f}}(\mathrm{HA})\right\}^{2}\right. \\ \left. + 4\left[\mathrm{MH}^{+}\right]/K_{\mathrm{f}}(\mathrm{HA})\right\}^{1/2} - \left\{\left[\mathrm{A}^{-}\right]_{\mathrm{total}} - 2\left[\mathrm{MH}^{+}\right] \\ + 1/K_{\mathrm{f}}(\mathrm{HA})\right\}\}/2\end{gathered}$$

3. [AHA^-] is determined using mass balance on A^-:

$$\left[\mathrm{A}^{-}\right]_{\mathrm{total}} = \left[\mathrm{A}^{-}\right] + \left[\mathrm{HA}\right] + 2\left[\mathrm{AHA}^{-}\right]$$

One does not directly know [HA], but the H^+ from reacted HA formed either [MH^+] or [AHA^-] (mass balance on H^+):

$$\left[\mathrm{MH}^{+}\right] + \left[\mathrm{AHA}^{-}\right] = \left[\mathrm{A}^{-}\right]_{\mathrm{total}} - \left[\mathrm{HA}\right]$$

and

$$\left[\mathrm{HA}\right] = \left[\mathrm{A}^{-}\right]_{\mathrm{total}} - \left[\mathrm{MH}^{+}\right] - \left[\mathrm{AHA}^{-}\right]$$

Substituting this expression for [HA] into the mass balance above:

$$[\mathrm{AHA}^-] = [\mathrm{MH}^+] - [\mathrm{A}^-]$$

4. [HA] is then computed from the mass balance:

$$[\mathrm{HA}] = [\mathrm{A}^-]_{\mathrm{total}} - [\mathrm{A}^-] - 2[\mathrm{AHA}^-]$$

5. All the values [A⁻], [HA], [M], and [MH⁺] are now known such that K_{eq} and thus $pK_a(MH^+) = pK_a(HA) - pK_{eq}$ can be computed.

A.3. Expressions for Hydricity and H Atom Donation

The hydricity of a metal hydride MH⁺ can be determined by thermodynamic cycles.[53,58,59] If the potentials $E_{1/2}[M]^{+/0}$ and $E_{1/2}[M]^{2+/+}$ are known, one can sum the four reactions

$$\begin{gathered}\mathrm{MH}^+ \rightleftharpoons \mathrm{M} + \mathrm{H}^+ \\ \mathrm{M} \rightleftharpoons \mathrm{M}^+ + \mathrm{e}^- \\ \mathrm{M}^+ \rightleftharpoons \mathrm{M}^{2+} + \mathrm{e}^- \\ \mathrm{H}^+ + 2\mathrm{e}^- \rightleftharpoons \mathrm{H}^-\end{gathered}$$

This affords

$$\mathrm{MH}^+ \rightleftharpoons \mathrm{M}^{2+} + \mathrm{H}^- \quad \text{(A9)}$$

Summing the free energy changes for the four reactions gives the change for eq A9:

$$\begin{aligned}\Delta G^\circ(\mathrm{H}^-) = (RT/\log_{10}\mathrm{e})pK_a + FE_{1/2}([\mathrm{M}]^{+/0}) \\ + FE_{1/2}([\mathrm{M}]^{2+/+}) - 2FE_{1/2}([\mathrm{H}]^{+/-})\end{aligned} \quad \text{(A10)}$$

where F = 96 485 C mol^{-1}, R = 8.314 J K^{-1} mol^{-1}, e = 2.718… and T is reported in kelvin.

Note that the last term accounts for the hydricity of H_2 itself. When data are collected in MeCN at T = 298 K, and $E_{1/2}$ values are each relative to $Fc^{+/0}$, eq A10 becomes eq A10′, in which the free energy change, in kcal mol^{-1}, is

$$\begin{aligned}\Delta G^\circ(\mathrm{H}^-) = 1.37pK_a + 23.06E_{1/2}([\mathrm{M}]^{+/0}) \\ + 23.06E_{1/2}([\mathrm{M}]^{2+/+}) + 76.6\end{aligned} \quad \text{(A10′)}$$

When data are instead collected in H_2O vs NHE, eq A10″ is appropriate:

$$\begin{aligned}\Delta G^\circ(\mathrm{H}^-) = 1.37pK_a + 23.06E_{1/2}([\mathrm{M}]^{+/0}) \\ + 23.06E_{1/2}([\mathrm{M}]^{2+/+}) + 34.2\end{aligned} \quad \text{(A10″)}$$

Alternatively, if the potential for the 2e$^-$ couple $E_{1/2}[\mathrm{M}]^{2+/0}$ is known, then the following equations are summed:

$$\begin{gathered}\mathrm{MH}^+ \rightleftharpoons \mathrm{M}+\mathrm{H}^+ \\ \mathrm{M} \rightleftharpoons \mathrm{M}^{2+}+2\mathrm{e}^- \\ \mathrm{H}^+ + 2\mathrm{e}^- \rightleftharpoons \mathrm{H}^-\end{gathered}$$

This once more gives eq A9, the free energy change of which is now equated in terms of

$$\begin{gathered}\Delta G^\circ(\mathrm{H}^-) = (RT/\log_{10}\mathrm{e})\mathrm{p}K_\mathrm{a} + 2FE_{1/2}([\mathrm{M}]^{2+/0}) \\ -2FE_{1/2}([\mathrm{H}]^{+/-})\end{gathered} \quad \text{(A11)}$$

Again, when data are collected in MeCN at T = 298 K, and $E_{1/2}$ values are each relative to Fc$^{+/0}$, eq A11 becomes eq A11′, in which the free energy change, in kcal mol^{-1}, is

$$\Delta G^\circ(\mathrm{H}^-) = 1.37\mathrm{p}K_\mathrm{a} + 46.1E_{1/2}([\mathrm{M}]^{2+/0}) + 76.6 \quad \text{(A11′)}$$

When data are instead collected in H_2O vs NHE, eq A11″ is appropriate:

$$\Delta G^\circ(\mathrm{H}^-) = 1.37\mathrm{p}K_\mathrm{a} + 46.1E_{1/2}([\mathrm{M}]^{2+/0}) + 34.2 \quad \text{(A11″)}$$

One can also consider MH$^+$ as a source of H$^\bullet$ instead of H$^+$. In this case, summing the reactions

$$\begin{gathered}\mathrm{MH}^+ \rightleftharpoons \mathrm{M}+\mathrm{H}^+ \\ \mathrm{M} \rightleftharpoons \mathrm{M}^+ + \mathrm{e}^- \\ \mathrm{H}^+ + \mathrm{e}^- \rightleftharpoons \mathrm{H}^\bullet\end{gathered}$$

affords the net conversion:

$$\mathrm{MH}^+ \rightleftharpoons \mathrm{M}^+ + \mathrm{H}^\bullet \quad \text{(A12)}$$

The free energy change of this reaction is

$$\begin{gathered}\Delta G^\circ(\mathrm{H}^\bullet) = (RT/\log_{10}\mathrm{e})\mathrm{p}K_\mathrm{a} + FE_{1/2}([\mathrm{M}]^{+/0}) \\ -FE_{1/2}([\mathrm{H}]^{+/0})\end{gathered} \quad \text{(A13)}$$

When data are collected in PhCN/MeCN at T = 298 K, and $E_{1/2}$ values are each relative to Fc$^{+/0}$, eq A13 becomes eq A13′, in which the free energy change, in kcal mol^{-1}, is

$$\Delta G^{\circ}(\mathrm{H}^{\bullet}) = 1.37\mathrm{p}K_{\mathrm{a}} + 23.06E_{1/2}([\mathrm{M}]^{+/0}) + 54.9 \quad \text{(A13}'\text{)}$$

When data are instead collected in H_2O vs NHE, eq A13″ is appropriate:

$$\Delta G^{\circ}(\mathrm{H}^{-}) = 1.37\mathrm{p}K_{\mathrm{a}} + 23.06E_{1/2}([\mathrm{M}]^{+/0}) + 52.8 \quad \text{(A13}''\text{)}$$

ABBREVIATIONS

Arg	arginine residue
adt^{2-}	azadithiolate ($^{-}SCH_2N(H)CH_2S^{-}$)
(adt^{R})$^{2-}$	substituted azadithiolate ($^{-}SCH_2N(R)$-CH_2S^{-})
BAr$^{F}_{4}$$^{-}$	$(3,5\text{-}(CF_3)_2C_6H_3)_4B^{-}$
bdt^{2-}	1,2-benzenedithiolate
Bn	benzyl
Bu	butyl
CODHase	carbon monoxide dehydrogenase
Cp^{-}	cyclopentadienide
Cp*$^{-}$	pentamethylcyclopentadienide
CV	cyclic voltammetry
Cy	cyclohexyl
Cys	cysteine residue
dcpe	1,2-bis(dicylcohexylphosphino)ethane
DBU	1,8-diazabicycloundec-7-ene
DFT	density functional theory
dmpe	1,2-bis(dimethylphosphino)ethane
dppbz	1,2-bis(diphenylphosphino)benzene
dppe	1,2-bis(diphenylphosphino)ethane
dppn	1,8-bis(diphenylphosphino)naphthalene
dppv	1,2-bis(diphenylphosphino)ethane
edt^{2-}	1,2-ethanedithiolate ($^{-}S(CH_2)_2S^{-}$)

ENDOR	electron nuclear double resonance
EPR	electron paramagnetic resonance
Et	ethyl
Fc	ferrocene
Fc*	decamethylferrocene
Fe-GP	Fe-guanylylpyridinol cofactor
FLP	frustrated Lewis pair
IR	infrared
H_2ase	hydrogenase
HER	hydrogen evolution reaction
Hmd	H_2-forming methylenetetrahydromethanopterin dehydrogenase
HYSCORE	hyperfine sublevel correlation
Lys	lysine residue
Me	methyl
methenyl-H_4MPT$^+$	methenyltetrahydromethanopterin
methylene-H_4MPT	methylenetetrahydromethanopterin
N_2ase	nitrogenase
NHE	normal hydrogen electrode
NMR	nuclear magnetic resonance
^{n}Pr	*n*-propyl
NRVS	nuclear resonance vibrational spectroscopy
OTf$^-$	triflate ($CF_3SO_3^-$)
PCET	proton-coupled electron transfer
pdpp^{2-}	1,3-propanedi(phenylphosphide) ($^-$PhP-$(CH_2)_3$PPh$^-$)
pdt^{2-}	1,3-propanedithiolate ($^-S(CH_2)_3S^-$)
Ph	phenyl
ppm	parts per million
Ser	serine residue

Tf	trifluoromethanesulfonyl
THF	tetrahydrofuran
TOF	turnover frequency
Ts	4-toluenesulfonyl

References

1. Immerdorf H. Contributions to the solution of the “nitrogen question”. Landwirtsch Jahrb. 1892; 21:281.
2. Tausz J, Donath H. On the oxidation of hydrogen and hydrocarbons by bacteria. Hoppe-Seyler’s Z Physiol Chem. 1930; 190:141.
3. Stephenson M, Stickland LH. XXVII. Hydrogenase: a bacterial enzyme activating molecular hydrogen. I. The properties of the enzyme. ochem J. 1931; 25:205–214.
4. Elsden SR. Hydrogenase 1931–1981. Trends Biochem Sci. 1981; 6:251–253.
5. Stripp ST, Happe T. How algae produce hydrogen—news from the photosynthetic hydrogenase. Dalton Trans. 2009:9960–9969. [PubMed: 19904421]
6. Thauer RK. Hydrogenases and the Global H_2 Cycle. Eur J Inorg Chem. 2011; 2011:919–921.
7. Lubitz W, Ogata H, Rüdiger O, Reijerse E. Hydrogenases. Chem Rev. 2014; 114:4081–4148. [PubMed: 24655035]
8. Frey M. Hydrogenases: Hydrogen-Activating Enzymes. Chem-BioChem. 2002; 3:153–160.
9. Shima S, Ermler U. Structure and Function of [Fe]-Hydrogenase and its Iron–Guanylylpyridinol (FeGP) Cofactor. Eur J Inorg Chem. 2011; 2011:963–972.
10. Farkas A, Farkas L, Yudkin J. The Decomposition of Sodium Formate by *Bacterium coli* in the Presence of Heavy Water. Proc R Soc London, Ser B. 1934; 115:373–379.
11. Krasna AI. Hydrogenase: properties and applications. Enzyme Microb Technol. 1979; 1:165–172.
12. Yagi T, Tsuda M, Inokuchi H. Kinetic studies on hydrogenase parahydrogen-orthohydrogen conversion and hydrogen-deuterium exchange reactions. J Biochem. 1973; 73:1069–1081. [PubMed: 4352847]
13. Pagliaro, M.; Konstandopoulos, AG. Solar Hydrogen: Fuel of the Future. RSC Publishing; 2012.
14. Peters JW, Schut GJ, Boyd ES, Mulder DW, Shepard EM, Broderick JB, King PW, Adams MWW. [FeFe]- and [NiFe]-hydrogenase diversity, mechanism, and maturation. Biochim Biophys Acta, Mol Cell Res. 2015; 1853:1350–1369.
15. Adams MWW, Stiefel EI. Organometallic iron: the key to biological hydrogen metabolism. Curr Opin Chem Biol. 2000; 4:214–220. [PubMed: 10742193]
16. Vignais PM, Billoud B. Occurrence, classification, and biological function of hydrogenases: an overview. Chem Rev. 2007; 107:4206–4272. [PubMed: 17927159]
17. Bethel, RD.; Darensbourg, MY. Bioorganometallic Chemistry: Applications in Drug Discovery, Biocatalysis, and Imaging. Jaouen, G.; Salmain, M., editors. Wiley-VCH Verlag GmbH & Co. KGaA; 2015.
18. Lawrence EJ, Clark ER, Curless LD, Courtney JM, Blagg RJ, Ingleson MJ, Wildgoose GG. Metal-free electrocatalytic hydrogen oxidation using frustrated Lewis pairs and carbon-based Lewis acids. Chem Sci. 2016; 7:2537–2543.
19. Artero V, Berggren G, Atta M, Caserta G, Roy S, Pecqueur L, Fontecave M. From enzyme maturation to synthetic chemistry: the case of hydrogenases. Acc Chem Res. 2015; 48:2380–2387. [PubMed: 26165393]
20. Darensbourg MY. Hydrogenase active sites: a new paradigm for natural product-inspired synthesis based on organometallic chemistry. Comments Inorg Chem. 2010; 31:144–152.
21. DuBois DL. Development of molecular electrocatalysts for energy storage. Inorg Chem. 2014; 53:3935–3960. [PubMed: 24555579]

22. Gloaguen F, Rauchfuss TB. Small molecule mimics of hydrogenases: hydrides and redox. Chem Soc Rev. 2009; 38:100–108. [PubMed: 19088969]
23. Heinekey DM. Hydrogenase enzymes: recent structural studies and active site models. J Organomet Chem. 2009; 694:2671–2680.
24. Simmons TR, Berggren G, Bacchi M, Fontecave M, Artero V. Mimicking hydrogenases: from biomimetics to artificial enzymes. Coord Chem Rev. 2014; 270–271:127–150.
25. Tard C, Pickett CJ. Structural and functional analogues of the active sites of the [Fe]-, [NiFe]-, and [FeFe]-hydrogenases. Chem Rev. 2009; 109:2245–2274. [PubMed: 19438209]
26. Xu T, Chen D, Hu X. Hydrogen-activating models of hydrogenases. Coord Chem Rev. 2015; 303:32–41.
27. Yang JY, Bullock RM, Rakowski DuBois M, DuBois DL. Fast and efficient molecular electrocatalysts for H_2 production: using hydrogenase enzymes as guides. MRS Bull. 2011; 36:39–47.
28. Matsumoto T, Kim K, Nakai H, Hibino T, Ogo S. Organometallic catalysts for use in a fuel cell. ChemCatChem. 2013; 5:1368–1373.
29. Matsumoto T, Kim K, Ogo S. Molecular catalysis in a fuel cell. Angew Chem, Int Ed. 2011; 50:11202–11205.
30. Tran PD, Morozan A, Archambault S, Heidkamp J, Chenevier P, Dau H, Fontecave M, Martinent A, Jousselme B, Artero V. A noble metal-free proton-exchange membrane fuel cell based on bio-inspired molecular catalysts. Chem Sci. 2015; 6:2050–2053.
31. Nakazawa H, Itazaki M. Fe–H complexes in catalysis. Top Organomet Chem. 2011; 33:27–81.
32. Crabtree RH. Dihydrogen complexation. Chem Rev. 2016; doi: 10.1021/acs.chemrev.6b00037
33. Kubas GJ. Metal–dihydrogen and σ-bond coordination: the consummate extension of the Dewar–Chatt–Duncanson model for metal–olefin π bonding. J Organomet Chem. 2001; 635:37–68.
34. Gordon JC, Kubas GJ. Perspectives on how nature employs the principles of organometallic chemistry in dihydrogen activation in hydrogenases. Organometallics. 2010; 29:4682–4701.
35. Kubas GJ. Fundamentals of H_2 binding and reactivity on transition metals underlying hydrogenase function and H_2 production and storage. Chem Rev. 2007; 107:4152–4205. [PubMed: 17927158]
36. Lill SON, Siegbahn PEM. An autocatalytic mechanism for NiFe-hydrogenase: reduction to Ni(I) followed by oxidative addition. Biochemistry. 2009; 48:1056–1066. [PubMed: 19138102]
37. Kubas GJ. Catalytic processes involving dihydrogen complexes and other sigma-bond complexes. Catal Lett. 2005; 104:79–101.
38. Rokob TA, Bakó I, Stirling A, Hamza A, Pápai I. Reactivity models of hydrogen activation by frustrated Lewis pairs: synergistic electron transfers or polarization by electric field? J Am Chem Soc. 2013; 135:4425–4437. [PubMed: 23432375]
39. Stephan DW, Erker G. Frustrated Lewis pair chemistry: development and perspectives. Angew Chem, Int Ed. 2015; 54:6400–6441.
40. Abdur-Rashid K, Fong TP, Greaves B, Gusev DG, Hinman JG, Landau SE, Lough AJ, Morris RH. An acidity scale for phosphorus-containing compounds including metal hydrides and dihydrogen complexes in THF: toward the unification of acidity scales. J Am Chem Soc. 2000; 122:9155–9171.
41. Morris RH. Estimating the acidity of transition metal hydride and dihydrogen complexes by adding ligand acidity constants. J Am Chem Soc. 2014; 136:1948–1959. [PubMed: 24410025]
42. Landau SE, Morris RH, Lough AJ. Acidic dicationic iron(II) dihydrogen complexes and compounds related by H_2 substitution. Inorg Chem. 1999; 38:6060–6068. [PubMed: 11671314]
43. Forde CE, Landau SE, Morris RH. Dicationic iron(II) complexes with dihydrogen *trans* to π-acid ligands: *trans*-$[Fe(H_2)(L)\text{-}(dppe)_2]^{2+}$ (L = CO or CNH). Is there Fe H_2 π-back bonding? J Chem Soc, Dalton Trans. 1997:1663–1664.
44. Morris RH. Brønsted-Lowry acid strength of metal hydride and dihydrogen Complexes. Chem Rev. 2016; doi: 10.1021/acs.chemrev.5b00695
45. Fong TP, Forde CE, Lough AJ, Morris RH, Rigo P, Rocchini E, Stephan T. Synthesis of the acidic dihydrogen complexes *trans*-$[M(H_2)(CN)L_2]^+$ and *trans*-$[M(H_2)(CNH)L_2]^{2+}$ where M = Fe, Ru, Os and L = dppm, dppe, dppp, depe, and dihydrogen substitution by the trifluoromethanesulfonate

anion to give *trans*-[Ru(OTf)(CN)L_2] or *trans*-[Ru(OTf)(CNH)L_2]OTf. J Chem Soc, Dalton Trans. 1999:4475–4486.

46. Chatt J, Kan CT, Leigh GJ, Pickett CJ, Stanley DR. Transition-metal binding sites and ligand parameters. J Chem Soc, Dalton Trans. 1980:2032.
47. Lever ABP. Electrochemical parametrization of metal complex redox potentials, using the ruthenium(III)/ruthenium(II) couple to generate a ligand electrochemical series. Inorg Chem. 1990; 29:1271–1285.
48. Moore EJ, Sullivan JM, Norton JR. Kinetic and thermodynamic acidity of hydrido transition-metal complexes. 3. Thermodynamic acidity of common mononuclear carbonyl hydrides. J Am Chem Soc. 1986; 108:2257–2263. [PubMed: 22175569]
49. Fourmond V, Jacques P-A, Fontecave M, Artero V. H_2 evolution and molecular electrocatalysts: determination of overpotentials and effect of homoconjugation. Inorg Chem. 2010; 49:10338–10347. [PubMed: 20964310]
50. Izutsu, K. Acid-Base Dissociation Constants in Dipolar Aprotic Solvents. Blackwell Scientific Publications; Oxford, U.K: 1990.
51. Kaljurand I, Kütt A, Sooväli L, Rodima T, Mäemets V, Leito I, Koppel IA. Extension of the self-consistent spectrophotometric basicity scale in acetonitrile to a full span of 28 pK_a units: unification of different basicity scales. J Org Chem. 2005; 70:1019–1028. [PubMed: 15675863]
52. Qi X-J, Fu Y, Liu L, Guo Q-X. Ab initio calculations of thermodynamic hydricities of transition-metal hydrides in acetonitrile. Organometallics. 2007; 26:4197–4203.
53. Berning DE, Noll BC, DuBois DL. Relative hydride, proton, and hydrogen atom transfer abilities of [HM(diphosphine)$_2$]PF_6 complexes (M = Pt, Ni). J Am Chem Soc. 1999; 121:11432–11447.
54. Tsay C, Livesay BN, Ruelas S, Yang JY. Solvation effects on transition metal hydricity. J Am Chem Soc. 2015; 137:14114–14121. [PubMed: 26466014]
55. Nimlos MR, Chang CH, Curtis CJ, Miedaner A, Pilath HM, DuBois DL. Calculated hydride donor abilities of five-coordinate transition metal hydrides [HM(diphosphine)$_2$]$^+$ (M = Ni, Pd, Pt) as a function of the bite angle and twist angle of diphosphine ligands. Organometallics. 2008; 27:2715–2722.
56. Raebiger JW, Miedaner A, Curtis CJ, Miller SM, Anderson OP, DuBois DL. Using ligand bite angles to control the hydricity of palladium diphosphine complexes. J Am Chem Soc. 2004; 126:5502–5514. [PubMed: 15113222]
57. Chen S, Rousseau R, Raugei S, Dupuis M, DuBois DL, Bullock RM. Comprehensive thermodynamics of nickel hydride bis(diphosphine) complexes: a predictive model through computations. Organometallics. 2011; 30:6108–6118.
58. Tilset M, Parker VD. Solution homolytic bond dissociation energies of organotransition-metal hydrides. J Am Chem Soc. 1989; 111:6711–6717.
59. Tilset M, Parker VD. Solution homolytic bond dissociation energies of organotransition-metal hydrides [J. Am. Chem. Soc. 1989, 111, 6711]. J Am Chem Soc. 1990; 112:2843.
60. Choi J, Pulling ME, Smith DM, Norton JR. Unusually weak metal–hydrogen bonds in HV(CO)$_4$(P–P) and their effectiveness as H• donors. J Am Chem Soc. 2008; 130:4250–4252. [PubMed: 18335937]
61. Tilset M, Fjeldahl I, Hamon J-R, Hamon P, Toupet L, Saillard J-Y, Costuas K, Haynes A. Theoretical, thermodynamic, spectroscopic, and structural studies of the consequences of one-electron oxidation on the Fe-X bonds in 17- and 18-electron Cp*Fe(dppe)X complexes (X = F, Cl, Br, I, H, CH_3. J Am Chem Soc. 2001; 123:9984–10000. [PubMed: 11592877]
62. Tilset, M. Electron Transfer in Chemistry. Balzani, V., editor. Wiley; 2001.
63. Barton BE, Rauchfuss TB. Hydride-containing models for the active site of the nickel-iron hydrogenases. J Am Chem Soc. 2010; 132:14877–14885. [PubMed: 20925337]
64. Page CC, Moser CC, Chen X, Dutton PL. Natural engineering principles of electron tunnelling in biological oxidation-reduction. Nature. 1999; 402:47–52. [PubMed: 10573417]
65. Cammack R, Fernandez VM, Hatchikian EC. [5] Nickel-iron Hydrogenases. Methods Enzymol. 1994; 243:43–68.

66. Camara JM, Rauchfuss TB. Combining acid–base, redox and substrate binding functionalities to give a complete model for the [FeFe]-hydrogenase. Nat Chem. 2011; 4:26–30. [PubMed: 22169868]

67. Tard C, Liu X, Ibrahim SK, Bruschi M, De Gioia L, Davies SC, Yang X, Wang L-S, Sawers G, Pickett CJ. Synthesis of the H-cluster framework of iron-only hydrogenase. Nature. 2005; 433:610–613. [PubMed: 15703741]

68. Connelly NG, Geiger WE. Chemical redox agents for organometallic chemistry. Chem Rev. 1996; 96:877–910. [PubMed: 11848774]

69. Pavlishchuk VV, Addison AW. Conversion constants for redox potentials measured versus different reference electrodes in acetonitrile solutions at 25 °C. Inorg Chim Acta. 2000; 298:97–102.

70. Krossing I, Raabe I. Noncoordinating anions—fact or fiction? A survey of likely candidates. Angew Chem, Int Ed. 2004; 43:2066–2090.

71. Nishida H, Takada N, Yoshimura M, Sonoda T, Kobayashi H. Tetrakis[3,5-bis(trifluoromethyl)phenyl]borate. Highly lipophilic stable anionic agent for solvent-extraction of cations. Bull Chem Soc Jpn. 1984; 57:2600–2604.

72. Geiger WE, Barrière F. Organometallic electrochemistry based on electrolytes containing weakly-coordinating fluoroarylborate anions. Acc Chem Res. 2010; 43:1030–1039. [PubMed: 20345126]

73. Rountree ES, McCarthy BD, Eisenhart TT, Dempsey JL. Evaluation of homogeneous electrocatalysts by cyclic voltammetry. Inorg Chem. 2014; 53:9983–10002. [PubMed: 25247280]

74. Best SP. Spectroelectrochemistry of hydrogenase enzymes and related compounds. Coord Chem Rev. 2005; 249:1536–1554.

75. Armstrong FA, Belsey NA, Cracknell JA, Goldet G, Parkin A, Reisner E, Vincent KA, Wait AF. Dynamic electrochemical investigations of hydrogen oxidation and production by enzymes and implications for future technology. Chem Soc Rev. 2009; 38:36–51. [PubMed: 19088963]

76. Nicholson RS, Shain I. Theory of stationary electrode polarography: single scan and cyclic methods applied to reversible, irreversible, and kinetic systems. Anal Chem. 1964; 36:706–723.

77. Savéant J-M, Vianello E. Potential-sweep chronoamperometry: kinetic currents for first-order chemical reaction parallel to electron-transfer process (catalytic currents). Electrochim Acta. 1965; 10:905–920.

78. Felton GAN, Glass RS, Lichtenberger DL, Evans DH. Iron-only hydrogenase mimics. Thermodynamic aspects of the use of electrochemistry to evaluate catalytic efficiency for hydrogen generation. Inorg Chem. 2006; 45:9181–9184. [PubMed: 17083215]

79. Roberts JAS, Bullock RM. Direct determination of equilibrium potentials for hydrogen oxidation/production by open circuit potential measurements in acetonitrile. Inorg Chem. 2013; 52:3823–3835. [PubMed: 23488870]

80. Appel AM, Helm ML. Determining the overpotential for a molecular electrocatalyst. ACS Catal. 2014; 4:630–633.

81. Felton GAN, Mebi CA, Petro BJ, Vannucci AK, Evans DH, Glass RS, Lichtenberger DL. Review of electrochemical studies of complexes containing the Fe_2S_2 core characteristic of [FeFe]-hydrogenases including catalysis by these complexes of the reduction of acids to form dihydrogen. J Organomet Chem. 2009; 694:2681–2699.

82. McCarthy BD, Martin DJ, Rountree ES, Ullman AC, Dempsey JL. Electrochemical reduction of Brønsted acids by glassy carbon in acetonitrile—implications for electrocatalytic hydrogen evolution. Inorg Chem. 2014; 53:8350–8361. [PubMed: 25076140]

83. Bard, AJ.; Faulkner, LR. Electrochemical Methods: Fundamentals and Applications. 2nd. John Wiley & Sons, Inc; Hoboken, NJ: 2001.

84. Costentin C, Drouet S, Robert M, Savéant J-M. Turnover numbers, turnover frequencies, and overpotential in molecular catalysis of electrochemical reactions. cyclic voltammetry and preparative-scale electrolysis. J Am Chem Soc. 2012; 134:11235–11242. [PubMed: 22670885]

85. Felton GAN, Vannucci AK, Chen J, Lockett LT, Okumura N, Petro BJ, Zakai UI, Evans DH, Glass RS, Lichtenberger DL. Hydrogen generation from weak acids: electrochemical and computational studies of a diiron hydrogenase mimic. J Am Chem Soc. 2007; 129:12521–12530. [PubMed: 17894491]

86. Bullock RM, Appel AM, Helm ML. Production of hydrogen by electrocatalysis: making the H–H bond by combining protons and hydrides. Chem Commun. 2014; 50:3125–3143.
87. Costentin C, Passard G, Savéant J-M. Benchmarking of homogeneous electrocatalysts: overpotential, turnover frequency, limiting turnover number. J Am Chem Soc. 2015; 137:5461–5467. [PubMed: 25757058]
88. Woińska M, Grabowsky S, Dominiak PM, WoŸniak K, Jayatilaka D. Hydrogen atoms can be located accurately and precisely by x-ray crystallography. Sci Adv. 2016; 2:e1600192. [PubMed: 27386545]
89. Ogata H, Nishikawa K, Lubitz W. Hydrogens detected by subatomic resolution protein crystallography in a [NiFe] hydrogenase. Nature. 2015; 520:571–574. [PubMed: 25624102]
90. Elias M, Liebschner D, Koepke J, Lecomte C, Guillot B, Jelsch C, Chabriere E. Hydrogen atoms in protein structures: high-resolution X-ray diffraction structure of the DFPase. BMC Res Notes. 2013; 6:308. [PubMed: 23915572]
91. Piccoli PMB, Koetzle TF, Schultz AJ. Single crystal neturon diffraction for the inorganic chemist - a practical guide. Comments Inorg Chem. 2007; 28:3–38.
92. Bau R, Drabnis MH. Structures of transition metal hydrides determined by neutron diffraction. Inorg Chim Acta. 1997; 259:27–50.
93. Gruene T, Hahn HW, Luebben AV, Meilleur F, Sheldrick GM. Refinement of macromolecular structures against neutron data with SHELXL2013. J Appl Crystallogr. 2014; 47:462–466. [PubMed: 24587788]
94. Hrobarik P, Hrobáriková V, Meier F, Repiský M, Komorovský S, Kaupp M. Relativistic four-component DFT calculations of ^{1}H NMR chemical shifts in transition-metal hydride complexes: unusual high-field shifts beyond the Buckingham–Stephens model. J Phys Chem A. 2011; 115:5654–5659. [PubMed: 21591659]
95. Lubitz W, Reijerse E, van Gastel M. [NiFe] and [FeFe] Hydrogenases studied by advanced magnetic resonance techniques. Chem Rev. 2007; 107:4331–4365. [PubMed: 17845059]
96. Whitehead JP, Gurbiel RJ, Bagyinka C, Hoffman BM, Maroney MJ. The Hydrogen Binding Site in Hydrogenase: 35-GHz ENDOR and XAS studies of the Ni-C active form and the Ni-L photoproduct. J Am Chem Soc. 1993; 115:5629–5635.
97. Socrates, G. Infrared and Raman Characteristic Group Frequencies: Tables and Charts. 3rd. Wiley; 2004.
98. Nakamoto, K. Infrared and Raman Spectra of Inorganic and Coordination Compounds. 4th. Wiley; 1986.
99. Sturhahn W. Nuclear resonant spectroscopy. J Phys Condens Matter. 2004; 16:S497–S530.
100. Sturhahn W, Toellner TS, Alp EE, Zhang X, Ando M, Yoda Y, Kikuta S, Seto M, Kimball CW, Dabrowski B. Phonon density of states measured by inelastic nuclear resonant scattering. Phys Rev Lett. 1995; 74:3832–3835. [PubMed: 10058308]
101. Seto M, Yoda Y, Kikuta S, Zhang XW, Ando M. Observation of nuclear resonant scattering accompanied by phonon excitation using synchrotron radiation. Phys Rev Lett. 1995; 74:3828–3831. [PubMed: 10058307]
102. Yoda Y, Yabashi M, Izumi K, Zhang XW, Kishimoto S, Kitao S, Seto M, Mitsui T, Harami T, Imai Y, Kikuta S. Nuclear resonant scattering beamline at SPring-8. Nucl Instrum Methods Phys Res, Sect A. 2001; 467–478:715–718.
103. Ogata H, Krämer T, Wang H, Schilter D, Pelmenschikov V, van Gastel M, Neese F, Rauchfuss TB, Gee LB, Scott AD, et al. Hydride bridge in [NiFe]-hydrogenase observed by nuclear resonance vibrational spectroscopy. Nat Commun. 2015; 6:7890–7897. [PubMed: 26259066]
104. Kamali S, Wang H, Mitra D, Ogata H, Lubitz W, Manor BC, Rauchfuss TB, Byrne D, Bonnefoy V, Jenny FE Jr, et al. Observation of the Fe–CN and Fe–CO vibrations in the active site of [NiFe] hydrogenase by nuclear resonance vibrational spectroscopy. Angew Chem, Int Ed. 2013; 52:724–728.
105. Nibbering ETJ, Fidder H, Pines E. Ultrafast chemistry: using time-resolved vibrational spectroscopy for interrogation of structural dynamics. Annu Rev Phys Chem. 2005; 56:337–367. [PubMed: 15796704]

106. Hunt NT, Wright JA, Pickett C. Detection of transient intermediates generated from subsite analogues of [FeFe] hydrogenases. Inorg Chem. 2016; 55:399–410. [PubMed: 26689103]

107. Greene BL, Wu C-H, McTernan PM, Adams MWW, Dyer RB. Proton-coupled electron transfer dynamics in the catalytic mechanism of a [NiFe]-hydrogenase. J Am Chem Soc. 2015; 137:4558–4566. [PubMed: 25790178]

108. Jablonskytë A, Wright JA, Fairhurst SA, Peck JNT, Ibrahim SK, Oganesyan VS, Pickett CJ. Paramagnetic bridging hydrides of relevance to catalytic hydrogen evolution at metallosulfur centers. J Am Chem Soc. 2011; 133:18606–18609. [PubMed: 22035325]

109. Vidossich P, Magistrato A. QM/MM molecular dynamics studies of metal binding proteins. Biomolecules. 2014; 4:616–645. [PubMed: 25006697]

110. Dal Peraro M, Ruggerone P, Raugei S, Gervasio FL, Carloni P. Investigating biological systems using first principles Car–Parrinello molecular dynamics simulations. Curr Opin Struct Biol. 2007; 17:149–156. [PubMed: 17419051]

111. Lin H, Truhlar DG. QM/MM: what have we learned, where are we, and where do we go from here? Theor Chem Acc. 2007; 117:185–199.

112. van der Kamp MW, Mulholland AJ. Combined quantum mechanics/molecular mechanics (QM/MM) methods in computational enzymology. Biochemistry. 2013; 52:2708–2728. [PubMed: 23557014]

113. Saunders MG, Voth GA. Coarse-graining methods for computational biology. Annu Rev Biophys. 2013; 42:73–93. [PubMed: 23451897]

114. Finkelmann AR, Stiebritz MT, Reiher M. Kinetic modeling of hydrogen conversion at [Fe] hydrogenase active-site models. J Phys Chem B. 2013; 117:4806–4817. [PubMed: 23560849]

115. Ginovska-Pangovska B, Ho M-H, Linehan JC, Cheng Y, Dupuis M, Raugei S, Shaw WJ. Molecular dynamics study of the proposed proton transport pathways in [FeFe]-hydrogenase. Biochim Biophys Acta, Bioenerg. 2014; 1837:131–138.

116. Sumner I, Voth GA. Proton transport pathways in [NiFe]-Hydrogenase. J Phys Chem B. 2012; 116:2917–2926. [PubMed: 22309090]

117. Kohn W, Sham LJ. Self-consistent equations including exchange and correlation effects. Phys Rev. 1965; 140:A1133–A1138.

118. Parr, RG.; Yang, W. Density-Functional Theory of Atoms and Molecules. Oxford University Press; New York: 1989.

119. Bruschi M, Zampella G, Fantucci P, De Gioia L. DFT investigations of models related to the active site of [NiFe] and [Fe] hydrogenases. Coord Chem Rev. 2005; 249:1620–1640.

120. Siegbahn PEM, Tye JW, Hall MB. Computational studies of [NiFe] and [FeFe] hydrogenases. Chem Rev. 2007; 107:4414–4435. [PubMed: 17927160]

121. Greco, C.; De Gioia, L. Bioinspired Catalysis. Wiley-VCH Verlag GmbH & Co. KGaA; 2014.

122. Jensen KP, Roos BO, Ryde U. Performance of density functionals for first row transition metal systems. J Chem Phys. 2007; 126:014103. [PubMed: 17212486]

123. Bühl M, Reimann C, Pantazis DA, Bredow T, Neese F. Geometries of third-row transition-metal complexes from density-functional theory. J Chem Theory Comput. 2008; 4:1449–1459. [PubMed: 26621431]

124. Narendrapurapu BS, Richardson NA, Copan AV, Estep ML, Yang Z, Schaefer HF III. Investigating the effects of basis set on metal–metal and metal–ligand bond distances in stable transition metal carbonyls: performance of correlation consistent basis sets with 35 density functionals. J Chem Theory Comput. 2013; 9:2930–2938. [PubMed: 26583976]

125. Lee C, Yang W, Parr RG. Development of the Colic-Salvetti correlation-energy formula into a functional of the electron density. Phys Rev B: Condens Matter Mater Phys. 1988; 37:785–789.

126. Becke AD. Density-functional thermochemistry. III. The role of exact exchange. J Chem Phys. 1993; 98:5648–5652.

127. Perdew JP. Density-functional approximation for the correlation energy of the inhomogeneous electron gas. Phys Rev B: Condens Matter Mater Phys. 1986; 33:8822–8824.

128. Becke AD. Density-functional exchange-energy approximation with correct asymptotic behavior. Phys Rev A: At, Mol, Opt Phys. 1988; 38:3098–3100.

129. Perdew JP, Burke K, Ernzerhof M. Generalized gradient approximation made simple. Phys Rev Lett. 1996; 77:3865–3868. [PubMed: 10062328]
130. Perdew JP, Burke K, Ernzerhof M. Generalized gradient approximation made simple [Phys. Rev. Lett. 77, 3865 (1996)]. Phys Rev Lett. 1997; 78:1396.
131. Adamo C, Barone V. Toward reliable density functional methods without adjustable parameters: The PBE0 model. J Chem Phys. 1999; 110:6158.
132. Tao J, Perdew JP, Staroverov VN, Scuseria GE. Climbing the density functional ladder: nonempirical meta–generalized gradient approximation designed for molecules and solids. Phys Rev Lett. 2003; 91:146401. [PubMed: 14611541]
133. Zhao Y, Truhlar DG. A new local density functional for main-group thermochemistry, transition metal bonding, thermochemical kinetics, and noncovalent interactions. J Chem Phys. 2006; 125:194101. [PubMed: 17129083]
134. Chai J-D, Head-Gordon M. Long-range corrected hybrid density functionals with damped atom–atom dispersion corrections. Phys Chem Chem Phys. 2008; 10:6615–6620. [PubMed: 18989472]
135. Hariharan PC, Pople JA. Influence of polarization functions on MO hydrogenation energies. Theoret Chim Acta. 1973; 28:213–222.
136. Clark T, Chandrasekhar J, Spitznagel GW, Schleyer PVR. Efficient diffuse function-augmented basis sets for anion calculations. III.† The 3-21+G basis set for first-row elements, Li–F. J Comput Chem. 1983; 4:294–301.
137. Hay PJ, Wadt WR. Ab initio effective core potentials for molecular calculations. Potentials for K to Au including the outermost core orbitals. J Chem Phys. 1985; 82:299–310.
138. Dolg M, Wedig U, Stoll H, Preuss H. Energy-adjusted ab initio pseudopotentials for the first row transition elements. J Chem Phys. 1987; 86:866–872.
139. Frenking G, Antes I, Böhme M, Dapprich S, Ehlers AW, Jonas V, Neuhaus A, Otto M, Stegmann R, Veldkamp A, Vyboishchikov SF. Pseudopotential calculations of transition metal compounds: scope and limitations. Rev Comput Chem. 1996; 8:63–144.
140. Cramer CJ, Truhlar DG. Density functional theory for transition metals and transition metal chemistry. Phys Chem Chem Phys. 2009; 11:10757–10816. [PubMed: 19924312]
141. Solis BH, Hammes-Schiffer S. Proton-coupled electron transfer in molecular electrocatalysis: theoretical methods and design principles. Inorg Chem. 2014; 53:6427–6443. [PubMed: 24731018]
142. Miertuš S, Scrocco E, Tomasi J. Electrostatic interaction of a solute with a continuum. A direct utilizaion of ab initio molecular potentials for the prevision of solvent effects. Chem Phys. 1981; 55:117–129.
143. Miertuš S, Tomasi J. Approximate evaluations of the electrostatic free energy and internal energy changes in solution processes. Chem Phys. 1982; 65:239–245.
144. Barone V, Cossi M. Quantum calculation of molecular energies and energy gradients in solution by a conductor solvent model. J Phys Chem A. 1998; 102:1995.
145. Cossi M, Rega N, Scalmani G, Barone V. Energies, structures, and electronic properties of molecules in solution with the C-PCM solvation model. J Comput Chem. 2003; 24:669–681. [PubMed: 12666158]
146. Marenich AV, Cramer CJ, Truhlar DG. Universal solvation model based on solute electron density and on a continuum model of the solvent defined by the bulk dielectric constant and atomic surface tensions. J Phys Chem B. 2009; 113:6378–6396. [PubMed: 19366259]
147. Klamt A, Schüürmann G. COSMO: A new approach to dielectric screening in solvents with explicit expressions for the screening energy and its gradient. J Chem Soc, Perkin Trans. 1993; 2:799–805.
148. Baik M-H, Friesner RA. Computing redox potentials in solution: density functional theory as a tool for rational design of redox agents. J Phys Chem A. 2002; 106:7407–7412.
149. Tsai M-K, Rochford J, Polyansky DE, Wada T, Tanaka K, Fujita E, Muckerman JT. Characterization of redox states of $Ru(OH_2)(Q)(tpy)^{2+}$ (Q = 3,5-di-*tert*-butyl-1,2-benzoquinone, tpy = 2,2′:6′,2″-terpyridine) and related species through experimental and theoretical studies. Inorg Chem. 2009; 48:4372–4383. [PubMed: 19425612]

150. Wang T, Brudvig G, Batista VS. Characterization of proton coupled electron transfer in a biomimetic oxomanganese complex: evaluation of the DFT B3LYP level of theory. J Chem Theory Comput. 2010; 6:755–760. [PubMed: 20607115]

151. Sundstrom EJ, Yang X, Thoi VS, Karunadasa HI, Chang CJ, Long JR, Head-Gordon M. Computational and experimental study of the mechanism of hydrogen generation from water by a molecular molybdenum-oxo electrocatalyst. J Am Chem Soc. 2012; 134:5233–5242. [PubMed: 22356562]

152. Keith JA, Grice KA, Kubiak CP, Carter EA. Elucidation of the selectivity of proton-dependent electrocatalytic CO_2 reduction by *fac*-Re(bpy)$(CO)_3$Cl. J Am Chem Soc. 2013; 135:15823–15829. [PubMed: 24053131]

153. Roy LE, Batista ER, Hay PJ. Theoretical studies on the redox potentials of Fe dinuclear complexes as models for hydrogenase. Inorg Chem. 2008; 47:9228–9237. [PubMed: 18811143]

154. Roy LE, Jakubikova E, Guthrie MG, Batista ER. Calculation of one-electron redox potentials revisited. Is it possible to calculate accurate potentials with density functional methods? J Phys Chem A. 2009; 113:6745–6750. [PubMed: 19459608]

155. Muckerman JT, Fujita E. Theoretical studies of the mechanism of catalytic hydrogen production by a cobaloxime. Chem Commun. 2011; 47:12456–12458.

156. Konezny SJ, Doherty MD, Luca OR, Crabtree RH, Soloveichik GL, Batista VS. Reduction of systematic uncertainty in DFT redox potentials of transition-metal complexes. J Phys Chem C. 2012; 116:6349–6356.

157. Fernandez LE, Horvath S, Hammes-Schiffer S. Theoretical analysis of the sequential proton-coupled electron transfer mechanisms for H_2 oxidation and production pathways catalyzed by nickel molecular electrocatalysts. J Phys Chem C. 2012; 116:3171–3180.

158. Solis BH, Hammes-Schiffer S. Theoretical analysis of mechanistic pathways for hydrogen evolution catalyzed by cobaloximes. Inorg Chem. 2011; 50:11252–11262. [PubMed: 21942543]

159. Chambers GM, Huynh MT, Li Y, Hammes-Schiffer S, Rauchfuss TB, Reijerse E, Lubitz W. Models of the Ni-L and Ni-SI_a states of the [NiFe]-hydrogenase active site. Inorg Chem. 2016; 55:419–431. [PubMed: 26421729]

160. Huynh MT, Schilter D, Hammes-Schiffer S, Rauchfuss TB. Protonation of nickel–iron hydrogenase models proceeds after isomerization at nickel. J Am Chem Soc. 2014; 136:12385–12395. [PubMed: 25094041]

161. Huynh MT, Wang W, Rauchfuss TB, Hammes-Schiffer S. Characterization of singly and doubly protonated intermediates and mechanistic insights. Inorg Chem. 2014; 53:10301–10311. [PubMed: 25207842]

162. Scott AP, Radom L. Harmonic vibrational frequencies: an evaluation of Hartree-Fock, Møller-Plesset, quadratic configuration interaction, density functional theory, and semiempirical scale factors. J Phys Chem. 1996; 100:16502–16513.

163. Alecu IM, Zheng J, Zhao Y, Truhlar DG. Computational thermochemistry: scale factor databases and scale factors for vibrational frequencies obtained from electronic model chemistries. J Chem Theory Comput. 2010; 6:2872–2887. [PubMed: 26616087]

164. Neugebauer J, Hess BA. Fundamental vibrational frequencies of small polyatomic molecules from density-functional calculations and vibrational perturbation theory. J Chem Phys. 2003; 118:7215–7225.

165. Schreckenbach G, Ziegler T. Calculation of the g-tensor of electron paramagnetic resonance spectroscopy using gauge-including atomic orbitals and density functional theory. J Phys Chem A. 1997; 101:3388–3399.

166. Kaupp, M. EPR of Free Radicals in Solids I. Lund, A.; Shiotani, M., editors. Springer; New York: 2003.

167. Kaupp M, Remenyi C, Vaara J, Malkina OL, Malkin VG. Density functional calculations of electronic g-tensors for semiquinone radical anions. The role of hydrogen bonding and substituent effects. J Am Chem Soc. 2002; 124:2709–2722. [PubMed: 11890822]

168. Neese F. Prediction of electron paramagnetic resonance *g* values using coupled perturbed Hartree–Fock and Kohn–Sham theory. J Chem Phys. 2001; 115:11080.

169. Kaupp M, Reviakine R, Malkina OL, Arbuznikov A, Schimmelpfennig B, Malkin VG. Calculation of electronic g tensors for transition metal complexes using hybrid density functionals and atomic meanfield spin-orbit operators. J Comput Chem. 2002; 23:794–803. [PubMed: 12012356]

170. Neese F. Efficient and accurate approximations to the molecular spin-orbit coupling operator and their use in molecular *g*-tensor calculations. J Chem Phys. 2005; 122:034107.

171. Munzarová M, Kaupp M. A critical validation of density functional and coupled-cluster approaches for the calculation of EPR hyperfine coupling constants in transition metal complexes. J Phys Chem A. 1999; 103:9966–9983.

172. Munzarová M, Kubáček P, Kaupp M. Mechanisms of EPR hyperfine coupling in transition metal complexes. J Am Chem Soc. 2000; 122:11900–11913.

173. Neese F. Prediction of molecular properties and molecular spectroscopy with density functional theory: from fundamental theory to exchange-coupling. Coord Chem Rev. 2009; 253:526–563.

174. Zhang Y, Mao J, Oldfield E. ^{57}Fe Mössbauer isomer shifts of heme protein model systems: electronic structure calculations. J Am Chem Soc. 2002; 124:7829–7839. [PubMed: 12083937]

175. Liu T, Lovell T, Han W-G, Noodleman L. DFT calculations of isomer shifts and quadrupole splitting parameters in synthetic iron-oxo complexes: applications to methane monooxygenase and ribonucleotide reductase. Inorg Chem. 2003; 42:5244–5251. [PubMed: 12924895]

176. Sinnecker S, Slep LD, Bill E, Neese F. Performance of nonrelativistic and quasi-relativistic hybrid DFT for the prediction of electric and magnetic hyperfine parameters in ^{57}Fe Mössbauer spectra. Inorg Chem. 2005; 44:2245–2254. [PubMed: 15792459]

177. Neese F. Metal and ligand hyperfine couplings in transition metal complexes: the effect of spin–orbit coupling as studied by coupled perturbed Kohn–Sham theory. J Chem Phys. 2003; 118:3939–3948.

178. Sonnenberg, JL.; Schlegel, HB.; Hratchian, HP. Encyclopedia of Inorganic and Bioinorganic Chemistry. John Wiley & Sons, Inc; 2011.

179. Kampa M, Pandelia M-E, Lubitz W, van Gastel M, Neese F. A Metal–metal bond in the light-induced state of [NiFe] hydrogenases with relevance to hydrogen evolution. J Am Chem Soc. 2013; 135:3915–3925. [PubMed: 23402569]

180. Schilter D, Nilges MJ, Chakrabarti M, Lindahl PA, Rauchfuss TB, Stein M. Mixed-valence nickel–iron dithiolate models of the [NiFe]-hydrogenase active site. Inorg Chem. 2012; 51:2338–2348. [PubMed: 22304696]

181. Stein M, Lubitz W. Relativistic DFT calculation of the reaction cycle intermediates of [NiFe] hydrogenase: a contribution to understanding the enzymatic mechanism. J Inorg Biochem. 2004; 98:862–877. [PubMed: 15134933]

182. Stein M, van Lenthe E, Baerends EJ, Lubitz W. Relativistic DFT calculations of the paramagnetic intermediates of [NiFe] hydrogenase. implications for the enzymatic mechanism. J Am Chem Soc. 2001; 123:5839–5840. [PubMed: 11403633]

183. Stadler C, de Lacey AL, Hernández B, Fernández VM, Conesa JC. Density functional calculations for modeling the oxidized states of the active site of nickel–iron hydrogenases. 1. Verification of the method with paramagnetic Ni and Co Complexes. Inorg Chem. 2002; 41:4417–4423. [PubMed: 12184758]

184. Hsieh C-H, Erdem OF, Harman SD, Singleton ML, Reijerse E, Lubitz W, Popescu CV, Reibenspies JH, Brothers SM, Hall MB, Darensbourg MY. Structural and spectroscopic features of mixed valent $Fe^{II}Fe^{I}$ complexes and factors related to the rotated configuration of diiron hydrogenase. J Am Chem Soc. 2012; 134:13089–13102. [PubMed: 22774845]

185. Silakov A, Olsen MT, Sproules S, Reijerse EJ, Rauchfuss TB, Lubitz W. EPR/ENDOR, Mössbauer, and quantum-chemical investigations of diiron complexes mimicking the active oxidized state of [FeFe] hydrogenase. Inorg Chem. 2012; 51:8617–8628. [PubMed: 22800196]

186. Filippi G, Arrigoni F, Bertini L, De Gioia L, Zampella G. DFT Dissection of the Reduction Step in H_2 catalytic production by [FeFe]-hydrogenase inspired models: can the bridging hydride become more reactive than the terminal isomer? Inorg Chem. 2015; 54:9529–9542. [PubMed: 26359661]

187. Greco C. Towards [NiFe]-hydrogenase biomimetic models that couple H_2 binding with functionally relevant intramolecular electron transfers: a quantum chemical study. Dalton Trans. 2013; 42:13845–13854. [PubMed: 23921968]

188. Greco C. H_2 binding and splitting on a new-generation [FeFe]-hydrogenase model featuring a redox-active decamethylferrocenyl phosphine ligand: a theoretical investigation. Inorg Chem. 2013; 52:1901–1908. [PubMed: 23374093]

189. Greco C, De Gioia L. A theoretical study on the enhancement of functionally relevant electron transfers in biomimetic models of [FeFe]-hydrogenases. Inorg Chem. 2011; 50:6987–6995. [PubMed: 21728321]

190. McGlynn SE, Mulder DW, Shepard EM, Broderick JB, Peters JW. Hydrogenase cluster biosynthesis: organometallic chemistry nature's way. Dalton Trans. 2009:4274–4285. [PubMed: 19662302]

191. Pandey AS, Harris TV, Giles LJ, Peters JW, Szilagyi RK. Dithiomethylether as a ligand in the hydrogenase H-cluster. J Am Chem Soc. 2008; 130:4533–4540. [PubMed: 18324814]

192. Adams MWW. The Mechanisms of H_2 activation and CO binding by hydrogenase I and hydrogenase II of *Clostridium pasteurianum*. J Biol Chem. 1987; 262:15054–15061. [PubMed: 2822711]

193. Pierik AJ, Roseboom W, Happe RP, Bagley KA, Albracht SPJ. Carbon monoxide and cyanide as intrinsic ligands to iron in the active site of [NiFe]-hydrogenases. J Biol Chem. 1999; 274:3331–3337. [PubMed: 9920874]

194. Knörzer P, Silakov A, Foster CE, Armstrong FA, Lubitz W, Happe T. Importance of the protein framework for catalytic activity of [FeFe]-hydrogenases. J Biol Chem. 2012; 287:1489–1499. [PubMed: 22110126]

195. Chernev P, Lambertz C, Brünje A, Leidel N, Sigfridsson KGV, Kositzki R, Hsieh C-H, Yao S, Schiwon R, Driess M, Limberg C, Happe T, Haumann M. Hydride binding to the active site of [FeFe]-hydrogenase. Inorg Chem. 2014; 53:12164–12177. [PubMed: 25369169]

196. Tschierlei S, Ott S, Lomoth R. Spectroscopically characterized intermediates of catalytic H_2 formation by [FeFe] hydrogenase models. Energy Environ Sci. 2011; 4:2340–2352.

197. Kramarz KW, Norton JR. Slow Proton-Transfer Reactions in Organometallic and Bioinorganic Chemistry. Prog Inorg Chem. 1994; 42:1–65.

198. Mulder DW, Ratzloff MW, Bruschi M, Greco C, Koonce E, Peters JW, King PW. Investigations on the Role of Proton-Coupled Electron Transfer in Hydrogen Activation by [FeFe]-Hydrogenase. J Am Chem Soc. 2014; 136:15394–15402. [PubMed: 25286239]

199. Berggren G, Adamska A, Lambertz C, Simmons TR, Esselborn J, Atta M, Gambarelli S, Mouesca J-M, Reijerse E, Lubitz W, Happe T, Artero V, Fontecave M. Biomimetic assembly and activation of [FeFe]-hydrogenases. Nature. 2013; 499:66–70. [PubMed: 23803769]

200. Esselborn J, Lambertz C, Adamska-Venkatesh A, Simmons T, Berggren G, Noth J, Siebel J, Hemschemeier A, Artero V, Reijerse E, Fontecave M, Lubitz W, Happe T. Spontaneous activation of [FeFe]-hydrogenases by an inorganic [2Fe] active site mimic. Nat Chem Biol. 2013; 9:607–610. [PubMed: 23934246]

201. Siebel JF, Adamska-Venkatesh A, Weber K, Rumpel S, Reijerse E, Lubitz W. Hybrid [FeFe]-hydrogenases with modified active sites show remarkable residual enzymatic activity. Biochemistry. 2015; 54:1474–1483. [PubMed: 25633077]

202. Adamska-Venkatesh A, Krawietz D, Siebel J, Weber K, Happe T, Reijerse E, Lubitz W. New redox states observed in [FeFe] hydrogenases reveal redox coupling within the H-cluster. J Am Chem Soc. 2014; 136:11339–11346. [PubMed: 25025613]

203. Adamska A, Silakov A, Lambertz C, Rüdiger O, Happe T, Reijerse E, Lubitz W. Identification and characterization of the "super-reduced" state of the H-cluster in [FeFe] hydrogenase: a new building block for the catalytic cycle? Angew Chem, Int Ed. 2012; 51:11458–11462.

204. Popescu CV, Münck E. Electronic structure of the H cluster in [Fe]-hydrogenases. J Am Chem Soc. 1999; 121:7877–7884.

205. Silakov A, Wenk B, Reijerse E, Lubitz W. ^{14}N HYSCORE investigation of the H-cluster of [FeFe] hydrogenase: evidence for a nitrogen in the dithiol bridge. Phys Chem Chem Phys. 2009; 11:6592–6599. [PubMed: 19639134]

206. Lemon BJ, Peters JW. Binding of exogenously added carbon monoxide at the active site of the iron-only hydrogenase (CpI) from *Clostridium pasteurianum*. Biochemistry. 1999; 38:12969–12973. [PubMed: 10529166]

207. de Lacey AL, Stadler C, Cavazza C, Hatchikian EC, Fernandez VM. FTIR characterization of the active site of the Fe-hydrogenase from *Desulfovibrio desulfuricans*. J Am Chem Soc. 2000; 122:11232–11233.

208. Silakov A, Reijerse EJ, Albracht SPJ, Hatchikian EC, Lubitz W. The electronic structure of the H-cluster in the [FeFe]-hydrogenase from *Desulfovibrio desulfuricans*: a Q-band ^{57}Fe-ENDOR and HYSCORE study. J Am Chem Soc. 2007; 129:11447–11458. [PubMed: 17722921]

209. Nicolet Y, de Lacey AL, Vernède X, Fernandez VM, Hatchikian EC, Fontecilla-Camps JC. Crystallographic and FTIR spectroscopic evidence of changes in Fe coordination upon reduction of the active site of the Fe-only hydrogenase from *Desulfovibrio desulfuricans*. J Am Chem Soc. 2001; 123:1596–1601. [PubMed: 11456758]

210. Silakov A, Kamp C, Reijerse E, Happe T, Lubitz W. Spectroelectrochemical characterization of the active site of the [FeFe] hydrogenase HydA1 from *Chlamydomonas reinhardtii*. Biochemistry. 2009; 48:7780–7786. [PubMed: 19634879]

211. Baffert C, Bertini L, Lautier T, Greco C, Sybirna K, Ezanno P, Etienne E, Soucaille P, Bertrand P, Bottin H, Meynial-Salles I, De Gioia L, Léger C. CO disrupts the reduced H-cluster of FeFe hydrogenase. A combined DFT and protein film voltammetry study. J Am Chem Soc. 2011; 133:2096–2099. [PubMed: 21271703]

212. Adams MWW. The structure and mechanism of iron-hydrogenases. Biochim Biophys Acta, Bioenerg. 1990; 1020:115–145.

213. Hambourger M, Gervaldo M, Svedruzic D, King PW, Gust D, Ghirardi M, Moore AL, Moore TA. [FeFe]-hydrogenase-catalyzed H_2 production in a photoelectrochemical biofuel Cell. J Am Chem Soc. 2008; 130:2015–2022. [PubMed: 18205358]

214. Reihlen H, Gruhl A, von Hessling G. Photochemical and oxidative degradation of carbonyls. Justus Liebigs Ann Chem. 1929; 472:268–287.

215. Winter A, Zsolnai L, Huttner G. Dinuclear and trinuclear carbonyliron complexes wth 1,2- and 1,3-dithiolato bridging ligands. Z Naturforsch, B: J Chem Sci. 1982; 37:1430–1436.

216. Li Y, Rauchfuss TB. Synthesis of diiron(I) dithiolato carbonyl complexes. Chem Rev. 2016

217. Jablonskytë A, Webster LR, Simmons TR, Wright JA, Pickett CJ. Electronic control of the protonation rates of Fe–Fe bonds. J Am Chem Soc. 2014; 136:13038–13044. [PubMed: 25116589]

218. Matthews SL, Heinekey DM. A carbonyl-rich bridging hydride complex relevant to the Fe-Fe hydrogenase active site. Inorg Chem. 2010; 49:9746–9748. [PubMed: 20883039]

219. Cordero B, Gómez V, Platero-Prats AE, Revés M, Echeverría J, Cremades E, Barragán F, Alvarez S. Covalent radii revisited. Dalton Trans. 2008:2832–2838. [PubMed: 18478144]

220. Green JC, Green MLH, Parkin G. The occurrence and representation of three-centre two-electron bonds in covalent inorganic compounds. Chem Commun. 2012; 48:11481–11503.

221. Mack AE, Rauchfuss TB. (1,3-Propanedithiolato)-hexacarbonyldiiron and Cyanide Derivatives. Inorg Synth. 2010; 35:142–147.

222. Cloirec AL, Davies SC, Evans DJ, Hughes DL, Pickett CJ, Best SP, Borg S. A di-iron dithiolate possessing structural elements of the carbonyl/cyanide sub-site of the H-centre of Fe-only hydrogenase. Chem Commun. 1999:2285–2286.

223. Lyon EJ, Georgakaki IP, Reibenspies JH, Darensbourg MY. Carbon monoxide and cyanide ligands in a classical organometallic complex model for Fe-only hydrogenase. Angew Chem, Int Ed. 1999; 38:3178–3180.

224. Schmidt M, Contakes SM, Rauchfuss TB. First generation analogues of the binuclear site in the Fe-only hydrogenases: $Fe_2(\mu\text{-}SR)_2(CO)_4(CN)_2^{2-}$. J Am Chem Soc. 1999; 121:9736–9737.

225. Gloaguen F, Lawrence JD, Rauchfuss TB. Biomimetic hydrogen evolution catalyzed by an iron carbonyl thiolate. J Am Chem Soc. 2001; 123:9476–9477. [PubMed: 11562244]

226. Fauvel K, Mathieu R, Poilblanc R. Protonation of the metal-metal bond in $[\mu(SCH_3)Fe(CO)_2L]_2$ complexes (L = P-$(CH_3)_{3-x}(C_6H_5)_x$). Experimental evidence of the variation of nucleophilicity

of the metal-metal bond with donor properties of phosphorus ligands. Inorg Chem. 1976; 15:976–978.

227. Capon J-F, El Hassnaoui S, Gloaguen F, Schollhammer P, Talarmin J. N-heterocyclic carbene ligands as cyanide mimics in diiron models of the all-iron hydrogenase active site. Organometallics. 2005; 24:2020–2022.
228. Morvan D, Capon J-F, Gloaguen F, Le Goff A, Marchivie M, Michaud F, Schollhammer P, Talarmin J, Yaouanc J-J, Pichon R, Kervarec N. N-heterocyclic carbene ligands in nonsymmetric diiron models of hydrogenase active sites. Organometallics. 2007; 26:2042–2052.
229. Tye JW, Lee J, Wang H-W, Mejia-Rodriguez R, Reibenspies JH, Hall MB, Darensbourg MY. Dual electron uptake by simultaneous iron and ligand reduction in an N-heterocyclic carbene substituted [FeFe] hydrogenase model compound. Inorg Chem. 2005; 44:5550–5552. [PubMed: 16060601]
230. Liu T, Darensbourg MY. A mixed-valent, Fe(II)Fe(I), diiron complex reproduces the unique rotated state of the [FeFe]hydrogenase active site. J Am Chem Soc. 2007; 129:7008–7009. [PubMed: 17497786]
231. Singleton ML, Jenkins RM, Klemashevich CL, Darensbourg MY. The effect of bridgehead steric bulk on the ground state and intramolecular exchange processes of (μ-$SCH_2CR_2CH_2S$)-[$Fe(CO)_3$][$Fe(CO)_2$L] complexes. C R Chim. 2008; 11:861–874.
232. Boyke CA, Rauchfuss TB, Wilson SR, Rohmer M-M, Bénard M. $[Fe_2(SR)_2(\mu\text{-}CO)(CNMe)_6]^{2+}$ and analogues: a new class of diiron dithiolates as structural models for the H_{ox}^{air} state of the Fe-only hydrogenase. J Am Chem Soc. 2004; 126:15151–15160. [PubMed: 15548012]
233. Hou J, Peng X, Liu J, Gao Y, Zhao X, Gao S, Han K. A binuclear isocyanide azadithiolatoiron complex relevant to the active site of Fe-only hydrogenases: synthesis, structure and electrochemical properties. Eur J Inorg Chem. 2006; 2006:4679–4686.
234. Lawrence JD, Rauchfuss TB, Wilson SR. New class of diiron dithiolates related to the Fe-only hydrogenase active site: synthesis and characterization of $[Fe_2(SR)_2(CNMe)_7]^{2+}$ Inorg Chem. 2002; 41:6193–6195. [PubMed: 12444758]
235. Nehring JL, Heinekey DM. Dinuclear iron isonitrile complexes: models for the iron hydrogenase active site. Inorg Chem. 2003; 42:4288–4292. [PubMed: 12844300]
236. Hsieh CH, Ding S, Erdem OF, Crouthers DJ, Liu T, McCrory CCL, Lubitz W, Popescu CV, Reibenspies JH, Hall MB, Darensbourg MY. Redox active iron nitrosyl units in proton reduction electrocatalysis. Nat Commun. 2014; doi: 10.1038/ncomms4684
237. Olsen MT, Bruschi M, De Gioia L, Rauchfuss TB, Wilson SR. Nitrosyl derivatives of diiron(I) dithiolates mimic the structure and Lewis acidity of the [FeFe]-hydrogenase active site. J Am Chem Soc. 2008; 130:12021–12030. [PubMed: 18700771]
238. Allen GC, Hush NS. Intervalence-transfer absorption. Part 1. Qualitative evidence for intervalence-transfer absorption in inorganic systems in solution and in the solid state. Prog Inorg Chem. 1967; 8:357–390.
239. Robin MB, Day P. Mixed-valence chemistry: a survey and classification. Adv Inorg Chem Radiochem. 1968; 10:247–422.
240. Day P, Hush NS, Clark RJH. Mixed valence: origins and developments. Philos Trans R Soc, A. 2008; 366:5–14.
241. Singh PS, Rudbeck HC, Huang P, Ezzaher S, Eriksson L, Stein M, Ott S, Lomoth R. (I,0) Mixed-valence state of a diiron complex with pertinence to the [FeFe]-hydrogenase active site: an IR, EPR, and computational study. Inorg Chem. 2009; 48:10883–10885. [PubMed: 19888734]
242. Streich D, Astuti Y, Orlandi M, Schwartz L, Lomoth R, Hammarström L, Ott S. High-turnover photochemical hydrogen production catalyzed by a model complex of the [FeFe]-hydrogenase active site. Chem - Eur J. 2010; 16:60–63. [PubMed: 19938018]
243. Mirmohades M, Pullen S, Stein M, Maji S, Ott S, Hammarström L, Lomoth R. Direct observation of key catalytic intermediates in a photoinduced proton reduction cycle with a diiron carbonyl complex. J Am Chem Soc. 2014; 136:17366–17369. [PubMed: 25419868]
244. Keizer PN, Krusic PJ, Morton JR, Preston KF. Thiolato- and selenato-bridged dinuclear iron carbonyl radicals. J Am Chem Soc. 1991; 113:5454–5456.

245. Wang W, Nilges MJ, Rauchfuss TB, Stein M. Isolation of a mixed valence diiron hydride: evidence for a spectator hydride in hydrogen evolution catalysis. J Am Chem Soc. 2013; 135:3633–3639. [PubMed: 23383865]
246. Yang D, Li Y, Wang B, Zhao X, Su L, Chen S, Tong P, Luo Y, Qu J. Synthesis and electrocatalytic property of diiron hydride complexes derived from a thiolate-bridged diiron complex. Inorg Chem. 2015; 54:10243–10249. [PubMed: 26479581]
247. Wang W, Rauchfuss TB, Zhu L, Zampella G. New reactions of terminal hydrides on a diiron dithiolate. J Am Chem Soc. 2014; 136:5773–5782. [PubMed: 24661238]
248. Heiden ZM, Zampella G, De Gioia L, Rauchfuss TB. [FeFe]-hydrogenase models and hydrogen: oxidative addition of dihydrogen and silanes. Angew Chem, Int Ed. 2008; 47:9756–9759.
249. Justice AK, Linck RC, Rauchfuss TB, Wilson SR. Dihydrogen activation by a diruthenium analogue of the Fe-only hydrogenase active site. J Am Chem Soc. 2004; 126:13214–13215. [PubMed: 15479062]
250. Zaffaroni R, Rauchfuss TB, Gray DL, De Gioia L, Zampella G. Terminal vs bridging hydrides of diiron dithiolates: protonation of Fe_2(dithiolate)$(CO)_2(PMe_3)_4$. J Am Chem Soc. 2012; 134:19260–19269. [PubMed: 23095145]
251. Cheah MH, Borg SJ, Bondin MI, Best SP. Electrocatalytic proton reduction by phosphido-bridged diiron carbonyl compounds: distant relations to the H-cluster? Inorg Chem. 2004; 43:5635–5644. [PubMed: 15332815]
252. Ezzaher S, Capon J-F, Gloaguen F, Pétillon FY, Schollhammer P, Talarmin J, Pichon R, Kervarec N. Evidence for the formation of terminal hydrides by protonation of an asymmetric iron hydrogenase active site mimic. Inorg Chem. 2007; 46:3426–3428. [PubMed: 17397148]
253. van der Vlugt JI, Rauchfuss TB, Whaley CM, Wilson SR. Characterization of a diferrous terminal hydride mechanistically relevant to the Fe-only hydrogenases. J Am Chem Soc. 2005; 127:16012–16013. [PubMed: 16287273]
254. Pelmenschikov V, Guo Y, Wang H, Cramer SP, Case DA. Fe–H/D stretching and bending modes in nuclear resonant vibrational, Raman and infrared spectroscopies: Comparisons of density functional theory and experiment. Faraday Discuss. 2011; 148:409–420. [PubMed: 21322496]
255. Brookhart M, Grant B, Volpe AF Jr. $[(3,5\text{-}(CF_3)_2C_6H_3)_4B]^-[H(OEt_2)_2]^+$: a convenient reagent for generation and stabilization of cationic, highly electrophilic organometallic complexes. Organometallics. 1992; 11:3920–3922.
256. Bertini L, Fantucci P, De Gioia L, Zampella G. Excited state properties of diiron dithiolate hydrides: implications in the unsensitized photocatalysis of H_2 evolution. Inorg Chem. 2013; 52:9826–9841. [PubMed: 23952259]
257. Zampella G, Fantucci P, De Gioia L. DFT characterization of the reaction pathways for terminal-to μ-hydride isomerisation in synthetic models of the [FeFe]-hydrogenase active site. Chem Commun. 2009; 46:8824–8826.
258. Carroll ME, Barton BE, Rauchfuss TB, Carroll PJ. Synthetic models for the active site of the [FeFe]-hydrogenase: catalytic proton reduction and the structure of the doubly protonated intermediate. J Am Chem Soc. 2012; 134:18843–18852. [PubMed: 23126330]
259. Barton BE, Rauchfuss TB. Terminal hydride in [FeFe]-hydrogenase model has lower potential for H_2 production than the isomeric bridging hydride. Inorg Chem. 2008; 47:2261–2263. [PubMed: 18333613]
260. Zampella G, Fantucci P, De Gioia L. Unveiling how stereoelectronic factors affect kinetics and thermodynamics of protonation regiochemistry in [FeFe] hydrogenase synthetic models: a DFT investigation. J Am Chem Soc. 2009; 131:10909–10917. [PubMed: 19621919]
261. Dong W, Wang M, Liu X, Jin K, Li G, Wang F, Sun L. An insight into the protonation property of a diiron azadithiolate complex pertinent to the active site of Fe-only hydrogenases. Chem Commun. 2006:305–307.
262. Ezzaher S, Gogoll A, Bruhn C, Ott S. Directing protonation in [FeFe] hydrogenase active site models by modifications in their second coordination sphere. Chem Commun. 2010; 46:5775–5777.

263. Jordan RF, Norton JR. Kinetic and Thermodynamic acidity of hydrido transition-metal complexes. 1. Periodic trends in group 6 complexes and substituent effects in osmium complexes. J Am Chem Soc. 1982; 104:1255–1263.

264. Barton BE, Zampella G, Justice AK, De Gioia L, Rauchfuss TB, Wilson SR. Isomerization of the hydride complexes $[HFe_2(SR)_2(PR_3)_x(CO)_{6-x}]^+$ ($x = 2, 3, 4$) relevant to the active site models for the [FeFe]-hydrogenases. Dalton Trans. 2010; 39:3011–3019. [PubMed: 20221534]

265. Zaffaroni R, Rauchfuss TB, Fuller A, De Gioia L, Zampella G. Contrasting protonation behavior of diphosphido vs dithiolato diiron(I) carbonyl complexes. Organometallics. 2013; 32:232–238.

266. Wang W, Rauchfuss TB, Moore CE, Rheingold AL, De Gioia L, Zampella G. Crystallographic characterization of a fully rotated, basic diiron dithiolate: model for the H_{red} state? Chem - Eur J. 2013; 19:15476–15479. [PubMed: 24130068]

267. Munery S, Capon J-F, De Gioia L, Elleouet C, Greco C, Pétillon FY, Schollhammer P, Talarmin J, Zampella G. New Fe^{I}–Fe^{I} complex featuring a rotated conformation related to the $[2Fe]_H$ subsite of [Fe–Fe] hydrogenase. Chem - Eur J. 2013; 19:15458–15461. [PubMed: 24127299]

268. Finkelmann AR, Stiebritz MT, Reiher M. Inaccessibility of the μ-hydride species in [FeFe] hydrogenases. Chem Sci. 2014; 5:215–221.

269. Angamuthu R, Chen C-S, Cochrane TR, Gray DL, Schilter D, Ulloa OA, Rauchfuss TB. N-Substituted derivatives of the azadithiolate cofactor from the [FeFe] hydrogenases: stability and complexation. Inorg Chem. 2015; 54:5717–5724. [PubMed: 26000618]

270. Li H, Rauchfuss TB. Iron carbonyl sulfides, formaldehyde, and amines condense to give the proposed azadithiolate cofactor of the Fe-only hydrogenases. J Am Chem Soc. 2002; 124:726–727. [PubMed: 11817928]

271. Lawrence JD, Li H, Rauchfuss TB, Benard M, Rohmer M-M. Diiron azadithiolates as models for the iron-only hydrogenase active site: synthesis, structure, and stereoelectronics. Angew Chem, Int Ed. 2001; 40:1768–1771.

272. Gilbert-Wilson R, Siebel JF, Adamska-Venkatesh A, Pham CC, Reijerse E, Wang H, Cramer SP, Lubitz W, Rauchfuss TB. Spectroscopic investigations of [FeFe] hydrogenase maturated with $[^{57}Fe_2(adt)(CN)_2(CO)_4]^{2-}$. J Am Chem Soc. 2015; 137:8998–9005. [PubMed: 26091969]

273. Belkova NV, Epstein LM, Filippov OA, Shubina ES. Hydrogen and dihydrogen bonds in the reactions of metal hydrides. Chem Rev. 2016

274. Yang X, Hall MB. Monoiron hydrogenase catalysis: hydrogen activation with the formation of a dihydrogen, $Fe–H^{\delta-}\cdots H^{\delta+}–O$, bond and methenyl-$H_4MPT^+$ triggered hydride transfer. J Am Chem Soc. 2009; 131:10901–10908. [PubMed: 19722671]

275. Gloaguen F. Electrochemistry of simple organometallic models of iron–iron hydrogenases in organic solvent and water. Inorg Chem. 2016; 55:390–398. [PubMed: 26641526]

276. Capon J-F, Gloaguen F, Pétillon FY, Schollhammer P, Talarmin J. Electron and proton transfers at diiron dithiolate sites relevant to the catalysis of proton reduction by the [FeFe]-hydrogenases. Coord Chem Rev. 2009; 253:1476–1494.

277. Pandey IK, Natarajan M, Kaur-Ghumaan S. Hydrogen generation: aromatic dithiolate-bridged metal carbonyl complexes as hydrogenase catalytic site models. J Inorg Biochem. 2015; 143:88–110. [PubMed: 25528677]

278. Borg SJ, Behrsing T, Best SP, Razavet M, Liu X, Pickett CJ. Electron transfer at a dithiolate-bridged diiron assembly: electrocatalytic hydrogen evolution. J Am Chem Soc. 2004; 126:16988–16999. [PubMed: 15612737]

279. Borg SJ, Bondin MI, Best SP, Razavet M, Liu X, Pickett CJ. Electrocatalytic proton reduction by dithiolate- bridged diiron carbonyl complexes: a connection to the H-cluster? Biochem Soc Trans. 2005; 33:3–6. [PubMed: 15667249]

280. Greco C, Zampella G, Bertini L, Bruschi M, Fantucci P, De Gioia L. Insights into the mechanism of electrocatalytic hydrogen evolution mediated by $Fe_2(S_2C_3H_6)(CO)_6$: the simplest functional model of the Fe-hydrogenase active site. Inorg Chem. 2007; 46:108–116. [PubMed: 17198418]

281. Bullock RM, Helm ML. Molecular electrocatalysts for oxidation of hydrogen using earth-abundant metals: shoving protons around with proton relays. Acc Chem Res. 2015; 48:2017–2026. [PubMed: 26079983]

282. Capon J-F, Ezzaher S, Gloaguen F, Pétillon FY, Schollhammer P, Talarmin J. Electrochemical insights into the mechanisms of proton reduction by $[Fe_2(CO)_6\{\mu\text{-}SCH_2N(R)CH_2S\}]$ complexes related to the $[2Fe]_H$ subsite of [FeFe]hydrogenase. Chem -Eur J. 2008; 14:1954–1964. [PubMed: 18067109]
283. Ezzaher S, Capon J-F, Dumontet N, Gloaguen F, Pétillon FY, Schollhammer P, Talarmin J. Electrochemical study of the role of a H-bridged, unsymmetrically disubstituted diiron complex in proton reduction catalysis. J Electroanal Chem. 2009; 626:161–170.
284. Becker R, Amirjalayer S, Li P, Woutersen S, Reek JNH. An iron-iron hydrogenase mimic with appended electron reservoir for efficient proton reduction in aqueous media. Sci Adv. 2016; 2:e1501014. [PubMed: 26844297]
285. Zhao X, Georgakaki IP, Miller ML, Mejia-Rodriguez R, Chiang C-Y, Darensbourg MY. Catalysis of H_2/D_2 scrambling and other H/D exchange processes by [Fe]-hydrogenase model complexes. Inorg Chem. 2002; 41:3917–3928. [PubMed: 12132916]
286. Razavet M, Borg SJ, George SJ, Best SP, Fairhurst SA, Pickett CJ. Transient FTIR spectroelectrochemical and stopped-flow detection of a mixed valence {Fe(I)–Fe(II)} bridging carbonyl intermediate with structural elements and spectroscopic characteristics of the di-iron sub-site of all-iron hydrogenase. Chem Commun. 2002:700–701.
287. Justice AK, Rauchfuss TB, Wilson SR. Unsaturated, mixed-valence Diiron dithiolate model for the H_{ox} state of the [FeFe]-hydrogenase. Angew Chem, Int Ed. 2007; 46:6152–6154.
288. Barton BE, Olsen MT, Rauchfuss TB. Aza- and oxadithiolates are probable proton relays in functional models for the [FeFe]-hydrogenases. J Am Chem Soc. 2008; 130:16834–16835. [PubMed: 19053433]
289. Esselborn J, Muraki N, Klein K, Engelbrecht V, Metzler-Nolte N, Apfel U-P, Hofmann E, Kurisu G, Happe T. A structural view of synthetic cofactor integration into [FeFe]-hydrogenases. Chem Sci. 2016; 7:959–968.
290. Olsen MT, Barton BE, Rauchfuss TB. Hydrogen activation by biomimetic diiron dithiolates. Inorg Chem. 2009; 48:7507–7509. [PubMed: 19603776]
291. Camara JM, Rauchfuss TB. Mild redox complementation enables H_2 activation by [FeFe]-hydrogenase models. J Am Chem Soc. 2011; 133:8098–8101. [PubMed: 21548619]
292. Lansing JC, Camara JM, Gray DL, Rauchfuss TB. Hydrogen production catalyzed by bidirectional, biomimetic models of the [FeFe]-hydrogenase active site. Organometallics. 2014; 33:5897–5906. [PubMed: 25364093]
293. Ghosh S, Hogarth G, Hollingsworth N, Holt KB, Kabir SE, Sanchez BE. Hydrogenase biomimetics: $Fe_2(CO)_4(\mu\text{-dppf})(\mu\text{-pdt})$(dppf = 1,1′-bis(diphenylphosphino)ferrocene) both a proton-reduction and hydrogen oxidation catalyst. Chem Commun. 2014; 50:945–947.
294. Ezzaher S, Capon J-F, Gloaguen F, Pétillon FY, Schollhammer P, Talarmin J, Kervarec N. Influence of a pendant amine in the second coordination sphere on proton transfer at a dissymmetrically disubstituted diiron system related to the $[2Fe]_H$ subsite of $[FeFe]H_2$ase. Inorg Chem. 2009; 48:2–4. [PubMed: 19053348]
295. Wang N, Wang M, Zhang T, Li P, Liu J, Sun L. A proton–hydride diiron complex with a base-containing diphosphine ligand relevant to the [FeFe]-hydrogenase active site. Chem Commun. 2008:5800–5802.
296. Wang N, Wang M, Wang Y, Zheng D, Han H, Ahlquist MSG, Sun L. Catalytic activation of H_2 under mild conditions by an [FeFe]-hydrogenase model via an active μ-hydride species. J Am Chem Soc. 2013; 135:13688–13691. [PubMed: 24001095]
297. Rauchfuss TB. Diiron azadithiolates as models for the [FeFe]-hydrogenase active site and paradigm for the role of the second coordination sphere. Acc Chem Res. 2015; 48:2107–2116. [PubMed: 26079848]
298. Leroux F, Dementin S, Burlat B, Cournac L, Volbeda A, Champ S, Martin L, Guigliarelli B, Bertrand P, Fontecilla-Camps J, Rousset M, Léger C. Experimental approaches to kinetics of gas diffusion in hydrogenase. Proc Natl Acad Sci U S A. 2008; 105:11188–11193. [PubMed: 18685111]

299. Goy R, Bertini L, Elleouet C, Görls H, Zampella G, Talarmin J, De Gioia L, Schollhammer P, Apfel U-P, Weigand W. A sterically stabilized Fe^{I}–Fe^{I} semi-rotated conformation of [FeFe] hydrogenase subsite model. Dalton Trans. 2015; 44:1690–1699. [PubMed: 25436832]
300. Liu T, DuBois DL, Bullock RM. An iron complex with pendent amines as a molecular electrocatalyst for oxidation of hydrogen. Nat Chem. 2013; 5:228–233. [PubMed: 23422565]
301. Vignais PM, Billoud B, Meyer J. Classification and phylogeny of hydrogenases. FEMS Microbiol Rev. 2001; 25:455–501. [PubMed: 11524134]
302. Shafaat HS, Rüdiger O, Ogata H, Lubitz W. [NiFe] hydrogenases: a common active site for hydrogen metabolism under diverse conditions. Biochim Biophys Acta, Bioenerg. 2013; 1827:986–1002.
303. Volbeda A, Charon M-H, Piras C, Hatchikian EC, Frey M, Fontecilla-Camps JC. Crystal structure of the nickel-iron hydrogenase from *Desulfovibrio gigas*. Nature. 1995; 373:580–587. [PubMed: 7854413]
304. Higuchi Y, Yagi T, Yasuoka N. Unusual ligand structure in Ni–Fe active center and an additional Mg site in hydrogenase revealed by high resolution X-ray structure analysis. Structure. 1997; 5:1671–1680. [PubMed: 9438867]
305. Volbeda A, Darnault C, Parkin A, Sargent F, Armstrong FA, Fontecilla-Camps JC. Crystal structure of the O_2-tolerant membrane-bound hydrogenase 1 from Escherichia coli in complex with its cognate cytochrome *b*. Structure. 2013; 21:184–190. [PubMed: 23260654]
306. Addison AW, Rao TN, Reedijk J, van Rijn J, Verschoor GC. Synthesis, structure, and spectroscopic properties of copper(II) compounds containing nitrogen-sulphur donor ligands; the crystal and molecular structure of aqua[1,7-bis(N-methylbenzimidazol-2′-yl)-2,6-dithiaheptane]copper(II) perchlorate. J Chem Soc, Dalton Trans. 1984:1349–1356.
307. Murphy BJ, Hidalgo R, Roessler MM, Evans RM, Ash PA, Myers WK, Vincent KA, Armstrong FA. Discovery of dark pH-dependent H^+ migration in a [NiFe]-hydrogenase and its mechanistic relevance: mobilizing the hydrido ligand of the Ni-C intermediate. J Am Chem Soc. 2015; 137:8484–8489. [PubMed: 26103582]
308. Amara P, Volbeda A, Fontecilla-Camps JC, Field MJ. A hybrid density functional theory/molecular mechanics study of nickel-iron hydrogenase: investigation of the active site redox states. J Am Chem Soc. 1999; 121:4468–4477.
309. Niu S, Thomson LM, Hall MB. Theoretical characterization of the reaction intermediates in a model of the nickel-iron hydrogenase of *Desulfovibrio gigas*. J Am Chem Soc. 1999; 121:4000–4007.
310. Yson RL, Gilgor JL, Guberman BA, Varganov SA. Protein induced singlet–triplet quasidegeneracy in the active site of [NiFe]-hydrogenase. Chem Phys Lett. 2013; 577:138–141.
311. Fan H-J, Hall MB. High-spin Ni(II), a surprisingly good structural model for [NiFe] hydrogenase. J Am Chem Soc. 2002; 124:394–395. [PubMed: 11792207]
312. Wang H, Yoda Y, Ogata H, Tanaka Y, Lubitz W. A strenuous experimental journey searching for spectroscopic evidence of a bridging nickel–iron–hydride in [NiFe] hydrogenase. J Synchrotron Radiat. 2015; 22:1334–1344. [PubMed: 26524296]
313. Evans RM, Brooke EJ, Wehlin SAM, Nomerotskaia E, Sargent F, Carr SB, Phillips SEV, Armstrong FA. Mechanism of hydrogen activation by [NiFe] hydrogenases. Nat Chem Biol. 2015; 12:46–50. [PubMed: 26619250]
314. Fichtner C, Laurich C, Bothe E, Lubitz W. Spectroelectrochemical characterization of the [NiFe] hydrogenase of *Desulfovibrio Vulgaris* Miyazaki F. Biochemistry. 2006; 45:9706–9716. [PubMed: 16893172]
315. Brecht M, van Gastel M, Buhrke T, Friedrich B, Lubitz W. Direct detection of a hydrogen ligand in the [NiFe] center of the regulatory H_2-sensing hydrogenase from *Ralstonia eutropha* in its reduced state by HYSCORE and ENDOR spectroscopy. J Am Chem Soc. 2003; 125:13075–13083. [PubMed: 14570480]
316. Krämer T, Kampa M, Lubitz W, van Gastel M, Neese F. Theoretical spectroscopy of the Ni^{II} intermediate states in the catalytic cycle and the activation of [NiFe] hydrogenases. ChemBioChem. 2013; 14:1898–1905. [PubMed: 23703916]

317. Foerster S, Stein M, Brecht M, Ogata H, Higuchi Y, Lubitz W. Single crystal EPR studies of the reduced active site of [NiFe] hydrogenase from *Desulfovibrio vulgaris* Miyazaki F. J Am Chem Soc. 2003; 125:83–93. [PubMed: 12515509]

318. Tai H, Nishikawa K, Inoue S, Higuchi Y, Hirota S. FT-IR Characterization of the light-induced Ni-L2 and Ni-L3 states of [NiFe] hydrogenase from *Desulfovibrio vulgaris* Miyazaki F. J Phys Chem B. 2015; 119:13668–13674. [PubMed: 25898020]

319. Roessler MM, Evans RM, Davies RA, Harmer J, Armstrong FA. EPR spectroscopic studies of the Fe–S clusters in the O_2-tolerant [NiFe]-hydrogenase Hyd-1 from *Escherichia coli* and characterization of the unique [4Fe–3S] cluster by HYSCORE. J Am Chem Soc. 2012; 134:15581–15594. [PubMed: 22900997]

320. Hidalgo R, Ash PA, Healy AJ, Vincent KA. Infrared spectroscopy during electrocatalytic turnover reveals the Ni-L active site state during H_2 oxidation by a NiFe hydrogenase. Angew Chem, Int Ed. 2015; 54:7110–7113.

321. Tai H, Nishikawa K, Suzuki M, Higuchi Y, Hirota S. Control of the transition between Ni-C and Ni-SI_a States by the Redox State of the Proximal Fe-S Cluster in the Catalytic Cycle of [NiFe]Hydrogenase. Angew Chem, Int Ed. 2014; 53:13817–13820.

322. Greene BL, Wu C-H, Vansuch GE, Adams MWW, Dyer RB. Proton inventory and dynamics in the Ni_a-S to Ni_a-C transition of a [NiFe] hydrogenase. Biochemistry. 2016; 55:1813–1825. [PubMed: 26956769]

323. Bleijlevens B, Faber BW, Albracht SPJ. The [NiFe] hydrogenase from *Allochromatium vinosum* studied in EPR-detectable states: H/D exchange experiments that yield new information about the structure of the active site. JBIC, J Biol Inorg Chem. 2001; 6:763–769. [PubMed: 11713683]

324. Montet Y, Amara P, Volbeda A, Vernede X, Hatchikian EC, Field MJ, Frey M, Fontecilla-Camps JC. Gas access to the active site of Ni-Fe hydrogenases probed by X-ray crystallography and molecular dynamics. Nat Struct Biol. 1997; 4:523–527. [PubMed: 9228943]

325. Bruschi M, Tiberti M, Guerra A, De Gioia L. Disclosure of key stereoelectronic factors for efficient H_2 binding and cleavage in the active site of [NiFe]-hydrogenases. J Am Chem Soc. 2014; 136:1803–1814. [PubMed: 24392667]

326. Smith DMA, Raugei S, Squier TC. Modulation of active site electronic structure by the protein matrix to control [NiFe] hydrogenase reactivity. Phys Chem Chem Phys. 2014; 16:24026–24033. [PubMed: 25285653]

327. Kampa M, Lubitz W, van Gastel M, Neese F. Computational study of the electronic structure and magnetic properties of the Ni–C state in [NiFe] hydrogenases including the second coordination sphere. *JBIC*. J Biol Inorg Chem. 2012; 17:1269–1281. [PubMed: 23053531]

328. Kaliakin DS, Zaari RR, Varganov SA. Effect of H_2 binding on the nonadiabatic transition probability between singlet and triplet states of the [NiFe]-hydrogenase active site. J Phys Chem A. 2015; 119:1066–1073. [PubMed: 25603170]

329. Delcey MG, Pierloot K, Phung QM, Vancoillie S, Lindh R, Ryde U. Accurate calculations of geometries and singlet–triplet energy differences for active-site models of [NiFe] hydrogenase. Phys Chem Chem Phys. 2014; 16:7927–7938. [PubMed: 24647807]

330. Wu H, Hall MB. Density functional theory on the larger active site models for [NiFe] hydrogenases: Two-state reactivity? C R Chim. 2008; 11:790–804.

331. Dong G, Ryde U. Protonation states of intermediates in the reaction mechanism of [NiFe] hydrogenase studied by computational methods. *JBIC*. J Biol Inorg Chem. 2016; 21:383–394. [PubMed: 26940957]

332. Fitch CA, Platzer G, Okon M, Garcia-Moreno E B, McIntosh LP. Arginine: its pK_a value revisited. Protein Sci. 2015; 24:752–761. [PubMed: 25808204]

333. Jones AK, Sillery E, Albracht SPJ, Armstrong FA. Direct comparison of the electrocatalytic oxidation of hydrogen by an enzyme and a platinum catalyst. Chem Commun. 2002:866–867.

334. Pershad HR, Duff JLC, Heering HA, Duin EC, Albracht SPJ, Armstrong FA. Catalytic electron transport in Chromatium Vinosum [NiFe]-hydrogenase: application of voltammetry in detecting redox-active centers and establishing that hydrogen oxidation is very fast even at potentials close to the reversible H^+/H_2 Value. Biochemistry. 1999; 38:8992–8999. [PubMed: 10413472]

335. Fontecilla-Camps JC, Volbeda A, Cavazza C, Nicolet Y. Structure/function relationships of [NiFe]- and [FeFe]-hydrogenases. Chem Rev. 2007; 107:4273–4303. [PubMed: 17850165]
336. Goldet G, Wait AF, Cracknell JA, Vincent KA, Ludwig M, Lenz O, Friedrich B, Armstrong FA. Hydrogen production under aerobic conditions by membrane-bound hydrogenases from *Ralstonia* Species. J Am Chem Soc. 2008; 130:11106–11113. [PubMed: 18661984]
337. Fourmond V, Baffert C, Sybirna K, Dementin S, Abou-Hamdan A, Meynial-Salles I, Soucaille P, Bottin H, Léger C. The mechanism of inhibition by H_2 of H_2-evolution by hydrogenases. Chem Commun. 2013; 49:6840–6842.
338. Léger C, Dementin S, Bertrand P, Rousset M, Guigliarelli B. Inhibition and aerobic inactivation kinetics of *Desulfovibrio fructosovorans* NiFe hydrogenase studied by protein film voltammetry. J Am Chem Soc. 2004; 126:12162–12172. [PubMed: 15382953]
339. van Haaster DJ, Hagedoorn P-L, Jongejan JA, Hagen WR. On the relationship between affinity for molecular hydrogen and the physiological directionality of hydrogenases. Biochem Soc Trans. 2005; 33:12–14. [PubMed: 15667251]
340. Kaur-Ghumaan S, Stein M. [NiFe] hydrogenases: how close do structural and functional mimics approach the active site? Dalton Trans. 2014; 43:9392–9405. [PubMed: 24846119]
341. Ohki Y, Tatsumi K. Thiolate-bridged iron–nickel models for the active site of [NiFe] hydrogenase. Eur J Inorg Chem. 2011; 2011:973–985.
342. Whaley CM, Rauchfuss TB, Wilson SR. Coordination chemistry of $[HFe(CN)_2(CO)_3]^-$ and its derivatives: toward a model for the iron subsite of the [NiFe]-hydrogenases. Inorg Chem. 2009; 48:4462–4469. [PubMed: 19374433]
343. Ceriotti A, Chini P, Fumagalli A, Koetzle TF, Longoni G, Takusagawa F. Synthesis of Bimetallic Fe-Ni Carbonyl Clusters: Crystal Structure of $[N(CH_3)_3CH_2Ph][Fe_3Ni(CO)_8(\mu\text{-}CO)_4(\mu_3\text{-}H)]$. Inorg Chem. 1984; 23:1363–1368.
344. Della Pergola R, Fumagalli A, Garlaschelli L, Manassero C, Manassero M, Sansoni M, Sironi A. Iron–nickel mixed metal nitrido clusters: Synthesis and solid state structure of the anions $[HFe_5NiN\text{-}(CO)_{14}]^{2-}$ and $[HFe_4Ni_2N(CO)_{13}]^{2-}$. Inorg Chim Acta. 2008; 361:1763–1769.
345. Barton BE, Whaley CM, Rauchfuss TB, Gray DL. Nickel-iron dithiolato hydrides relevant to the [NiFe]-hydrogenase active site. J Am Chem Soc. 2009; 131:6942–6943. [PubMed: 19413314]
346. Zhu W, Marr AC, Wang Q, Neese F, Spencer DJE, Blake AJ, Cooke PA, Wilson C, Schröder M. Modulation of the electronic structure and the Ni–Fe distance in heterobimetallic models for the active site in [NiFe]hydrogenase. Proc Natl Acad Sci U S A. 2005; 102:18280–18285. [PubMed: 16352727]
347. Schilter D, Pelmenschikov V, Wang H, Meier F, Gee LB, Yoda Y, Kaupp M, Rauchfuss TB, Cramer SP. Synthesis and vibrational spectroscopy of ^{57}Fe-labeled models of [NiFe] hydrogenase: first direct observation of a nickel–iron interaction. Chem Commun. 2014; 50:13469–13472.
348. Carroll ME, Barton BE, Gray DL, Mack AE, Rauchfuss TB. Active-site models for the nickel-iron hydrogenases: effects of ligands on reactivity and catalytic properties. Inorg Chem. 2011; 50:9554–9563. [PubMed: 21866886]
349. Shafaat HS, Weber K, Petrenko T, Neese F, Lubitz W. Key hydride vibrational modes in [NiFe] hydrogenase model compounds studied by resonance Raman spectroscopy and density functional calculations. Inorg Chem. 2012; 51:11787–11797. [PubMed: 23039071]
350. Hugenbruch S, Shafaat HS, Krämer T, Delgado-Jaime MU, Weber K, Neese F, Lubitz W, DeBeer S. In search of metal hydrides: an X-ray absorption and emission study of [NiFe] hydrogenase model complexes. Phys Chem Chem Phys. 2016; 18:10688–10699. [PubMed: 26924248]
351. Ulloa OA, Huynh MT, Richers CP, Bertke JA, Nilges MJ, Hammes-Schiffer S, Rauchfuss TB. Mechanism of H_2 Production by Models for the [NiFe]-Hydrogenases: Role of Reduced Hydrides. J Am Chem Soc. 2016; doi: 10.1021/jacs.6b04579
352. Chambers GM, Angamuthu R, Gray DL, Rauchfuss TB. Organo ruthenium–nickel dithiolates with redox-responsive nickel sites. Organometallics. 2013; 32:6324–6329.
353. Schilter D, Fuller AL, Gray DL. Nickel-molybdenum and nickel-tungsten dithiolates: hybrid models for hydrogenases and hydrodesulfurization. Eur J Inorg Chem. 2015; 2015:4638–4642.

354. Chojnacki SS, Hsiao Y-M, Darensbourg MY, Reibenspies JH. X-ray structure and solution characterization of Ni-$(SCH_2CH_2PPh_2)_2Mo(CO)_4$. Inorg Chem. 1993; 32:3573–3576.
355. Weber K, Krämer T, Shafaat HS, Weyhermüller T, Bill E, van Gastel M, Neese F, Lubitz W. A functional [NiFe]-hydrogenase model compound that undergoes biologically relevant reversible thiolate protonation. J Am Chem Soc. 2012; 134:20745–20755. [PubMed: 23194246]
356. Canaguier S, Vaccaro L, Artero V, Ostermann R, Pécaut J, Field MJ, Fontecave M. Cyclopentadienyl ruthenium–nickel catalysts for biomimetic hydrogen evolution: electrocatalytic properties and mechanistic DFT studies. Chem - Eur J. 2009; 15:9350–9364. [PubMed: 19670195]
357. Fourmond V, Canaguier S, Golly B, Field MJ, Fontecave M, Artero V. A nickel–manganese catalyst as a biomimic of the active site of NiFe hydrogenases: a combined electrocatalytical and DFT mechanistic study. Energy Environ Sci. 2011; 4:2417–2427.
358. Song L-C, Li J-P, Xie Z-J, Song H-B. Synthesis, structural characterization, and electrochemical properties of dinuclear Ni/Mn model complexes for the active site of [NiFe]-hydrogenases. Inorg Chem. 2013; 52:11618–11626. [PubMed: 24063734]
359. Chambers GM, Mitra J, Rauchfuss TB, Stein M. Ni^{I}/Ru^{II} model for the Ni–L state of the [NiFe]hydrogenases: synthesis, spectroscopy, and reactivity. Inorg Chem. 2014; 53:4243–4249. [PubMed: 24684697]
360. Denny JA, Darensbourg MY. Metallodithiolates as ligands in coordination, bioinorganic, and organometallic chemistry. Chem Rev. 2015; 115:5248–5273. [PubMed: 25948147]
361. Ogo S, Kabe R, Uehara K, Kure B, Nishimura T, Menon SC, Harada R, Fukuzumi S, Higuchi Y, Ohhara T, Tamada T, Kuroki R. A dinuclear Ni(μ-H)Ru complex derived from H_2. Science. 2007; 316:585–587. [PubMed: 17463285]
362. Ogo S. Electrons from hydrogen. Chem Commun. 2009:3317–3325.
363. Kure B, Matsumoto T, Ichikawa K, Fukuzumi S, Higuchi Y, Yagi T, Ogo S. pH-Dependent isotope exchange and hydrogenation catalysed by water-soluble NiRu complexes as functional models for [NiFe]hydrogenases. Dalton Trans. 2008:4747–4755. [PubMed: 18728883]
364. Kim K, Kishima T, Matsumoto T, Nakai H, Ogo S. Selective redox activation of H_2 or O_2 in a [NiRu] complex by aromatic ligand effects. Organometallics. 2013; 32:79–87.
365. Kishima T, Matsumoto T, Nakai H, Hayami S, Ohta T, Ogo S. A high-valent iron(IV) peroxo core derived from O_2. Angew Chem, Int Ed. 2016; 55:724–727.
366. Wulff P, Day CC, Sargent F, Armstrong FA. How oxygen reacts with oxygen-tolerant respiratory [NiFe]-hydrogenases. Proc Natl Acad Sci U S A. 2014; 111:6606–6611. [PubMed: 24715724]
367. Ogo S, Ichikawa K, Kishima T, Matsumoto T, Nakai H, Kusaka K, Ohhara T. A functional [NiFe]hydrogenase mimic that catalyzes electron and hydride transfer from H_2. Science. 2013; 339:682–684. [PubMed: 23393260]
368. Manor BC, Rauchfuss TB. Hydrogen activation by biomimetic [NiFe]-hydrogenase model containing protected cyanide cofactors. J Am Chem Soc. 2013; 135:11895–11900. [PubMed: 23899049]
369. Begum A, Moula G, Sarkar S. A nickel(II) –sulfur-based radical-ligand complex as a functional model of hydrogenase. Chem - Eur J. 2010; 16:12324–12327. [PubMed: 20853299]
370. Sellmann D, Geipel F, Moll M. [Ni(NHP*n*Pr_3)('S3')], the first nickel thiolate complex modeling the nickel cysteinate site and reactivity of [NiFe] hydrogenase. Angew Chem, Int Ed. 2000; 39:561–563.
371. Connelly SJ, Zimmerman AC, Kaminsky W, Heinekey DM. Synthesis, structure, and reactivity of a nickel dihydrogen complex. Chem - Eur J. 2012; 18:15932–15934. [PubMed: 23138965]
372. He T, Tsvetkov NP, Andino JG, Gao X, Fullmer BC, Caulton KG. Mechanism of heterolysis of H_2 by an unsaturated d^8 nickel center: via tetravalent nickel? J Am Chem Soc. 2010; 132:910–911. [PubMed: 20043681]
373. Tsay C, Peters JC. Thermally stable N_2 and H_2 adducts of cationic nickel(II). Chem Sci. 2012; 3:1313–1318.
374. Yang JY, Chen S, Dougherty WG, Kassel WS, Bullock RM, DuBois DL, Raugei S, Rousseau R, Dupuis M, Rakowski DuBois M. Hydrogen oxidation catalysis by a nickel diphosphine complex with pendant *tert*-butyl amines. Chem Commun. 2010; 46:8618–8620.

375. Raugei S, Helm ML, Hammes-Schiffer S, Appel AM, O'Hagan M, Wiedner ES, Bullock RM. Experimental and computational mechanistic studies guiding the rational design of molecular electrocatalysts for production and oxidation of hydrogen. Inorg Chem. 2016; 55:445–460. [PubMed: 26653114]

376. Horvath S, Fernandez LE, Soudackov AV, Hammes-Schiffer S. Insights into proton-coupled electron transfer mechanisms of electrocatalytic H_2 oxidation and production. Proc Natl Acad Sci U S A. 2012; 109:15663–15668. [PubMed: 22529352]

377. Helm ML, Stewart MP, Bullock RM, Rakowski DuBois M, DuBois DL. A synthetic nickel electrocatalyst with a turnover frequency above 100,000 s^{-1} for H_2 production. Science. 2011; 333:863–866. [PubMed: 21836012]

378. Schilter D, Rauchfuss TB, Stein M. Connecting [NiFe]- and [FeFe]-hydrogenases: mixed-valence nickel–iron dithiolates with rotated structures. Inorg Chem. 2012; 51:8931–8941. [PubMed: 22838645]

379. Schilter D. Nickel–iron hydrogenases: high-resolution crystallography resolves the hydride, but not the debate. ChemBioChem. 2015; 16:1712–1714. [PubMed: 26083003]

380. Behnke SL, Shafaat HS. Heterobimetallic models of the [NiFe] hydrogenases: a structural and spectroscopic comparison. Comments Inorg Chem. 2016; 36:123–140.

381. Thauer RK, Kaster A-K, Goenrich M, Schick M, Hiromoto T, Shima S. Hydrogenases from methanogenic archaea, nickel, a novel cofactor, and H_2 storage. Annu Rev Biochem. 2010; 79:507–536. [PubMed: 20235826]

382. Shima S, Thauer RK. A third type of hydrogenase catalyzing H_2 activation. Chem Rec. 2007; 7:37–46. [PubMed: 17304591]

383. Zirngibl C, Hedderich R, Thauer RK. N^5,N^{10}-Methylenetetrahydromethanopterin dehydrogenase from *Methanobacterium thermoautotrophicum* has hydrogenase activity. FEBS Lett. 1990; 261:112–116.

384. Stiebritz MT, Reiher M. Hydrogenases and oxygen. Chem Sci. 2012; 3:1739–1751.

385. Berkessel A. Activation of dihydrogen without transition metals. Curr Opin Chem Biol. 2001; 5:486–490. [PubMed: 11578920]

386. Lyon EJ, Shima S, Buurman G, Chowdhuri S, Batschauer A, Steinbach K, Thauer RK. UV-A/blue-light inactivation of the 'metal-free' hydrogenase (Hmd) from methanogenic archaea The enzyme contains functional iron after all. Eur J Biochem. 2004; 271:195–204. [PubMed: 14686932]

387. Lyon EJ, Shima S, Boecher R, Thauer RK, Grevels F-W, Bill E, Roseboom W, Albracht SPJ. Carbon monoxide as an intrinsic ligand to iron in the active site of the iron-sulfur-cluster-free hydrogenase H_2-forming methylenetetrahydromethanopterin dehydrogenase as revealed by infrared spectroscopy. J Am Chem Soc. 2004; 126:14239–14248. [PubMed: 15506791]

388. Guo Y, Wang H, Xiao Y, Vogt S, Thauer RK, Shima S, Volkers PI, Rauchfuss TB, Pelmenschikov V, Case DA, Alp EE, Sturhahn W, Yoda Y, Cramer SP. Characterization of the Fe Site in iron-sulfur cluster-free hydrogenase (Hmd) and of a model compound via nuclear resonance vibrational spectroscopy (NRVS). Inorg Chem. 2008; 47:3969–3977. [PubMed: 18407624]

389. Shima S, Lyon EJ, Sordel-Klippert M, Kauß M, Kahnt J, Thauer RK, Steinbach K, Xie X, Verdier L, Griesinger C. The cofactor of the iron–sulfur cluster free hydrogenase Hmd: structure of the light inactivation product. Angew Chem, Int Ed. 2004; 43:2547–2551.

390. Hiromoto T, Ataka K, Pilak O, Vogt S, Stagni MS, Meyer-Klaucke W, Warkentin E, Thauer RK, Shima S, Ermler U. The crystal structure of C176A mutated [Fe]-hydrogenase suggests an acyl-iron ligation in the active site iron complex. FEBS Lett. 2009; 583:585–590. [PubMed: 19162018]

391. Hiromoto T, Warkentin E, Moll J, Ermler U, Shima S. The crystal structure of an [Fe]-hydrogenase–substrate complex reveals the framework for H_2 activation. Angew Chem, Int Ed. 2009; 48:6457–6460.

392. Tamura H, Salomone-Stagni M, Fujishiro T, Warkentin E, Meyer-Klaucke W, Ermler U, Shima S. Crystal structures of [Fe]-hydrogenase in complex with inhibitory isocyanides: implications for the H_2-activation site. Angew Chem, Int Ed. 2013; 52:9656–9659.

393. Bartoschek S, Buurman G, Thauer RK, Geierstanger BH, Weyrauch JP, Griesinger C, Nilges M, Hutter MC, Helms V. *Re*face stereospecificity of methylenetetrahydromethanopterin and methylenetetrahydrofolate dehydrogenases is predetermined by intrinsic properties of the substrate. ChemBioChem. 2001; 2:530–541. [PubMed: 11828486]

394. Shima S, Pilak O, Vogt S, Schick M, Stagni MS, Meyer-Klaucke W, Warkentin E, Thauer RK, Ermler U. The crystal structure of [Fe]-hydrogenase reveals the geometry of the active site. Science. 2008; 321:572–575. [PubMed: 18653896]

395. Stiebritz MT, Reiher M. A unifying structural and electronic concept for Hmd and [FeFe] hydrogenase active sites. Inorg Chem. 2010; 49:5818–5823. [PubMed: 20527808]

396. Dey A. Density functional theory calculations on the mononuclear non-heme iron active site of Hmd hydrogenase: role of the internal ligands in tuning external ligand binding and driving H_2 heterolysis. J Am Chem Soc. 2010; 132:13892–13901. [PubMed: 20831194]

397. Finkelmann AR, Senn HM, Reiher M. Hydrogen-activation mechanism of [Fe] hydrogenase revealed by multi-scale modeling. Chem Sci. 2014; 5:4474–4482.

398. Vogt S, Lyon EJ, Shima S, Thauer RK. The exchange activities of [Fe] hydrogenase (iron–sulfur-cluster-free hydrogenase) from methanogenic archaea in comparison with the exchange activities of [FeFe] and [NiFe] hydrogenases. *JBIC*. J Biol Inorg Chem. 2008; 13:97–106. [PubMed: 17924153]

399. Wright JA, Turrell PJ, Pickett CJ. The third hydrogenase: more natural organometallics. Organometallics. 2010; 29:6146–6156.

400. Royer AM, Rauchfuss TB, Gray DL. Oxidative addition of thioesters to iron(0): active-site models for Hmd, Nature's third hydrogenase. Organometallics. 2009; 28:3618–3620.

401. Royer AM, Salomone-Stagni M, Rauchfuss TB, Meyer-Klaucke W. Iron acyl thiolato carbonyls: structural models for the active site of the [Fe]-hydrogenase (Hmd). J Am Chem Soc. 2010; 132:16997–17003. [PubMed: 21062066]

402. Fujishiro T, Kahnt J, Ermler U, Shima S. Protein-pyridinol thioester precursor for biosynthesis of the organometallic acyl-iron ligand in [Fe]-hydrogenase cofactor. Nat Commun. 2015; 6:6895. [PubMed: 25882909]

403. Obrist BV, Chen D, Ahrens A, Schünemann V, Scopelliti R, Hu X. An iron carbonyl pyridonate complex related to the active site of the [Fe]-hydrogenase (Hmd). Inorg Chem. 2009; 48:3514–3516. [PubMed: 19320470]

404. Song L-C, Xie Z-J, Wang M-M, Zhao G-Y, Song H-B. Biomimetic models for the active site of [Fe]hydrogenase featuring an acylmethyl(hydroxymethyl)pyridine ligand. Inorg Chem. 2012; 51:7466–7468. [PubMed: 22757742]

405. Turrell PJ, Hill AD, Ibrahim SK, Wright JA, Pickett CJ. Ferracyclic carbamoyl complexes related to the active site of [Fe]-hydrogenase. Dalton Trans. 2013; 42:8140–8146. [PubMed: 23595606]

406. Turrell PJ, Wright JA, Peck JNT, Oganesyan VS, Pickett CJ. The third hydrogenase: a ferracyclic carbamoyl with close structural analogy to the active site of Hmd. Angew Chem, Int Ed. 2010; 49:7508–7511.

407. Chen D, Scopelliti R, Hu X. [Fe]-hydrogenase models featuring acylmethylpyridinyl ligands. Angew Chem, Int Ed. 2010; 49:7512–7515.

408. Song L-C, Hu F-Q, Wang M-M, Xie Z-J, Xu K-K, Song H-B. Synthesis, structural characterization, and some properties of 2-acylmethyl-6-ester group difunctionalized pyridine-containing iron complexes related to the active site of [Fe]-hydrogenase. Dalton Trans. 2014; 43:8062–8071. [PubMed: 24718303]

409. Song L-C, Zhao G-Y, Xie Z-J, Zhang J-W. A novel acylmethylpyridinol ligand containing dinuclear iron complex closely related to [Fe]-hydrogenase. Organometallics. 2013; 32:2509–2512.

410. Song L-C, Xu K-K, Han X-F, Zhang J-W. Synthetic and structural studies of 2-acylmethyl-6-R-difunctionalized pyridine ligand-containing iron complexes related to [Fe]-hydrogenase. Inorg Chem. 2016; 55:1258–1269. [PubMed: 26756374]

411. Shima S, Chen D, Xu T, Wodrich MD, Fujishiro T, Schultz KM, Kahnt J, Ataka K, Hu X. Reconstitution of [Fe]-hydrogenase using model complexes. Nat Chem. 2015; 7:995–1002. [PubMed: 26587715]

412. Chen D, Scopelliti R, Hu X. A five-coordinate iron center in the active site of [Fe]-hydrogenase: hints from a model study. Angew Chem, Int Ed. 2011; 50:5671–5673.

413. Wodrich MD, Hu X. Electronic elements governing the binding of small molecules to a [Fe]-hydrogenase mimic. Eur J Inorg Chem. 2013; 2013:3993–3999.

414. Hu B, Chen D, Hu X. Synthesis and reactivity of mononuclear iron models of [Fe]-hydrogenase that contain an acylmethylpyridinol ligand. Chem - Eur J. 2014; 20:1677–1682. [PubMed: 24402840]

415. Durgaprasad G, Xie Z-L, Rose MJ. Iron hydride detection and intramolecular hydride transfer in a synthetic model of mono-iron hydrogenase with a CNS chelate. Inorg Chem. 2016; 55:386–389. [PubMed: 26405810]

416. Xu T, Yin C-JM, Wodrich MD, Mazza S, Schultz KM, Scopelliti R, Hu X. A functional model of [Fe]-hydrogenase. J Am Chem Soc. 2016; 138:3270–3273. [PubMed: 26926708]

417. Kalz KF, Brinkmeier A, Dechert S, Mata RA, Meyer F. Functional model for the [Fe] hydrogenase inspired by the frustrated Lewis pair concept. J Am Chem Soc. 2014; 136:16626–16634. [PubMed: 25353322]

418. Escalante-Semerena JC, Kenneth L, Rinehart J, Wolfe RS. Tetrahydromethanopterin, a carbon carrier in methanogenesis. J Biol Chem. 1984; 259:9447–9455. [PubMed: 6547718]

419. Igarashi RY, Laryukhin M, Dos Santos PC, Lee H-I, Dean DR, Seefeldt LC, Hoffman BM. Trapping H^- bound to the nitrogenase FeMo-cofactor active site during H_2 evolution: characterization by ENDOR spectroscopy. J Am Chem Soc. 2005; 127:6231–6241. [PubMed: 15853328]

420. Hoffman BM, Lukoyanov D, Yang Z-Y, Dean DR, Seefeldt LC. Mechanism of nitrogen fixation by nitrogenase: the next stage. Chem Rev. 2014; 114:4041–4062. [PubMed: 24467365]

421. Jeoung J-H, Dobbek H. Carbon dioxide activation at the Ni,Fe-cluster of anaerobic carbon monoxide dehydrogenase. Science. 2007; 318:1461–1464. [PubMed: 18048691]

422. Amara P, Mouesca J-M, Volbeda A, Fontecilla-Camps JC. Carbon monoxide dehydrogenase reaction mechanism: a likely case of abnormal CO_2 insertion to a Ni-H^- Bond. Inorg Chem. 2011; 50:1868–1878. [PubMed: 21247090]

423. Fontecilla-Camps JC, Amara P, Cavazza C, Nicolet Y, Volbeda A. Structure–function relationships of anaerobic gas-processing metalloenzymes. Nature. 2009; 460:814–822. [PubMed: 19675641]

424. Armstrong FA, Hirst J. Reversibility and efficiency in electrocatalytic energy conversion and lessons from enzymes. Proc Natl Acad Sci U S A. 2011; 108:14049–14054. [PubMed: 21844379]

425. Chavarot-Kerlidou, M.; Chenevier, P.; Artero, V. Bioorganometallic Chemistry: Applications in Drug Discovery, Biocatalysis, and Imaging. Jaouen, G.; Salmain, M., editors. Wiley-VCH Verlag GmbH & Co. KGaA; 2015.

426. Cabot P-L, Alcaide F, Brillas E. Hydrogen reaction at open circuit in alkaline media on Pt in a gas-diffusion electrode. J Electroanal Chem. 2009; 626:183–191.

427. Barton BE, Olsen MT, Rauchfuss TB. Artificial hydrogenases. Curr Opin Biotechnol. 2010; 21:292–297. [PubMed: 20356731]

428. Kiss G, Zhang K, Mukerjee SL, Hoff CD, Roper GC. Heat of reaction of the $Cr(CO)_3(C_5Me_5)$ radical with H_2 and related reactions. Relative and absolute bond strengths in the complexes H–$Cr(CO)_2(L)(C_5R_5)$. J Am Chem Soc. 1990; 112:5657–5658.

429. Gladysz JA, Bedford RB, Fujita M, Gabbaï FP, Goldberg KI, Holland PL, Kiplinger JL, Krische MJ, Louie J, Lu CC, Norton JR, Petrukhina MA, Ren T, Stahl SS, Tilley TD, Webster CE, White MC, Whiteker GT. Organometallics roundtable 2013–2014. Organometallics. 2014; 33:1505–1527.

430. Gewirth AA, Thorum MS. Electroreduction of dioxygen for fuel-cell applications: materials and challenges. Inorg Chem. 2010; 49:3557–3566. [PubMed: 20380457]

431. Mealli C, Rauchfuss TB. Models for the hydrogenases put the focus where it should be—hydrogen. Angew Chem, Int Ed. 2007; 46:8942–8944.

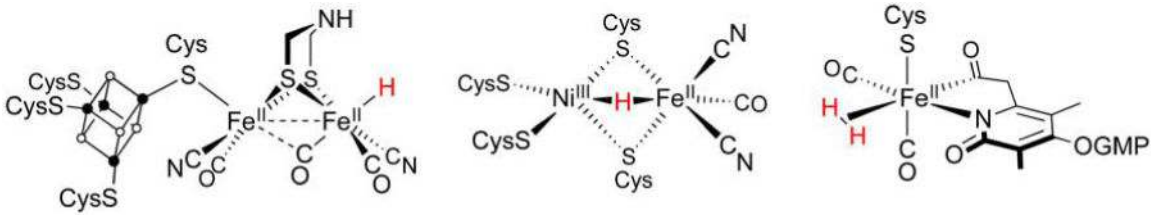

Figure 1.

Schematic representations of the active sites in [FeFe]-H_2ase (left), [NiFe]-H_2ase (center), and [Fe]-H_2ase (right). The presence of H^- and H_2 ligands in [FeFe]-H_2ase and [Fe]-H_2ase, respectively, has yet to be confirmed.

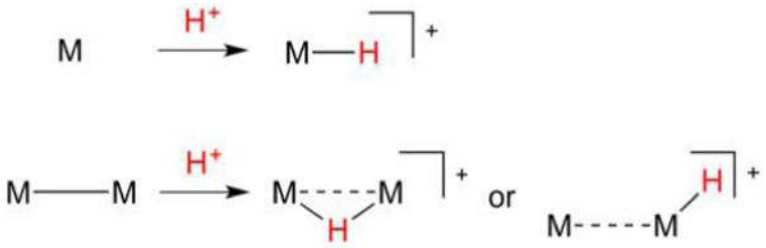

Figure 2.

Formation of mono- and dinuclear metal hydrides from low valent metals and H^+. In the latter case, both bridging and terminal hydrido products are possible.

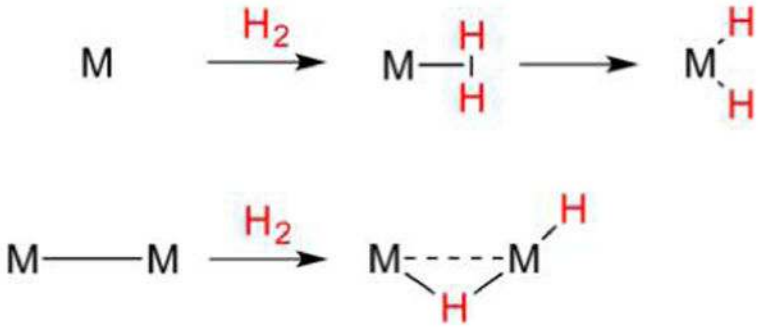

Figure 3.

Interactions of low-valent metal sites with H_2. The η^2-H_2 ligand can cleave through oxidative addition to afford dihydride complexes.

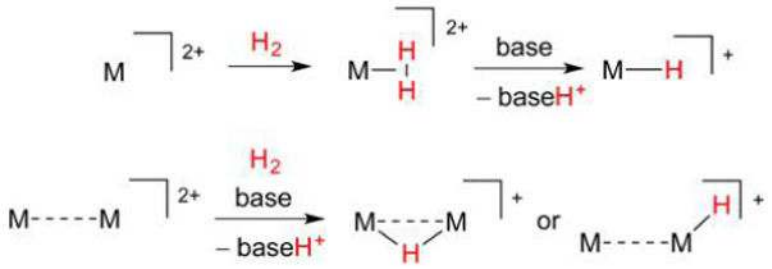

Figure 4.

Interactions of high-valent metal sites with H_2. The η^2-H_2 ligand in high-valent complexes can be acidic and is cleaved through deprotonation (heterolysis).

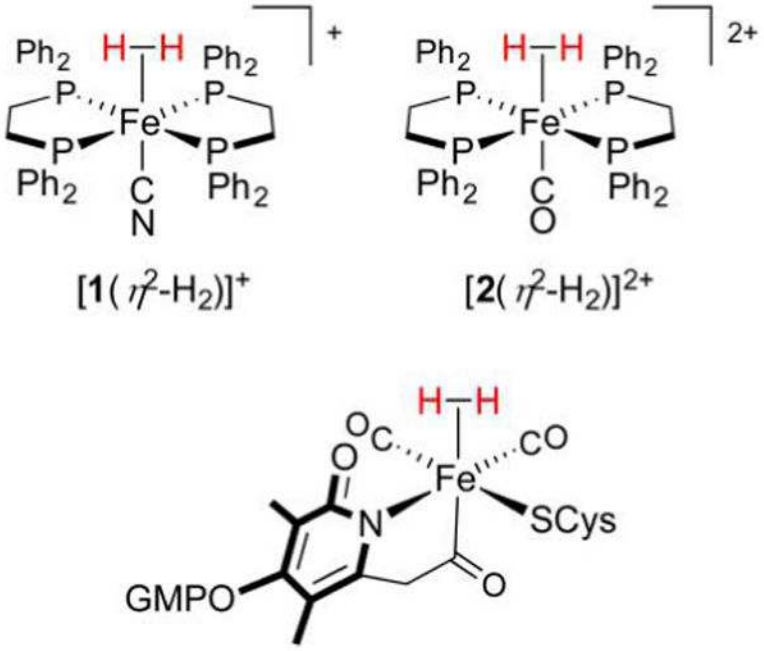

Figure 5.

Fe(η^2-H_2) complexes in the laboratory (top left and right) and in Nature (bottom). Note the presence of five strong-field ligands that serve to support the low-spin Fe(II) electrophile.

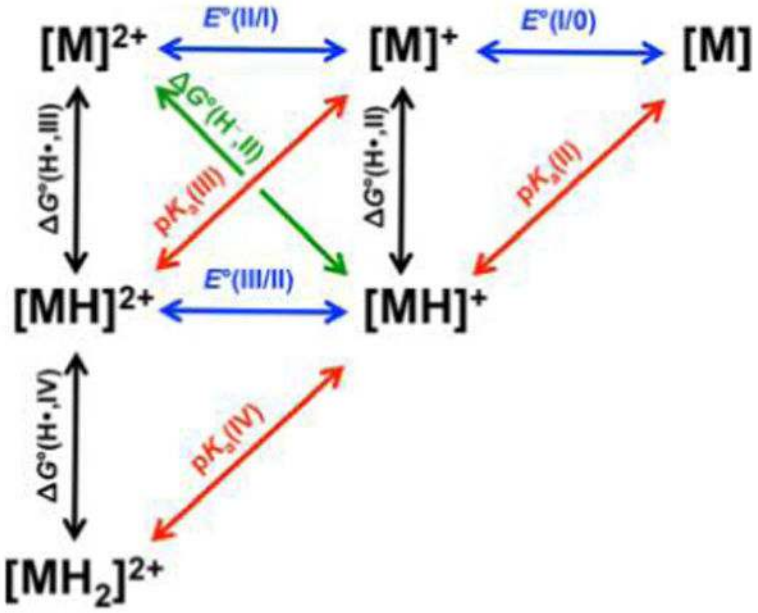

Figure 6.

Thermodynamic parameters for redox and acid–base processes for a metal complex M. Colored arrows denote transfer of an electron (blue), proton (red), $H^{\bullet}$ (black), and H^{-} (green). Adapted from ref 57. Copyright 2012 American Chemical Society.

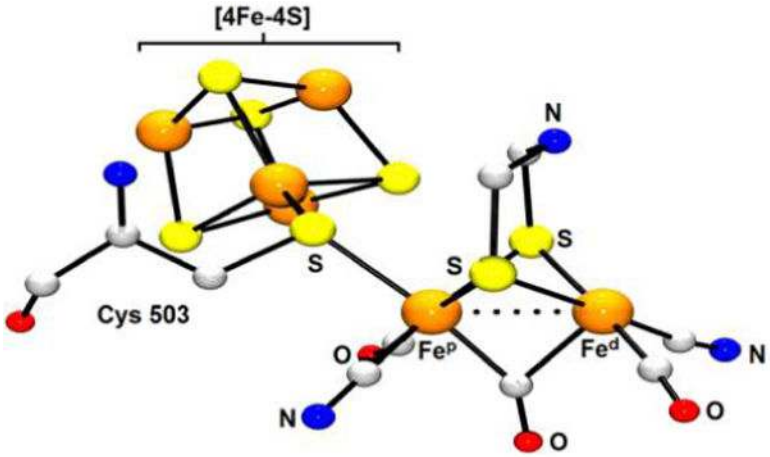

Figure 7.

X-ray structure of the [FeFe]-H_2ase active site from *Clostridium pasteurianum* (PDB code 3C8Y).[191] H atoms are omitted for clarity.

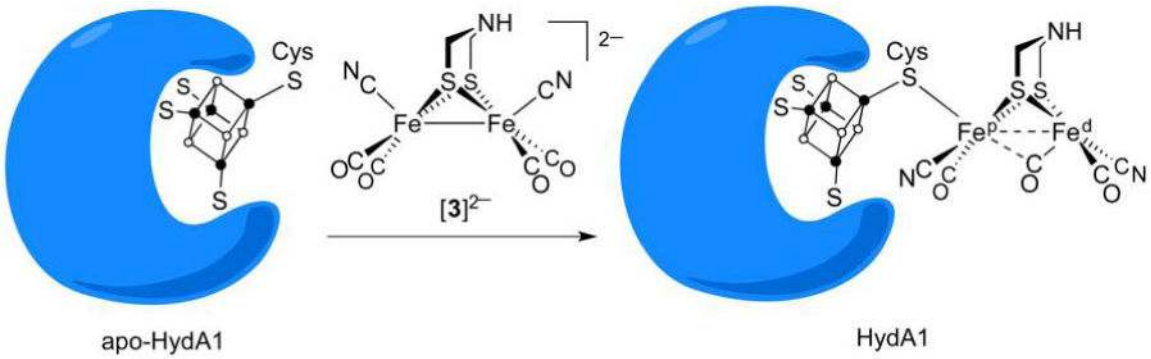

Figure 8.

Reconstitution of apo-[FeFe]-H_2ase from *Chlamydomonas reinhardtii* with $[NC(CO)_2Fe(adt)Fe(CO)_2CN]^{2-}$.[199,200]

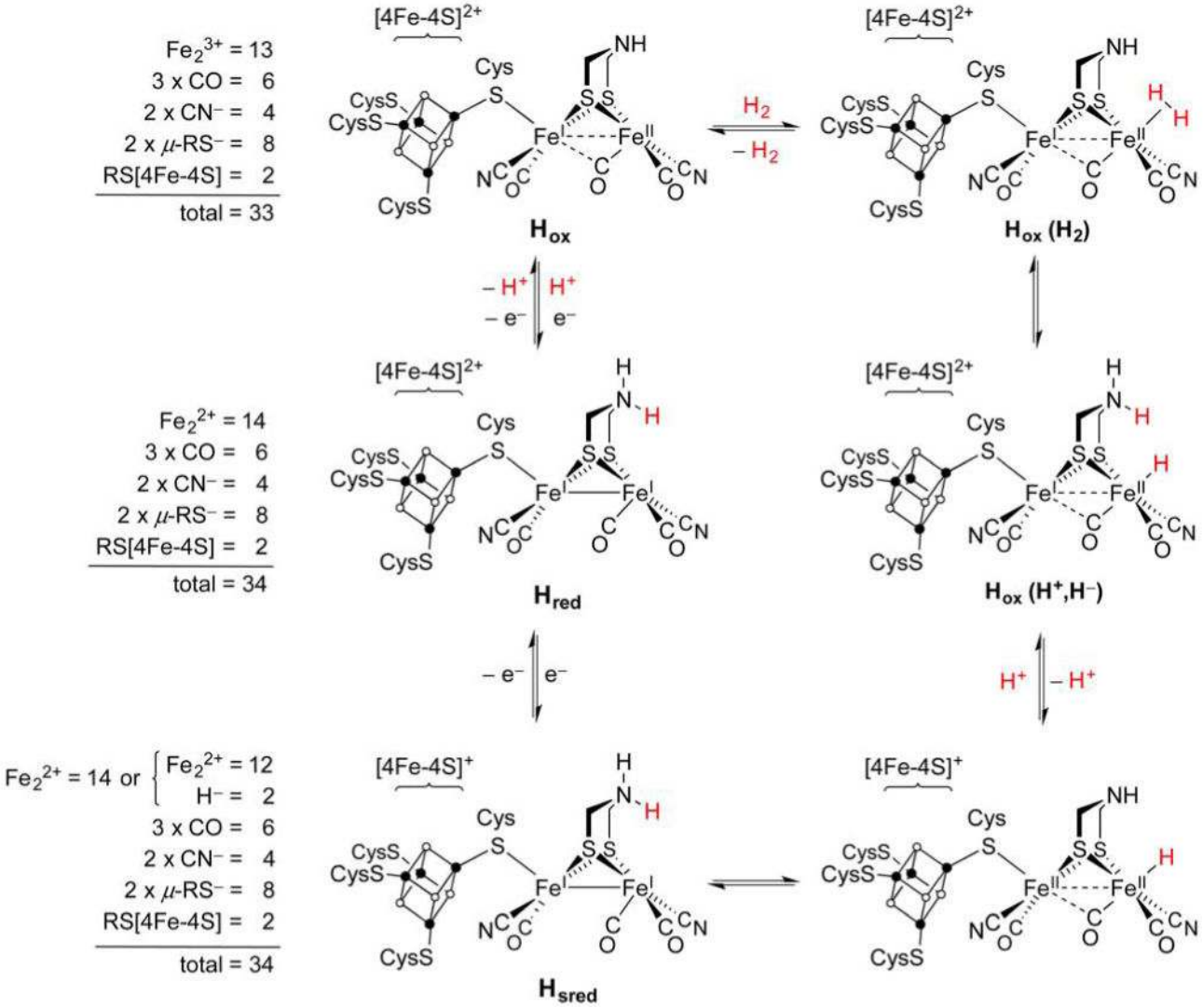

Figure 9.

Catalytic cycle proposed for [FeFe]-H_2ase (right)[203] and electron counting for the [2Fe] unit in the three characterized states (left). The totals include Fe 3d electrons and bonding electron pairs from donor atoms. The substrate H atoms are in red for emphasis, although they cannot be distinguished from the amine H atoms.

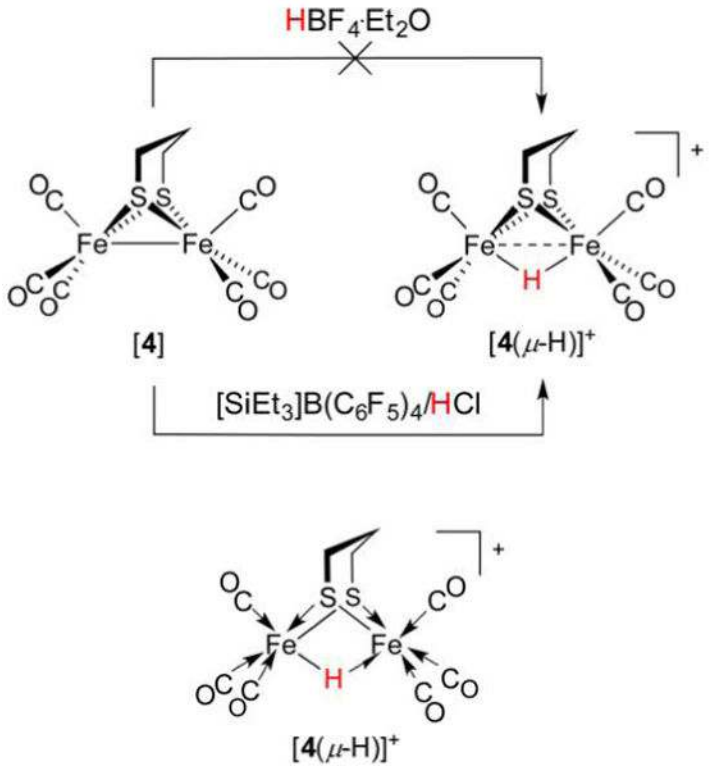

Figure 10.

Archetypal diiron thiolato hexacarbonyl [**4**] can be converted to its hydride [**4**(μ-H)]$^+$ only with very strong acids.[44] An alternative structural representation of [**4**(μ-H)]$^+$, using full arrow and half-arrow notation, is provided below.

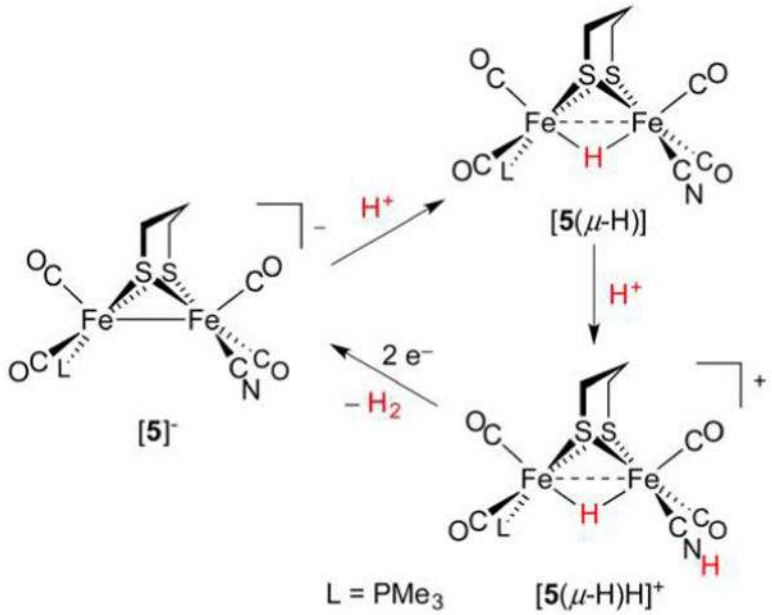

Figure 11.
Catalytic cycle for electrocatalytic proton reduction mediated by [**5**(μ-H)].[23]

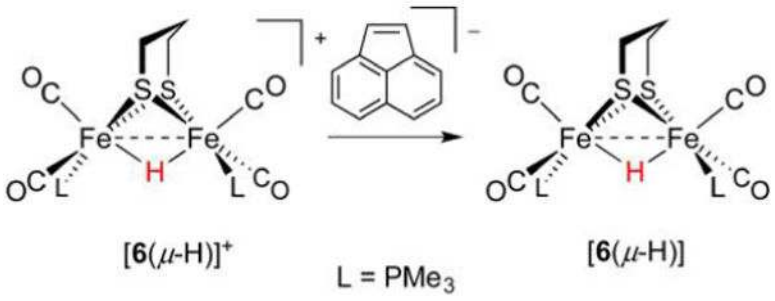

Figure 12.

The 1e⁻ reduction of a diamagnetic Fe(II)(μ-H)Fe(II) hydride affords a Fe(1.5)(μ-H)Fe(1.5) mixed-valent hydride.[108]

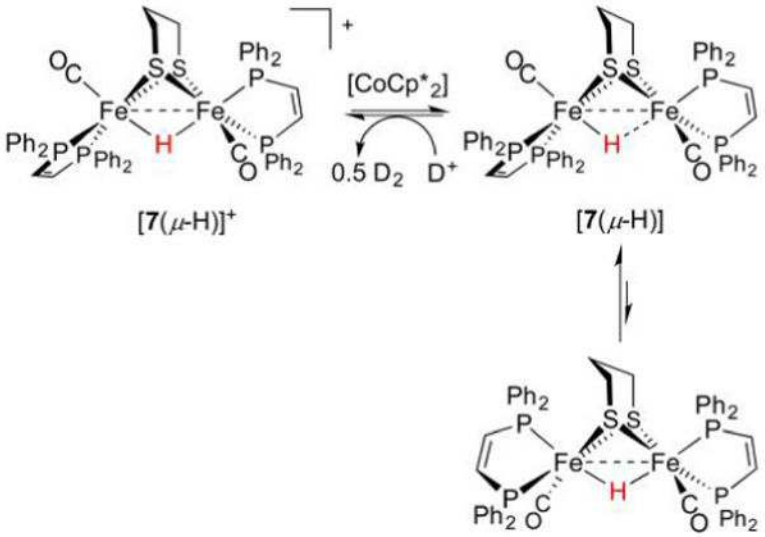

Figure 13.

Formation and isomerism of the mixed-valent hydride [7(μ-H)]. The μ-H$^-$ ligand is unaffected by acid.[245]

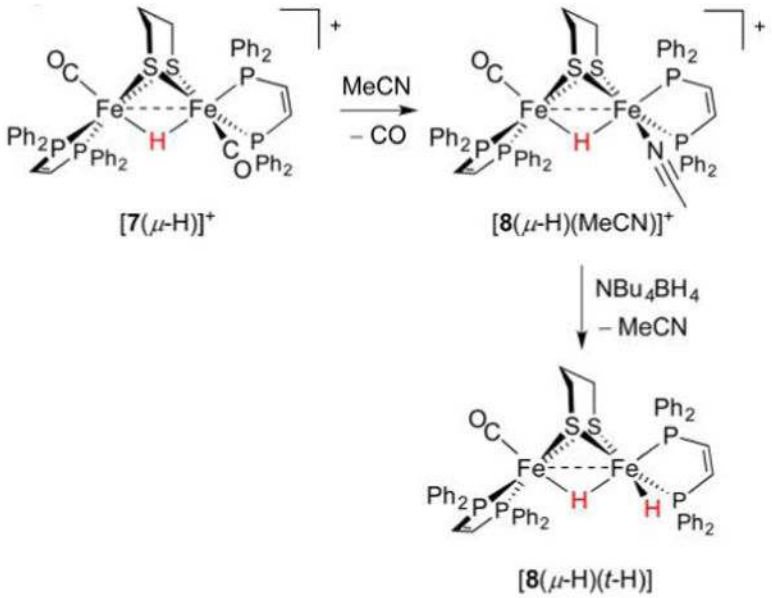

Figure 14.
Preparation of the dihydride [**8**(μ-H)(t-H)] from sources of H^+ and H^-.[247]

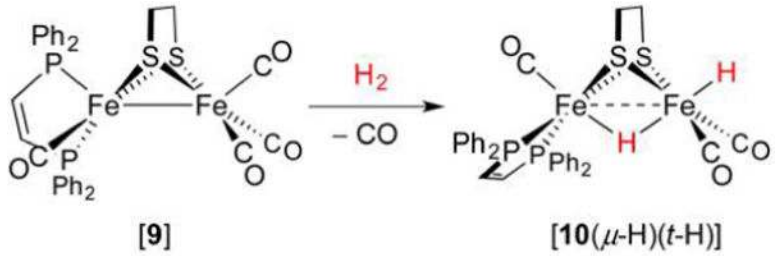

Figure 15.
Preparation of a dihydride through oxidative addition.[248]

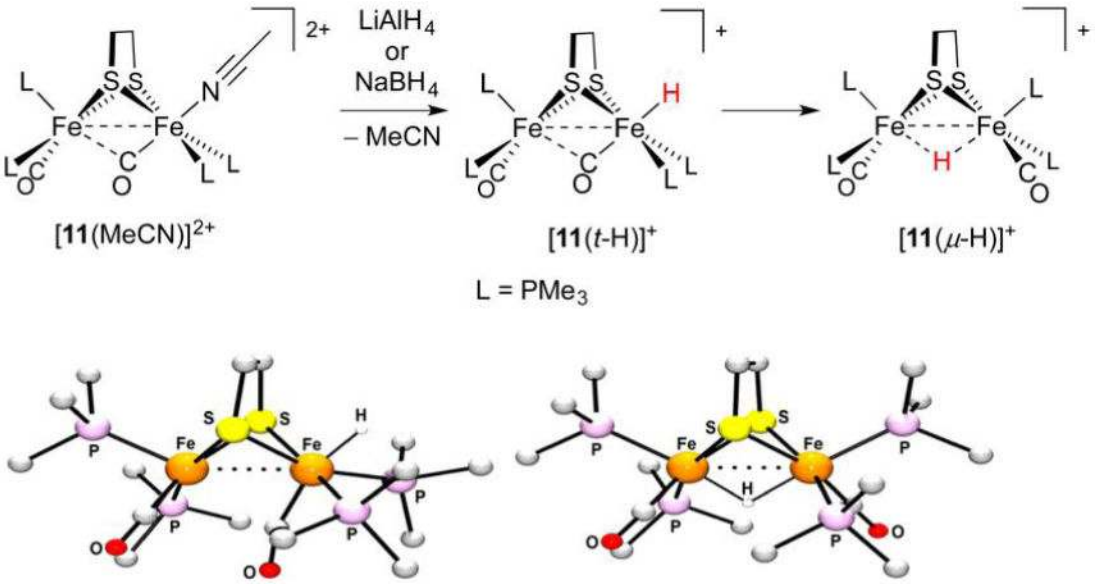

Figure 16.

Preparation (top) and X-ray structures of [**11**(*t*-H)]$^{+}$ and ([**11**(μ-H)]$^{+}$ (bottom). Non-hydride H atoms are omitted for clarity.[253]

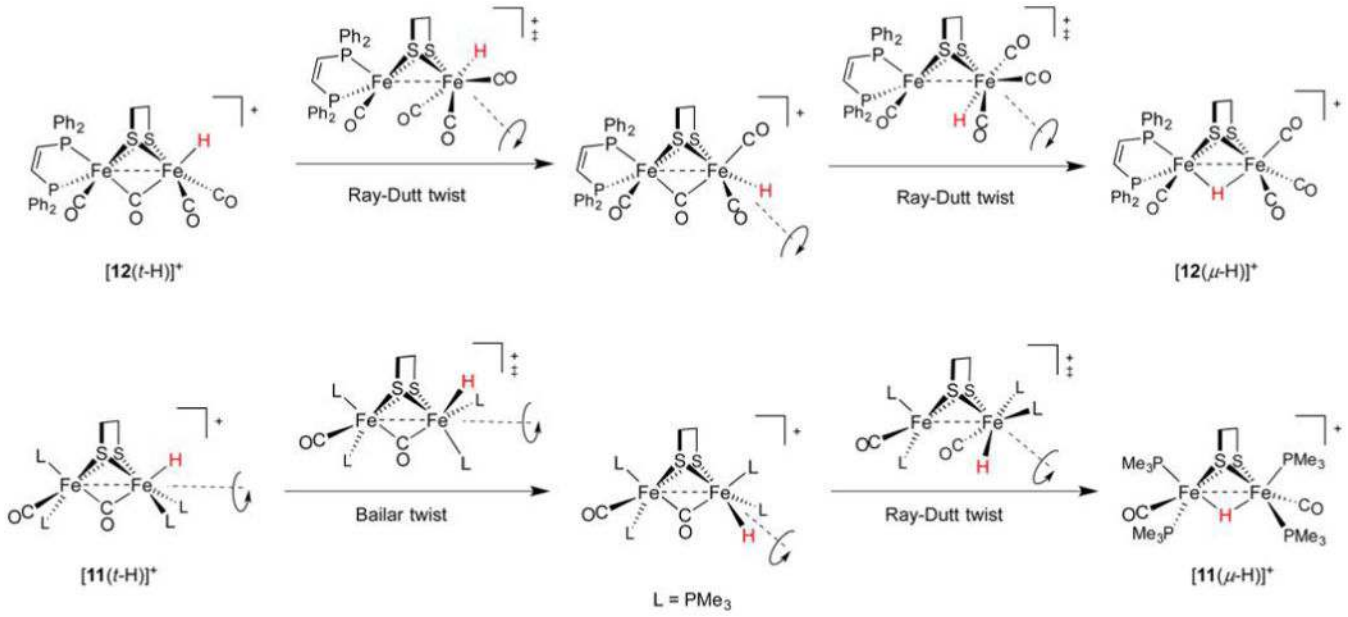

Figure 17.
Mechanisms for the isomerization of terminal to bridging hydride complexes.

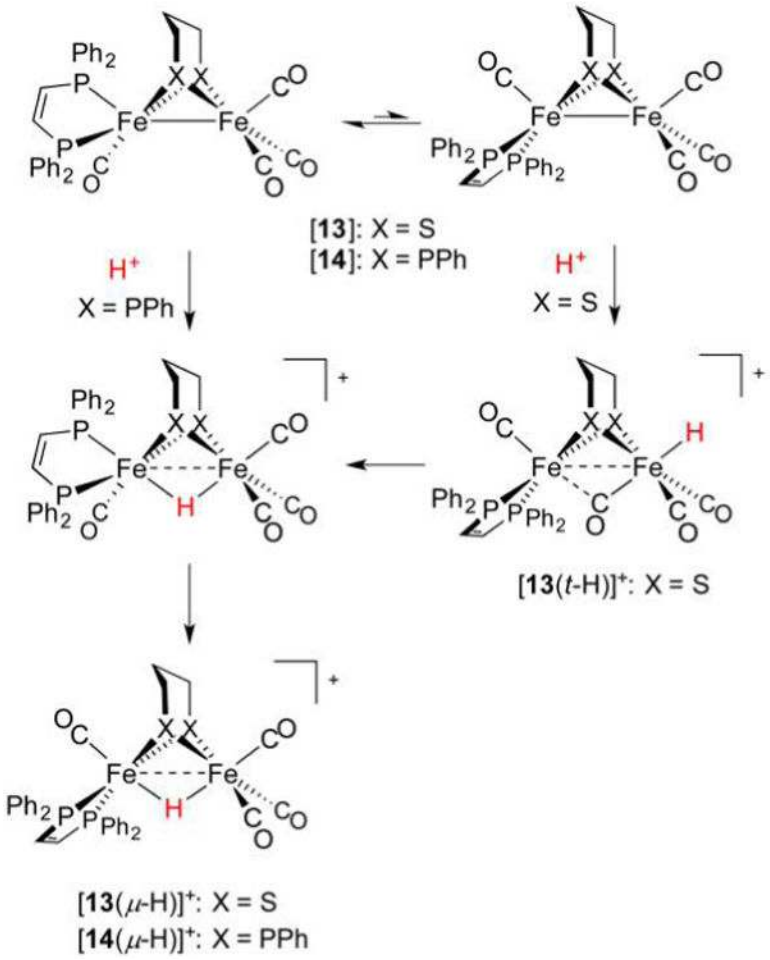

Figure 18.

Bridging secondary phosphido ligands do not represent sites for protonation, and only bridging hydrides are observed.[265] In contrast, bridging thiolato ligands can be protonated, and serve as relays to afford terminal and bridging hydride complexes.[264]

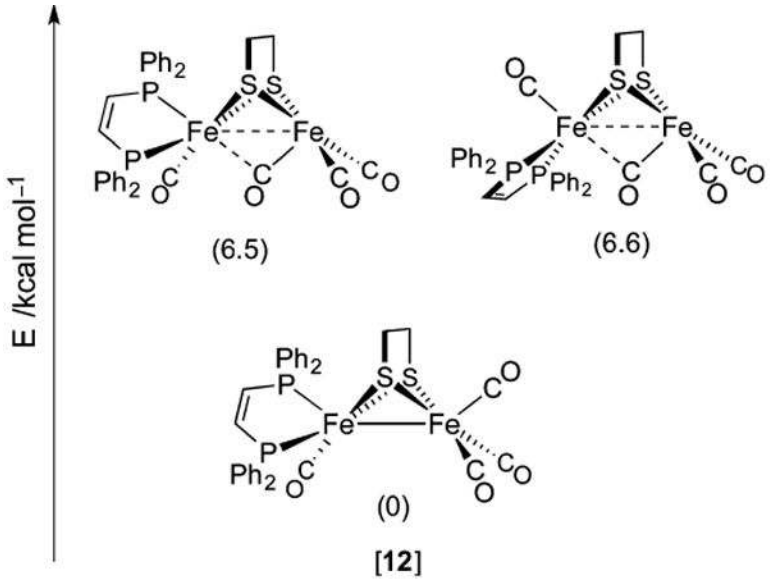

Figure 19.
Rotated and unrotated isomers of [**12**], an Fe(I)Fe(I) model for H_{red}.[265]

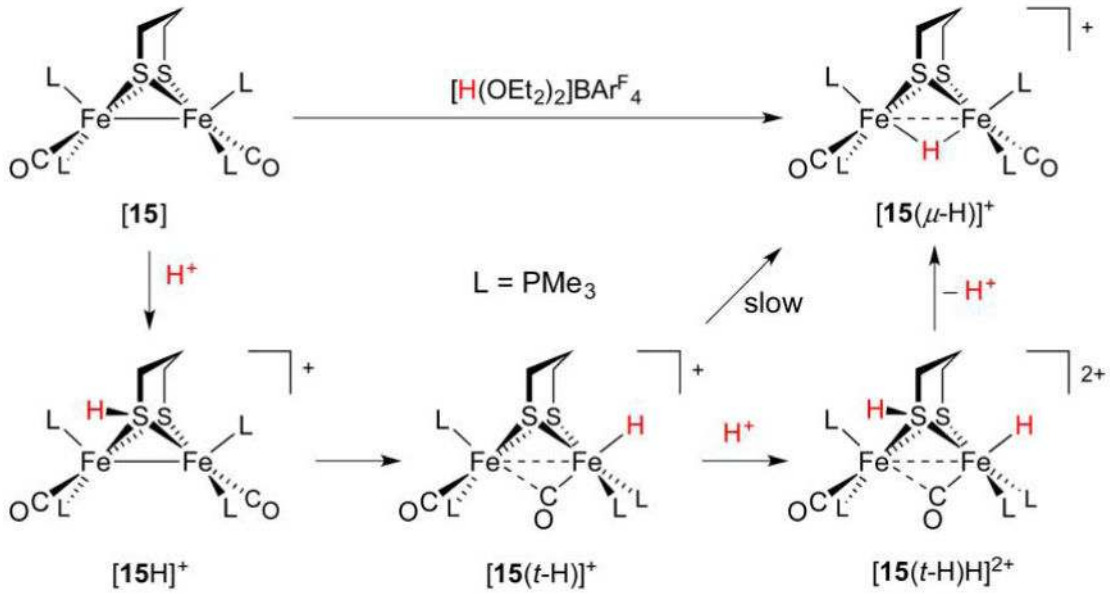

Figure 20.

Protonation of [**15**] affords a thiol intermediate en route to a terminal hydride. Formation of the bridging hydride thermodynamic product is acid-catalyzed.[250]

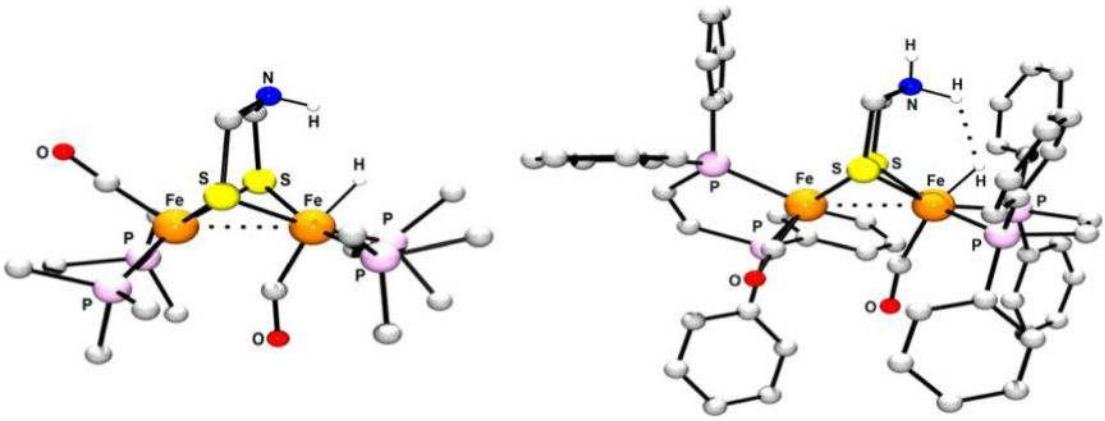

Figure 21.

X-ray structures of [**16**(*t*-H)]$^{+}$ and [**17**(*t*-H)H]$^{2+}$. Nonionizable H atoms are omitted for clarity.[250,258]

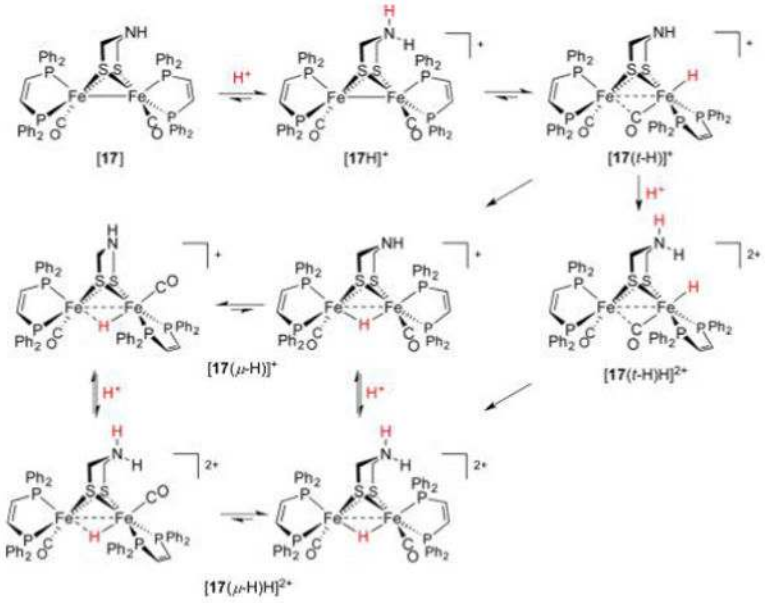

Figure 22.

Conformational dynamics accompanying the protonation of [**17**] (inversion of ammonium/amine centers not depicted).[161]

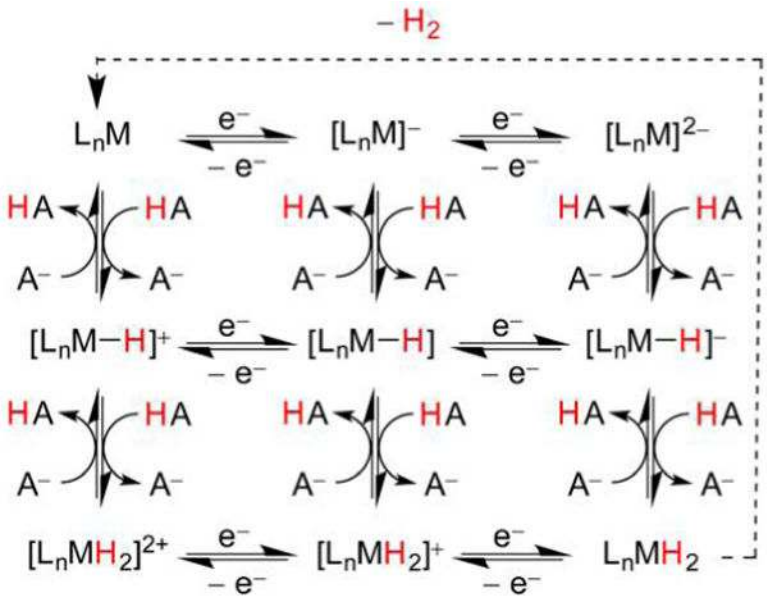

Figure 23.
Many proton and electron transfers that can be involved in the HER.

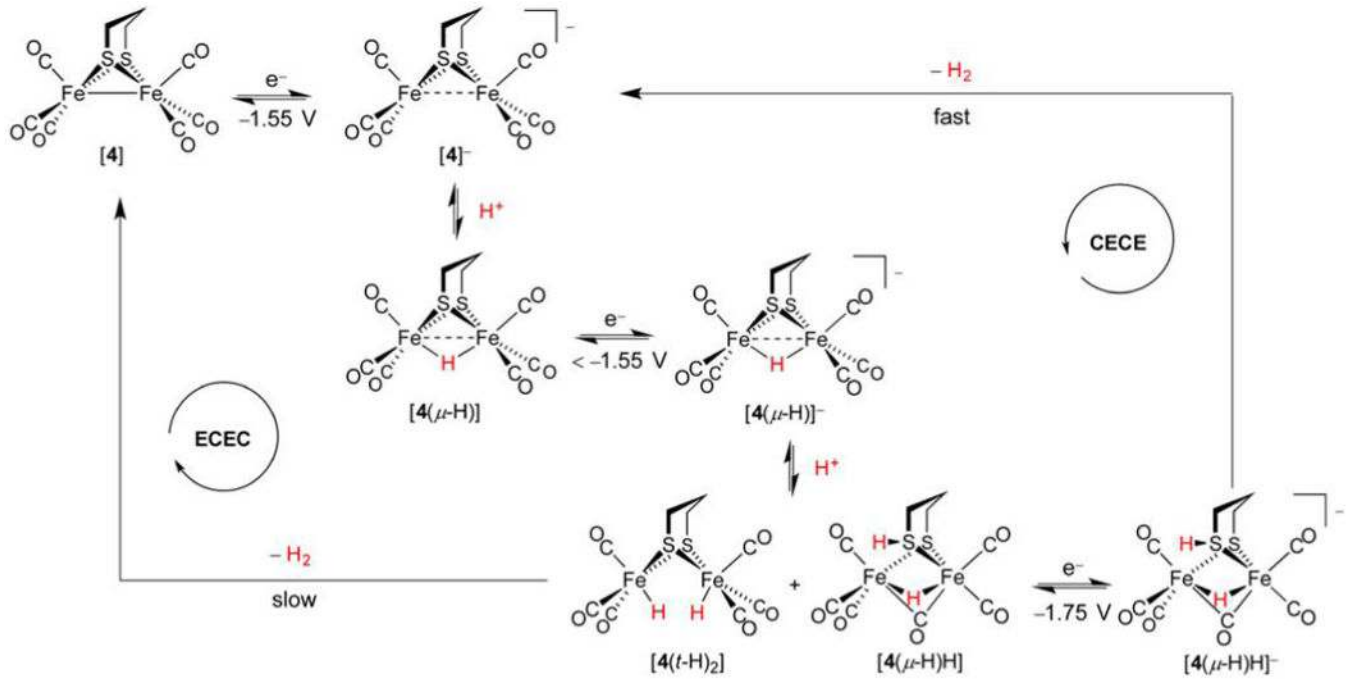

Figure 24.
HER mechanism associated with [**4**].[280]

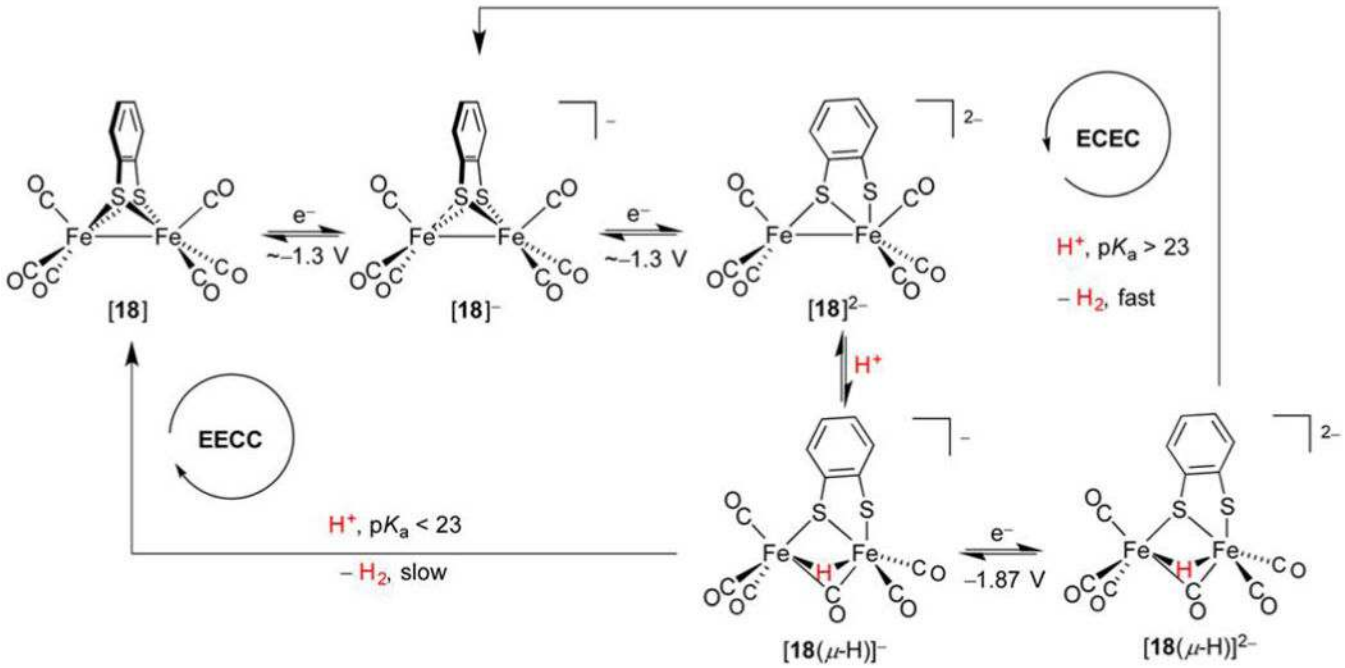

Figure 25.
HER mechanism associated with [**18**].[85]

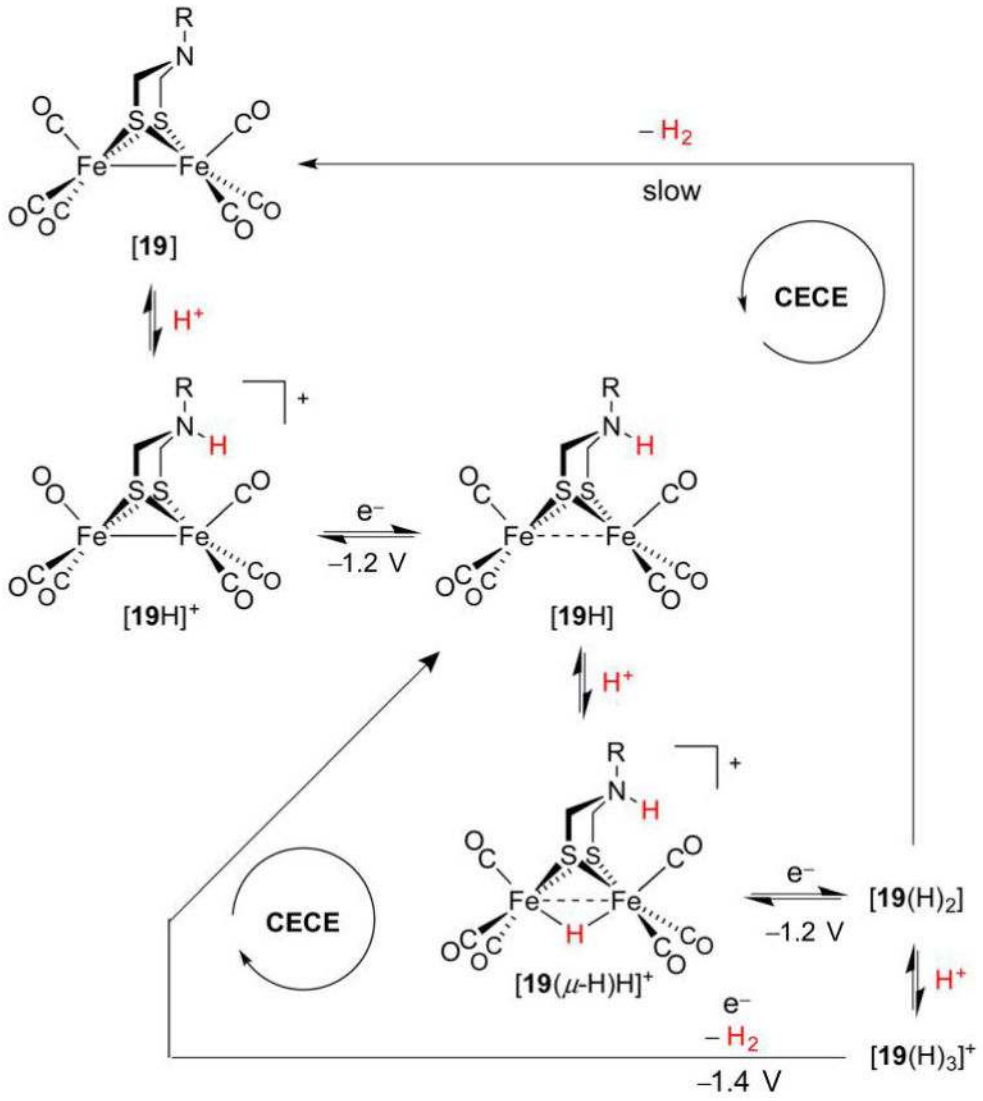

Figure 26.
HER mechanism associated with [**19**].[282]

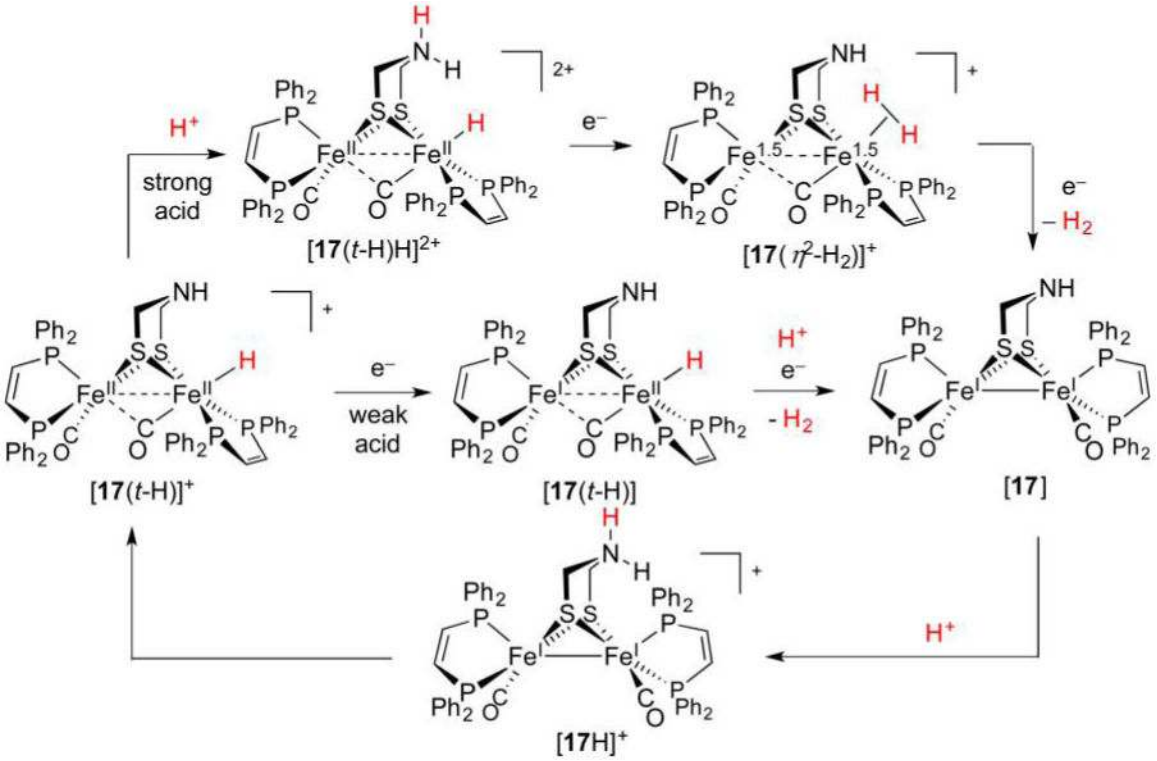

Figure 27.

Highly active HER catalyst [**17**] operates by different mechanisms that depend on acid strength.[258]

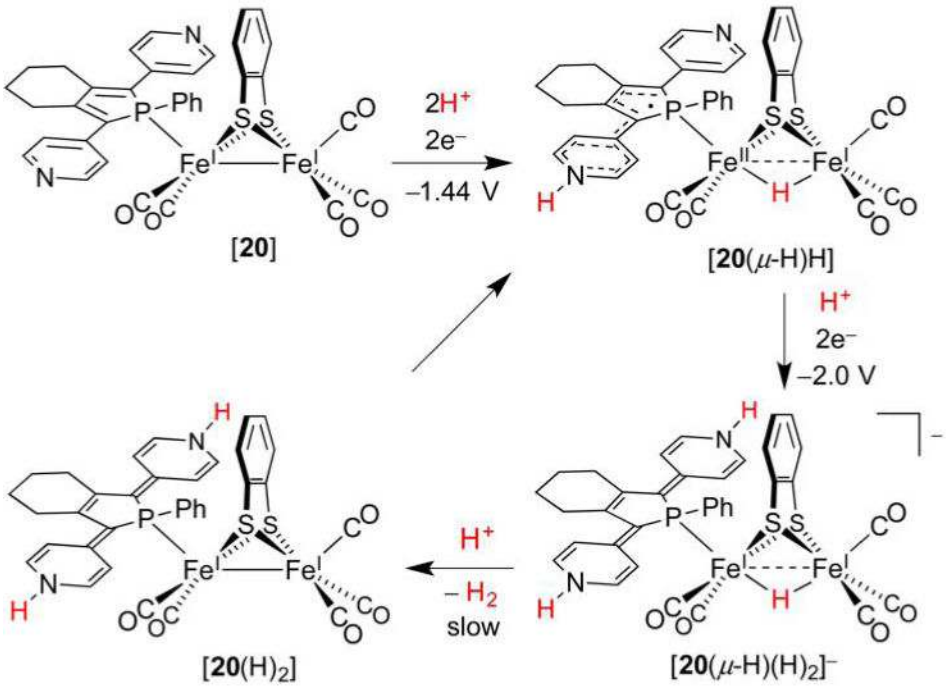

Figure 28.
HER catalytic cycle proposed for [**20**], which bears a redox-active phosphole ligand.[284]

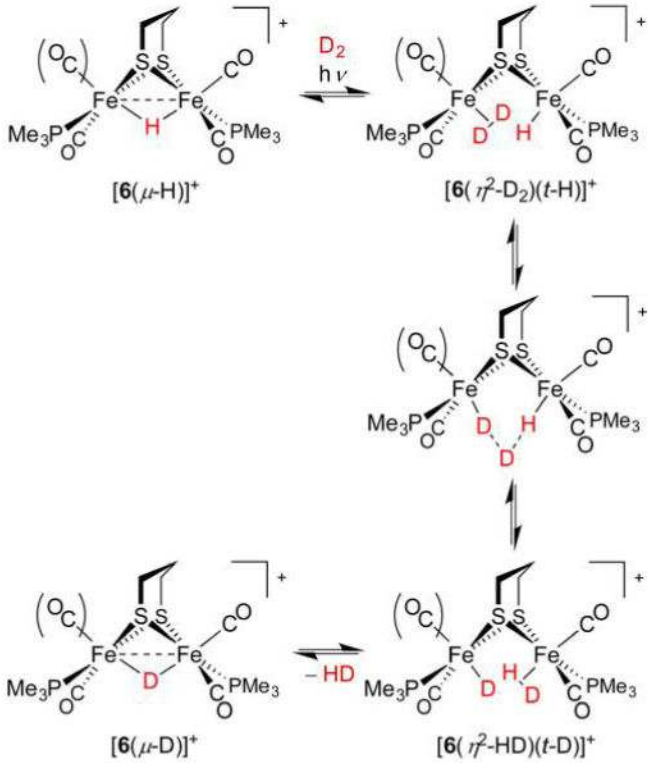

Figure 29.

H/D scrambling mediated by [**6**(μ-H)]$^+$. This complex may undergo either decarbonylation or μ-H → *t*-H isomerization such that a vacant site for D_2 binding is accessible.[285]

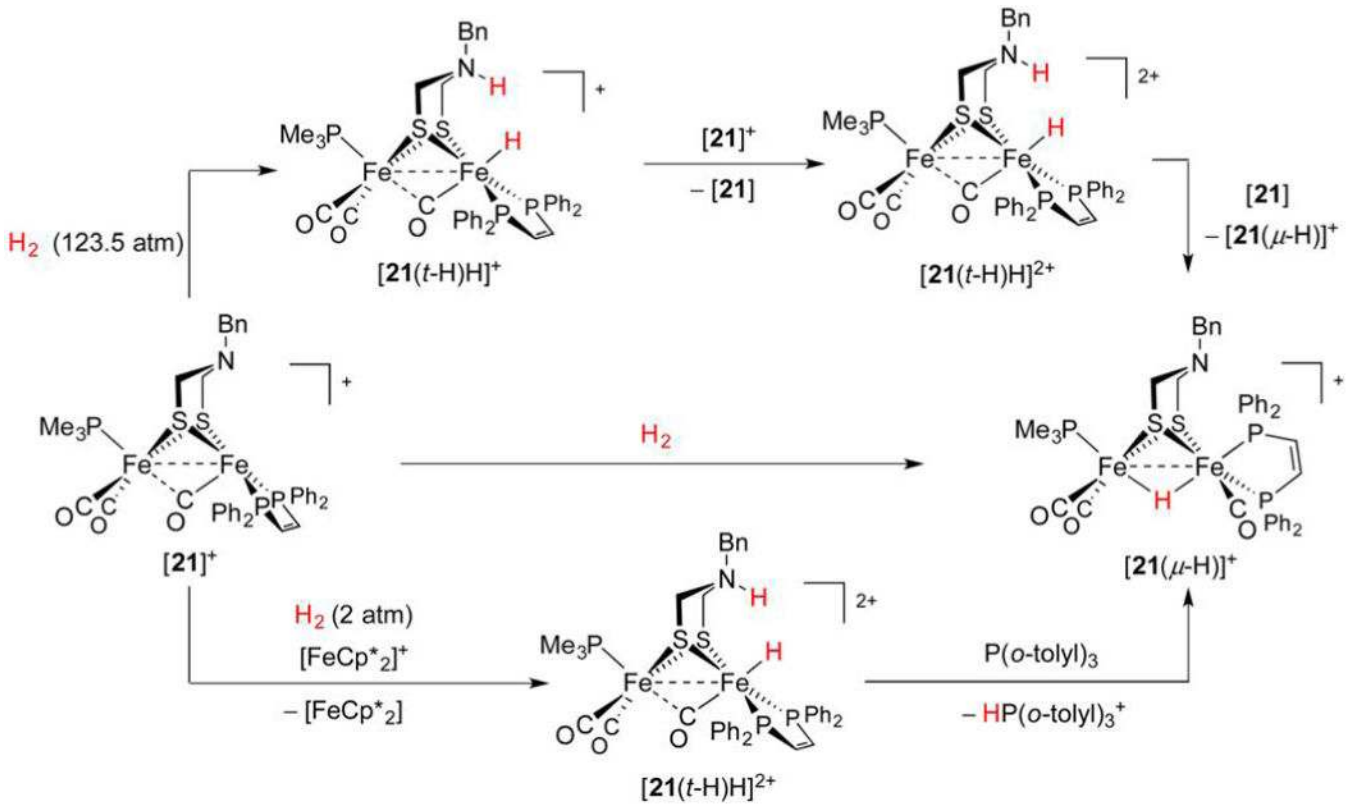

Figure 30.

Stoichometric activation of H_2 with [**21**]$^+$ in the presence[291] and absence[290] of an external oxidant.

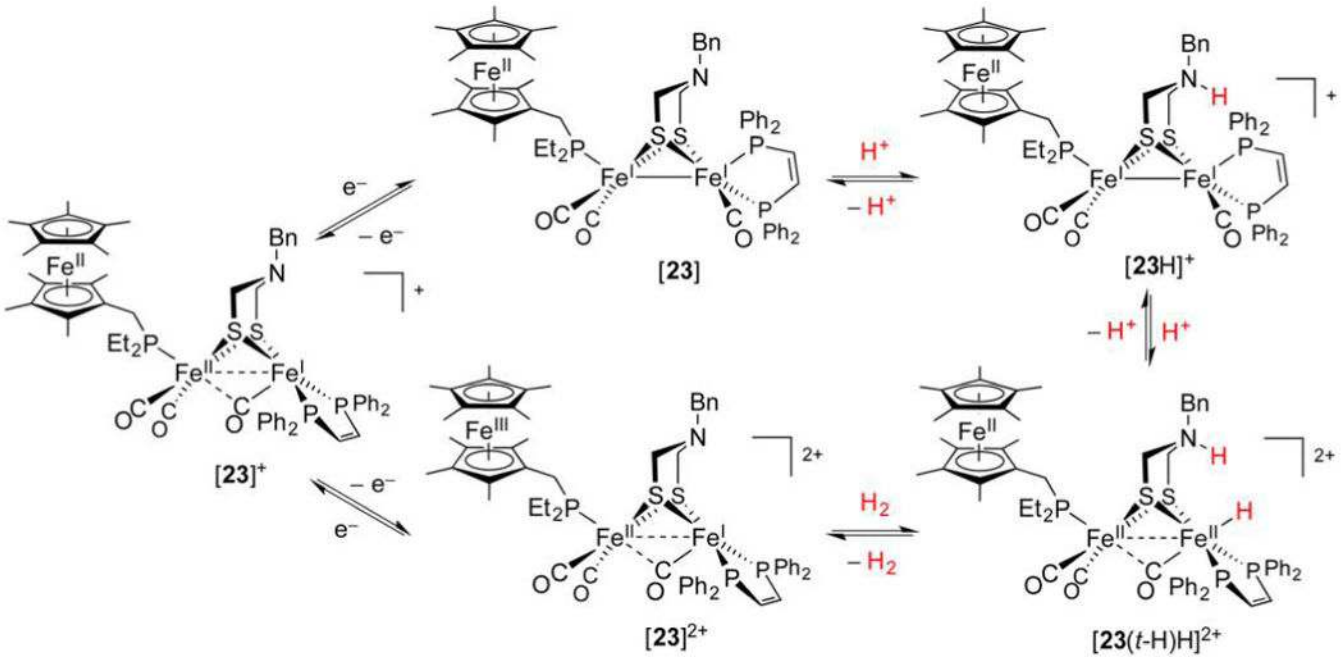

Figure 31.

Catalytic cycle proposed for [**23**]-mediated H_2 evolution and oxidation (clockwise and counterclockwise, respectively).[66,292]

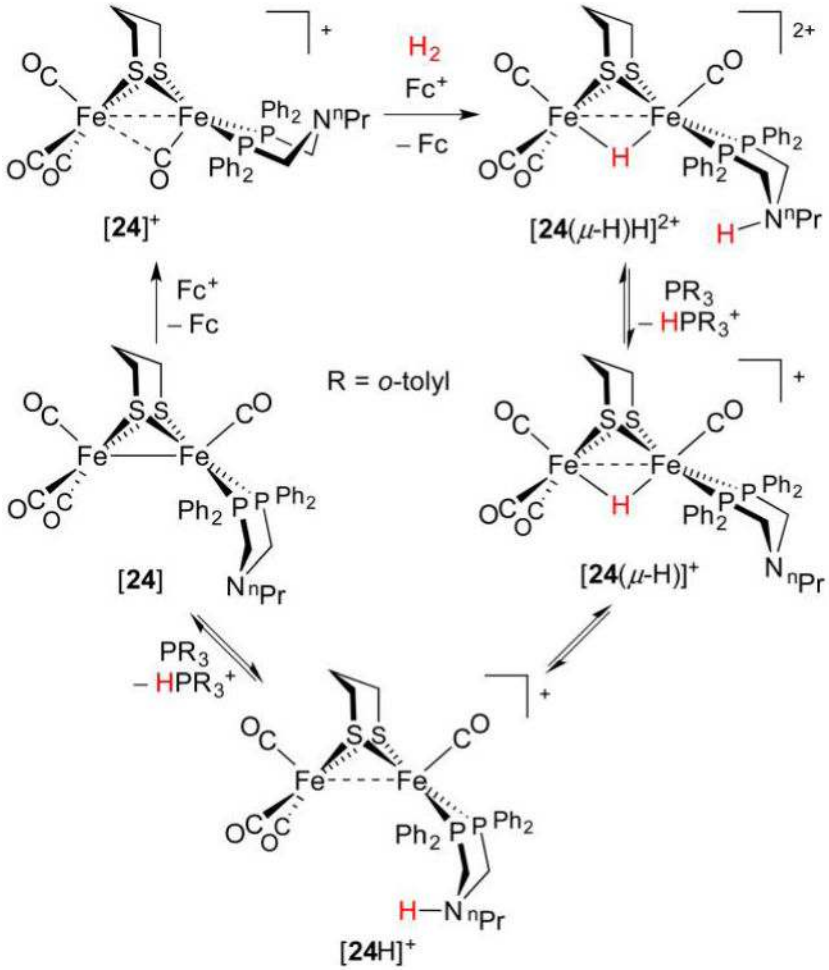

Figure 32.
Catalytic cycle proposed for H_2 oxidation mediated by PNP complex [**24**(μ-H)]$^+$.[295]

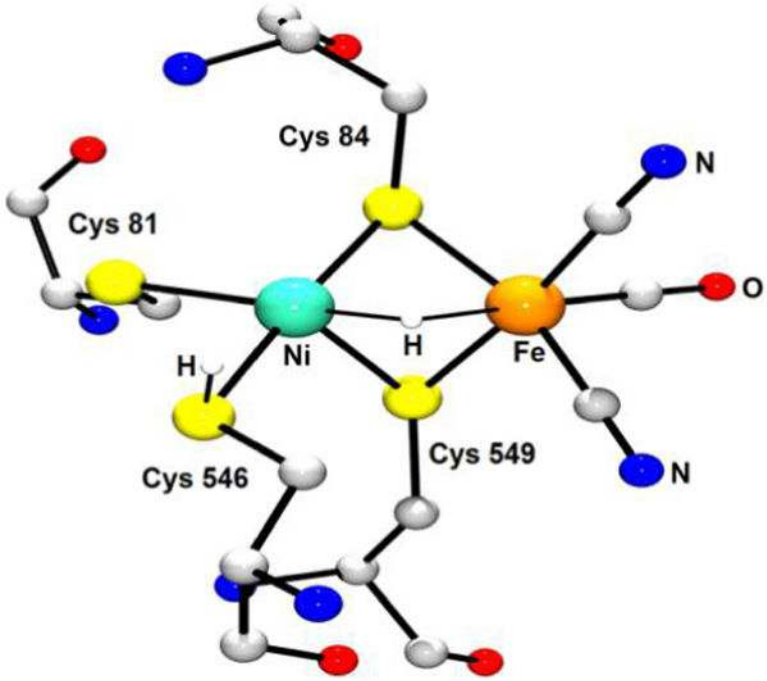

Figure 33.

X-ray structure of the [NiFe]-H_2ase active site from *Desulfovibrio vulgaris* Miyazaki F (PDB code 4U9H).[89] Nonionizable H atoms are omitted for clarity.

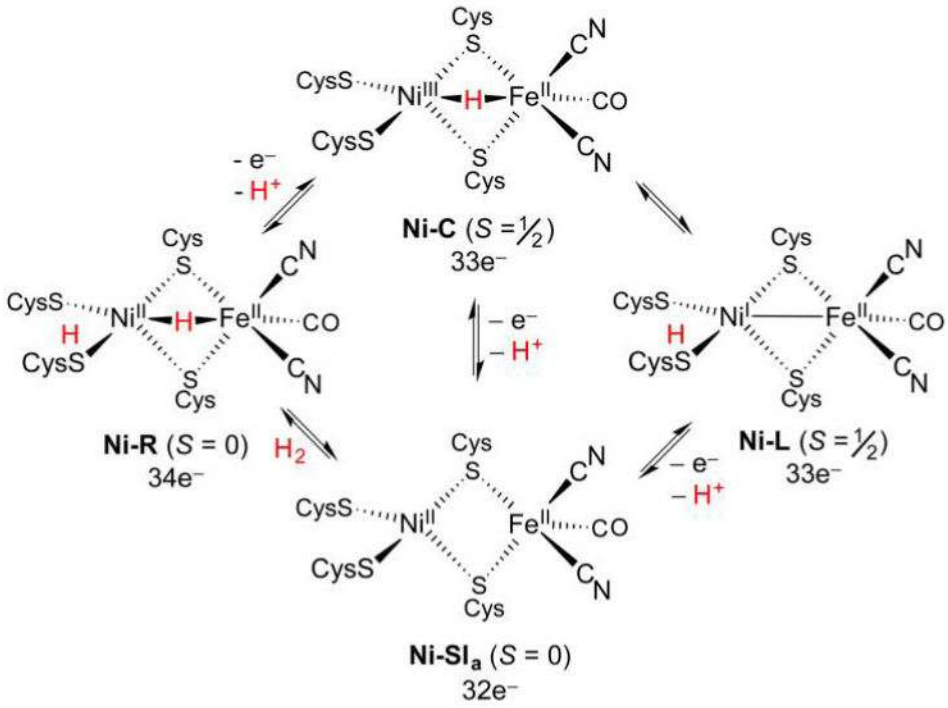

Figure 34.

Catalytic cycles proposed for [NiFe]-H_2ase. The electronic spin (S) and electron count of the NiFe cores (the sum of 3d electrons and electrons in metal–ligand bonds) are presented below each structure.[307] A H_2O ligand may be weakly bound to Ni in Ni-SI_a.

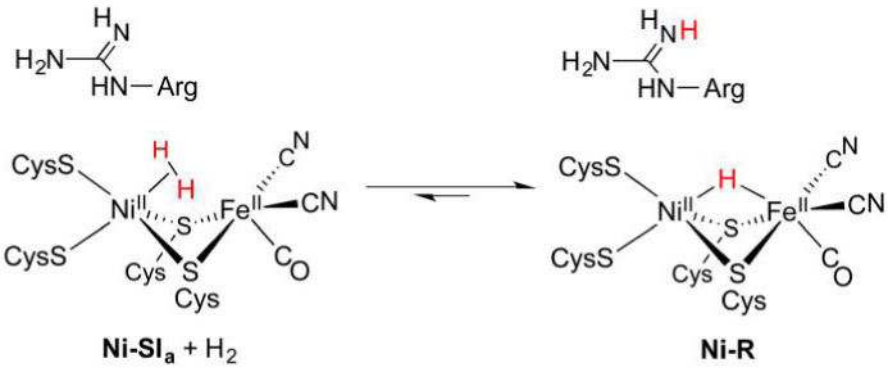

Figure 35.

Alternative mechanism for H_2 activation by [NiFe]-H_2ase, in which a proximal Arg residue (rather than a terminal Cys ligand) relays H^+ to and from the active site.[313]

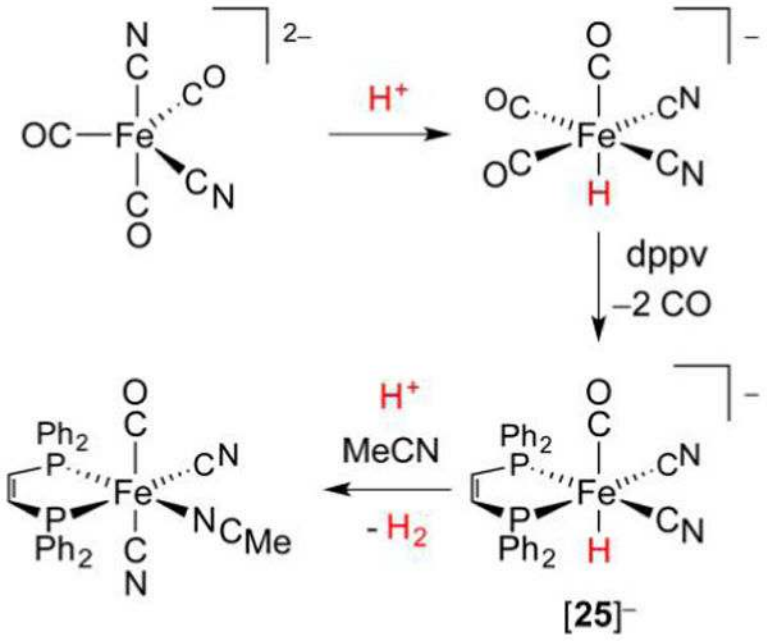

Figure 36.

Initial work on hydride-containing [NiFe]-H_2ase models focused on the Fe subsite, whose $Fe(CO)(CN)_2H$ fragment is replicated by [**25**]$^-$.[342]

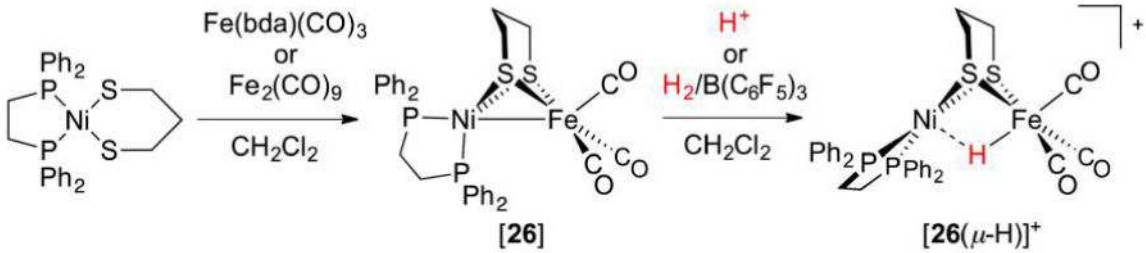

Figure 37.

Synthesis of a Ni(I)Fe(I) thiolate [**26**],[63] which can accept H^+ either from acid or from H_2 heterolysis to afford the hydride derivative [**26**(μ-H)]$^+$.[345]

Figure 38.

X-ray structure of [**26**(μ-H)]$^{+}$. Non-hydride H atoms are omitted for clarity.[345]

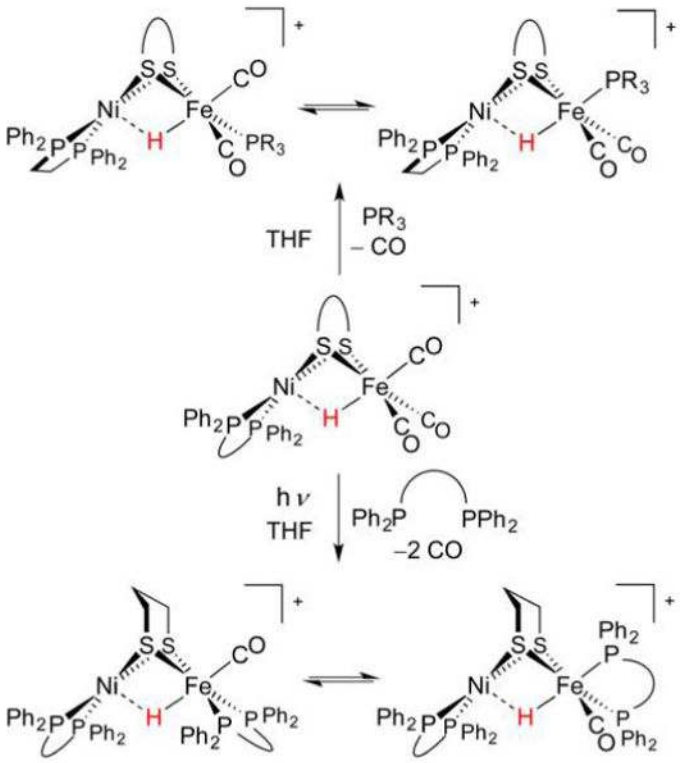

Figure 39.

Synthesis of phosphine-substituted Ni(pdt)(μ-H)Fe derivatives is best performed from hydrido tricarbonyl [**26**(μ-H)]$^{+}$.[63]

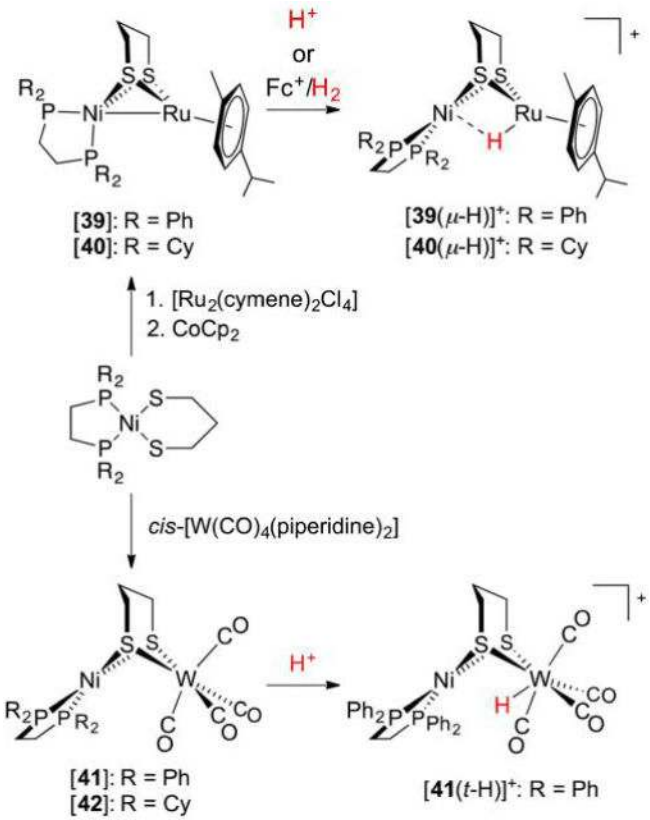

Figure 40.
Synthesis of NiRu[352] and NiW dithiolates[353] and their respective hydrides.

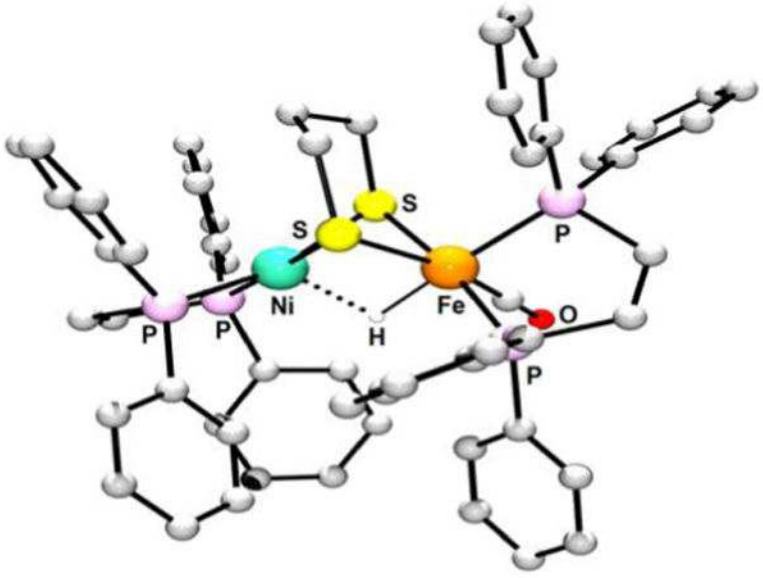

Figure 41.

X-ray structure of [**36**(μ-H)]$^{+}$, one of the most active synthetic NiFe HER catalysts. Non-hydride H atoms are omitted for clarity.[351]

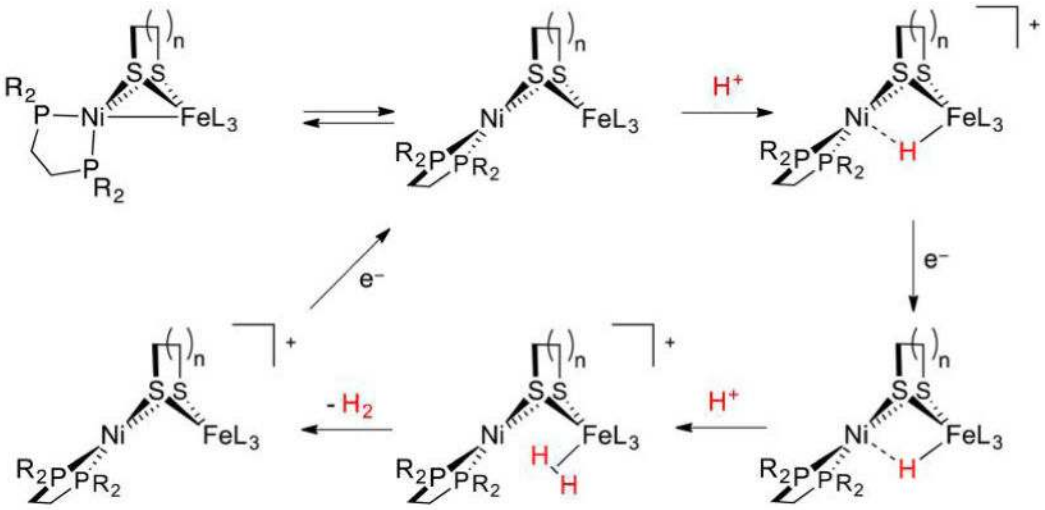

Figure 42.
HER catalytic cycle proposed for the present NiFe dthiolato hydrides.[160]

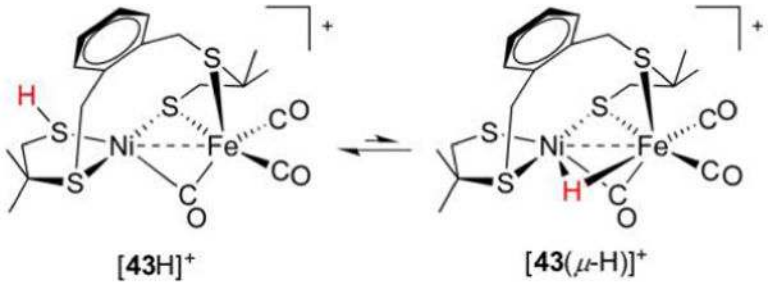

Figure 43.

Interconversion between thiol and hydride tautomers of [**43**H]$^{+}$.[355] There is evidence for both thiol and hydride moieties in the structure for Ni-R.

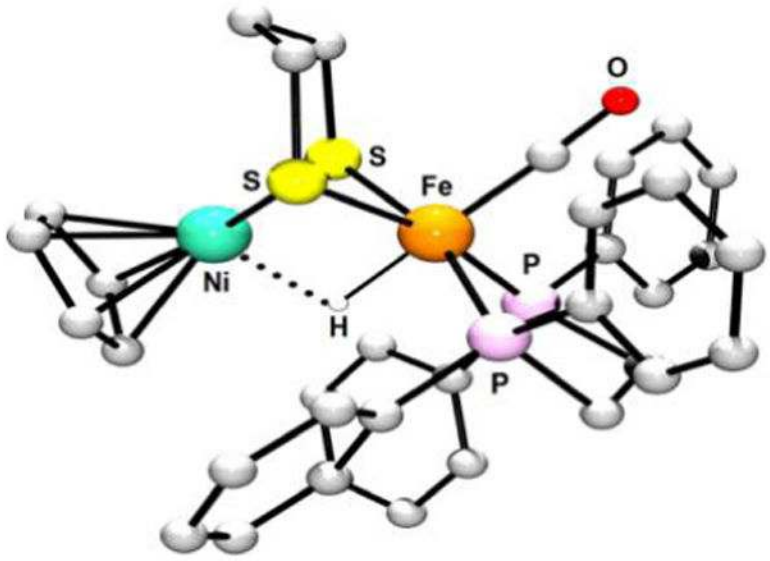

Figure 44.

DFT-calculated structure for the putative species [**44**(μ-H)]$^{+}$, whose Ni(III)(μ-H)Fe(II) core mimics that in Ni-C. Non-hydride H atoms omitted for clarity.[159]

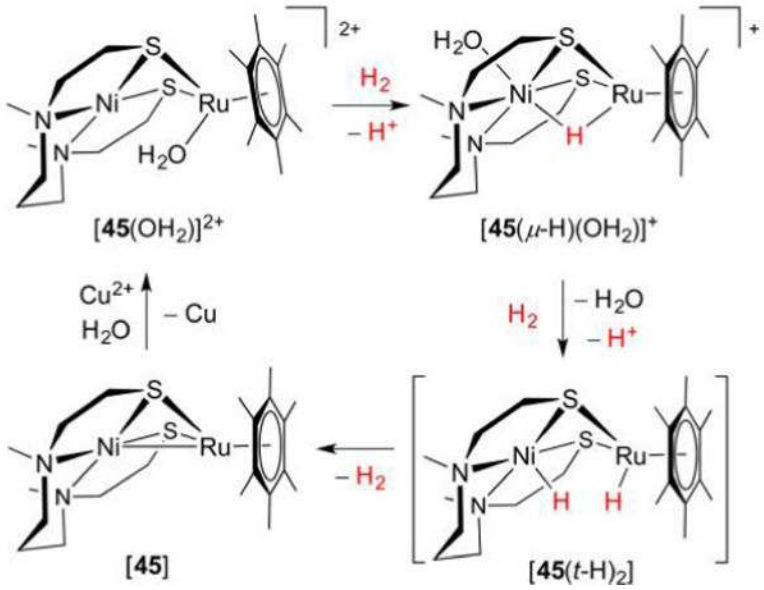

Figure 45.

NiRu dithiolate [**45**$(OH_2)]^{2+}$ activates H_2 to afford hydride [**45**(μ-H)$(OH_2)]^{+}$. Catalytic H_2 oxidation, using Cu^{2+} as the electron acceptor, is proposed to involve a dihydride intermediate.[361]

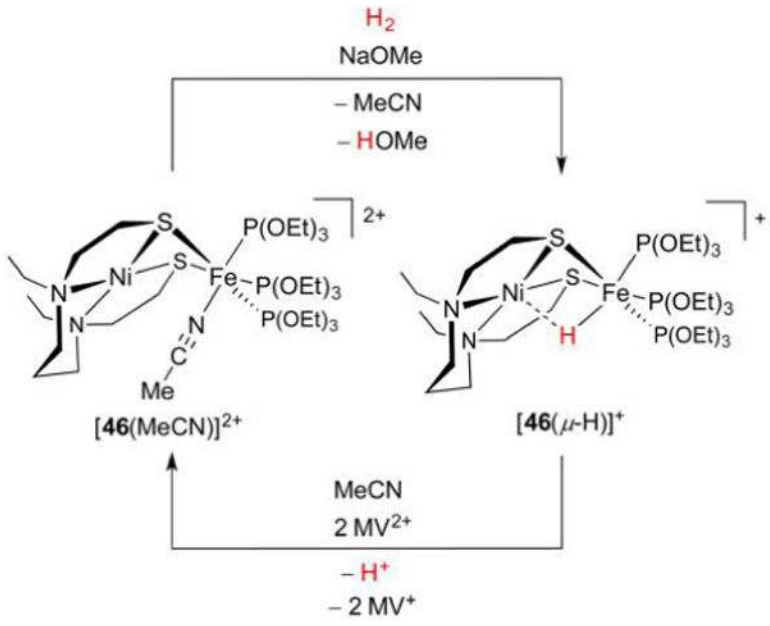

Figure 46.

Activation of H_2 by Ni(II)Fe(II) species [**46**(MeCN)]$^{2+}$ affords hydride [**46**(μ-H)]$^{+}$ (top). X-ray structure of [**46**(μ-H)]$^{+}$ (bottom; non-hydride H atoms omitted for clarity).[367]

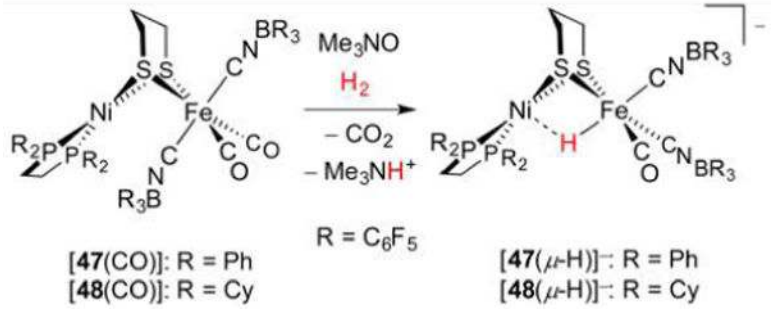

Figure 47.

Activation of H_2 by in situ generated coordinatively unsaturated Ni(II)Fe(II) species affords hydride models for Ni-R (top). X-ray crystal structure of anion [**47**(μ-H)]$^-$ (bottom; F and non-hydridic H atoms omitted for clarity).[368]

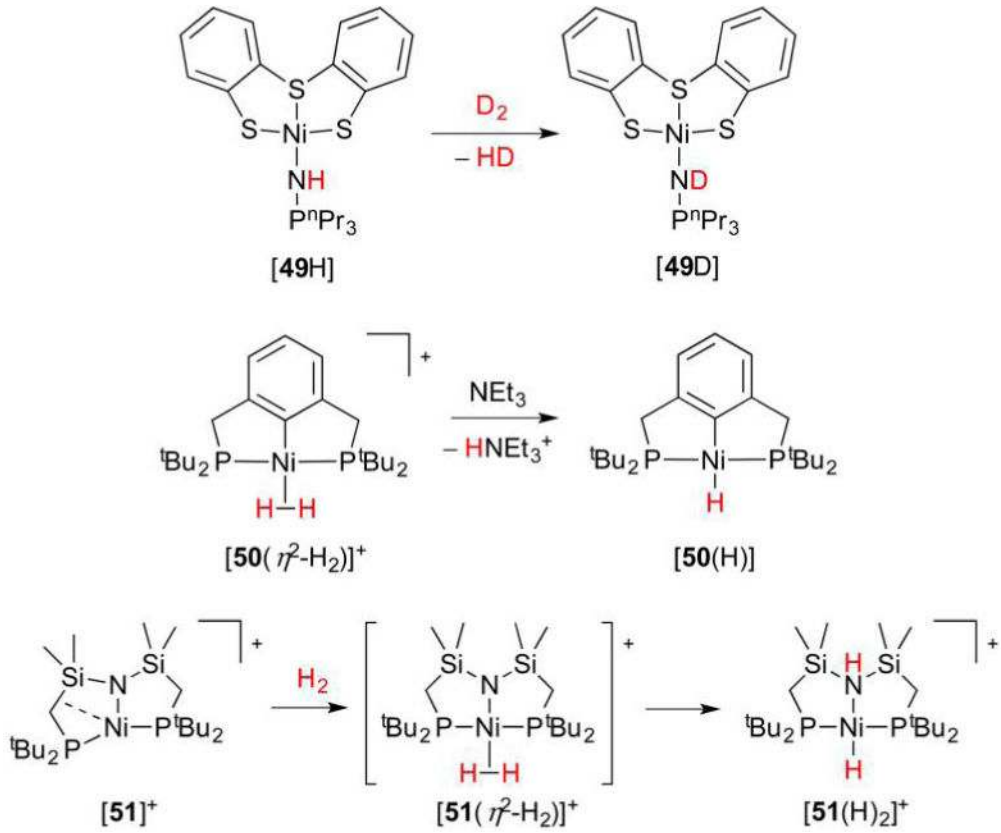

Figure 48.

H/D scrambling implies a Ni(η^2-H_2) intermediate (top).[370] Such Ni(η^2-H_2) species can exhibit heterolysis with[371] and without an external base[372] (middle and bottom, respectively).

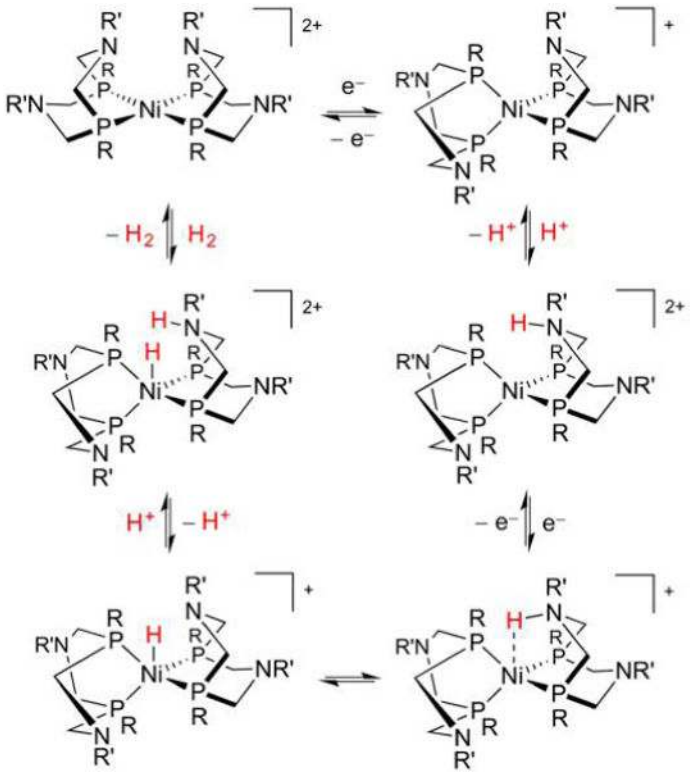

Figure 49.

Examples of the $[Ni(P_2N_2)_2]$ family of electrocatalysts mediate both H_2 oxidation (counterclockwise) and evolution (clockwise).[86] This cycle is a simplification that neglects certain side pathways, and the order of the steps depends on the identities of substituents R and R′.

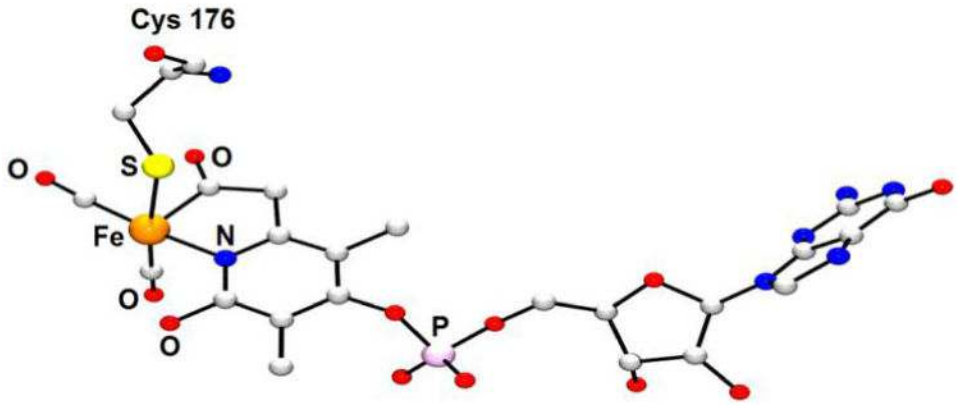

Figure 50.

X-ray structure of the [Fe]-H_2ase active site from *Methanocaldococcus jannaschii* (PDB code 3F4Z).[390] H atoms are omitted for clarity.

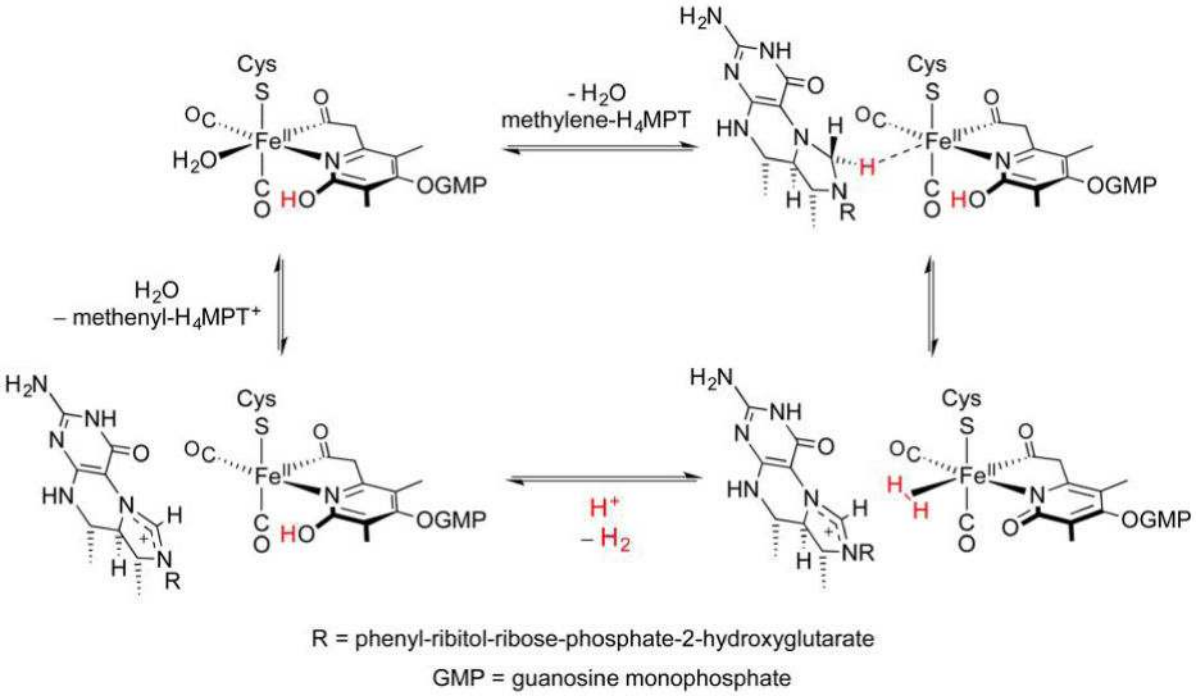

R = phenyl-ribitol-ribose-phosphate-2-hydroxyglutarate

GMP = guanosine monophosphate

Figure 51.

Catalytic cycle proposed for [Fe]-H_2ase.[9]

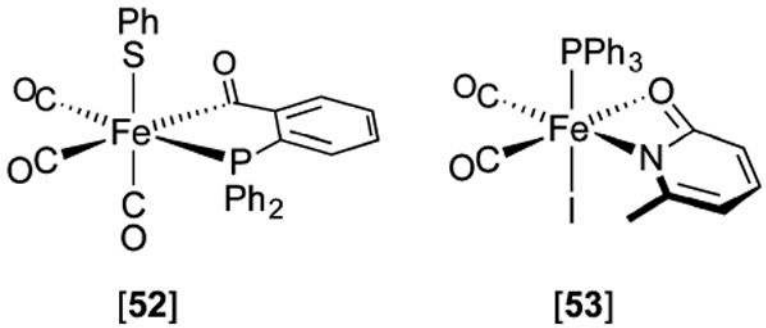

[52] [53]

Figure 52.

Early models for CO-inhibited [Fe]-H_2ase feature some of the donor groups present in the enzyme.[400,401,403]

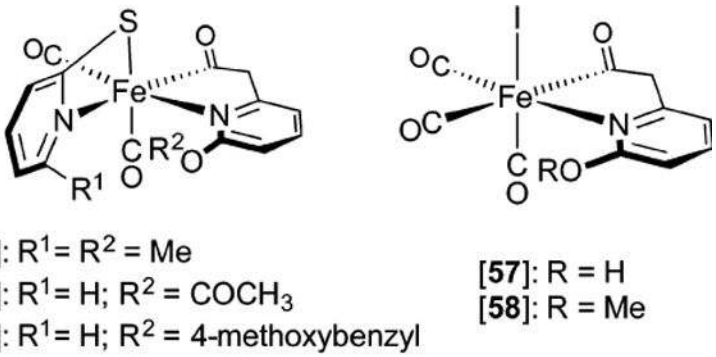

[54]: $R^1 = R^2 = Me$
[55]: $R^1 = H$; $R^2 = COCH_3$
[56]: $R^1 = H$; R^2 = 4-methoxybenzyl

[57]: R = H
[58]: R = Me

Figure 53.
Acyl- and carbamoylpyridine models for CO-inhibited [Fe]-H_2ase.

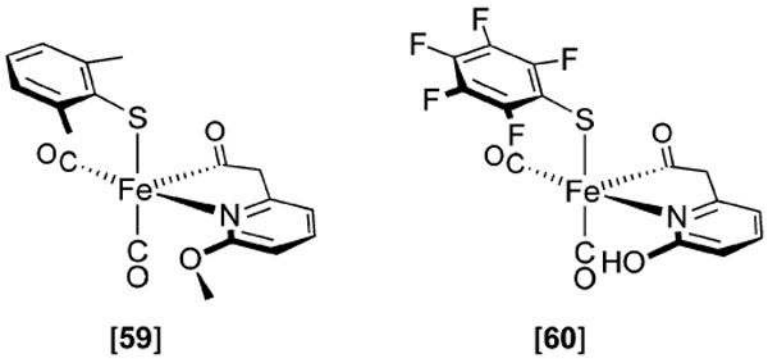

Figure 54.

Pentacoordinate acylpyridine models [**59**] and [**60**] replicate inner Fe coordination sphere of the active [Fe]-H_2ase states, yet do not bind H_2.[412,414]

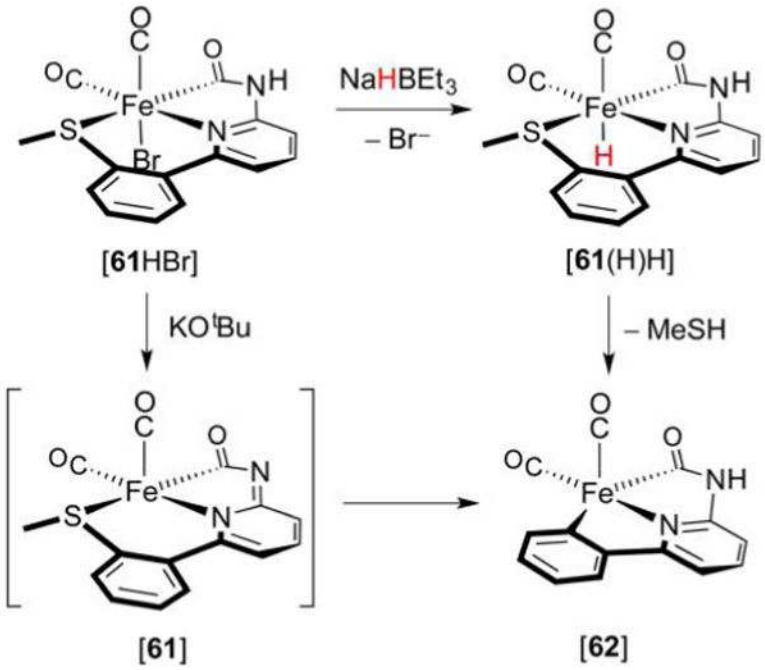

Figure 55.
Preparation and reactivity of the Fe hydrido carbamoyl [**61**(H)H].[415]

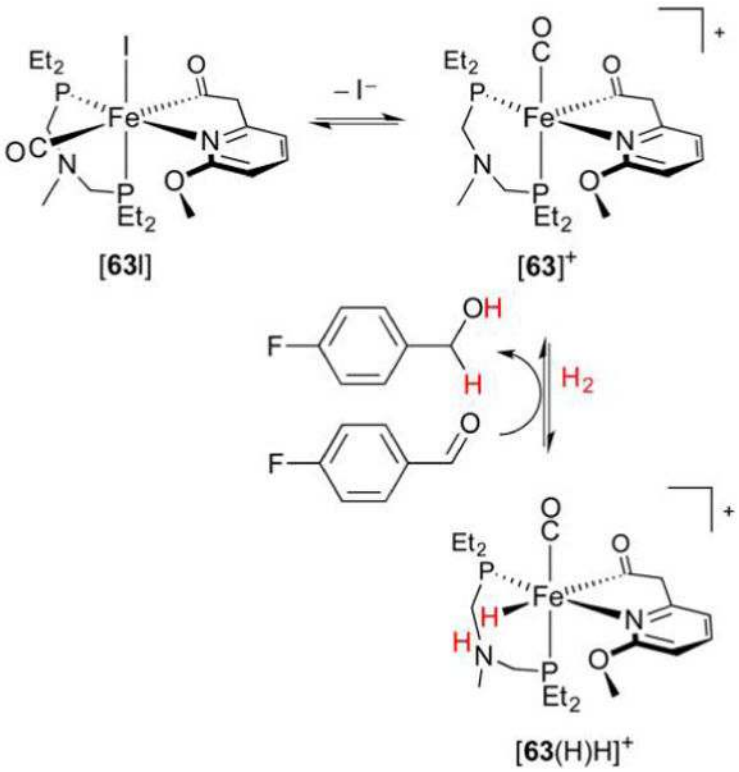

Figure 56.
Polar hydrogenation of an aldehyde catalyzed by [**63**]$^{+}$.[416]

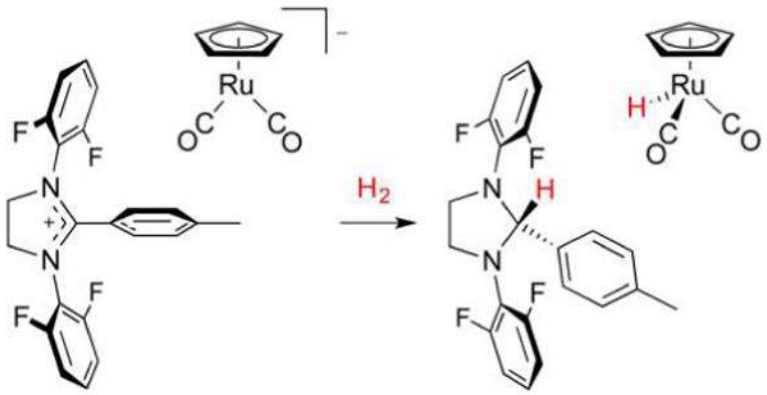

Figure 57.

Complex $[RuCp(CO)_2]^-$ exhibits [Fe]-H_2ase behavior, effecting H_2 heterolysis and delivery of H^- to an imidazolium substrate resembling methenyl-H_4MPT^+.[417]

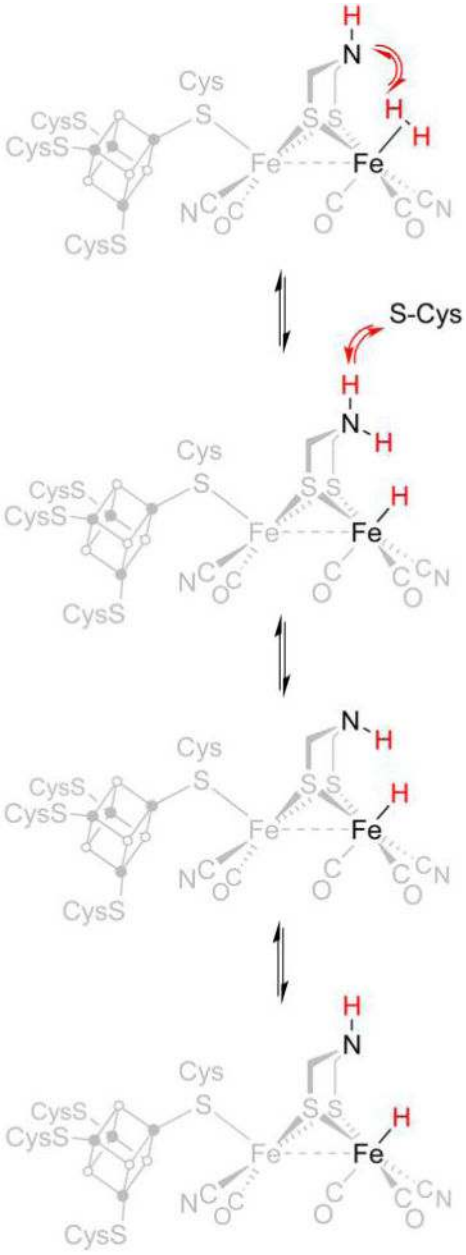

Figure 58.

Proton transport to and from the [2Fe] site in [FeFe]-H_2ase (formal charges omitted). This involves H^+ movement, denoted by red arrows, between Fe^d, the adt^{2-} cofactor, and the protein (via Cys299), and likely requires pyramidal inversion of the amine.

Table 1

Oxidation States and Spectroscopic Parameters for [FeFe]-H_2ase HydA1 from *Chlamydomonas reinhardtii*[a]

state	$[Fe_4S_4]^{n+}$	[2Fe]	ν_{CO}/cm^{-1}	ν_{CN}/cm^{-1}	*g*
H_{ox}	$[Fe_4S_4]^{2+}$	$Fe^p(II)Fe^d(I)$ or $Fe^p(I)Fe^d(II)$	1964, 1940, 1800	2088, 2072	2.10, 2.04, 2.00
H_{red}	$[Fe_4S_4]^{2+}$	$Fe^p(I)Fe^d(I)$	1935, 1891, 1793	2088, 2072	–
H_{sred}	$[Fe_4S_4]^{+}$	$Fe^p(I)Fe^d(I)$	1954, 1919, 1882	2070, 2026	2.08, 1.94, 1.87

[a]Proteins from other strains afford similar data for H_{OX} and H_{red}.[7,202].

Table 2

Redox and Catalytic Properties of FeFe Dithiolato Hydrides

hydride complex	abbreviation	$\delta(^1H)$/ppm	$E_{1/2}$[a]	E_{cat}[a]	acid used	TOF/s^{-1}	η/V
$[(OC)_2(Me_3P)Fe(pdt)(\mu\text{-}H)Fe(CO)_2(CN)]$	[**5**(μ-H)]	−17.08	−1.57	−1.47	HOTs	–	0.75
$[(OC)_2(PMe_3)Fe(pdt)(\mu\text{-}H)Fe(CO)_2(PMe_3)]^+$	[**6**(μ-H)]$^+$	−15.3	−1.39[b]	−1.4	HOTs	–	0.75
$[dppv(OC)Fe(adt)Fe(t\text{-}H)(dppv)(CO)]^+$	[**17**(t-H)]$^+$	−4.2	−1.64[b]	−1.49	$ClCH_2CO_2H$	5000	0.71
$[dppv(OC)Fe(adtH)Fe(t\text{-}H)(dppv)(CO)]^{2+}$	[**17**(t-H)H]$^{2+}$	−4.95	−1.4[b]	−1.11	CF_3CO_2H	58000	0.51
$[dppv(OC)Fe(adt)(\mu\text{-}H)Fe\ (dppv)(CO)]^+$	[**17**(μ-H)]$^+$	−14.8,[c] −13.7[d]	−1.86	−1.72	$ClCH_2CO_2H$	20	0.90
$[dppv(OC)Fe(adtH)(\mu\text{-}H)Fe(dppv)(CO)]^{2+}$	[**17**(μ-H)H]$^{2+}$	−15.5,[c] −14.3[d]	−1.77				
$[dppv(OC)Fe(pdt)Fe(t\text{-}H)(dppv)(CO)]^+$	[**7**(t-H)]$^+$	−3.5	−1.67[e]	−1.49[e]	$HBF_4{\cdot}Et_2O$	5	1.32
$[dppv(OC)Fe(pdt)(\mu\text{-}H)Fe(dppv)(CO)]^+$	[**7**(μ-H)]$^+$	−15.6,[c] −3.5[d]	−1.8[e]	−1.78[e]	$ClCH_2CO_2H$	3	0.95

[a] Relative to $Fc^{+/0}$ in CH_2Cl_2/NBu_4BArF_4.

[b] Irreversible.

[c] Symmetric isomer.

[d] Unsymmetric isomer.

[e] In CH_2Cl_2/NBu_4PF_6.

Table 3

Structural and Spectroscopic Parameters of Active [NiFe]-H_2ase States

state	core	r_{Ni-Fe}/Å	r_{Ni-H}/Å	r_{Fe-H}/Å	ν_{CO}/cm^{-1}	ν_{CN}/cm^{-1}	g
Ni-R	Ni(II)(μ-H)Fe(II)	2.57[a]	1.58[a]	1.78[a]	1944	2074, 2061	–
Ni-C	Ni(III)(μ-H)Fe(II)	2.57[b]	1.59[b]	1.70[b]	1961	2085, 2074	2.21, 2.15, 2.02
Ni-L	Ni(I)Fe(II)	2.56[c]	–	–	1911	2062, 2048	2.28, 2.11, 2.05
Ni-SI_a	Ni(II)Fe(II)	2.61[d]	–	–	1943	2086, 2075	–

[a]Distances from X-ray structure.[89]

[b]DFT-calculated values.[316]

[c]DFT-calculated values.[179]

[d]DFT-calculated value from a structure bearing a H_2O ligand and protonated Cys ligand. IR bands from *Desulfovibrio vulgaris* Miyazaki F.[314] EPR g-values from *Allochromatium vinosum*.[323]

Table 4

Spectroscopic and Structural Parameters for NiFe Thiolato Hydrides

hydride complex[a]		$\delta(^1H)$/ppm	ν_{CO}/cm^{-1}	pK_a[d]	r_{Ni-Fe}/Å	r_{Ni-H}/Å	r_{Fe-H}/Å
[(dppe)Ni(pdt)(μ-H)Fe(CO)$_3$]$^+$	[**26**(μ-H)]$^+$	−3.53	2082, 2024	10.7	2.613	1.637	1.460
[(dcpe)Ni(pdt)(μ-H)Fe(CO)$_3$]$^+$	[**27**(μ-H)]$^+$	−3.00	2078, 2017	13.6	2.684	1.905	1.535
[(dppe)Ni(edt)(μ-H)Fe(CO)$_3$]$^+$	[**28**(μ-H)]$^+$	−5.7	2084, 2025	11.3	2.596	1.843	1.578
[(dppe)Ni(pdt)(μ-H)Fe(CO)$_2$PPh$_3$]$^+$	[**29**(μ-H)]$^+$	−3.08[b]	2016, 1964	14.9	2.643	1.890[b]	1.487[b]
[(dppe)Ni(pdt)(μ-H)Fe(CO)$_2$PPh$_2$(2-py)]$^+$	[**30**(μ-H)]$^+$	−3.19[b]	2022, 1971				
[(dppe)Ni(pdt)(μ-H)Fe(CO)$_2$P(OPh)$_3$]$^+$	[**31**(μ-H)]$^+$	−3.45[b]	2031, 1981				
[(dcpe)Ni(edt)(μ-H)Fe(CO)$_3$]$^+$	[**32**(μ-H)]$^+$	−5.3	2080, 2019	13.6			
[(dppe)Ni(edt)(μ-H)Fe(CO)$_2$PPh$_3$]$^+$	[**33**(μ-H)]$^+$	−8.15,[b] −5.13[c]	2068, 1912	14.0			
[(dppe)Ni(pdt)(μ-H)Fe(dppe)CO]$^+$	[**34**(μ-H)]$^+$	−6.34,[b] −3.01[c]	1954, 1938	2.656[c]	1.847[c]	1.555[c]	
[(dppe)Ni(pdt)(μ-H)Fe(dppbz)CO]$^+$	[**35**(μ-H)]$^+$	−6.01,[b] −3.14[c]	1949, 1935	2.671[a]	1.788[a]	1.798[a]	
[(dppv)Ni(pdt)(μ-H)Fe(dppv)CO]$^+$	[**36**(μ-H)]$^+$	−5.79[b]	1962, 1952	16.6	2.646[b]	1.79[b]	1.56[b]

[a] Isolated as BF_4^- salts.

[b] Asymmetric isomer.

[c] Symmetric isomer.

[d] pK_a is in PhCN.

Table 5

Redox and Catalytic Properties of NiFe Dithiolato Hydrides

hydride complex[a]		E(NiHFe$^{+/0}$)[b]	$E_{cat/2}$[b,c]	acid used	TOF/s^{-1}	η/V
[(dppe)Ni(pdt)(μ-H)Fe(CO)$_3$]$^+$	[**26**(μ-H)]$^+$	−1.34	−1.20	CF_3CO_2H	20	0.50
[(dcpe)Ni(pdt)(μ-H)Fe(CO)$_3$]$^+$	[**27**(μ-H)]$^+$	−1.56	−1.46	$ClCH_2CO_2H$	50	0.59
[(dppe)Ni(edt)(μ-H)Fe(CO)$_3$]$^+$	[**28**(μ-H)]$^+$	−1.33	−1.23	CF_3CO_2H	240–310	0.49
[(dppe)Ni(pdt)(μ-H)Fe(CO)$_2$PPh$_3$]$^+$	[**29**(μ-H)]$^+$	−1.49	−1.30	CF_3CO_2H	50	0.60
[(dppe)Ni(pdt)(μ-H)Fe(CO)$_2$PPh$_2$(2-py)]$^+$[d]	[**30**(μ-H)]$^+$	−1.49	−1.30	CF_3CO_2H	50	0.60
[(dppe)Ni(pdt)(μ-H)Fe(CO)$_2$P(OPh)$_3$]$^+$	[**31**(μ-H)]$^+$	−1.44	−1.32	CF_3CO_2H	50	0.62
[(dcpe)Ni(edt)(μ-H)Fe(CO)$_3$]$^+$	[**32**(μ-H)]$^+$	−1.47	−1.45	$ClCH_2CO_2H$	20	0.59
[(dppe)Ni(edt)(μ-H)Fe(CO)$_2$PPh$_3$]$^+$	[**33**(μ-H)]$^+$	−1.47	−1.45	$ClCH_2CO_2H$	60–120	0.54
[(dppe)Ni(pdt)(μ-H)Fe(dppe)CO]$^+$	[**34**(μ-H)]$^+$	N/D	−1.61, −1.65	$ClCH_2CO_2H$	23	0.85
[(dppe)Ni(pdt)(μ-H)Fe(dppbz)CO]$^+$	[**35**(μ-H)]$^+$	N/D	−1.61, −1.70	$ClCH_2CO_2H$	30	0.85
[(dppv)Ni(pdt)(μ-H)Fe(dppv)CO]$^+$	[**36**(μ-H)]$^+$	N/D	−1.54	$ClCH_2CO_2H$	29	0.75

[a] Isolated as BF_4^- salts.

[b] In volts, determined in CH_2Cl_2, relative to $Fc^{+/0}$.

[c] Potential at $i_{cat}/2$.

[d] 2-py =2-pyridyl.

Table 6

CO-Stretching Bands for Active and CO-Inhibited Forms of [Fe]-H_2ase, as well as for Selected Synthetic Models

species	ν_{CO}/cm^{-1}
[Fe]-H_2ase	2011, 1944
[Fe]-H_2ase-CO	2074, 2020, 1981
[**52**]	2075, 2020, 1981
[**53**]	2032, 1987
[**54**]	2026, 1961
[**55**]	2027, 1964
[**56**]	2022, 1958
[**57**]	2068, 2050, 1996
[**58**]	2084, 2018, 2003
[**59**]	2013, 1950
[**60**]	2022, 1958
[**61**HBr]	2030, 1974
[**62**]	2003, 1940
[**63**I]	1945
$[RuCp(CO)_2]^-$	1887, 1802